BRIDGE DECK CRACKING EVALUATION

FHWA/MT-21-005/9696-700

Final Report

prepared for
THE STATE OF MONTANA
DEPARTMENT OF TRANSPORTATION

in cooperation with
THE U.S. DEPARTMENT OF TRANSPORTATION
FEDERAL HIGHWAY ADMINISTRATION

October 2021

prepared by
Todd Nelson
Le Pham
Paul Krauss
Elizabeth Wagner
Eisa Rahmani
Jack Dai

Wiss Janney Elstner (WJE) Associates
Northbrook, IL

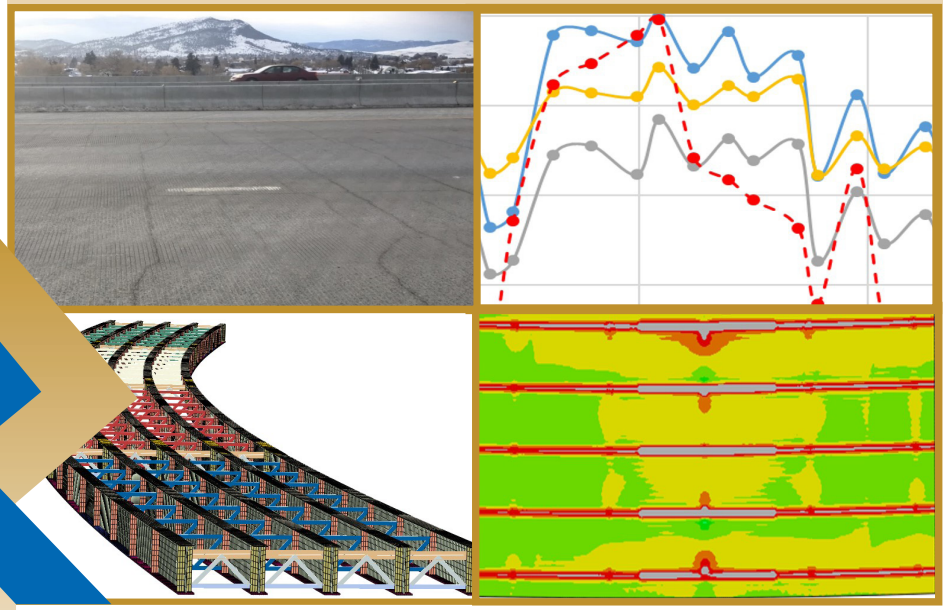

RESEARCH PROGRAMS

MDT

WJE

Bridge Deck Cracking Evaluation

Final Report

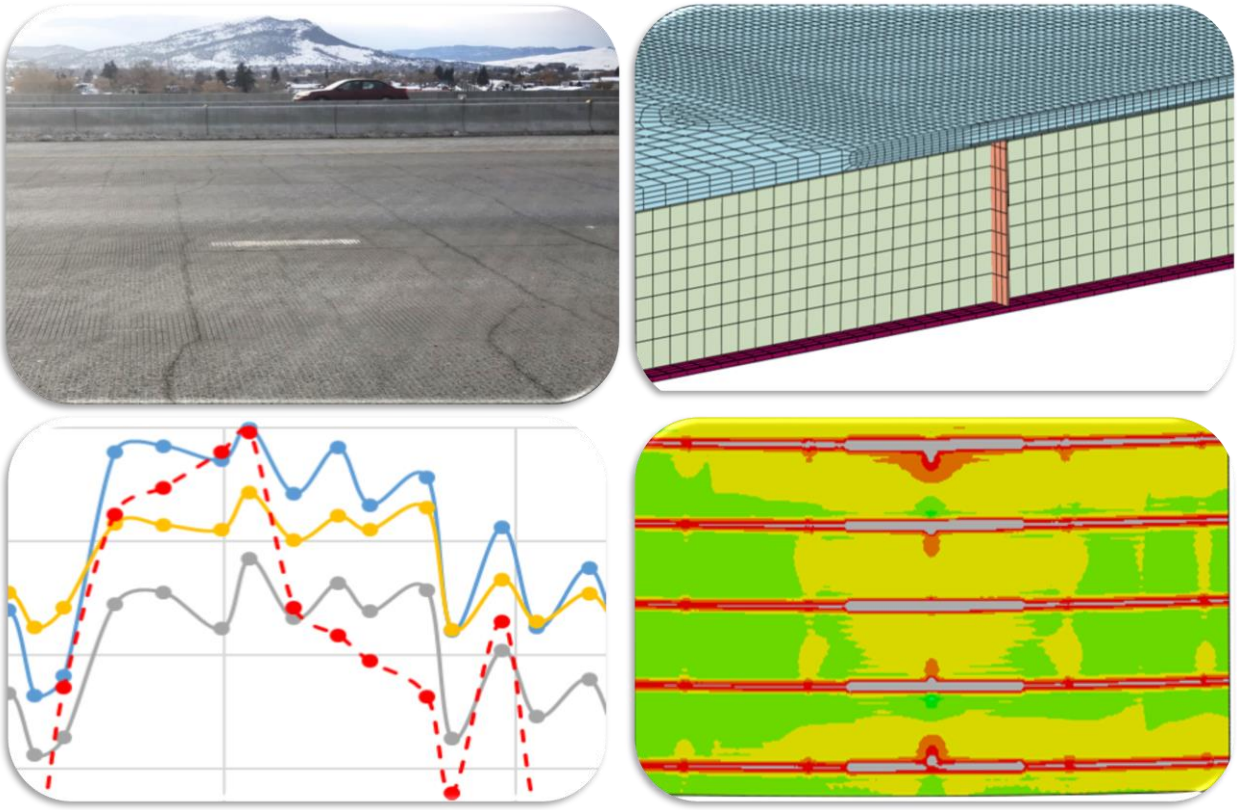

FINAL REPORT

October 6, 2021

WJE No. 2019.2214

PREPARED FOR THE:

MONTANA DEPARTMENT OF TRANSPORTATION
in cooperation with the
U.S. DEPARTMENT OF TRANSPORTATION
FEDERAL HIGHWAY ADMINISTRATION

PREPARED BY:

Wiss, Janney, Elstner Associates, Inc.
330 Pfingsten Road
Northbrook, Illinois 60062
847.272.7400 tel

1. Report No. FHWA-MT-21-005/9696-700	**2. Government Accession No.**	**3. Recipient's Catalog No.**
4. Title and Subtitle *Bridge Deck Cracking Evaluation*		**5. Report Date** October, 2021
		6. Performing Organization Code MDT
7. Author(s) Todd Nelson, WJE Le Pham, WJE Paul Krauss, WJE Elizabeth Wagner, WJE Eisa Rahmani, WJE Jack Dai, WJE		**8. Performing Organization Report No.** 1
9. Performing Organization Name and Address Wiss Janney Elstner Associates (WJE) 330 Pfingsten Road Northbrook, IL 60062		**10. Work Unit No.**
		11. Contract or Grant No. MDT - 313162, Project #9696-700
12. Sponsoring Agency Name and Address Research Programs Montana Department of Transportation (SPR) 2701 Prospect Avenue PO Box 201001		**13. Type of Report and Period Covered** Final Report July, 2019 to October, 2021
		14. Sponsoring Agency Code 5401

15. Supplementary Notes

Conducted in cooperation with the U.S. Department of Transportation, Federal Highway Administration. This report can be found at https://www.mdt.mt.gov/research/projects/const/deckcracking.shtml DOI: https://doi.org/10.21949/1518315

Recommended Citation: Nelson, T. 2020. *Bridge Deck Cracking Consulting Services. Montana Department of Transportation. Wiss, Janney, Elstner Associates, Inc. DOI: https://doi.org/10.21949/1518315*

16. Abstract

Transverse cracking of concrete bridge decks continues to be an issue for the Montana Department of Transportation (MDT) and is considered a common issue reported among many state departments of transportation (DOTs). In the last 25 years with the introduction of high performance concrete (HPC) in bridge decks to lower permeability and with the use of finer ground cements (to increase early age strength gain and construction schedule), the susceptibility of bridge deck cracking has increased. Cracking commonly leads to a reduction in service life and increased maintenance costs, primarily due to accelerated corrosion of reinforcing steel in the deck. Identifying the causes of bridge deck cracking and providing prevention can be complex and challenging, but is very important for maintaining longevity of the bridge deck.

To assist MDT with diagnosing and mitigating the causes of transverse cracking of bridge decks, WJE implemented a multi-disciplinary approach including a literature review, field inspections, bridge deck instrumentation, laboratory evaluations, and finite element modeling (FEM). From this research, WJE found the primary causes were related to non-uniform moisture gradients, drying shrinkage, and specific winter curing procedures. Based on these findings, WJE recommended improvements to mixture proportions, construction practices, and design considerations.

17. Key Words Bridge deck cracking, bridge deck inspection, crack mapping, cracking severity, transverse cracking, finite element modeling, moisture gradients, and drying shrinkage.	**18. Distribution Statement** No restrictions. This document is available through the National Technical Information Service, Springfield, VA 22161. Enter any other agency mandated distribution statements. Remove NTIS statement if it does not apply.

19. Security Classif. (of this report) Unclassified	**20. Security Classif. (of this page)** Unclassified	**21. No. of Pages** 247	**22. Price**
Form DOT F 1700.7 (8-72)	Reproduction of completed page authorized		

Disclaimer Statement

This document is disseminated under the sponsorship of the Montana Department of Transportation (MDT) and the United States Department of Transportation (USDOT) in the interest of information exchange. The State of Montana and the United States assume no liability for the use or misuse of its contents.

The contents of this document reflect the views of the authors, who are solely responsible for the facts and accuracy of the data presented herein. The contents do not necessarily reflect the views or official policies of MDT or the USDOT.

The State of Montana and the United States do not endorse products of manufacturers.

This document does not constitute a standard, specification, policy or regulation.

Alternative Format Statement

MDT attempts to provide accommodations for any known disability that may interfere with a person participating in any service, program, or activity of the Department. Alternative accessible formats of this information will be provided upon request. For further information, call 406/444.7693, TTY 800/335.7592, or Montana Relay at 711.

CONTENTS

LIST OF FIGURES

LIST OF TABLES

STANDARD CONVERSION CHART

STANDARD CONVERSION TABLE – ENGLISH TO METRIC				
Symbol	To convert from	Multiply by	To determine	Symbol
		LENGTH		
IN	inch	25.4	millimeters	mm
FT	feet	0.3048	meters	m
YD	yards	0.9144	meters	m
MI	miles	1.609344	kilometers	km
		AREA		
SI	square inches	645.16	square millimeters	mm^2
SF	square feet	0.09290304	square meters	m^2
SY	square yards	0.83612736	square meters	m^2
A	acres	0.4046856	hectares	ha
MI^2	square miles	2.59	square kilometers	km^2
		VOLUME		
CI	cubic inches	16.387064	cubic centimeters	cm^3
CF	cubic feet	0.0283168	cubic meters	m^3
CY	cubic yards	0.764555	cubic meters	m^3
GAL	gallons	3.78541	liters	L
OZ	fluid ounces	0.0295735	liters	L
MBM	thousand feet board	2.35974	cubic meters	m^3
		MASS		
LB	pounds	0.4535924	kilograms	kg
TON	short tons (2000 lbs)	0.9071848	metric tons	t
		PRESSURE AND STRESS		
PSF	pounds per square foot	47.8803	pascals	Pa
PSI	pounds per square inch	6.89476	kilopascals	kPa
PSI	pounds per square inch	0.00689476	megapascals	Mpa
		DISCHARGE		
CFS	cubic feet per second	0.02831	cubic meters per second	$m^3/_s$
		VELOCITY		
FT/SEC	feet per second	0.3048	meters per second	m/s
		INTENSITY		
IN/HR	inch per hour	25.4	millimeters per hour	mm/hr
		FORCE		
LB	pound (force)	4.448222	newtons	N
		POWER		
HP	horsepower	746.0	watts	W
		TEMPERATURE		
°F	degrees Fahrenheit	5 X (°F – 32)/9	degrees Celsius	°C
		DENSITY		
lb/ft^3	pounds per cubic foot	16.01846	kilograms per cubic meter	kg/m^3
		ACCELERATION		
g	freefall, standard	9.807	meters per second squared	m/s^2

TO CONVERT FROM METRIC TO ENGLISH, DIVIDE BY THE ABOVE CONVERSION FACTORS.

ITEM 1 - PROBLEM STATEMENT

Transverse cracking of concrete bridge decks continues to be an issue nationally and for the Montana Department of Transportation (MDT) and is a common issue reported among many state departments of transportation (DOTs) and other transportation agencies. Numerous recent research projects have investigated the possible causes of cracking in bridge decks [1, 2, 3, 4] that continue to add to our knowledge and understanding, but cracking still remains a primary problem for many new bridges. In the last 25 years with the introduction of concrete mixtures with low water/cement ratios, including high performance concrete (HPC), in bridge decks to lower permeability and with the use of finer ground cements (to increase early age strength gain and construction schedule), the susceptibility of bridge deck cracking has increased, primarily due to the increased volume changes and early age modulus (stiffness) development. For these reasons, an increase in cracking potential has been reported by numerous state agencies [1, 2, 3, 4, 5, 6]. Cracking commonly leads to a reduction in service life and increased maintenance costs, primarily due to accelerated corrosion of reinforcing steel in the deck and substructure but occasionally due to structural failure of the deck. Identifying the causes of bridge deck cracking and providing prevention methods can be complex and challenging, but it is very important for maintaining longevity of the bridge deck. The complexity of transverse bridge deck cracking is created by many variables associated with time dependent interactions of the cement hydration chemical reaction, differential volumetric movement of the deck concrete, associated interactions with girders, internal reinforcing steel, end restraint, and the environment. In addition, deck designs and construction practices can further contribute and add to the complexity to the manifestation of transverse bridge deck cracking.

In its most basic form, the primary driving cause of transverse bridge deck cracking is the restraint of volumetric movement. Material degradation mechanisms can cause cracking, but these typically occur at later ages and do not cause transverse deck cracking. There are many contributing factors to the volume change of the concrete and associated restraint needed for bridge decks to crack; however, the most common contributing factors are identified below:

- **Autogenous Shrinkage** - Autogenous shrinkage is a reduction in concrete volume due to the consumption of water from the capillary pores during cement hydration. Autogenous shrinkage manifests itself at very early ages while the concrete is still developing strength, so relatively small autogenous deformations may generate relatively large tensile stresses compared to the material's tensile strength. Typically, for notable autogenous shrinkage to occur, the concrete must have a water to cementitious ratio (w/cm) less than about 0.40 [7]. High-performance concrete (HPC) mixtures with w/cm of 0.40 or less and mixes containing fine mineral admixtures, such as silica fume, are especially susceptible. As HPC has become more common in the construction of bridge decks, autogenous shrinkage and its related cracking have become a greater concern for state DOTs.
- **Temperature Changes** - Thermal-induced movements (strains) occur in bridge deck concrete as a consequence of cement hydration, daily fluctuations in ambient temperatures and solar radiation. Because the process of cement hydration is exothermic, the temperature of the concrete initially increases while the concrete is still in a plastic state. After setting, the concrete temperature continues to rise until it reaches a peak, typically within the first day or two of placement. As the concrete cools from its peak hydration temperature, it will begin to shrink, generating non-linear temperature gradients and thermal stresses while the concrete's tensile strength is still not fully developed.

Cracking during this stage may be very narrow and difficult to see, but these very fine, early-age cracks provide a weakened plane that can widen and extend due to diurnal temperature changes and additional drying. The early implementation of HPC mixes included high paste contents which generate more heat of hydration and worsen the cooling effects. One other cause for the increase in the incidence of deck cracking in the last 25 years is the gradual changes in portland cement chemistry and fineness that result in faster setting and compressive strength gain but also higher heat of hydration. Cement producers claim that it is not cost competitive to provide a coarser, low heat (Type IV) cement due to the lack of demand and existing silo storage procedures. Therefore, engineers are limited to exploring options to mitigate the effects of the currently available cement types.

The daily fluctuations in ambient temperature also contribute to volumetric movement and development of stresses in bridge decks and can be additive to the hydration effects at early ages. Daily ambient fluctuations not only cause global expansion and contraction of the bridge superstructure but can also cause thermal gradients through the concrete deck which creates stresses in the bridge deck. Furthermore, tensile stresses can be caused by the concrete deck wanting to contract or expand more than the supporting girders due to the lag effect of the ambient temperature changes have on the deck versus the girders and further exacerbated by differences in the coefficient of thermal expansion of the girders (steel girders), a key factor.

- **Drying Shrinkage and Differential Drying -** Drying shrinkage is a natural process as the concrete loses moisture to the environment. The loss of moisture in concrete is a two-phase process. The first phase consists of loss of free water due to bleeding, which causes little volumetric movement. Inadequate bleeding and high evaporation rates can result in random surface cracks in the plastic concrete that are different than the typical transverse cracking being studied. The second phase consists of loss of adsorbed water from the concrete, which results in volume change essentially equal to the volume of water lost. Drying will continue until the available moisture inside the concrete reaches equilibrium with the surroundings. When considering drying shrinkage of bridge decks, not only does the bulk volume change have to be considered, but also the volume change caused by differential drying. Typically, the exposed surfaces of a bridge deck will dry faster than the center, creating a differential drying gradient through the concrete's thickness. Furthermore, changes in the daily ambient relative humidity will exacerbate this condition, another key factor. With daily fluctuations in relative humidity, the exposed surface will contract or expand more than the central region, creating steeper moisture gradients through the deck thickness. The stresses developed in bridge decks resulting from differential drying and changes in ambient relative humidity can be very large.
- **Restraint Conditions** - The potential for cracking in bridge decks is directly affected by the amount of restraint of the concrete. This restraint comes in many forms. For bridge decks, the primary source of restraint are composite girders, through stirrups protruding from prestressed concrete girders or shear connectors attached to steel girders, and the reinforcing steel which restrains bulk volumetric changes in the deck. Because such restraint conditions are largely unavoidable, commonly employed crack mitigation methods tend to focus on reducing the effects of volume change mechanisms of the concrete not the superstructure restraint.

In June 2016, MDT noted severe cracking on two bridge decks in the Missoula District along Interstate 90. Both bridges exhibited closely spaced transverse cracking through the full thickness of the deck, which led

to holes in the deck after small sections of the concrete deck fell through. The decks for these bridges were relatively new, having been replaced in 2010 and 2011. Further review of additional bridge decks in western Montana by MDT staff revealed widespread transverse cracking in more than 20 additional bridge decks constructed within the previous 10 years.

MDT commissioned WJE in 2016 to investigate the cause(s) of the transverse cracking and provide recommendations on mitigation. WJE's 2016 investigation consisted of a document review, field investigations, laboratory evaluations, and simple analytical modeling of the bridge decks. As reported by WJE on April 21, 2017, the most prominent cracking feature observed during WJE's field investigation were closely spaced transverse cracks, which subsequent laboratory testing and analytical studies indicated that they initiated at very early ages primarily due to thermal changes within the bridge deck; additional stresses generated by drying and autogenous shrinkage likely further contributed to crack-generating stresses, crack growth and extension in-line with deck reinforcing bars, and eventual deck failure. WJE provided recommendations to revise concrete mix design, construction practices, and design considerations employed by MDT with the intent of reducing early age transverse cracking.

Since implementation of the recommendations, MDT personnel reported a notable decrease in early-age transverse cracking due to these changes, but MDT then observed later age development of transverse cracks in some of their bridge decks resulting in similar, sometimes severe, cracking. Therefore, WJE was commissioned to perform additional investigations to further assess the benefits of the previous recommendations and to take a focused look at the later age development of transverse cracking. WJE implemented a multi-disciplinary approach including literature review, field inspections, bridge instrumentation, laboratory evaluations, and finite element modeling as briefly described below:

- A literature review was performed incorporating most recent research on transverse bridge deck cracking with a focus on other DOT's research. The literature review was focused on cause(s) and mitigation techniques used for transverse bridge deck cracking.
- Detailed inspections were performed of recently constructed bridge decks (with implementation of WJE's previous recommendations) to quantify the type, amount, and extent of transverse cracking on the decks, and analyze the data for any trends in the cracking severity. As part of this task, WJE reviewed available documentation from these recent bridge deck construction projects to review which recommendations were implemented, construction practices, concrete mix designs, concrete temperature monitoring records, weather data, quality control results, and design drawings.
- Instrumentation of one bridge deck was performed to monitor internal concrete temperatures, relative humidity, and strains. Ambient conditions were also monitored including temperature, relative humidity, wind speed, and solar radiation. The goal of the instrumentation was to better understand the impact of environmental changes on the internal deck temperatures, relative humidity, and strains. The data collected from the instrumentation was also used to validate finite element modeling. The Rarus/Silver Bow Creek Structure, Bridge D, located in Butte, Montana was selected for this monitoring, and data collection is still ongoing.
- Laboratory evaluations of the concrete mix design used for the construction of the Rarus/Silver Bow Creek Structure, Bridge D, were performed to measure the physical properties of this mix, especially at early ages, and to accurately model physical characteristics in the finite element modeling.

- Nonlinear finite element (FE) simulations were conducted to help gain further insight into the effect of environmental factors and material properties on concrete deck stresses that lead to transverse deck cracking and to further refine previous WJE crack-mitigation recommendations. To investigate the deck performance, a three-dimensional (3D) finite element model of Rarus/Silver Bow Creek, Bridge D, was constructed and analyzed in the general-purpose FE program Abaqus v2020. The finite element modeling effort was divided into two broad categories: (1) those related to the early-age concrete deck (short-term) performance and (2) those corresponding to aged concrete typically after 90 days of placement (long-term). The objective of the FE modeling was to identify the factors that have the greatest impact on the maximum tensile stresses within the concrete deck at early or later ages that pose the greatest risk to cause transverse cracking.

ITEM 2 - SUMMARY OF RESEARCH AND RELEVANT FINDINGS

A summary of the research including relevant findings are presented in the following paragraphs, with details of the research included in Item 4.1 through Item 4.5b. The relevant findings are presented as important findings to the development of transverse cracking in Montana bridge decks. The details of the analyses and supporting documentation for these findings are presented in the specific section.

Bridge Deck Cracking Inspections (Item 4.4a)

Field inspection trips were performed on two different occasions to document cracking conditions of Montana bridge decks, as detailed in Item 4.4a (page 28). In December of 2019, the first inspection was performed on a total of nine bridge decks with the goal to document crack characteristics of bridge decks installed with WJE's previous curing recommendations and to help identify any trends of the cracking density relative to deck placement time (month), ambient and concrete temperatures, deck thickness, mix designs, bridge bearing type, span length, span bearing type, placement location, and placement length. The second site visit was performed in the Summer of 2020 and included 14 bridge decks with the intent to document any progression of the cracks noted during the first site visit with additional bridges added that might supplement the first field trip. As part of this task, WJE reviewed available documents for each inspected bridge related to the construction practices, mix designs, concrete curing temperatures, design drawings, weather data, and quality control records.

A list of inspected bridges is presented in Item 4.4a (page 28) showing location, time of deck placement and inspection, and key characteristics of the structure. Although the quantity of bridge decks inspected and detailed for cracking characteristics are not statistically sufficient, some potential trends were observed in the cracking severity of the inspected bridge decks:

- Cracking appears to be less severe in decks with greater deck thicknesses, consistent with WJE's literature review, previous investigation findings, and finite element modeling (See Item 4.5b, page 122).
- The placement of concrete during the winter months, actively heated from the top, is likely a contributing factor to transverse cracking severity, (further discussed in the modeling section, Item 4.5b, page 122). It is likely the concrete temperature gradients through the deck thickness due to uneven heating during curing and the temperature differentials between the deck and the girders results in early-age transverse cracks, with those cracks further propagating and widening with subsequent thermal and moisture changes. These curing conditions were performed on Russel Street

Phase I (potentially Phase II as well), as this bridge had some of the most severe cracking density, with closely spaced transverse cracking. Alternatively, Rarus/Silver Bow Creek Structure, Bridge D, was cast in the winter but heated from the bottom, including the steel girders, and exhibited very little transverse deck cracking (further discussed in the modeling section, Item 4.5b, page 122).

- Differences in cracking condition between spans and placements within the same bridge were observed; however, the trends were not consistent on every bridge deck. At some bridges, placements over piers have more severe cracking than those near mid-spans while at other bridges the trend was reversed or there was no trend between the two groups of placements.
- The following factors did not yield any consistent trends in the development of transverse cracking severity: bridge bearing type, span length, span bearing type, placement location, and placement length.
- Cracking conditions in 2019 and 2020 were generally similar at most of the bridges without significant progression of the cracking. At several bridges, a polymer concrete overlay was placed between the two inspections, which prevented observations of the original deck topside in the 2020 inspection and altered the exposure condition of the decks. No reflective cracking was noted in the overlays at the time of inspection.
- GPR surveys at transverse crack locations on the topside of the bridge decks indicate that the transverse cracks were generally in line with the transverse (topmost) deck reinforcement.
- Based on observations from both the deck topside and underside, it appears that the majority of transverse cracks are through the deck thickness.

Field Instrumentation and Monitoring (Item 4.4b)

To achieve a better understanding of the internal concrete temperature, relative humidity, and associated strains in Montana bridge decks, WJE instrumented a new bridge deck prior to concrete placement with thermocouples, relative humidity probes, and strain gages. The details of the instrumentation plan and collected data are presented in Item 4.4b (page 105) and summarized in the following paragraphs.

The Rarus/Silver Bow Creek Structure, Bridge D, was selected for the instrumentation based on schedule of the research plan and location relative to previously observed decks with transverse cracking issues. This bridge is located on southbound I-90 and spans over the Silver Bow Creek in Butte, Montana. This bridge is a four-span bridge (134, 165, 165, and 134 feet) spanning a total of 598 feet with the bridge deck being approximately 40 feet wide and supported by five steel plate girders spaced approximately 8 feet, 6 inches on center. The concrete deck thickness is 7.75 inches and is reinforced with stainless steel reinforcement. Concrete placement No. 7 was selected for the instrumentation and is located over a pier.

During the week of November 25 and December 1, 2019, WJE instrumented four locations (1-4) within the concrete on Placement No. 7 with locations being at the beginning and end of the concrete placement including interior, edge, and perimeter conditions. At each location, WJE embedded five thermocouples and three relative humidity probes at varying depths of the deck to obtain the temperature and relative humidity profiles. WJE also embedded three vibrating wire strain gages (VWSGs) at each location; one near the top and bottom surfaces and one at mid-depth. Field instrumentation also included ambient temperature, relative humidity, wind speed, and solar radiation measurements; all of which were powered

by a solar panel and battery system. Concrete was placed on December 5, 2019 utilizing winter curing methods (immediate application of wetted blankets, plastic sheeting, insultation blankets and heated from below). After concrete placement, data from each gage was collected every 5 minutes with accessing and downloading of the data performed via wireless modem with cloud-based storage.

At the date of this report, all installed gages are still being recorded every 5 minutes, and the instrumentation has been in-place for a period of 18 months. The data collected from the field instrumentation was used to provide a better understanding of the effect of environmental conditions on the temperature and relative humidity profiles and associated strains. The data was also used to validate finite element modeling (FEM) efforts (See Item 4.5b, page 105). The following relevant findings were observed in the collected data:

1. None of the 12 installed strain gages showed any indication of cracking (sudden change in strain). This is consistent with the field inspection performed by WJE that showed minimal transverse cracking (or any cracking) on the underside of this deck with no cracking observed to be near any of the installed gages. MDT reported to WJE on multiple occasions that no observed transverse cracking was apparent in the first couple months after construction.
2. No tensile strains developed in the deck concrete during the winter heating from below and wet-curing methods (first 11 days). Compressive strains developed in the deck immediately after removal of the winter curing procedures (insulation and underside heating), and the steel girders cooled. For this bridge, this early age compression likely provided benefits to negate net tensile stresses in the deck that can occur during the summer. Over the summer months, the compressive strains dissipated with the warmer temperatures and drying of the deck concrete, but with the top of the deck eventually developing only small tensile strains.
3. Large daily ambient temperature changes were observed with associated temperature gradients within the deck, with changes being most pronounced during the summer and early fall months. For example, in early September of 2020, daily ambient temperature increases and decreases of 55 to 60°F (30 to 33°C) were observed, see Figure 1. In this chart, the internal deck temperatures are graphed (as measured at five depths through the concrete deck at location No. 4, with 4-5 being at the top of the deck, 4-1 being at the bottom of the deck, and (4-4 and 4-3 are middle of the deck). These large ambient temperature changes create temperature gradients within the concrete deck, primarily during heating. This time period is an example of one of the extreme recorded events; however, daily ambient temperature variations during the summer and fall months are commonly 35 to 45°F (19 to 25°C). The implications of these large ambient temperature variations are further discussed and analyzed in the finite element modeling section and have an impact on alpine bridges in Montana.

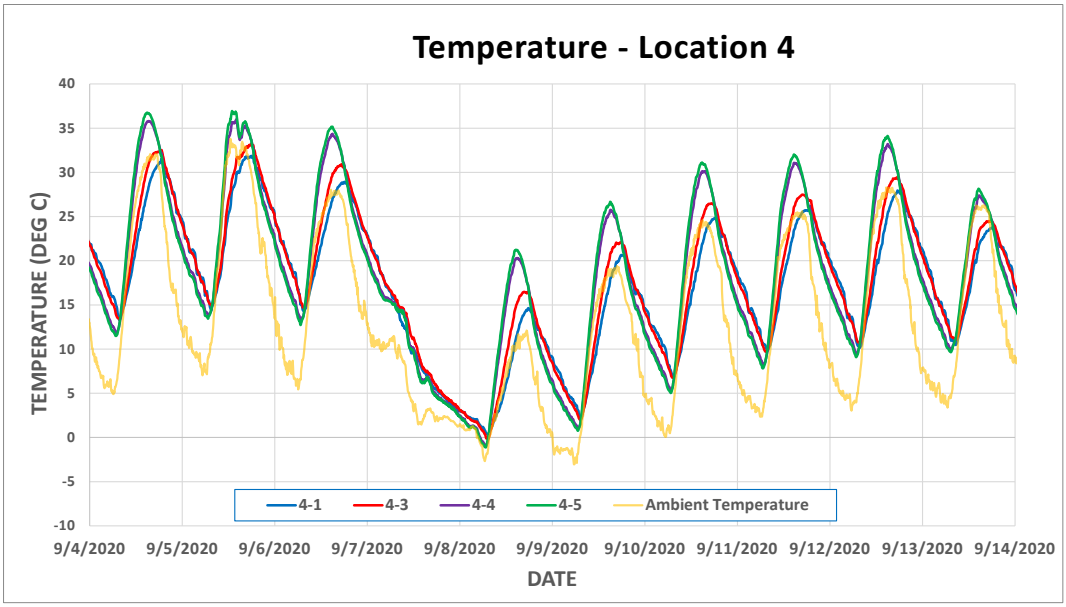

Figure 1. Ambient and internal deck concrete temperatures measured at Location No. 4, early September of 2020.

4. Large daily ambient relative humidity changes were observed, particularly in the spring and summer months, with associated large relative humidity changes and gradients within the deck concrete. For example, in early June 2020 (See Figure 2), the ambient relative humidity increased from approximately 20 to 100 percent within a 24 hour period, during a reported rain event. In this graph, the internal concrete deck relative humidity measurements are plotted at location No. 4. The measurement 4-3 represents the internal concrete relative humidity near the top of the deck; 4-2 mid-depth; and 4-1 near the bottom of the deck. This rain event created a relative humidity gradient, from top surface to bottom surface of the deck concrete, of approximately 25 to 30 percent. Prior to this rain event, the ambient relative humidity was generally low, and the concrete surface relative humidity dropped below the mid-depth relative humidity, and an approximate 5 to 10 percent relative humidity gradient was measured between the top and bottom of the deck. After the rain event, the surface of the deck went to 100 percent relative humidity and the bottom increased to 70 to 75 percent relative humidity.

   This particular rain event was one of the more extreme examples of ambient relative humidity changes observed in the data; but daily ambient relative humidity changes of 40 to 50 percent during the spring and summer months were common. The implications of these high daily relative humidity changes are further analyzed in Item 4.5b (page 122) and are of significant importance for alpine bridges in Montana.

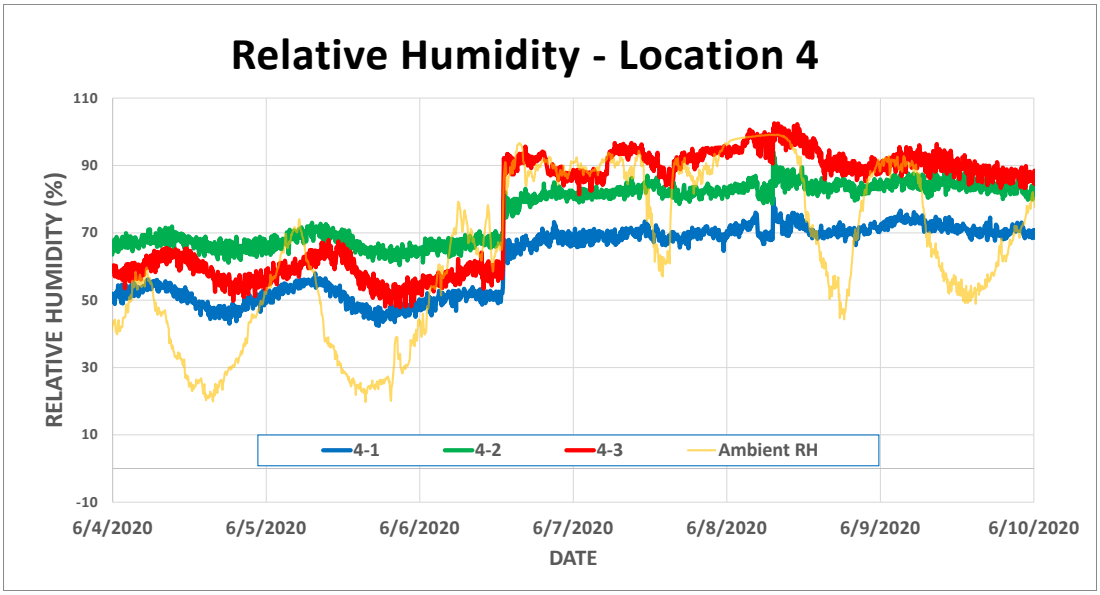

Figure 2. Graph shows the ambient and internal concrete relative humidity measurements at Location 4 during early June .RH probe 4-1 represents the bottom side of the deck and probe 4-3 represents the top side of the deck, with 4-2 in the middle.

Laboratory Evaluations (Item 4.5a)

Laboratory evaluations were performed on mix identification "MDT 1.5 DECK2", which was used for the concrete placements of Bridge D of the Rarus/Silver Bow Creek Structures (instrumented bridge deck). The primary goal of the laboratory evaluations was to measure physical properties of the concrete in order to accurately model stresses and strains in the bridge deck and to assess physical properties of the mix related to the potential development of cracking. Physical testing included compressive strength, splitting tensile strength, modulus of elasticity (MoE), drying shrinkage, creep, and coefficient of thermal expansion (CTE).

The compressive strength testing performed by WJE was consistent with the 4,000 psi design strength and consistent with the submitted mix design performance. With respect to the compressive strength, the modulus of elasticity (MoE) development at early ages was slightly higher than expected with the splitting tensile strength development slightly lower than expected based on industry standard relationships [8]. At later ages, the MoE and splitting tensile strength were measured to be more consistent with respect to the compressive strength.

A surprising and significant reduction in unrestrained drying shrinkage (and ultimate shrinkage) was noted when the wet-curing was increased from 5 to 14 days, with an approximate 25 percent reduction. The drying shrinkage (and ultimate shrinkage) can have a significant impact on the stresses that may develop in the bridge deck and potential for transverse deck cracking (further discussed and analyzed in Item 4.5b, page 122).

As anticipated, the creep characteristics of the concrete are much greater when loaded at earlier ages compared to later ages. For comparison, the creep at 90 days of loading is reduced by approximately 35 percent when increasing the wet-cure (i.e. age of loading) from 5 to 28 days. This means that an elastic

strain applied at an earlier age will result in greater creep than when that same strain is applied at a later age. Since creep dissipates stresses in concrete, early-age creep may potentially be beneficial in reducing tensile stresses in the concrete deck. When assessing the significance of creep and age of loading on the potential for cracking, the early age benefits of creep have to be evaluated relative to the volume changes, MoE, and tensile strength of the concrete. All of these variables effect the cracking potential of the concrete deck, and all change with time. The volume change due to drying applied to early age concrete (shorter curing period) may be larger than if applied at later ages (longer curing period); therefore, potentially negating some of the benefits of early age creep. The MoE increases with time, so for any given strain applied at early ages a lower associated stress will result than if applied at later ages. However, the concrete deck will also gain tensile strength over time, so larger stresses can be resisted by the concrete prior to cracking. Therefore, the interaction between these variables is quite complex and should be assessed uniquely with each mix design and curing conditions for transverse cracking potential.

The CTE of the concrete was slightly lower than anticipated and did not change significantly from 5 to 28 days of testing. The measured concrete CTE (4.14×10^{-6} in/in/°F) is less than the CTE of the supporting steel girders (5.76×10^{-6} in/in/°F), as utilized in the finite element modeling (Item 4.5b, page 122).

Finite Elemental Modeling (Item 4.5b)

Nonlinear FE simulations were performed to investigate the stresses developed due to environmental actions on the concrete bridge deck on steel girders. A 3D finite element model of the Rarus/Silver Bow Creek, Bridge D, was constructed and analyzed in Abaqus v2020. The FE model included the full-length deck geometry, girders, and lateral braces. The modeling was divided into short term modeling (first 14 days after placement) and long-term (greater than 90 days after placement). Effects of nonuniform temperature, moisture gradients and drying shrinkage on tensile stress development were investigated in the long-term modeling. Cross-sectional temperature histories were identified for diurnal summer and winter temperatures focusing on rigorous ambient temperature drops and rises. The nonuniform moisture gradient effect was investigated considering severe relative humidity gains and losses before and after a rain event, as measured and recorded during field monitoring of the Bridge D. Early-age stress analyses were conducted aiming to compare the early-age deck performance subjected to different curing methods and placement times. For late-age FE simulations, temperature histories, changing mechanical properties with age, and creep effects were included. Additionally, analyses were carried out for the sensitivity of the tensile stress in the concrete deck to variations in the degree of restraint and deck thickness.

Based on the FE analyses performed, the following conclusions are drawn:

1. Stresses in concrete deck due to restrained thermal, moisture and shrinkage are nonlinear across the depth of deck.
2. In the morning and afternoon hours, the temperature gradient is generally higher. The largest cross-sectional temperature gradient is observed when the top surface of the deck is warmest. At this time, due to the effect of solar radiation, the top of the deck is always warmer than the ambient temperature.

3. At the warmest time of a summer day, there can exist a nonlinear temperature gradient of 50°F (27˚C) between the top and bottom of the concrete deck. Such a thermal gradient can create tensile stress of 200 psi in magnitude near the top surface of the deck.
4. The analysis of stresses due to large ambient temperature swings show that with an ambient temperature change of 55°F (30°C) (the maximum daily ambient temperature change recorded with the field instrumentation), an increase in tensile stress amplitude (increase in tensile stress) of 400 psi can develop at the top surface. The largest net tensile stress; however, was predicted to happen at the bottom of the deck. The net tensile stress magnitude due to ambient 55°F (30°C) was predicted to be 250 to 300 psi (net tensile stresses decrease due to thermal compressive stresses applied at early ages).
5. The development of tensile stresses in the deck due to bridge warming or compressive stresses due to bridge cooling is mainly attributed to the difference between the coefficient of thermal expansion of steel girders and concrete deck. In the composite deck system, steel girders have higher stiffness and thermal expansion coefficient that are prone to more expansion and contraction resulting in deck tensile and compressive stresses, respectively.
6. The FE simulation showed that the tensile stresses developed due to restraint to normal drying shrinkage of the concrete deck alone can be as high as 300 psi. Shrinkage stress simulation was conducted for up to 150 days after concrete placement. The FE simulation results signify the long-term importance of the drying shrinkage effect, especially when combined with diurnal temperature and relative humidity changes that can result in elevated tensile stresses and increased cracking risk of the concrete deck.
7. The stress analysis of nonuniform moisture gradient suggested that there can exist a significant relative humidity gradient throughout the deck after a rain event that can lead to higher relative humidity at the top surface causing elevated tensile stresses at the bottom of the deck. Due to the moisture gradient alone, tensile stresses as high as 250 to 300 psi were predicted to develop at the lower depths of the concrete deck.
8. FE analysis of the combined moisture and temperature gradient showed that the effect of these two phenomena can be subtractive. It was shown that the higher tensile stresses at the centroid and bottom of the deck due to the moisture gradient were partially offset by compressive stresses that developed as a result of the bridge cooling down during the rain event. Further modeling of varying relative humidity and temperature variations, as measured in the field, would be needed to assess whether this phenomena is always subtractive.
9. The early-age simulation results for the summer placement showed that application of insulation after peak hydration temperature (WJE's previous recommendations) after placement can effectively keep the tensile stresses low when compared to the case with no insulation. Within the two cases considered for the summer placement, no significant tensile stresses were predicted after the removal of the insulation and curing measures.
10. In general, the early age stress analysis of the winter placement with heating enclosure from the bottom of the deck showed a better performance in terms of limiting the development of tensile stresses. Deck stresses due to the application of insulation from the top and heating from the bottom resulted in no tensile stresses in the concrete deck during curing. After removal of the insulation and

heat and exposure to the cold ambient temperature, concrete and girder temperatures sharply dropped which caused beneficial compressive stresses to develop within the concrete deck. These compressive stresses help reduce the tensile stresses due to subsequent drying shrinkage, relative humidity changes, and thermal movement and ultimately help reduce the likelihood of cracking.

11. On the contrary, in cold-weather placement, the application of a heating source only from the top increases the tensile stresses and risk of cracking. There exists a large temperature gradient from the top of the concrete deck compared to the steel girders that are left exposed to cold ambient temperatures. The thermal gradient through the deck and differential movement of the girders will cause the development of tensile stresses as high as 300 psi and increased top-surface cracking risk within the first 3 days after placement and upon removal of curing.

ITEM 3 - RECOMMENDATIONS

MDT has experienced severe cracking in new concrete decks cast on alpine bridges that has sometimes resulted in localized through-thickness loss of the deck concrete (holes in the deck). Cracking was typically noted within the first weeks or month after concrete placement. This very early age cracking is likely caused by temperature changes and gradients within the deck during cement hydration and diurnal temperature fluctuations of the deck and supporting girders. Concrete hydration, physical properties, and ambient conditions change rapidly with time during the initial curing periods making accurate modeling of deck stresses and cracking risk difficult. Therefore, a one-size-fits-all approach is not likely to be completely successful for all projects. This current research project has improved our understanding of the volumetric movement of the deck and superstructures at early- and late-ages; such that, general curing recommendations can be refined for different seasons of construction. Further research is needed to optimize curing recommendations based on actual deck designs, early- and late-age concrete properties, and anticipated construction and environmental conditions for a particular project.

In many parts of the United States avoiding deck cracking within the first several months bodes well for the long-term durability and crack resistance of a new bridge deck. However, findings of this current study suggest that diurnal and seasonal changes in ambient temperature and humidity in the alpine regions of Montana may provide sufficient strain within decks to cause transverse cracking at later ages. Typical bridge superstructure designs include moderately thin reinforced concrete decks supported on composite steel girders. For the instrumented bridge, the concrete had a lower thermal coefficient of expansion compared to the steel girders, so the girders compress the deck during cooling events and expand or stretch the deck during heating events. Essentially the thin concrete deck is "along for the ride" as the deep steel girders respond to temperature changes. Thinking of the superstructure in these terms allows for a better understanding of basic deck movements and for considering innovative solutions to reduce deck cracking.

This study also identified a characteristic of the alpine environment not previously recognized as a potential potent cause of deck cracking and that is large diurnal variations in ambient relative humidity. WJE's previous belief was that concrete tends to rapidly absorb and hold water (e.g. similar to a dry, hard sponge) but that drying is a slow process and that diurnal changes in humidity would have only superficial effect on concrete deck shrinkage and stress. Instrumentation of Bridge D indicated significant and rapid changes of the relative humidity within the concrete deck in response to the significant natural diurnal ambient humidity changes, similar and comparable to the large temperature variation effects. This finding

may be important nationally but is especially significant to alpine decks in Montana, since daily fluctuations in humidity (and temperature) are some of the highest in the nation (see Figure 3 and Figure 4).

Based on research performed by WJE [9], the large ambient relative humidity changes and potential for significant moisture gradients within the deck may be somewhat unique to certain areas of Montana. In Figure 3, the average daily ambient relative humidity swings by month is presented for Montana as compared to other US cities. This chart shows the average absolute daily change for each month (i.e., the absolute daily ambient relative humidity changes, whether positive or negative, are averaged over the month and plotted). Missoula shows the highest average daily ambient relative humidity change during March through October as compared to any other US city. Helena and Billings show similar high ambient relative humidity changes compared to other US cities but not to the extent as Missoula.

As previously researched and discussed by WJE in April 21, 2017, daily ambient temperature variations in Montana can regularly exceed 30°F (17°C) in summer months (Figure 4) with extremes reaching 55°F (30°C), giving rise to thermal gradients within placed bridge decks. These thermal gradients and associated stresses may be additive or subtractive to the stresses created by humidity gradients. In Figure 4, the average daily temperature changes per month is plotted for various cities in the US, including Missoula, Helena, and Billings. The ambient changes of parts of Montana are most extreme during the summer months. Other areas of the country, like Denver, have yearly fluctuations on average higher but do not reach these extremes.

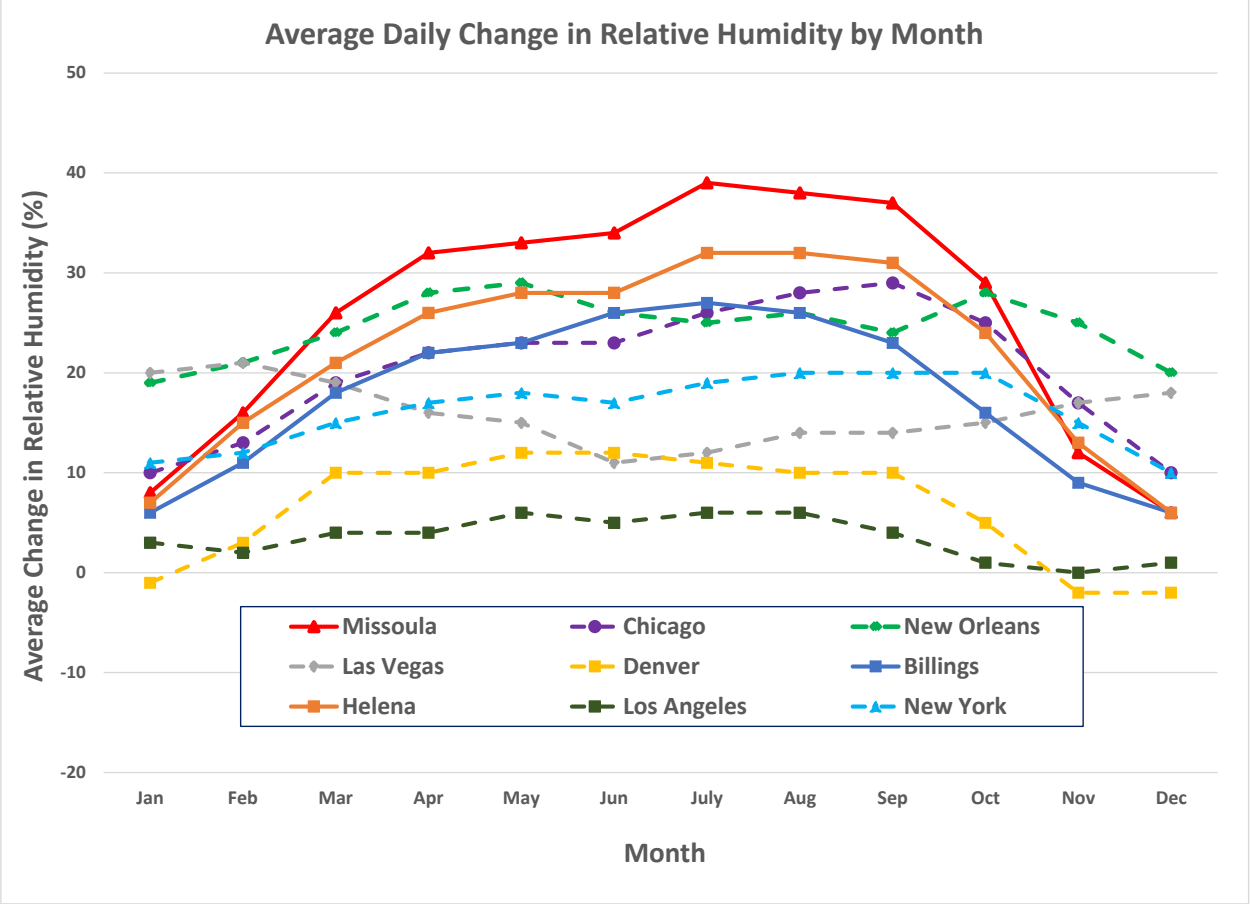

Figure 3. Average daily changes in ambient relative humidity by month for Missoula, Helena, and Billings compared to other cities in the US.

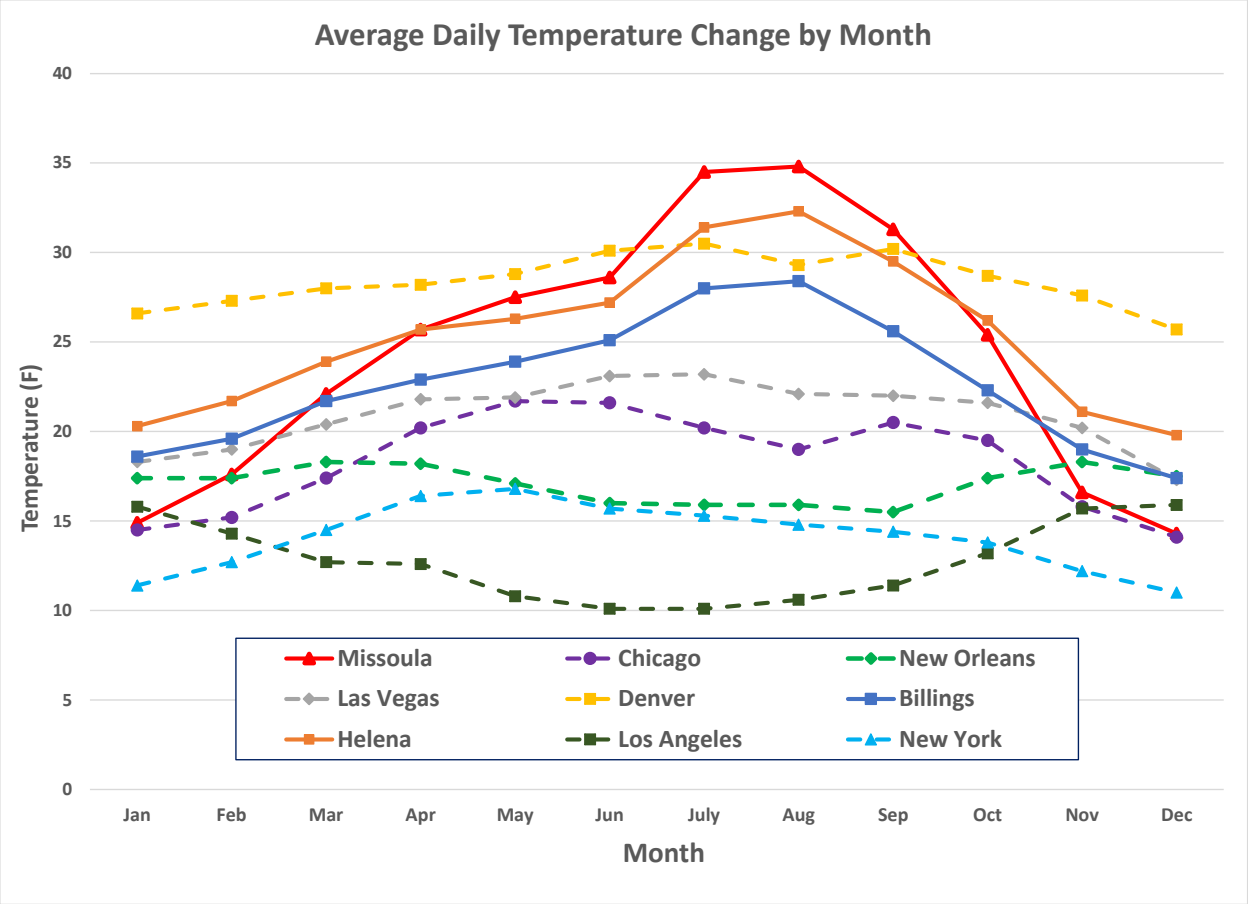

Figure 4. Average daily temperature changes by month for various cities in the US.

Based on the relevant findings, the following recommendations are provided to MDT for consideration of implementation on bridge decks to mitigate transverse bridge deck cracking. All of WJE's previous recommendations, as reported on April 20, 2017, are still recommended, with any modifications as noted in the following.

Concrete Mixture Proportions

The primary goal of the concrete mixture proportion recommendations is reducing the drying shrinkage and ultimate shrinkage of the concrete mix designs and associated strain development. In the FE modeling, it was found that the stress developed by drying shrinkage alone could potentially be half of the cracking potential of the concrete. With any mix recommendation, other factors have to be considered, such as maintaining a low permeable mix, cohesiveness, workability (ability to easily place and consolidate), and finishability (ability to easily finish and close-up the surface). The following are presented as mix recommendations:

1. Maintain total cementitious content below 600 pounds per cubic yard (lb/yd^3) and ideally below 550 lb/yd^3 with water to cementitious ratios (w/cm) between 0.40 to 0.45. Drying shrinkage occurs because of the loss of moisture from the cement paste in the concrete; therefore, limiting the paste content

helps keep the total moisture loss low and reduces drying shrinkage. Furthermore, the limits on w/cm ensure a low permeable concrete (resistance to chloride ingress) while limiting the amount of free evaporable moisture in the paste. The recommended w/cm range essentially eliminates the effect of autogenous shrinkage on volume change and is important to mitigate early age shrinkage during curing. With the reduction in paste volume and associated reduction in yield of the concrete mix, the recommended practice is to replace the paste with equivalent volume of coarse aggregate. These recommendations are consistent with other researchers [3, 6, 10].

2. Limit silica fume to a 5 percent maximum replacement rate. This has been previously recommended by WJE in 2017 but is still important based on this current research. The use of silica fume provides a very dense, low permeability paste in the concrete; however, it comes with additional risks of increased early age shrinkage and finishing and curing issues. For these reasons, the use of silica fume should be limited to 5 percent. For one of the investigated bridges, West Laurel Interchange, Phase I, the concrete contained 9 percent silica fume replacement for cement. This was likely a contributing factor to the observed map cracking, transverse cracking, and scaling (which was likely due to difficulty in finishing).
3. The use of supplementary cementitious materials (SCMs) is recommended, with fly ash and slag cement being the preferrable SCMs. The goal of this recommendation has three benefits: lower concrete permeability, lower heat generation, and lower modulus of elasticity development at early ages. The recommended replacement rates for fly ash is 15 to 30 percent and for slag cement is 25 to 40 percent, and a maximum of 50 percent in combination. The optimization of this recommendation is further discussed as future MDT research. As part of this recommendation, consideration should be given to a design compressive strength at 56 days instead of 28 days, as this would encourage mix designs that develop strength slower (less heat) and lessen the early age modulus of elasticity. A 28-day strength could be still used for acceptability of the concrete but be less than the needed design strength.
4. Some states have had success using shrinkage reducing chemical admixtures (SRAs) in reducing deck cracking of high performance concrete (HPC) mixes [11, 12, 13]. SRAs operate by lowering the surface tension of pore water in the concrete. When concrete dries, tension from the evaporation is transferred to the concrete creating drying shrinkage. By lowering the surface tension, SRAs reduce this tension and associated internal concrete stresses, decreasing short- and long-term drying shrinkage [14]. There is also potential for these admixtures to provide benefit in the daily ambient relative humidity changes and associated moisture gradients within the concrete, as this surface tension may decrease the stresses associated with moisture changes. While these admixtures may have benefits, they do increase cost and require proper mix design and construction considerations. Further research into SRAs additives may be of interest, as discussed in the recommendation for future research.
5. Optimized aggregate gradations are recommended to ensure that the mixes maintain cohesiveness, workability, and constructability with the recommended paste reductions. With a decrease in paste content (as recommended above), optimization of the aggregate gradation may be needed to maintain a mix that consolidates and finishes well. Optimization programs include the Tarantula Curve developed by Oklahoma State [15]. Optimized concrete mixes can be evaluated for cracking tendency and tensile strength development as discussed in recommended research below.

6. The use of internal concrete curing via lightweight aggregates (LWAs), as a replacement of a percentage of the fine aggregate, should be considered for use in mix designs. LWAs have been used in bridge deck construction as "Internal Curing" to reduce early- and late-age shrinkage and improve cracking resistance [16]. DOTs have had success with reduction in cracking of bridge decks [12, 17]. Furthermore, some research suggests that an additional benefit is the reduction in stresses due to daily ambient temperature changes. [17, 18]. The use of LWAs for concrete in Montana bridge decks should be considered for additional research.

Design and Construction Practices

Strategies are needed to address deck stresses during both the curing period and at later ages. Deck tensile stresses that cause transverse cracking tend to be the highest during hot summer months. Consideration of the seasonal and diurnal exposure conditions are of primary importance to reduce the incidence of deck cracking of alpine bridges. Modifying curing practices to avoid incipient cracking is generally understood and workable but is in vain without consideration of the alpine exposure.

Based on the observed large ambient relative humidity changes and associated moisture gradients within the deck, reducing the moisture gradients within the deck is important. Methods or techniques to reduce the moisture fluctuations and gradients through the deck thickness should reduce the risk of deck cracking. The following options might be considered:

1. Bottom Side of Deck: The largest variations in humidity and resultant stress can occur along the bottom of the deck. Any options that seal the bottom surface of the deck and mitigate the moisture changes from the bottom of the deck should reduce cracking risk. These might include sealing of the bottom side with a barrier coating or using stay-in-place forms. Sealing options would include epoxies, urethanes, or other barrier type coatings. Penetrating, silane type, sealers are not likely to be effective, but may be worth evaluating due to their ease of application. The use of stay in-place (SIP) forms or form liners could be very effective, but corrugated forms or any forms that increase restraint should be investigated before implementation. Products such as polymer-laminated and fiber reinforced polymer (FRP) SIP forms have been used in bridge deck applications; Wisconsin DOT has performed research on the use of FRP for SIP forms [19].
2. Top Side of the Deck: Application of a thin-polymer concrete overlay on the top-side of the deck, preferably prior to the first mid-summer heat, may be beneficial to reduce the risk of cracking. Thin polymer overlays have a low moisture permeability to both moisture vapor and liquid transport, which will reduce the impact of the daily ambient relative humidity fluctuations and the rain events. The importance of sealing both top and bottom sides or only one side has not been investigated and would be interesting to study further to refine these recommendations and potential impacts on moisture gradient reduction and durability.
3. Modifying the superstructure design has the potential to reduce deck cracking; however, the practicality may vary. Thin concrete decks should be avoided. As with WJE's previous recommendations and previously cited research, a minimum deck thickness of 8 inches is recommended. With non-linear temperature and moisture gradients, thinner concrete decks will develop higher stresses. From the FE modeling, thermal stresses are larger in thin decks than thicker

decks, especially at early ages. A 1.75-inch increase in the thickness of the deck (e.g., from 6 inches to 7.75 inches) can reduce the magnitude of thermal stresses generated in the deck by 10 to 20 percent.

4. Any methods to reduce the difference in thermal movement potentials between the concrete deck and steel girders will reduce cracking risk as well, such as adding thermal insulation or using steel with lower thermal coefficient of expansion (and closer to the CTE of concrete). Precompressing the deck by heating the steel girders during concrete placement may be effective.

Summer Curing

Previous WJE recommendations of the application of insultation blankets immediately after peak concrete hydration is still recommended for summer concrete placements. Based on the finite element modeling performed by WJE, the installation of insultation at post peak hydration is effective in keeping early age tensile stresses low. WJE measured a surprising reduction in ultimate drying shrinkage of the concrete mix used for (Bridge D) Rarus/Silver Bow Creek bridge when the wet curing was extended from 5 days to 14 days. Research is somewhat conflicting with respect to length of wet-cure and reduction of drying shrinkage and cracking tendency [20, 21].

Based on WJE's laboratory testing of the concrete mix design used for Bridge D, a 25 percent reduction in drying shrinkage potential was measured when the wet curing time was extended from 5 to 14 days (as presented and discussed in the Laboratory Evaluations section). This mix also contained slag cement (ggbfs) and silica fume which likely influences the effectiveness of moist curing and ultimate drying shrinkage. For these mixtures, extending the wet curing period to 14 days is likely to be beneficial. The optimization of moisture cure duration and concrete mixture proportions for mitigating transverse cracking could be part of future research, as discussed in Recommendations for Future Research.

For reference, WJE's previous curing recommendations and modifications *(italic)* based on this current research are presented:

- Apply fogging (if needed) and wet curing as soon as possible after finishing procedures. Monitor concrete temperatures and apply insulation blankets only after the peak hydration temperatures are achieved. This requires concrete temperature monitoring during placement and while curing. Thermocouples should be installed at the beginning and end of each placement, at least 10 feet from any edge. Logging equipment should be able to record once every 15 minutes. Continue to monitor temperatures for the entire curing period. Within three hours after peak hydration temperatures are reached, apply insulating blankets. Do not remove top side insulation until concrete temperatures are within 5°F of ambient; and concrete is a minimum of 72 hours old (or 96 hours old if concrete contains silica fume), preferably in the evening hours. *If concrete mixture contains slag cement, fly ash, and/or silica fume, continue wet curing for 14 days*. Remove all curing and allow deck to dry. After the surface has dried, apply white-pigmented curing compound to slow the initial rate of drying and shrinkage and the white pigment will reduce peak diurnal temperatures of the deck surface.

Winter Curing

MDT's current winter curing procedures generally include placing pre-soaked wet burlap immediately behind the concrete finish operations, covering the wet burlap with plastic sheeting, and then covering with insulation blankets and maintaining until the design strength is met. Based on WJE's review of

provided curing documentation, the heating of the concrete decks has been achieved by two methods: 1) enclosing the underside of the deck and heating the girders and bottom side of the deck or 2) applying heating tubes between the plastic sheeting and the insulation.

Based on the modeling performed by WJE and the performance of the Russel Street Bridge, Phase I, heat from the top can lead to severe early age transverse cracking. From the internal concrete temperature data obtained from the Russel Street Bridge and from the modeling, a large temperature gradient is created from the top of the concrete deck to the steel girders that are left exposed to cold ambient temperatures. This will cause the development of high tensile stresses in the top of the deck. This is due not only from the thermal gradient through the deck thickness but also from the differential movement of the deck and the girders (girders respond to ambient temperature changes). There is significant risk of cracking if heat is applied only from the top during winter deck construction. Based on these research findings, the following is recommended:

- Heating from the bottom of the bridge deck is recommended as opposed to heating from the top as bottom side heating ultimately reduces tensile stresses in the deck while top side heating increases deck tensile stresses.
- At the end of the wet-curing period, it is also recommended that the heat and insulation be slowly removed instead of complete removal all at once, as performed on the Rarus/Silver Bow Creek, Bridge D. Even though this did not cause any cracking issues with Bridge D, under certain conditions this could lead to cracking. It is recommended that the insulation be kept in place until the concrete temperature is within 35°F (19°C) of the anticipated average daily temperature for the subsequent three days; the objective is to avoid a sudden drop in concrete temperatures that could cause cracking (thermal shock).

Recommendations on Future Research

The following topics are provided for consideration for future research:

1. Concrete mix and curing optimization using Montana aggregate and commonly available cements and cementitious material combinations. In addition, the use of SRAs and internal curing with LWAs could be included in this research. The goal is to determine optimized mixture proportions, including aggregate gradations, admixtures, and curing durations to reduce cracking tendencies of concrete mix designs. Based on the complex interaction between strength development, modulus of elasticity, creep, and drying shrinkage (as discussed in the Laboratory Evaluation section), a laboratory testing plan should include measurement of early-age mechanical properties, such as compressive strength, splitting tensile strength, and modulus of elasticity gain while measuring the drying shrinkage and cracking tendency after different wet-curing durations. Modeling of optimized mixes and curing would quantify the stresses developed by these mixes over time due to nonuniform moisture gradients for typical or specific bridge projects.
2. Evaluate options to reduce differential thermal movements of bridge superstructures by modeling. Examples included alternate steel compositions, increased thermal coefficient of the concrete, or girder insulation.
3. Evaluate options to reduce the effect of alpine humidity fluctuations on deck cracking by laboratory testing and modeling. Consider effects of sealing the top and bottom surfaces or installation of SIPS.

4. Research innovative means to add precompression into the deck. Heating the steel girders during concrete placement may be effective.

ITEM 4.1 - LITERATURE REVIEW

Transverse Cracking of Concrete Bridge Decks

Cracking of concrete bridge decks continues to be a common issue reported among state departments of transportation (DOTs) and other transportation agencies. In a survey of U.S. and international transportation agencies conducted as part of the NCHRP Report 380, "Transverse Cracking in Bridge Decks," WJE found that, on average, transverse cracks initiated within the first month in 53 percent of all bridge decks placed [22]. In the 30 years since the NCHRP report was first published, transverse cracking has remained a primary issue for new bridge decks.

In the last 25 years with the introduction of concrete mixtures with low water/cement ratios, including high performance concrete (HPC), in bridge decks to lower permeability and with the use of finer ground cements (to increase early age strength gain and construction schedule), the susceptibility of bridge deck cracking has increased, primarily due to the increased early-age volume changes and early age modulus (stiffness) development. For these reasons, an increase in cracking potential has been reported by numerous state agencies [1, 2, 3, 4, 5, 23]. Cracking commonly leads to a reduction in service life and increased maintenance costs, primarily due to accelerated corrosion of reinforcing steel in the deck and substructure but occasionally due to structural failure of the deck. Identifying the causes of bridge deck cracking and providing prevention methods can be complex and challenging, but is very important for maintaining longevity of the bridge deck. The complexity of transverse bridge deck cracking is created by many variables associated with time dependent interactions of the cement hydration chemical reaction, differential volumetric movement of the deck concrete, associated interactions with girders, internal reinforcing steel, and end restraint, and the environment conditions. In addition, deck designs and construction practices can further contribute and add to the complexity to the manifestation of transverse bridge deck cracking.

Transverse cracking is cracking that occurs along the transverse dimension of a concrete bridge deck, roughly perpendicular to its length. Transverse cracks are typically full-depth cracks and often span the entire width of the bridge deck. They most commonly occur directly over transverse reinforcing steel, are typically 10 to 20 mils (1 mil = 0.001 inch) in width and are often spaced between 5 and 10 feet.

Transverse cracks are predominantly caused by restraint of volumetric movement of the bridge deck concrete. Nationally, most bridge decks develop transverse cracks. While many bridge decks develop cracking at very early ages (within the first couple of days after placement), others develop much later, after exposure to traffic.

Causes of Transverse Cracking

The primary cause of transverse cracking is restrained volumetric movement. This volumetric movement can occur as the combined result of autogenous shrinkage, drying shrinkage, temperature changes, and differential drying of the concrete. All four of these volumetric influences can be additive and should be considered when assessing volume change and its effect on transverse cracking.

Autogenous Shrinkage

Autogenous shrinkage is a reduction in concrete volume caused by the consumption of water from the capillary porosity during cement hydration. This shrinkage is sometimes referred to as self-desiccation shrinkage because, as the available internal moisture is consumed by the hydration process, the pores dry out (self-desiccate), resulting in shrinkage of the cement paste. Because autogenous shrinkage is driven by cement hydration, it manifests at very early ages (often within the first 7 to 28 days) while the concrete is still developing strength, so even small autogenous deformations may generate large tensile stresses relative to the material's tensile strength. Typical autogenous shrinkage for concrete ranges between 40 and 100 microstrain of linear deformation [24].

Autogenous shrinkage increases for concrete mixtures with reduced w/cm's, higher replacement rates of slag cement and silica fume, rapid-setting cements, and high total cementitious materials contents. Although notable autogenous shrinkage will typically not occur unless the concrete has a w/cm less than about 0.40 [7], high-performance concrete (HPC) mixtures with w/cm's less than 0.35 and/or containing fine mineral admixtures, such as silica fume, are increasingly being used in bridge deck construction, making autogenous shrinkage and its related early-age cracking a greater concern. Autogenous shrinkage can be mitigated during the design phase by proper selection of cementitious materials and mixture proportions, or through the use of internal curing agents or shrinkage reducing admixtures.

Thermal Changes

Temperature changes in concrete occur as a consequence of cement hydration and daily fluctuations in ambient temperature. At early ages, temperature changes occur primarily due to cement hydration. Because the process of cement hydration is exothermic, the temperature of the concrete initially increases while the concrete is still in a plastic state. After setting, the concrete temperature continues to rise until it reaches a peak, typically within the first day or two of placement. As the concrete cools from its peak hydration temperature, it will begin to shrink, generating thermal stresses while the concrete's tensile strength is not fully developed. Cracking during this stage may be narrow and very difficult to see, but these fine early-age thermal cracks can widen and extend due to diurnal temperature changes and subsequent drying of the bridge deck.

The magnitude of stresses generated by temperature changes is a function of the degree of restraint in the deck (see below), the modulus of elasticity of the bridge deck, and most significantly, the coefficient of thermal expansion (CTE) of the concrete. The CTE is a property of a material that defines how much the material will expand or contract as its temperature changes. The CTE of concrete typically ranges between 5 to 7 microstrain per degree F (9 to 13 microstrain per degree C), with concrete mixtures containing calcareous (e.g., limestone) aggregates having CTE values on the lower end of the range and concrete mixtures containing siliceous and quartzite aggregates having CTE values on the upper end of the range [25]. Concrete with higher CTE values will exhibit greater deformation due to temperature changes and may therefore exhibit an increased likelihood of developing thermally-induced cracks at early ages.

In addition to early-age temperature changes arising from cement hydration, thermal stresses can also be generated across the thickness of the deck due to daily ambient temperature fluctuations. Daily fluctuations in ambient temperature force the top surface of the deck to cool or heat more rapidly than the interior, generating non-linear temperature gradients and associated stresses. Furthermore, tensile

stresses can be caused by the concrete deck contracting or expanding more than the supporting girders due to a lag effect of the ambient temperature changes have on the deck versus the girders and further exacerbated by differences in the coefficient of thermal expansion of the girders (steel girders), a key factor. Daily ambient temperature variations in Montana can regularly exceed 30°F (17°C) in summer months (Figure 4), with extremes reaching 55°F (30°C) degrees, potentially giving rise to large thermal gradients within placed bridge decks. In the figure below, the average daily temperature changes per month is plotted for various cities in the US, including Missoula, Helena, and Billings. The ambient changes of parts of Montana are most extreme during the summer months. Other areas of the country, like Denver, have yearly fluctuations on average higher but do not reach these extremes.

Drying Shrinkage

Drying shrinkage refers to the volumetric movement of concrete that occurs as it naturally loses moisture to the environment. The loss of moisture from concrete occurs in two phases. The first phase consists of loss of free water in plastic (fresh) concrete due to bleeding, which causes little volumetric movement. Inadequate bleeding and high evaporation rates can result in random surface cracks in the plastic concrete due to a localized form of drying shrinkage called plastic shrinkage.

The second phase of moisture loss consists of loss of adsorbed water from the hardened concrete, which results in a volume change that is essentially equal to the volume of water lost. This drying will continue until the internal relative humidity of the concrete reaches an equilibrium with its surroundings. The amount of drying shrinkage in concrete will vary depending on the concrete mixture proportions, the relative humidity of the exposure conditions, and the element geometry, but will typically range between 200 and 800 microstrain of linear deformation [26]. Factors that can contribute to an increase in drying shrinkage include a low aggregate content (or inversely, a high total cementitious materials content), a high total water content (high w/cm), low ambient relative humidity, short curing durations (less than 4 days), and element designs with high surface area-to-volume ratios, such as thin bridge decks [26].

Differential Drying

Related to drying shrinkage is differential drying across the bridge deck's cross-section. Typically, the exposed surfaces of a bridge deck will dry faster than the center, resulting in a differential drying gradient through the element's thickness. Due to this differential drying, the exposed surfaces of the deck may shrink more than the concrete at the interior, generating bending stresses across the top and/or bottom surface of the deck. Bridge decks can be particularly susceptible to rapid rates of drying and significant moisture gradients across their cross-section as a result of their usually large surface-area-to-volume ratios.

The stresses developed in bridge decks resulting from differential drying can be very large and can be additive to the stresses developed due to uniform drying shrinkage or other forms of volume change. Because relative humidity in Montana cycles over relatively wide ranges daily (see Figure 3), it is possible that large stresses may be developed due to steep gradients in relative humidity through the deck thickness. The average daily ambient humidity swings by month is presented for Montana as compared to other US cities. This chart shows the average absolute daily change for each month, i.e. the absolute daily ambient relative humidity changes, whether positive or negative, are averaged over the month and plotted. Missoula shows the highest average daily ambient relative humidity changes during March

through October as compared to any other US city. Helena and Billings show similar high ambient relative humidity changes compared to other US cities but not to the extent as Missoula.

Restraint

Volume change alone will not cause cracking of the bridge decks; rather, it is restrained volume change that increases the risk of cracking. Restraint in bridge decks can come in many forms. The primary source of *external* restraint in bridge decks is composite action with the girders at connection points, such as stirrups protruding from prestressed concrete girders or shear connectors attached to steel girders, while the primary sources of *internal* restraint are the reinforcing steel, which restrains bulk volumetric changes, and the concrete itself, which resists differential movement. The amount of restraint provided by these sources is related to the dimensions of the restrained element and to the relative stiffness of the restrained and restraining elements [25].

The stresses generated in concrete by restrained volumetric movement can be generally represented as Equation (1) [25]:

$$f = KE_c\Delta \quad (1)$$

where f is the stress, K is the degree of restraint, E_c is the modulus of elasticity of the concrete over the duration of the volumetric change, and Δ is the volumetric change generating the stress. Because volumetric movement often occurs over a period of time (rather than instantaneously), the modulus of elasticity E_c may be reduced from the static modulus of elasticity to a lower "effective" value based on creep [27].

Fatigue

Fatigue refers to the reduction in an element's mechanical strength over time due to cyclic loading. While fatigue is commonly considered as a limiting condition for the design of steel structures, it is not as frequently considered in the design of reinforced concrete structures. The primary result of fatigue in reinforced concrete structures is a progressive cracking and loss of reinforcing bond over time, with failure occurring due to either fracture of the reinforcing steel (which carries a greater load as the bond fails) or progressive cracking and spalling of the concrete [28]. Fatigue can also result in the opening of existing cracks from temperature, shrinkage, and other early-age sources.

Among reinforced concrete structures, bridge decks are one of the elements most vulnerable to fatigue [29]. However, because fatigue cracks often appear visually indistinguishable from cracking due to other causes, fatigue is not often cited as a primary cause of bridge deck failures [28], although it may be a contributing factor. The most significant cause of fatigue in reinforced concrete bridge decks is vehicle traffic; however, diurnal and seasonal cycles of temperature and relative humidity will also contribute. Yazdani [30] also found that cycles of freezing and thawing can contribute to fatigue damage in reinforced concrete elements. While vehicle traffic represents "high-cycle" fatigue, with typically several thousand cycles occurring per day; temperature, relative humidity, and freezing and thawing represent "low-cycle" fatigue, with typically no more than one cycle occurring per day. Because the strength of an element will gradually decline upon cyclic loading, the stresses due to temperature and humidity cycling will be additive to those caused by vehicle traffic [29]. Therefore, diurnal and seasonal changes in temperature

and relative humidity can contribute to progressive opening of cracks and reductions in the tensile and compressive strength of the concrete over time.

State DOT Experience with Cracking in Bridge Decks

Cracking in bridge decks continues to be one of the most common issues encountered on new concrete bridge decks. Consequently, several states have sponsored research projects focused on understanding causes of cracking and providing recommendations to mitigate these challenges. Commonly employed crack mitigation methods tend to focus on reducing the effects of volume change mechanisms in the concrete, changing the deck restraint conditions, and modifying construction practices to reduce the potential for cracking to occur.

A selection of relevant studies performed by other state DOTs is presented in the following section. Montana's experience with bridge deck cracking is summarized at the end of this section, along with a summary of recommendations from the various studies discussed.

Colorado

In a study of more than 70 bridge decks constructed in Colorado between 1993 and 2002, Xi et al. [31] found that 82 percent of newly-constructed bridge decks in Colorado exhibited cracking problems. The causes of cracking related to material, design, construction, and environmental factors were examined, with the most common cause of cracking identified to be early-age shrinkage of the concrete, combined with various design parameters that contribute to areas of negative bending moments above the girders and piers. The primary cause of early-age shrinkage addressed by the study was plastic shrinkage cracking, which is related to environmental conditions during and immediately after placement. Recommendations included using Type I or Type II cements with up to 25 percent Class F fly ash, by weight of cementitious material to control heat of hydration; limiting cement content to less than 470 pounds per cubic yard if possible; limiting rate of strength gain to reduce the tendency for early-age cracking; limiting the chloride ion penetrability of the concrete (likely a surrogate for limiting the water content), as well as performing drying shrinkage and crack resistance testing for acceptance; reducing longitudinal end restraint wherever possible; using concrete girders where possible to better match the coefficient of thermal expansion of the deck concrete; limiting deck thickness to no less than 8.5 inches; and placing concrete in a manner that minimizes surface evaporation and large temperature changes.

Idaho

To address an increase in cracking observed by the Idaho Department of Transportation (IDT) in concrete bridge decks, researchers from the University of Idaho instrumented two bridge decks to identify potential causes of cracking [32]. The decks were placed in November 2003 and subject to cold-weather concreting practices shortly after placement (heated enclosure and insulating blankets). Cracking occurred within the first month after placement in both decks and was attributed to restraint from the deck by the girders, integral abutment, parapet wall, and the bridge deck skew. Tensile stresses were reportedly developed in the deck due to the high heat of hydration of the concrete mixture (high cement content) and compounded by low creep and high modulus of elasticity of the concrete.

Iowa

Deng et al. [33] analyzed cracking on 22 bridge decks in Iowa, and summarized the factors that contributed to their cracking. Cracks were mostly perpendicular to girders irrespective of skew were observed to be present in both steel girder bridges and prestressed concrete girder bridges, and were most commonly found near piers and spaced 3 to 8 feet apart. Leaching observed on the underside of the decks was found to be an indicator that the crack had reached full-depth. Factors that were observed to contribute to crack severity included the cement type, content, and mixture proportions; aggregate contents and type; air content; admixtures; slump (water content); concrete strength; span type; girder type; end restraint; top transverse bars; girder depth/spacing; cross-frame location; expansion joints; reinforcement mesh; concrete cover; ambient conditions; vibration; finishing; curing; placement time; wind speed; construction sequence. The impact of each of these factors on early-age cracking is discussed in the report and summarized (in part) in Table 1 at the end of this section.

Kansas

Darwin et al. [34] performed a 10-year survey of bridge deck cracking in Kansas. Cracking was found to be more prevalent in bridges with steel girders than in bridges with concrete girders. The density of cracking was found to increase as a function of cement and water content (both associated with increased paste content) and concrete strength, and was also found to be more prevalent in the end spans of decks integral with abutments as compared to simply-supported or pin-supported spans. Cracking was observed to appear early, but was also observed to continue to increase over time. It was additionally observed that bridge decks cast in the 1980s exhibited less cracking than those in the 1990s, likely associated with increases in cement fineness, and shifts in construction practices to pumping (which encourages higher paste contents) and vibrating roller screeds (which locally increase paste contents at the surface). Although the highest crack densities were observed in decks with silica fume overlays, much of this cracking was attributed to plastic shrinkage, which was noted to be reduced in more recent years due to greater emphasis on limiting evaporation from freshly finished concrete surfaces.

Minnesota

Minnesota DOT has compiled a database of bridge deck construction and early-age cracking information in database. In 2014, American Engineering Testing, Inc., (AET) performed 20 bridge deck surveys and a statistical review of the data stored in the database [35]. Although the data was somewhat limited in its usefulness, AET found that restraint was a significant contributor to bridge deck cracking, especially at integral abutments. Correlations between bridge deck cracking and other evaluated parameters; such as concrete mixture design, construction practices, and other aspects of the bridge deck design were not found to be significant; however, the weak correlations were attributed to the limitations of the available data and did not necessarily indicate that these factors were insignificant. AET's recommendations were therefore primarily based on research by others, and included using Type II cements with cement contents less than 470 pounds per cubic yard; w/cm between 0.40 and 0.45; paste fractions less than 27 percent by volume; SCMs including 20 percent fly ash and no more than 6 percent silica fume; reducing or limiting compressive strength to less than 6000 psi to reduce "brittleness" of the concrete mixture; and limiting placement to daily ambient temperature swings to less than 50°F (28°C). Many of these recommendations were originally proposed by other researchers cited in this section [36].

New Jersey

Researchers working on behalf of the New Jersey Department of transportation [36] performed 2D and 3D linear and nonlinear finite element models to examine design factors that can contribute to cracking. Factors examined included girder stiffness, deck thickness, girder spacing, relative stiffnesses of the deck and girder, and the amount of reinforcing steel. The most significant contributors to cracking were found to be restraint of the deck and girders and the stiffness of the deck concrete. Recommendations included specifying an upper limit on concrete strength to reduce cracking issues related to high modulus of elasticity; reducing end restraint where possible; minimizing the ratio of girder to deck stiffness; using concrete mixture designs with low tendency for cracking; placing the concrete in the deck in a single placement, if possible; and when multiple placements must be made in a continuous span bridge, placing concrete in the center of the positive moment region first and delaying adjacent placements at least 72 hours.

Pennsylvania

A thorough study of the causes, prevention, and remediation of bridge deck cracking in Pennsylvania was conducted by Hopper, et al. [37]. In a survey of PennDOT personnel, 84 percent of respondents indicated that cracking is typically observed within 3 months after placement of concrete bridge decks. Common crack-prevention methods cited by DOT personnel included extended curing durations of 7 to 14 days; placement sequences that consider both the positive and negative moment areas of the deck; placing an upper limit on compressive strengths; and limiting restraint in the deck. In a review of more than 40 bridge decks in Pennsylvania, the researchers further found that high compressive strength and higher cementitious materials contents correlated with higher crack density, consistent with findings by others. They also found that decks constructed using half-width construction cracked approximately 4 times more than decks using detours (i.e., partial loading of the deck during construction resulted in an increase in crack frequency), while decks supported by prestressed concrete girders cracked approximately 3 times less than decks supported by steel girders. Recommendations for prevention of cracking were consistent with the findings of the literature review, DOT surveys, and bridge inspections.

Wisconsin

Researchers for the Wisconsin Department of Transportation [38] inspected and performed finite element analyses of 31 recently completed bridge deck structures in Wisconsin. Although limited information about the concrete mixtures and their performance characteristics was available, the researchers identified two primary causes of cracking: high shrinkage of the concrete mixtures and high restraint from the element design (continuous spans exhibited more restraint and greater cracking than simple spans). For two bridges investigated, researchers found very rapid compressive strength gain, with a 28-day result that often greatly exceeded design strength. Rapid strength and modulus of elasticity development can significantly increase early-age shrinkage stresses in the deck, resulting in increased tendency for early-age cracking. Based on the rapid rates of strength gain, they predicted cracking to initiate within the first week after placement. Designs incorporating simply-supported spans and concrete mixtures with controlled shrinkage and strength development rates were recommended as methods to reduce early-age cracking potential.

Montana

In August 2016, WJE performed a detailed investigation to identify the root cause(s) of bridge deck cracking in the Montana Department of Transportation (MDT) Missoula District. Severe cracking had been noted by MDT personnel in June 2016 on two bridge decks along Interstate 90 that had been constructed in 2010 and 2011. Upon further review, MDT found that more than 20 additional bridge decks in the Missoula District constructed in the prior 10 years were showing similarly widespread transverse cracking. Many of the bridge decks were located along Interstate 90 and represented replacement decks over existing bridge substructures originally constructed between 1960 and 1980.

Based on the results of a field investigation, laboratory studies, and thermal modeling, WJE provided the following recommendations to MDT to reduce the potential for early-age cracking:

1. Immediately fog-mist concrete placements until wet curing media is in place to provide surface evaporation and to cool the concrete.
2. Monitor concrete temperatures and apply insulation blankets when peak hydration temperatures are obtained to insulate the deck from the environment, to improve strength gain and curing, and to slow the rate of cooling, thereby decreasing early-age tensile stress development.
3. Consider placing concrete in the late afternoon or early evening, preferably between 4 pm and 8 pm, to avoid peak concrete temperatures occurring just prior to cool evening hours. This recommendation provides benefit as the cooling of the concrete from peak hydration does not coincide with ambient cooling. In addition, the tensile strength development at the time of cooling will be greater, reducing early-age tensile strength development.
4. Limit plastic concrete temperature at the time of placement to less than 75°F (24°C), or as cool as practical, to reduce the heat of hydration of the concrete.
5. Increase the design deck thickness to a minimum 8 inches to reduce the effects of non-linear temperature and drying profiles and associated stresses at the top and bottom of the deck.
6. Modify specifications to require staggering of top and bottom transverse reinforcing mats to reduce the alignment that can lead to full-depth cracks and holes.
7. Limit cementitious materials contents to no more than 600 pounds per cubic yard to reduce autogenous shrinkage, drying shrinkage, and total heat of hydration.
8. Limit silica fume replacement to 5 percent to reduce the potential for autogenous and plastic shrinkage cracking.
9. Specify a w/cm for deck concrete between 0.42 and 0.45 to ensure adequate concrete durability without increasing the risk of autogenous shrinkage.
10. Consider optimizing aggregate gradations to reduce paste volume and cracking tendency.

WJE's 2016 recommendations are generally consistent with the recommendations developed by others; however, due to the unique climate of the Missoula area (i.e., large diurnal variations in temperature and relative humidity), emphasis was placed on practices that would limit stresses developed by temperature and relative humidity gradients.

Summary of Findings

As seen in the preceding discussion, a number of factors have been identified by others as contributing to bridge deck cracking. These factors can be largely grouped into factors related to the concrete mixture design, concrete strength, restraint conditions, element design, and construction practices. Common recommendations from the reviewed literature are summarized in Table 1. While there is general agreement on many of these recommendations, some recommendations (e.g., limits on w/cm and total cement content) do not have broad consensus at this time. Further, many of the states reviewed are likely to experience less severe diurnal variations in temperature and relative humidity as compared to some regions of Montana; therefore, while the guidance summarized in this table may be applicable to the states listed above, the potential impact of Montana's local climate may also need to be considered.

Table 1. Summary of Factors Affecting Bridge Deck Cracking

Factor	Effect on Bridge Deck Cracking
Concrete Mixture Design	▪ Thermal and autogenous shrinkage are influenced by cement type; using Type II cements can help reduce thermal stresses, while using fly ash and slag can reduce both thermal stresses and shrinkage stresses. Finely ground cements, such as Type III cements, may increase heat of hydration and associated thermal stresses. ▪ Using high volume of coarse aggregates with low coefficient of thermal expansion can reduce both shrinkage and thermal stresses. ▪ Reducing paste content can reduce thermal stresses. ▪ Conflicting recommendations have been provided in the literature regarding recommended w/cm. Some researchers recommend a minimum w/cm of 0.40, while others recommend a maximum of 0.40. Recommending a minimum w/cm of 0.40 ignores the potential for increased autogenous shrinkage at these ratios.
Concrete Strength	▪ High strength concrete has a greater tendency to crack due to its higher modulus of elasticity (i.e., larger stresses associated with thermal or shrinkage strains). ▪ Modulus of elasticity develops faster than tensile strength for the first 3 to 5 hours after initial set of the concrete.
Restraint Conditions	▪ Restraint is greatest in interior spans (due to intermediate supports) and at integral abutments (due to fixed-end conditions). ▪ Simply-supported or pin connections can reduce crack tendency. ▪ Curved girders and skew can increase restraint.
Element Design	▪ Cracking increases when girders provide more stiffness than the deck. This includes designs with thin decks (< 8.5 inches), composite steel plate girders, wide flanges, and cross framing. Larger spacing and thicker decks can reduce crack tendency. ▪ Concrete girders can provide less restraint than steel girders due to their lower coefficient of thermal expansion. ▪ Offsetting the top and bottom transverse reinforcing bars can reduce the risk of full-depth crack formation. ▪ Increased cover will increase crack widths but will reduce crack frequency.
Construction Practices	▪ Practices that limit evaporation from freshly placed concrete surfaces can reduce the potential for early plastic shrinkage cracking. ▪ Mechanical vibration can close plastic shrinkage cracks; however, roller screeding may increase the risk of cracking due to local increases in near-surface paste content. ▪ Large temperature variations during placement can exacerbate thermal stresses.

Source: [33, 35, 31, 36]

ITEM 4.4A - BRIDGE DECK INSPECTIONS

Two separate field inspection trips were performed to document the crack conditions for bridge decks constructed in the last few years. The goal of the first field investigation was to document crack characteristics of bridge decks installed with WJE's previous curing recommendation and to help identify any trends of the cracking density relative to deck placement time (month), ambient and concrete

temperatures, the deck thickness, mix designs, bridge bearing type, span length, span bearing type, placement location, and placement length. The second site visit was intended to document any progression of the cracks noted during the first site visit with additional bridges added that might supplement the first field trip.

From December 2 to 7, 2019, WJE staff performed field inspections of nine bridges, and in addition, evaluated cracking conditions of one bridge (West Laurel Interchange) based on ortho mosaic photos provided by MDT. Of the nine investigated bridge decks, detailed crack mapping, visual inspections, and delamination surveys were performed on select deck sections of five of the bridges with only visual inspections of accessible portions of the deck surface and underside (no lane closures or traffic control) being performed on the remaining four decks.

From August 25 to August 30, 2020, WJE staff performed follow-up field inspections of 14 bridges. Of the 14 inspected bridge decks, detailed crack mapping and visual inspections were performed on select deck sections of five of the bridges with visual inspections of accessible portions of the deck being performed on the remaining nine bridges.

A list of inspected bridges is presented in Table 2 showing location, time of deck placement and inspection, and key characteristics of the structure. Mix designs for the concrete decks are presented in Table 3. All of the bridge decks except for the Capitol-Cedar Bridge - Phase I were reportedly constructed in general accordance with WJE's modified curing recommendations (detailed in WJE's report dated April 21, 2017). When available, the in-place concrete curing temperature records were reviewed to aid in the evaluation of the cracking tendencies (Appendix A.). Findings of the field inspections, crack mapping, delamination survey, and photo evaluation are discussed in the following sections.

Field Inspections

During the field inspections, WJE took notes and photographs of the deck cracking conditions and mapped the cracks on select bridges and deck placements. In general, the field inspections focused on the frequency and density of transverse cracks (with anomalous conditions of other cracks noted). For the detailed crack mapping, transverse cracks were mapped on digital plan drawings with associated typical crack widths. In addition, the transverse cracks were surveyed with ground penetrating radar (GPR) at select bridges to assess the location of the crack relative to any transverse deck reinforcing steel. WJE also performed a delamination survey on select bridge deck placements by chain dragging, and visual surveys were performed of the underside of assessable deck locations. All documentation was collected and saved using WJE's Plannotate software. WJE's Plannotate software allows MDT to store the inspection results (cracking, delamination, photographs, petrography, etc.) in a database that can be used for future inspection comparisons or quantification of the data.

In the following sections, key observations are presented for each bridge, generally in the order of inspection time. A subjective overall visual rating of the cracking condition, numbered 1 to 5 for the comparative best to worst condition, was assigned. In addition, the cracking severity of each concrete placement was subjectively rated during visual examinations of the bridges. The detailed crack maps for each bridge deck generated from Plannotate are presented in Appendix B.

Table 2. List of Inspected Bridges

Bridge ID	Bridge Short Name	Location	Route	Bridge Over	No. of Spans	Span Lengths (ft)	Superstructure Type	Nominal Deck Thickness (in)	Deck Placement Time
07006	Russell Street Bridge - Phase I (NB)	Missoula County	Russell Street	Clark Fork River	3	142+175+142	Steel Plate Girders	8.25	March, 2019
07006	Russell Street Bridge - Phase II (SB)	Missoula County	Russell Street	Clark Fork River	3	142+175+142	Steel Plate Girders	8.25	Jan - Feb, 2020
06253	Garrison Bridge	Powell County	N-88	MRL Railroad	3	55+94+55	Steel Beams	7.5	September, 2018
05943	Whitehall Bridge	Jefferson County	P-55	Big Pipestone Creek	3	47+47+47	Prestressed concrete tri-deck beams	5.75 to 7.75	May, 2018
01642	Capitol-Cedar Bridge - Phase I (NB)	Lewis and Clark County	I-15	MRL Railroad	4	180+212+212+180	Steel Plate Girders	8.5	2016
01641	Capitol-Cedar Bridge - Phase II (SB)	Lewis and Clark County	I-15	MRL Railroad	4	180+212+212+180	Steel Plate Girders	8.5	August, 2017
01434	Bonner Bridge - Phase I (EB)	Missoula County	I-90	Blackfoot River	3	158+210+113	Steel Plate Girders	9.5	October, 2018
01435	Bonner Bridge - Phase II (WB)	Missoula County	I-90	Blackfoot River	3	158+210+113	Steel Plate Girders	9.5	September, 2019
01741	West Laurel Bridge - Phase 1 (EB)	Yellowstone County	I-90	MRL Railroad	3	153+218+186	Steel Plate Girders	8.25	June, 2018
01742	West Laurel Bridge - Phase 2 (WB)	Yellowstone County	I-90	MRL Railroad	3	150+170+150	Steel Plate Girders	8.25	October, 2019
01104	Rarus-Silver Bow Creek - Phase I - Bridge A	Silver Bow County	I-15	BAP Railroad	3	90+137+139	Steel Plate Girders	7.75	October, 2018

Bridge ID	Bridge Short Name	Location	Route	Bridge Over	No. of Spans	Span Lengths (ft)	Superstructure Type	Nominal Deck Thickness (in)	Deck Placement Time
01105	Rarus-Silver Bow Creek - Phase I - Bridge B	Silver Bow County	I-15	BAP Railroad	3	90+137+139	Steel Plate Girders	7.75	December, 2019
01106	Rarus-Silver Bow Creek - Phase I - Bridge C	Silver Bow County	I-15	Silver Bowl Creak & BNSF Railroad	4	134+165+165+134	Steel Plate Girders	7.75	December, 2018
01107	Rarus-Silver Bow Creek - Phase I - Bridge D	Silver Bow County	I-15	Silver Bowl Creak & BNSF Railroad	4	134+165+165+134	Steel Plate Girders	7.75	December, 2019

Table 3. Mix Designs for Concrete Decks (pounds per cubic yard unless otherwise noted)

Bridge ID	Bridge Short Name	Cement	Fly Ash	GGBFS	Silica Fume	Fine Aggregate	Coarse Aggregate 1	Coarse Aggregate 2	w/cm	Air Content	Target Slump
07006	Russell Street Bridge - Phase I (NB)	381		163	20	1294	1732		0.42	7%	5 in.
07006	Russell Street Bridge - Phase II (SB)	381		163	20	1294	1732		0.42	7%	5 in.
06253	Garrison Bridge	--	--	--	--	--	--	--	--	--	--
05943	Whitehall Bridge	--	--	--	--	--	--	--	--	--	--
01642	Capitol-Cedar Bridge - Phase I (NB)	--	--	--	--	--	--	--	--	--	--
01641	Capitol-Cedar Bridge - Phase II (SB)	439	90		35	1339	1719		0.42	6%	5 in.
01434	Bonner Bridge - Phase I (EB)	434	81		25	1286	772	770	0.43	6%	5 in.
01435	Bonner Bridge - Phase II (WB)	434	81		25	1286	772	770	0.43	6%	5 in.
01741	West Laurel Bridge - Phase 1 - (EB)	382	108		49	1420	1645		0.39	7.8%	4 in.
01742	West Laurel Bridge - Phase 2 - (WB)	--	--	--	--	--	--	--	--	--	--
01104	Rarus-Silver Bow Creek - Phase I - Bridge A	--	--	--	--	--	--	--	--	--	--
01105	Rarus-Silver Bow Creek - Phase II - Bridge B	--	--	--	--	--	--	--	--	--	--
01106	Rarus-Silver Bow Creek - Phase I - Bridge C	--	--	--	--	--	--	--	--	--	--
01107	Rarus-Silver Bow Creek - Phase II - Bridge D	--	--	--	--	--	--	--	--	--	--

Note: "--" indicate data is not available.

Russel Street Bridge - Phase I (Northbound)

The bridge has three continuous spans of steel plate girders with span lengths of 142, 175, and 142 feet and new substructure. The nominal concrete deck thickness is 8-1/4 inches. Strip seal expansion joints are used between the superstructure and two abutments. This bridge deck was constructed in March of 2019 reportedly using WJE's modified curing recommendations from 2017 with five placements as shown on the crack map in Appendix A.

Based on the memorandum dated April 5, 2019, titled "Construction Engineering Services - Project Review Report" and the SiteManager Daily Work Reports provided by MDT, the following cold-weather placement procedures were used for this bridge deck:

- Reinforcing steel and deck forms were covered with insulating blankets and glycol-filled heater hoses during the night before placement to maintain temperatures of at least 35°F.
- The insulation blankets and heater hoses were temporarily removed for placing concrete.
- The concrete deck was covered with wet burlap and plastic sheeting.
- Heater hoses were placed on top of the concrete as needed.
- The deck was covered with insulation blankets.
- Insulation blankets were removed after concrete temperatures were within 5°F of the ambient temperature.

Based on the project records, the heater hoses were placed on the top of the concrete at the following times:

- For Placement 1: the same day of the concrete placement.
- For Placements 2, 3, 4, and 5: the day following the concrete placement. The insulation blankets were temporarily uncovered for installation of the heater hoses and re-covered after the heater hoses were in place.

It was reported in the April 5, 2019 memorandum mentioned above that after the cold weather protection and curing materials were removed, minimal transverse cracks were visible in most of the bridge deck, except that Placement 2 at mid-span of the bridges appeared to have significantly more transverse cracks than the other placements. The severe cracking at Placement 2 reported is generally consistent with WJE's visual inspections in 2019 and 2020; however, WJE's crack mapping survey indicates that the cracking condition at Placement 1 at the time of inspection was similar to Placement 2 (see Crack Data Summary). It is possible that the early cracks at Placement 1 were narrow when curing materials were removed and not readily visible, but they subsequently widened due to additional thermal and drying shrinkage movements. Possible effects of heating and low ambient temperatures during curing are discussed later.

2019 Inspection

The deck inspection was performed by Robert Firman and Todd Nelson (both of WJE) on 12/2/2019. It was mostly cloudy with ambient temperatures from 25 to 35°F (-4 to 2°C). Bridge deck cracks were observed from the east sidewalk, as lane closures were not allowed. Crack widths could only be measured on the sidewalks and were likely wider in the driving lanes. The survey focused on the first driving lane adjacent

to the sidewalk. The second lane from sidewalk was crack mapped, but the cracks were more difficult to see due to the distance and thus the results likely underestimate the amount of cracking.

Overall, there were a lot of transverse cracks for such an early age bridge, with the average transverse crack spacing of 2 to 4 feet and crack widths typically from 15 to 25 mils (0.015 to 0.025 inches). Reportedly, transverse cracks were observed by MDT within a couple months of construction. Photos of typical transverse cracks on the topside and underside are presented in Figure 5 through Figure 7. Placement 5 has map cracking along the center of the bridge in between lanes (see Figure 8). Ranking of the deck placements in cracking condition from worst to best was Placement 2, 1, 4, 5, and 3 based on visual inspection. No delamination was noted during chain dragging of the sidewalk. Placement 2 is the middle span and Placements 1 and 3 are end spans. Placement sequencing did not appear to have much effect on the amount of cracking at this bridge. This bridge has an overall rating of 3.

Figure 5. Russell Street Bridge - Phase I, 2019 Inspection - Placement 1, topside. Typical transverse crack at arrows.

Figure 6. Russell Street Bridge - Phase I, 2019 Inspection - Placement 1, topside. A 15-mil transverse crack at arrow.

Figure 7. Russell Street Bridge - Phase I, 2019 Inspection - Placement 3, underside. Typical transverse cracks at arrows.

Figure 8. Russell Street Bridge - Phase I, 2019 Inspection - Map cracking in placement 5.

2020 Inspection

The deck inspection was performed from the underside of the deck by Robert Frazier of WJE on 8/29/2020 (no traffic control). At the time of the inspection, it was unknown that there was a polymer overlay applied on the topside of the deck since WJE's last inspections. Crack mapping was performed from the underside of deck for the entire Placement 1, the south end of Placement 4 (approximately 47 feet long), and the north end of Placement 3 (approximately 66 feet long). For other parts of the deck, visual inspection with photos was performed, but crack mapping was not due to the limited access.

Overall, there were a lot of transverse cracks with the typical transverse crack spacing of approximately 2 feet in Spans 1 and 3. A photo of typical transverse cracks on the underside is presented in Figure 9. Intersecting cracks, exhibiting as multiple short longitudinal cracks intersecting transverse cracks, are present in Placements 1 and 2 near midspans; an example is shown in Figure 10. These appeared to have developed or become more observable since the 2019 inspections. Ranking of the deck placements in cracking condition from worst to best was 2, 1, 3, 4 and 5 based on visual inspection from the underside, which is generally consistent with the inspection in 2019. This bridge has the same overall rating of 3 as in the 2019 inspection.

Figure 9. Russell Street Bridge - Phase I, 2020 Inspection - Placement 1, underside. A typical transverse crack at arrows.

Figure 10. Russell Street Bridge - Phase I, 2020 Inspection - Placement 1, underside. Intersecting cracks in red oval.

Russel Street Bridge - Phase II (Southbound)

The span layout, deck thickness, and expansion joints are the same as the Russel Street Bridge - Phase I (northbound). This bridge deck was constructed in January to February 2020 reportedly using WJE's modified curing recommendations with five placements as shown on the crack map in Appendix A. It is unclear if the cold-weather placement procedures used in the Phase I bridge were implemented for Phase II.

2020 Inspection

The deck inspection was performed from the underside of the deck by Robert Frazier of WJE (no traffic control). There is a polymer overlay on the topside of the deck. Crack mapping was performed from the underside of deck for the entire Placement 1, the south end of Placement 4 (approximately 47 feet long), and the north end of Placement 3 (approximately 66 feet long). For other parts of the deck, visual inspection with photos was performed, but crack mapping was not due to the limited access.

Overall, transverse cracking was present but appeared to be milder than the Phase I bridge. A photo of typical transverse cracks on the underside is presented in Figure 11. Intersecting cracks, like those reported in the Phase I bridge, were not observed. Ranking of the deck placements in cracking condition from worst to best was 2, 4, 1, 3 and 5 based on visual inspection and crack mapping from the underside. Placement sequencing did not appear to have much effect on the amount of cracking at this bridge.

This bridge has an overall rating of 1.5 based on inspection from the deck underside.

Figure 11. Russell Street Bridge - Phase II, 2020 Inspection - Typical transverse cracks (arrows) in placement 1, underside.

Garrison Bridge

This bridge deck was constructed on August 29 and 30, 2019 with three night placements reportedly using WJE's modified curing recommendations from 2017. The bridge has three spans of steel beams with span lengths of 55, 94, and 55 feet and was constructed with existing substructure and deck girders. The end spans cantilever 11 feet over each interior pier into the middle span and support a 72-foot long suspended span with pins and hangers. The nominal concrete deck thickness is 7-1/2 inches in the cantilever spans and varies from 8 to 9.25 inches in the suspended span. Strip seal expansion joints are used between the cantilever and suspended spans. At the abutments, the concrete deck was cast continuously over the gap between the end of a steel beam and the abutment backwall, and rests on the top of the backwall. Per the project drawings, two control (contraction) joints are placed in the deck at center lines of the piers (Figure 12). These control joints were either formed during finishing or saw-cut after placement (then sealed), possibly to locate and control cracks due to negative moments. The bridge has one lane in each direction with low traffic volume.

According to a provided MDT construction report (dated September 25, 2018), Class Deck Concrete was batched with a portable batch plant; and ambient temperatures during placement were between 40 (4°C) and 60°F (16°C) with no wind. The contractor used wet burlap and soaker hoses for curing, and insulation was applied after peak hydration. Minimal cracking was noted after removal of the curing, but early age crack mapping was not performed.

Figure 12. Garrison Bridge - Sealed control joint (at arrow) in concrete deck. Photo taken in 2020.

2019 Inspection

The deck was visually inspected (from the shoulder with no lane closures nor traffic control) by Todd Nelson on 12/3/2019 from both the topside and underside of the deck. It was partly cloudy with ambient temperatures at about 35°F (2°C). Overall, the bridge deck is in very good condition with very few transverse cracks. Transverse crack spacing was estimated to be at 8 to 10 feet. No observable plastic shrinkage cracking or longitudinal cracking was noted. The deck underside was in good condition with only a few transverse cracks observed over the entire deck underside. Photos of typical conditions on the topside and underside are presented in Figure 13 and Figure 14, respectively. Minimal amounts of efflorescence were observed at deck construction joints (Figure 15). This bridge deck has an overall rating of 1.

Figure 13. Garrison Bridge - 2019 inspection - Typical deck topside condition.

Figure 14. Garrison Bridge - 2019 inspection - Typical deck underside condition. Transverse cracks at arrows.

Figure 15. Garrison Bridge - 2019 inspection - Efflorescence on the deck underside at a construction joint (at arrows).

2020 Inspection

The deck was visually inspected (no detailed inspection was performed with no lane closures nor traffic control) by Robert Frazier on 8/30/2020 from both the topside and underside of the deck. Overall, the bridge deck remains in very good condition with no significant changes from the 2019 inspection. On the topside, a few clusters of tight transverse cracks were observed in Span 1 at about 15 feet and 23 feet the south abutment and in Span 2 at one and three quarter points in span (Figure 16). No longitudinal cracking was noted. A photo of typical condition on the underside is presented in Figure 17.

Additional observations of the cracking condition are as follows:

- Span 1 (South): cracking is most prevalent at mid-span in Placement 4 and reduces near transition area from Placement 4 to Placement 7 and within Placement 7.
- Span 2: the cracking is most prevalent at mid-span in Placement 3.
- Span 3: cracking is most prevalent over the railroad (Placement 2); minimal cracking elsewhere.

This bridge deck has the same overall rating of 1 as in the 2019 inspection.

Figure 16. Garrison Bridge - 2020 inspection - Deck topside showing a cluster of fine transverse cracks.

Figure 17. Garrison Bridge - 2020 inspection - Typical deck underside condition (suspended span). Transverse cracks at arrows.

Whitehall Bridge (I-55)

This bridge deck was constructed in May 2018 reportedly using WJE's modified curing recommendations from 2017. The bridge has three simply supported spans of triple-T precast prestressed concrete beams (Tri-deck beams) with a 4-inch thick flange. A cast-in-place reinforced concrete deck was placed on top of the beams continuously over the three spans, with thickness varying from 5 3/4 inches at mid-span to 7 3/4 inches at piers. The bridge has one lane in each direction with low traffic volume.

2019 Inspection

A visual inspection (no lane closures or traffic control) of the deck was performed by Todd Nelson on 12/4/2019. It was partly cloudy with ambient temperatures from 25 to 30°F (-4 to -1°C). Overall, the bridge deck is in very good condition with very minimal transverse cracks noted from topside or underside. A couple of long longitudinal cracks were noted, likely at the joints between precast elements. Some minor map cracking was noted. Photos of typical conditions on the topside and underside are presented in Figure 18 and Figure 19, respectively. Crack mapping was not performed for this bridge.

This bridge has an overall rating of 1.

Figure 18. Whitehall Bridge - 2019 inspection - Typical deck topside condition. Arrows point to a longitudinal crack.

Figure 19. Whitehall Bridge - 2019 inspection - Typical deck underside condition.

2020 Inspection

A visual inspection (no lane closures or traffic control) of the deck was performed by Robert Frazier on 8/27/2020 from both the topside and underside of the deck. Overall, the bridge deck remains in very good condition with no significant changes from the 2019 inspection. A photo of typical condition on the topside is presented in Figure 20. Crack mapping was not performed for this bridge.

Additional observations of the cracking condition are as follows:

- Four full-length longitudinal cracks align with precast T-beam flange joints.
- Map cracking observed primarily in shoulders.

This bridge has the same overall rating of 1 as in the 2019 inspection.

Figure 20. Whitehall Bridge - 2020 inspection - Typical deck topside condition. Arrows point to longitudinal cracking.

Capitol-Cedar Interchange Bridge - Phase I (Northbound)

This bridge deck was constructed in 2016 prior to WJE's modified curing recommendations in 2017. The bridge has four continuous spans of steel plate girders with span lengths of 180, 212, 212, and 180 feet. The nominal concrete deck thickness is 8-1/2 inches. Modular expansion joints are used between the superstructure and two abutments. Significant transverse deck cracking was reported on this bridge immediately after removal of curing back in 2016.

2019 Inspection

The deck inspection was performed by Robert Schulman and Todd Nelson on 12/6/2019. It was mostly cloudy with ambient temperatures from 30 to 40°F (-1 to 4°C). The bridge has three traffic lanes and very high traffic volume. Crack mapping and delamination surveys were performed on deck placements 3 and 5, with visual assessments performed for the other placements. The crack mapping was performed from the farthest right driving lane (only the far-right lane was closed to traffic) and shoulder; therefore, the most accurate crack maps are in the right lane and shoulder with visual inspections of the other lanes being less reliable.

In general, the bridge deck has severe transverse cracking throughout, with placements 2 and 3 (interior mid-span) having the worst cracking conditions with many characteristic "jump" cracks. When the transverse cracks propagate past one another in close proximity, the crack tips bend toward one another, eventually "jumping" from one crack to another. Such "jump" crack patterns were observed and reported in WJE's April 21, 2017 report. Transverse cracking on placements 3 and 5 were typically spaced every 4 feet, with wide crack widths averaging 20 mils (0.020-in.), and the majority of the cracks were located over reinforcing steel (based on ground penetrating radar (GPR) survey). Typical transverse cracks on the topside and underside are shown in Figure 21 and Figure 22. Significant map cracking was observed at the beginning and end of placements 3 and 5 (Figure 23 and Figure 24). Observed from the deck underside, cracking in placements 2 and 3 looked worse than in placements 5 and 7. Cracking appears more frequent over and adjacent to the steel girders manifesting the additional restraint provided by the composite girders. The cracking in the mid-span placements looked worse than in the placements over piers. Ranking of the placements in cracking condition from worst to best is 3, 2, 4, 1, 7, 6, and 5 based on visual inspection. No delamination was noted.

This bridge has an overall rating of 4.

Figure 21. Capitol-Cedar Bridge Phase I (NB)- Typical deck topside transverse cracks, Placement 3.

Figure 22. Capitol-Cedar Bridge Phase I (NB) - Typical deck underside transverse cracks at arrows (Placement 3).

Figure 23. Map cracking at beginning of placement 3.

Figure 24. Map cracking at the end of placement 5.

2020 Inspection

A visual deck inspection was performed from the underside of the deck by Robert Frazier on 8/29/2020 (no traffic control). Visual inspection with photos was performed from the deck underside; crack mapping was not performed. Crack conditions in the underside appeared similar to those observed during the 2019 inspection, but with more efflorescence at crack locations. A typical photo of the deck underside is shown in Figure 25. Overall, cracking conditions in the mid-span regions (Placements 1, 2, 3 and 4) are worse than the placements over the piers (Placements 5, 6 and 7).

Additional observations of the cracking condition per span are as follows:

- Span 1 (South): the worst cracking condition at mid-span in Placement 4; cracking reduces near transition area from Placement 4 to Placement 7 and within Placement 7.
- Span 2: the worst cracking condition is at mid-span in Placement 3.
- Span 3: the worst cracking condition over the railroad (Placement 2); minimal cracking elsewhere.
- Span 4: the worst cracking at mid-span in Placement 1; minimal cracking within Placement 6 north of Bent 4.

This bridge has the same overall rating of 4 as in the 2019 inspection.

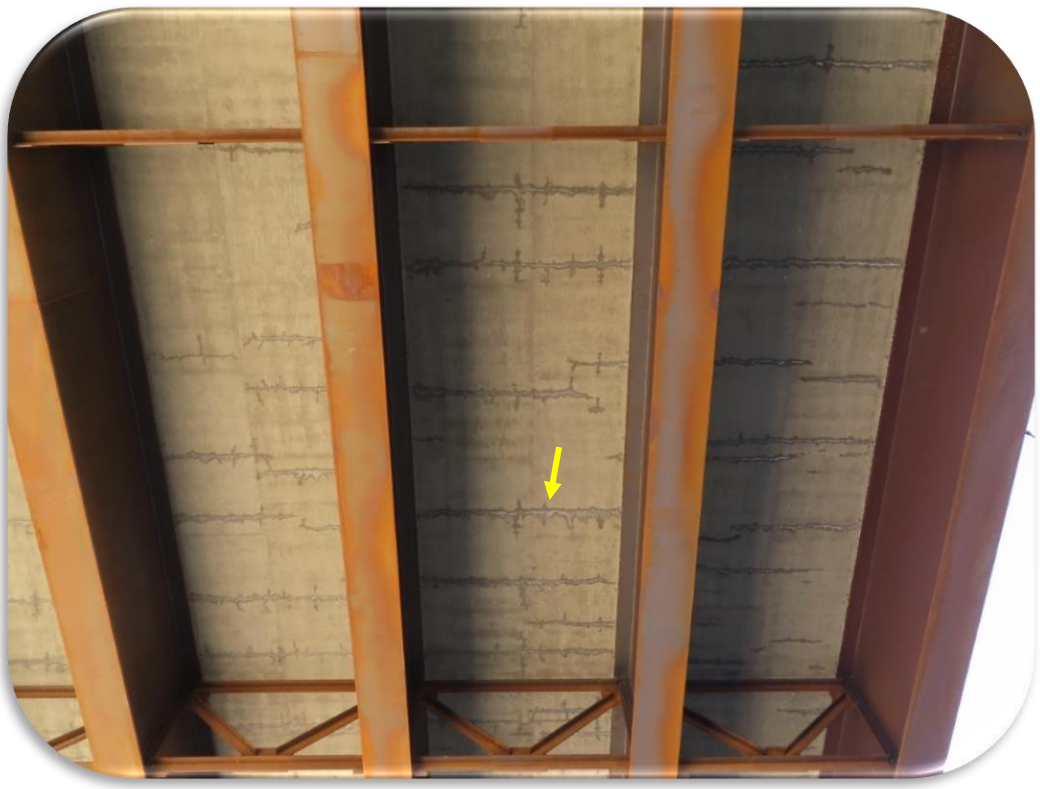

Figure 25. Capitol-Cedar Bridge Phase I (NB) - 2020 inspection - Typical deck underside transverse cracks. The arrow points to the same transverse crack noted in Figure 22.

Capitol-Cedar Interchange Bridge - Phase II (Southbound)

The bridge was constructed in August of 2017 with WJE's curing recommendations. The superstructure is generally the same as the Phase I, northbound bridge described above. The bridge has three lanes and has a very high traffic volume. When curing was removed from this bridge deck back in 2017, no observable cracking was noted. In addition, approximately one month after construction, WJE performed a brief visual review of the bridge deck and did not note any cracking. However, transverse cracking was reported to be observed after the winter months, approximately 4 to 6 months after construction, and progressively became more severe.

2019 Inspection

A deck inspection was performed by Robert Schulman and Todd Nelson on 12/6/2019. It was mostly cloudy with ambient temperatures from 30 to 40°F (-1 to 4°C). Crack mapping and delamination surveys were performed on deck placements 2 and 5, with visual assessments performed for the other placements. The crack mapping was performed from the farthest right (travel) lane and shoulder (lane closure of only the travel lane); therefore, the most accurate crack maps are in the right lane and shoulder with visual inspections of the other lanes being less reliable.

Typical transverse cracks on the topside are shown in Figure 26. There were one or two possible locations of "jump" cracks at transverse cracks spaced 2 to 3 feet apart (Figure 27). Location of the "jump" part relative to the steel girders shown in these figures appears to be consistent with observations in WJE previous investigations in which it was hypothesized that the transverse cracks originated from the girders where the restraint is the greatest, then propagated away from the girders with time, and finally bent towards each other, resulting in the "jump". These "jump" cracks, however, were atypical compared to "jump" cracks observed on previous investigations and on Phase I deck, as the transverse cracking was spaced farther apart (6 to 18 inches is typical based on previous bridge deck investigations). Typical transverse cracks were spaced at 4 to 5 feet with an average crack width of 20 mils (0.020-in.), and the majority of the cracks were located over reinforcing steel (based on GPR survey). Placements 5 and 7 (over piers) were in the best condition (similar to Phase I), with placement 1 and 3 the visually worst (similar to Phase I). Placement 1 looked much worse than placement 4. A longitudinal crack was observed over the entire length of placements 2 and 5 along the second girder from the right/east barrier. Ranking of the placements in visual cracking condition from worst to best: 1, 3, 2, 4, 7, 6, and 5; generally similar to Phase I. No delamination was noted on the deck.

From the deck underside, placements 5 and 7 were in good condition while placement 3 was visually the worst. Typical transverse cracks on the underside in placement 3 are shown in Figure 28. As shown in this figure, short, hairline longitudinal cracks are present along many transverse cracks. These hairline cracks are uncommon, and their origin is not well understood.

This bridge has an overall rating of 3.

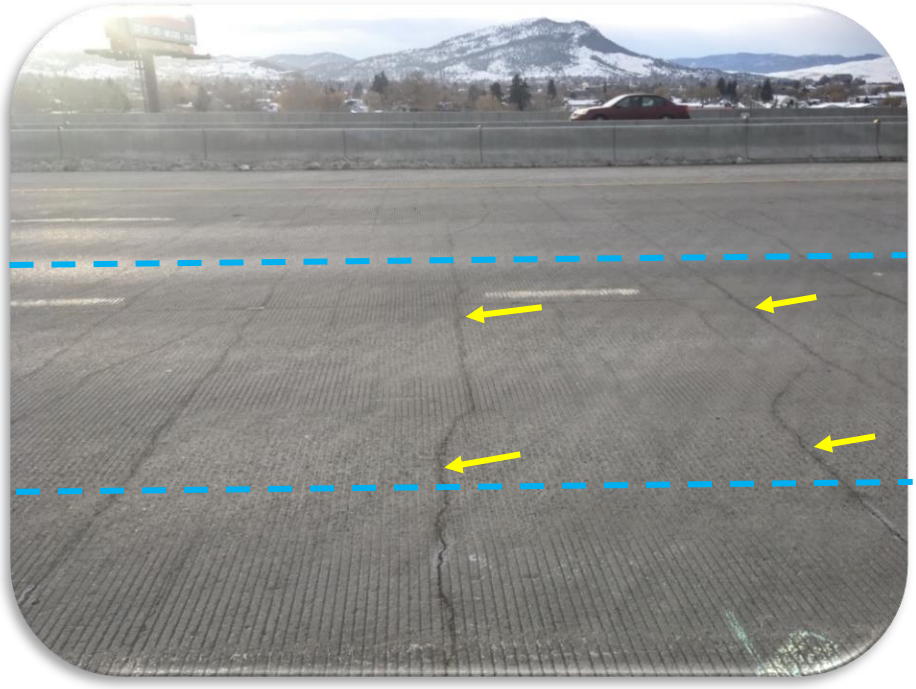

Figure 26. Capitol-Cedar Bridge Phase II (SB) - 2019 inspection. Typical deck topside transverse cracks at arrows. Blue dotted lines indicate approximate locations of two adjacent steel girders.

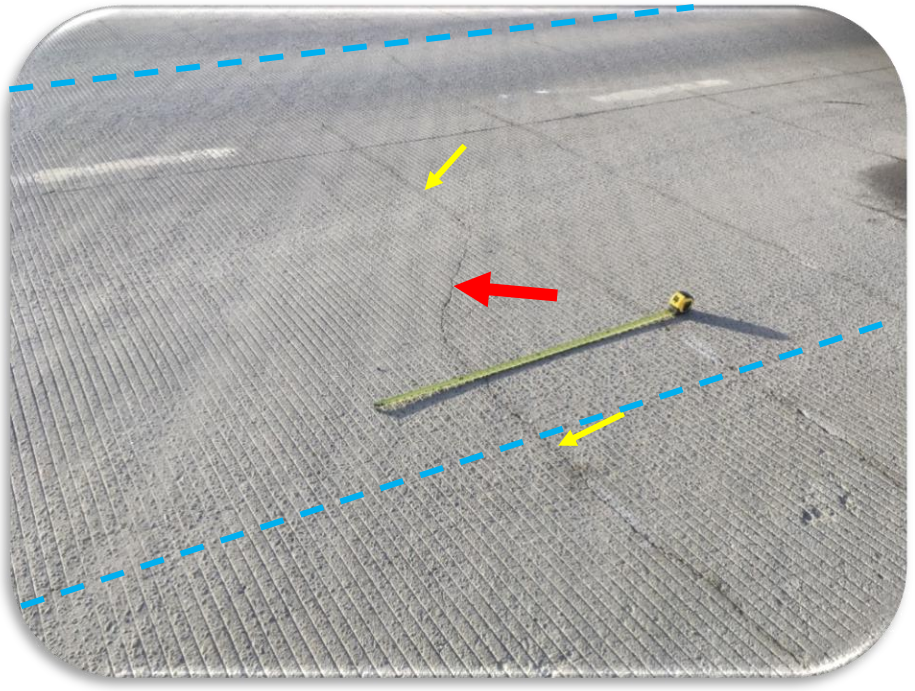

Figure 27. Capitol-Cedar Bridge Phase II (SB) - 2019 inspection. Jump (transverse) crack at arrows. Red arrow indicates the "jump" part. Blue dotted lines indicate approximate locations of two adjacent steel girders.

Figure 28. Capitol-Cedar Bridge Phase II (SB) - 2019 inspection. Placement 3. Typical deck underside transverse cracks at yellow arrows; short, hairline longitudinal cracks at red arrows.

2020 Inspection

A visual inspection was performed from the underside of the deck by Robert Frazier on 8/29/2020 (no traffic control). Crack mapping was not performed. Crack conditions generally looked similar to those observed during the 2019 inspection. A typical photo of the deck underside is given in Figure 29, showing typical transverse cracks and short, hairline longitudinal cracks similar to those observed in 2019. Overall, cracking conditions in the mid-span regions (Placements 1, 2, 3 and 4) are worse than the placements over the piers (Placements 5, 6 and 7).

Additional observations of the cracking condition are as follows:

- Span 1 (South): considerable cracking starting near the south abutment and reducing to minimal cracking near transition area from Placement 4 to Placement 7. Cracking returns over Bent 2.
- Span 2: the worst cracking condition at mid-span in Placement 3.
- Span 3: minimal cracking observed. Note: a portion of the span was not observable due to the presence of railroad and train.

- Span 4: considerable cracking starting near the north abutment and reducing to minimal cracking near transition area from Placement 1 to Placement 6 and Bent 4.

This bridge has the same overall rating of 3 as in the 2019 inspection.

Figure 29. Capitol-Cedar Bridge Phase II (SB) - 2020 inspection. Typical deck underside transverse cracks at yellow arrows); short, hairline longitudinal cracks at red arrows.

Bonner Bridge - Phase I (Eastbound)

This bridge deck was constructed in September 2018 reportedly using WJE's modified curing recommendations. The bridge has three continuous spans of steel plate girders with span lengths of 158, 210, and 113 feet. The nominal concrete deck thickness is 9-1/2 inches. Strip seal expansion joints are used between the superstructure and two abutments.

2019 Inspection

The deck inspection was performed Robert Schulman and Todd Nelson on 12/7/2019. It was mostly cloudy with ambient temperatures from 25°F to 35°F (-4 to 2°C). The crack mapping and delamination survey were performed from the driving lane (driving lane was the only lane closed), with visual crack assessment performed in the passing lane. The deck was generally in good condition on both topside and underside. The placements over the piers (4 and 5) had worse cracking than the mid-span placement (1) and end placements (2 and 4). On average, the transverse cracking was spaced at 13, 10, 20, 4, and 3 feet for placements 1, 2, 3, 4 and 5, respectively. Transverse crack widths were typically between 15 and 20 mils (0.015 to 0.020-in.) and approximately half of the cracks were located over reinforcing steel (based on GPR survey). Typical conditions of the deck topside and underside are shown in Figure 30 and Figure 31

respectively. Minor map cracking was observed on the topside in most of the placements (Figure 32). The cracking in the placements over piers was more severe than the placements in mid-span regions. Ranking of the placements in visual cracking condition from worst to best: 5, 4, 2, 1, 3.

This bridge has an overall rating of 1.5.

Figure 30. Bonner Bridge Phase I (EB) - 2019 inspection - Typical deck topside transverse cracks, placement 5.

Figure 31. Bonner Bridge Phase I (EB) - 2019 Inspection - Typical deck underside condition, placement 3. Transverse crack at arrows.

Figure 32. Bonner Bridge Phase I (EB) - 2019 Inspection - Typical map cracking, placement 5.

2020 Inspection

The deck inspection was performed by Robert Frazier on 8/29/2020. Visual inspection was performed from both the topside and underside of the deck, as traffic control was unavailable to perform a detailed survey. Crack mapping was performed from the topside. Crack conditions generally look similar to those observed during the 2019 inspection. Transverse crack widths were typically between 15 and 20 mils (0.015 to 0.020-in.), consistently with data from the 2019 survey. Typical conditions of the deck topside and underside are shown in Figure 33 and Figure 34, respectively. Ranking of the placements in visual cracking condition from worst to best: 4, 5, 3, 2, and 1.

Additional observations of the cracking condition on the underside are as follows:

- Span 1 (East): minimal cracking.
- Span 2: mild cracking in Placement 3; minimal cracking elsewhere.
- Span 3: minimal cracking except just west of transition area from Placement 2 to Placement 5.

This bridge has the same overall rating of 1.5 as in the 2019 inspection.

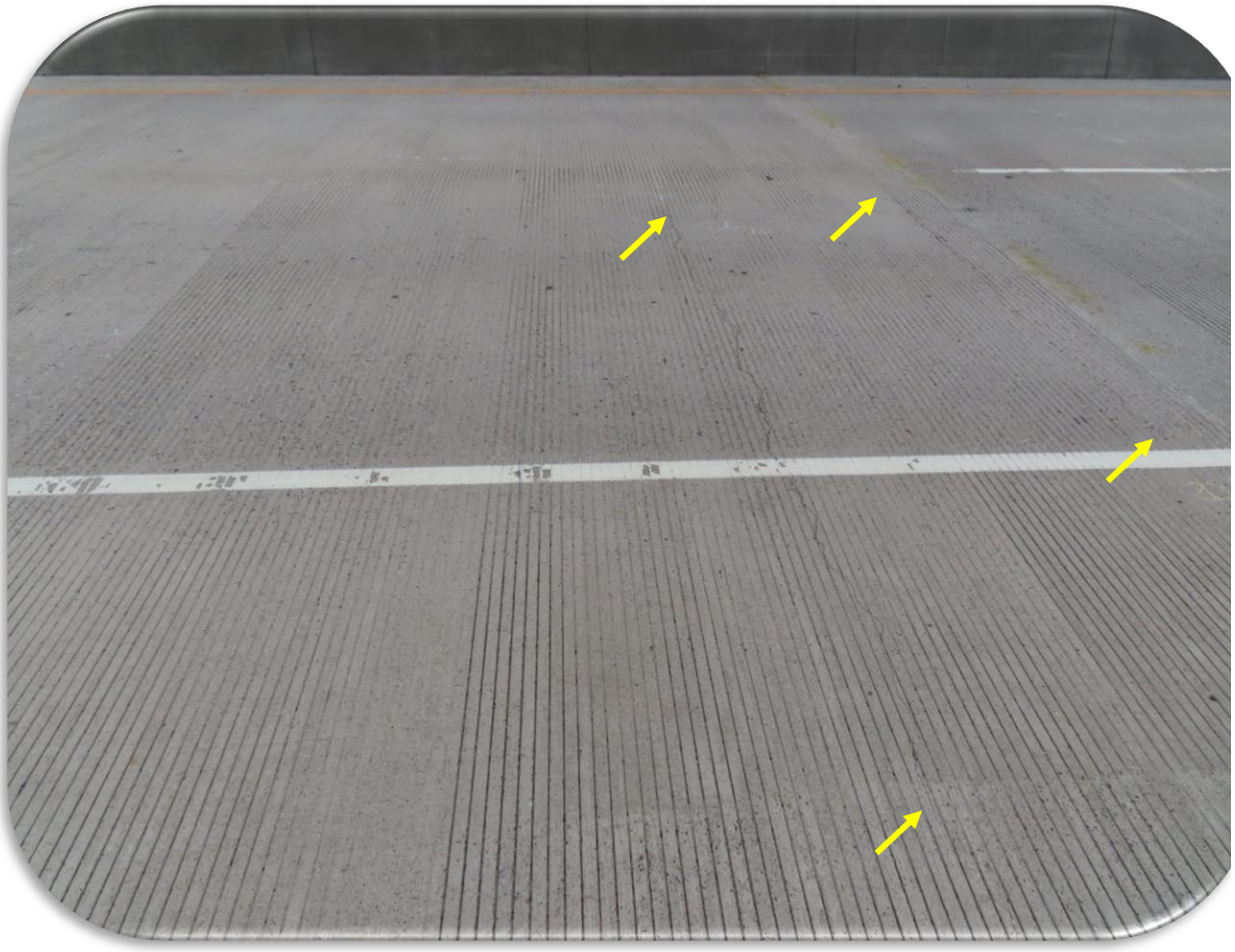

Figure 33. Bonner Bridge Phase I (EB) - 2020 inspection - Typical deck topside transverse cracks, placement 5.

Figure 34. Bonner Bridge Phase I (EB) - 2020 inspection - Typical deck underside condition, placement 3.

Bonner Bridge - Phase II (Westbound)

This bridge deck was constructed in September 2019 reportedly using WJE's modified curing recommendations and opened to traffic in November 2019. The structure is generally the same as the Phase I, as described above.

2019 Inspection

The deck inspection was performed by Robert Schulman and Todd Nelson on 12/7/2019. It was mostly cloudy with ambient temperatures from 25 to 35°F (-4 to 2°C). The crack mapping and delamination survey were performed from the driving lane, with visual crack assessment performed in the passing lane.

Overall, the bridge is in very good condition. Transverse cracks were very tight, most of them were 5 mils (0.05-in.) wide or less, and very difficult to see. Approximately half of the cracks were located over reinforcing steel (based on GPR survey). A couple of cracks appeared to have been previously repaired. No map cracking was observed. The deck underside was in very good condition with no observable transverse cracks. Typical conditions of the deck topside and underside are shown in Figure 35 and Figure 36, respectively.

This bridge has an overall rating of 1.

Figure 35. Bonner Bridge Phase II (WB)- Typical deck topside condition, placement 1.

Figure 36. Bonner Bridge Phase II (WB) - 2019 Inspection - Typical deck underside condition, Span 2 - Looking east.

2020 Inspection

A visual inspection was performed from the underside of the deck by Robert Frazier on 8/29/2020 (no traffic control). Crack mapping was not performed, as traffic control was unavailable to WJE. Crack conditions generally look similar to those observed during the 2019 inspection. Typical conditions of the deck underside are shown in Figure 37. Ranking of the spans in visual cracking condition from worst to best: 2, 3 and 1.

Additional observations of the cracking condition on the underside are as follows:

- Span 1 (East): minimal to mild cracking.
- Span 2: moderate cracking in Placement 3; minimal cracking elsewhere.
- Span 3: minimal cracking except just west of transition area from Placement 2 to Placement 5.

This bridge has the same overall rating of 1 as in the 2019 inspection.

Figure 37. Bonner Bridge Phase II (WB) - 2020 inspection - Typical deck underside condition, Span 2 - Looking east.

Rarus/Silver Bow Creek - Phase I - Bridge A

This bridge was constructed in October of 2018 reportedly using WJE's modified curing recommendations and consists of three spans with span lengths of 90, 137, and 139 feet. Concrete deck thickness is 7-3/4 inches, which is supported on steel plate girders.

2019 Inspection

A visual inspection of this bridge was performed from the underside only (no traffic control). The underside condition of this bridge is very good, with minimal transverse cracking noted (see Figure 38).

This bridge has an overall rating of 1.

Figure 38. Underside of Rarus/Silver Bow Creek Bridge A - 2019 inspection, condition is very good (Span 2 shown).

2020 Inspection

The deck inspection was performed by Robert Frazier on 8/27/2020. A polymer concrete overlay was placed between the 2019 and 2020 inspection. Visual inspection was performed from the underside only (no traffic control). Crack conditions appear to be slightly worse than in the 2019 inspection, with more efflorescence observed (see Figure 39). Ranking of the spans in visual cracking condition from worst to best: 1, 2 and 3.

Additional observations of the cracking condition on the underside are as follows:

- Span 1 (South): moderate cracking in Placement 1.
- Span 2: routine cracking throughout.
- Span 3: low-density routine cracking.

This bridge has an overall rating of 1.5.

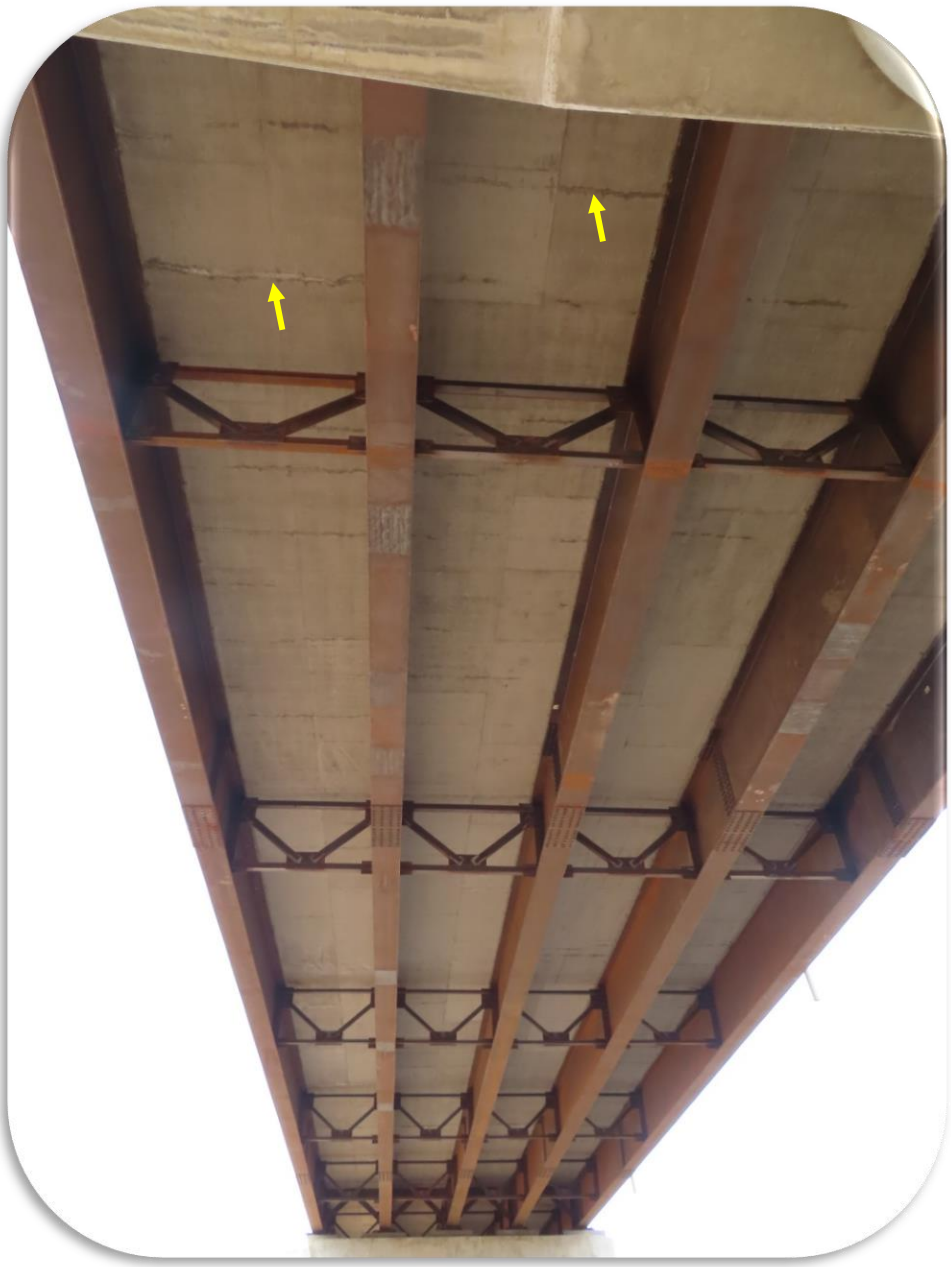

Figure 39. Underside of Rarus/Silver Bow Creek Bridge A - 2020 inspection - Span 2, Typical transverse cracks at arrows.

Rarus/Silver Bow Creek - Phase II - Bridge B

This bridge was constructed in December of 2019 using WJE's curing recommendations and consists of three spans with span lengths of 90, 137, and 139 feet. Concrete deck thickness is 7-3/4 inches, which is supported on steel plate girders.

2020 Inspection

The deck inspection was performed by Robert Frazier on 8/27/2020. A polymer concrete overlay is present on the topside, and visual inspection was performed from the underside only (no traffic control). The underside condition of this bridge is good, with minimal transverse cracking noted (see Figure 40 and Figure 41). Ranking of the spans in visual cracking condition from worst to best: 2, 1 and 3.

Additional observations of the cracking condition on the underside are as follows:

- Span 1 (South): minimal cracking except at mid-span.
- Span 2: routine cracking starting north of transition area between Placements 2 and 3.
- Span 3: low-density routine cracking.

This bridge has an overall rating of 1.

Figure 40. Underside of Rarus/Silver Bow Creek Bridge B - 2020 inspection - Span 1, Typical transverse crack at arrows.

Figure 41. Underside of Rarus/Silver Bow Creek Bridge B - 2020 inspection - Span 2, Typical transverse cracks at arrows.

Rarus/Silver Bow Creek - Phase I - Bridge C

This bridge was constructed in December of 2018 reportedly using WJE's curing recommendations and consists of four spans with span lengths of 134, 165, 165, and 134 feet. Concrete deck thickness is 7-3/4 inches, which is supported on steel plate girders.

2019 Inspection

A visual inspection of this bridge was performed from the underside only (no traffic control). The underside condition of this bridge is good, with minimal transverse cracking noted (see Figure 42 and Figure 43). This bridge has an overall rating of 1.5.

.
Figure 42. Underside of Rarus Structures - Silver Bow Creek - Bridge C - 2019 inspection.

Figure 43. Underside of Rarus Structures - Silver Bow Creek - Bridge C - 2019 inspection.

2020 Inspection

The deck inspection was performed by Robert Frazier on 8/27/2020. A polymer concrete overlay is present on the topside, and visual inspection was performed from the underside only (no traffic control). Crack conditions look similar to those observed during the 2019 inspection. Typical conditions of the deck underside are provided in Figure 44 and Figure 45. Ranking of the spans in visual cracking condition from worst to best: 3, 2, 1 and 4.

Additional observations of the cracking condition on the underside are as follows:

- Span 1 (South): low-density cracking.
- Span 2: low-density cracking.
- Span 3: moderate cracking at mid-span.

This bridge has the same overall rating of 1.5 as in the 2019 inspection.

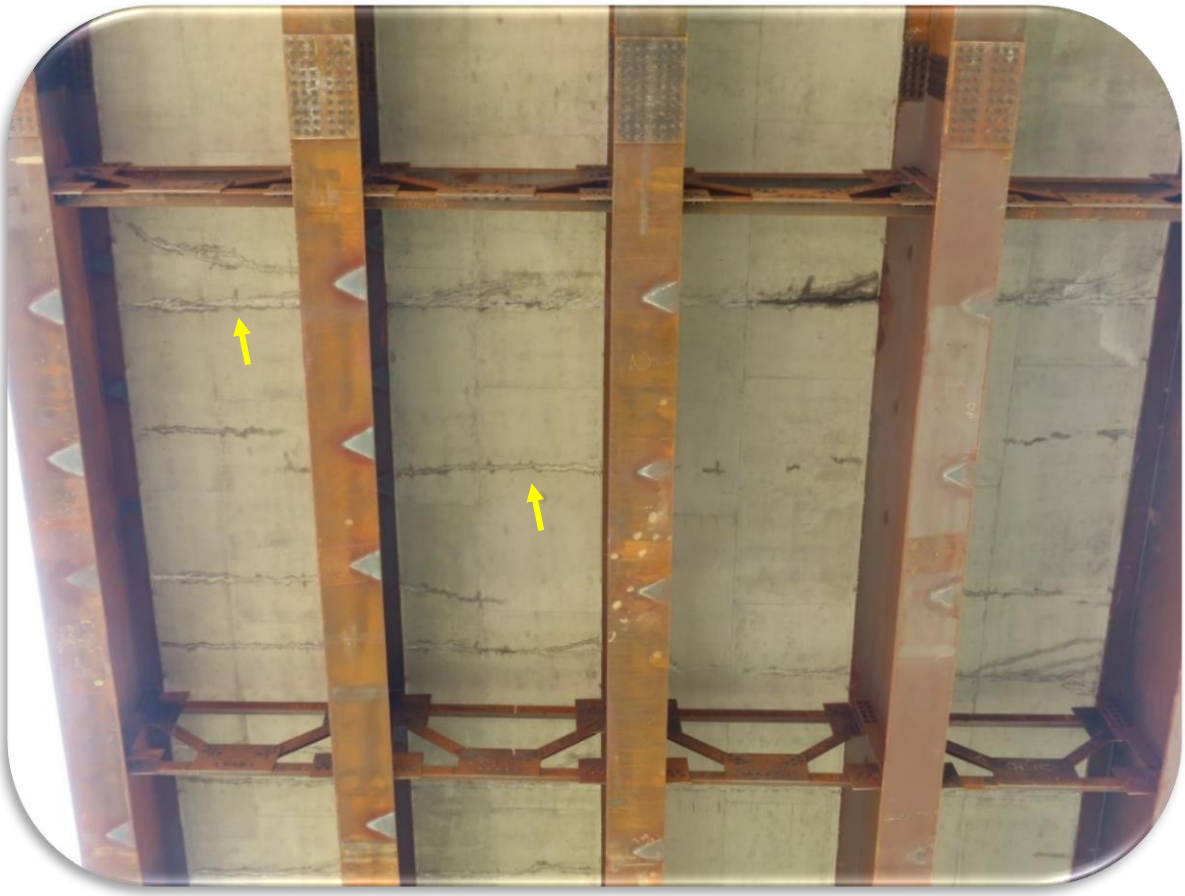

Figure 44. Underside of Rarus Structures - Silver Bow Creek - Bridge C - 2020 inspection, Span 3; typical transverse cracks at arrows.

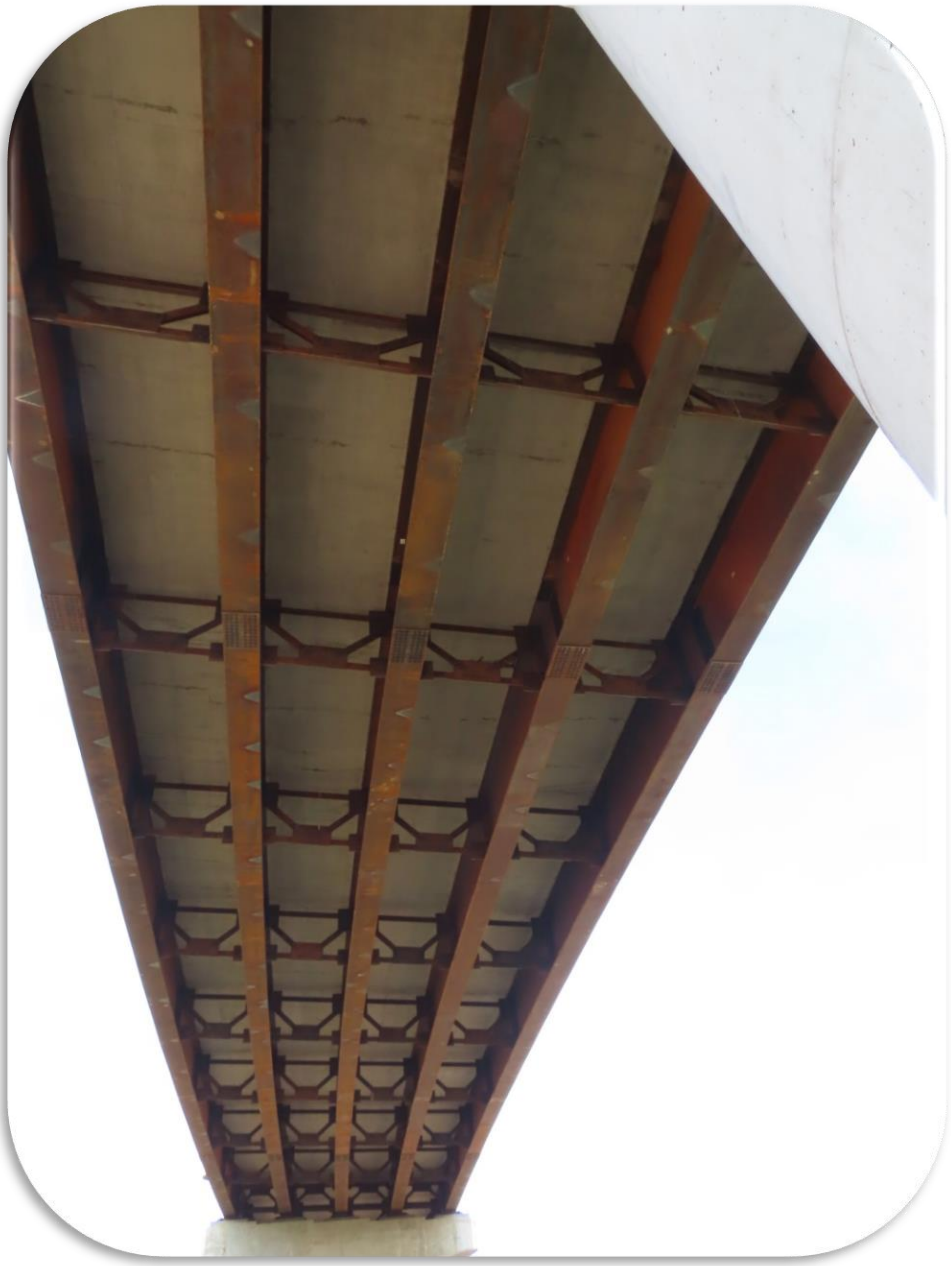

Figure 45. Underside of Rarus Structures - Silver Bow Creek - Bridge C - 2020 inspection, Span 2 overall view.

Rarus/Silver Bow Creek - Phase II - Bridge D

This bridge was constructed in December of 2019 using WJE's curing recommendations and consists of four spans with span lengths of 134, 165, 165, and 134 feet. Concrete deck thickness is 7-3/4 inches, which is supported on steel plate girders. During construction, placement No. 7 of this bridge deck was instrumented and monitored by WJE for temperature, relative humidity, and strain measurements (See Item 4.4b, page 105). The goal of this inspection was to document transverse cracks and correlate to the monitored data: temperature, relative humidity, and strain. Unfortunately, a polymer overly was installed (reportedly in July) and topside cracks could not be documented, so a visual inspection was performed from the underside of the bridge.

2020 Inspection

The deck inspection was performed by Robert Frazier on 8/27/2020. A polymer concrete overlay was present on the topside. Visual inspection and crack mapping were performed from the underside of deck (no traffic control). The underside condition of this bridge is good, with minimal transverse cracking noted (see Figure 46 and Figure 47). Ranking of the placements in visual cracking condition from worst to best: 3, 2, 1, 6, 7, 4, and 5. The cracking in the mid-span placements generally looked worse than in the placements over piers with the exception of Placement 4 which exhibited minimal cracking.

This bridge has an overall rating of 1.5.

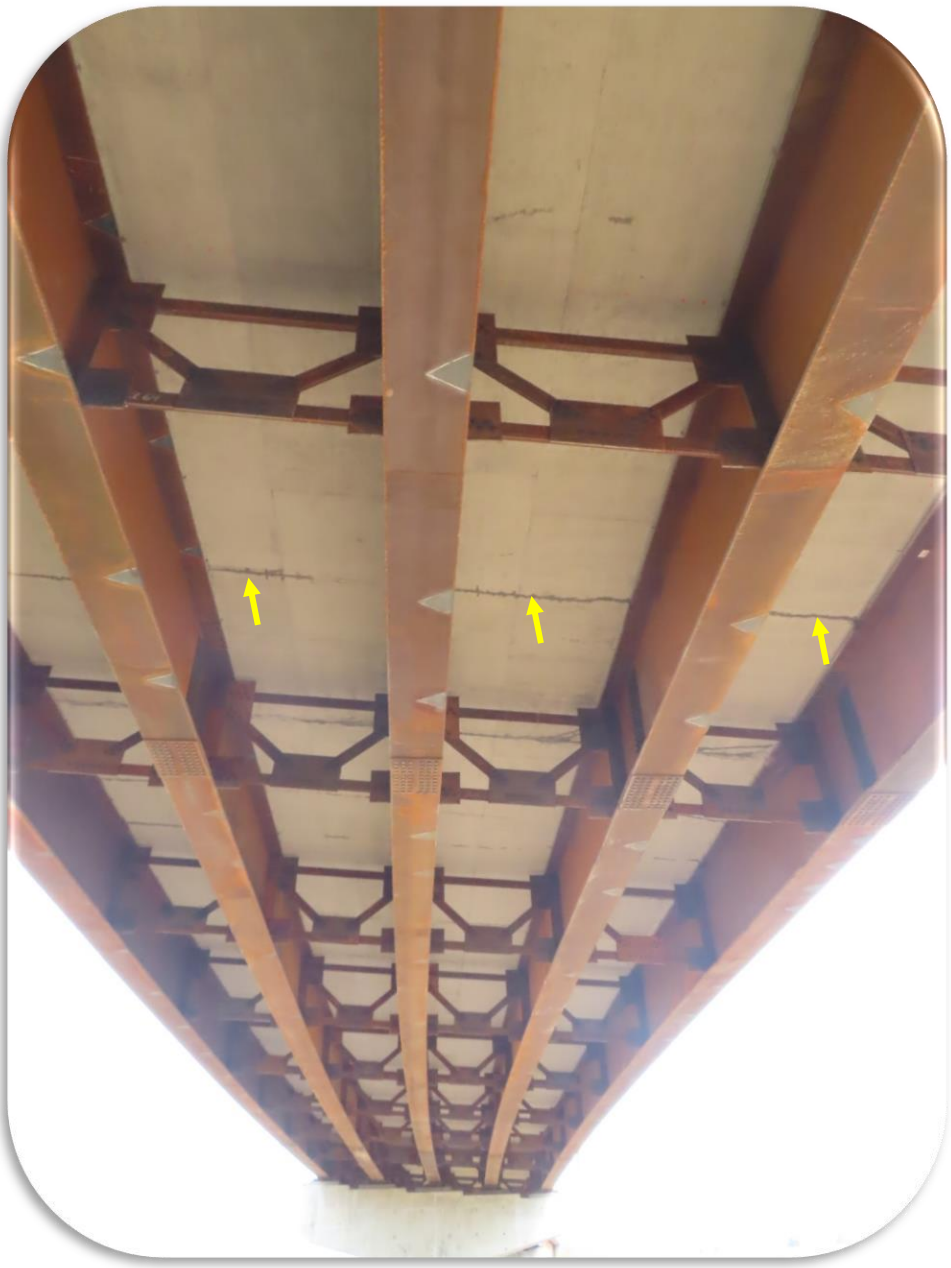

Figure 46. Underside of Rarus/Silver Bow Creek Bridge D - 2020 inspection - Span 2, Typical transverse crack at arrows.

Figure 47. Underside of Rarus/Silver Bow Creek Bridge D - 2020 inspection - Span 3, Typical transverse crack at arrows.

West Laurel Interchange - Phase I (Eastbound)

This bridge was constructed in June 2018 reportedly using WJE's curing recommendations and consists of three spans (153, 218, and 186 feet) with steel plate girders. Concrete deck thickness is 8-1/4 inches. Transverse deck cracking was reportedly noticed fairly early after construction, with some cracks reported during concrete placement of subsequent spans. Map cracking was reportedly observed but not until the Spring of 2019 and covers most of the deck. This deck also has isolated areas of near surface scaling. The map cracking and scaling were briefly investigated by WJE in 2020 by petrographically evaluating four concrete cores extracted from the deck. The petrographic evaluations were not conclusive on the cause of the scaling, but the map cracking was identified as plastic shrinkage cracking.

2019 Inspection

This bridge was not inspected by WJE, but an aerial photo taken in November 2019 (provided by MDT) was converted to a crack map and included in Appendix A. The cracking in the mid-span placements generally looked worse than in the placements over piers. Ranking of the placements in visual cracking condition from worst to best: 2, 1, 3, 5 and 4.

This bridge has an overall rating of 3.

2020 Inspection

A visual inspection was performed from the deck underside by Robert Frazier on 8/27/2020 (no traffic control). Crack mapping was performed from the underside for Placement 2 only; crack map is included in Appendix A. Ranking of the placements in visual cracking condition from worst to best: 2, 1, 3, 5, and 4. Notably in Placement 2, transverse cracks are closely spaced at 2 feet or less near the east end, and there are some areas exhibiting intersecting cracks. Typical crack conditions are shown in Figure 48 and Figure 49.

Additional observations of the cracking condition are as follows:

- Span 1 (East): moderate cracking one brace bay east of transition area from Placement 1 to Placement 4.
- Span 2: regular cracking in Placement 3; minimal cracking in Placements 4 and 5.
- Span 3: considerable cracking in Placement 2 (worst in this bridge).

This bridge has the same overall rating of 3 as in 2019 inspection.

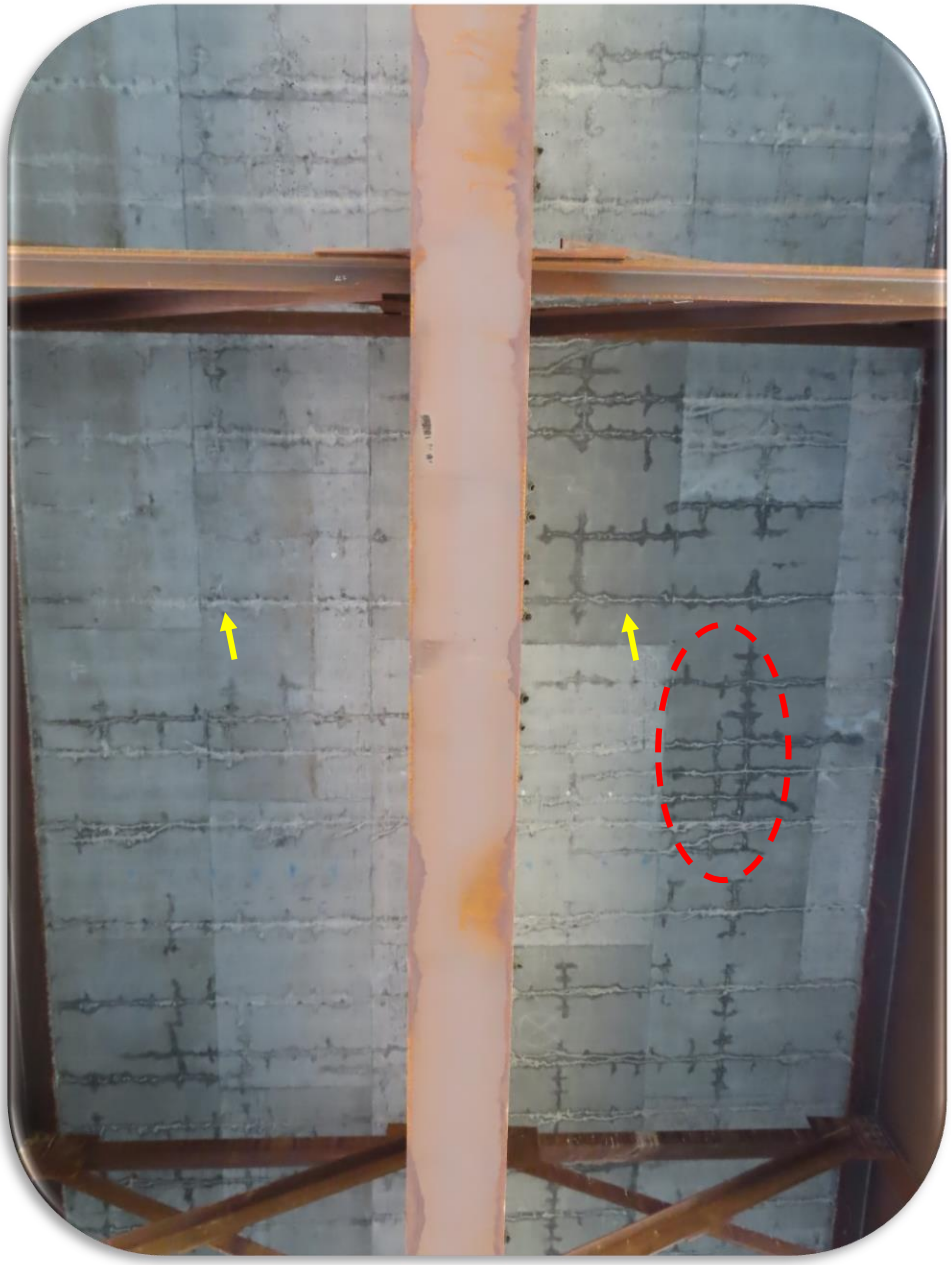

Figure 48. West Laurel Interchange - Phase I - 2020 inspection - Placement 2. Typical transverse crack at arrows. Red dotted oval indicates an area with intersecting cracks.

Figure 49. West Laurel Interchange - Phase I - 2020 inspection - Placement 1. Typical transverse crack at arrows.

West Laurel Interchange - Phase II (Westbound)

This bridge was constructed in October 2019 reportedly using WJE's curing recommendations and consists of three spans (150, 170, and 150 feet) with steel plate girders. Concrete deck thickness is 8-1/4 inches.

2020 Inspection

A visual inspection was performed from the deck underside by Robert Frazier on 8/27/2020 (no traffic control). Crack mapping was not performed. Overall, the bridge deck is in good condition with few transverse cracks. Some areas exhibiting intersecting cracks are observed in Placement 2. Typical crack conditions are shown in Figure 50 and Figure 51. The cracking in the mid-span placements generally looked worse than in the placements over piers. Ranking of the placements in visual cracking condition from worst to best: 2, 1, 3, 5, and 4.

Additional observations of the cracking condition are as follows:

- Span 1 (East): mild cracking one brace bay east of transition area from Placement 1 to Placement 4.
- Span 2: minimal cracking.
- Span 3: minimal cracking except for one brace bay west of transition area from Placement 2 to Placement 5.

This bridge has an overall rating of 1.5.

Figure 50. West Laurel Interchange - Phase II - 2020 inspection - Placement 1. Typical transverse crack at arrows.

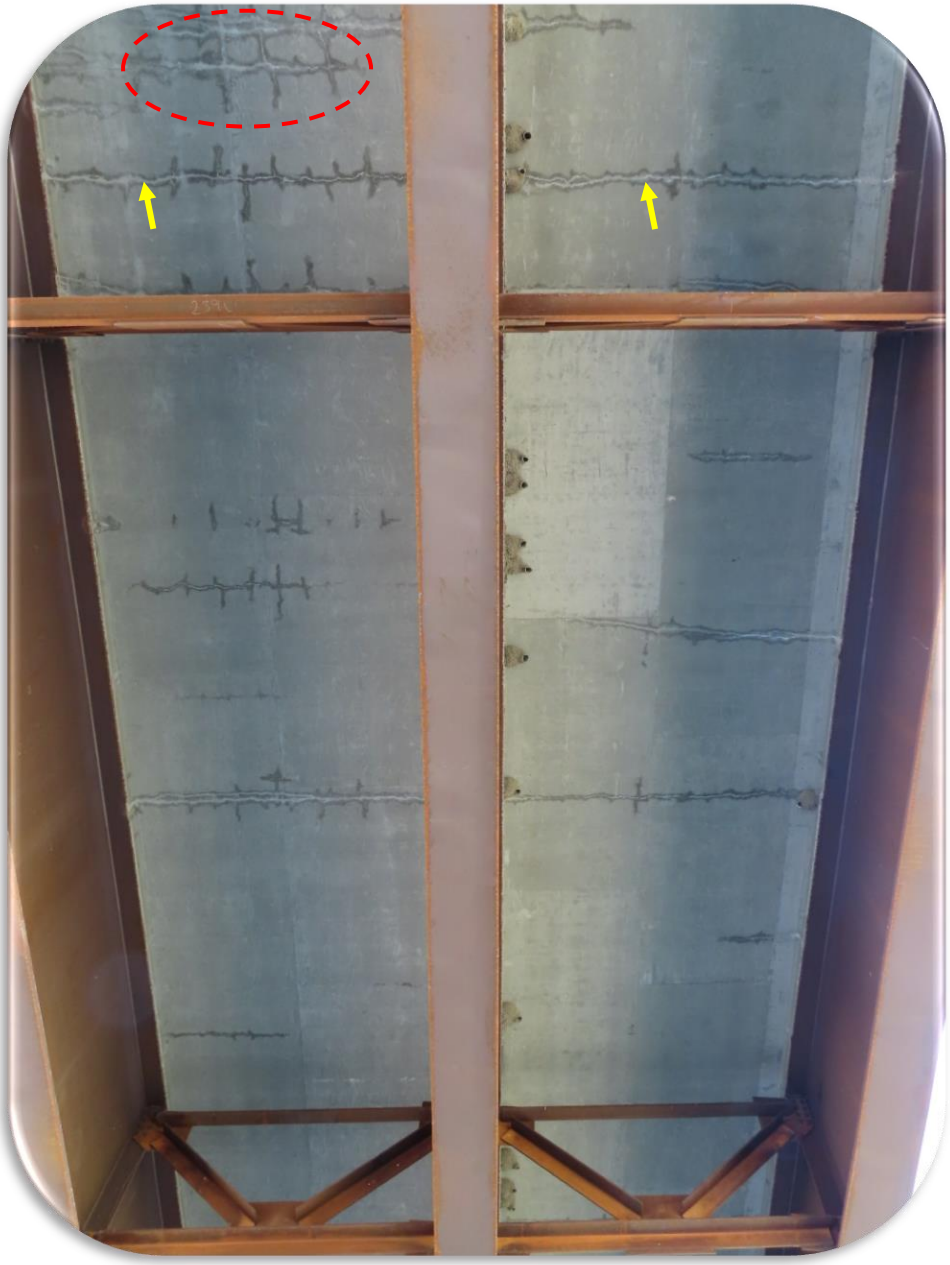

Figure 51. West Laurel Interchange - Phase II - 2020 inspection - Placement 2. Typical transverse crack at arrows. Red oval indicates an area with intersecting cracks.

Cracking Data Summary

In order to better understand the cracking characteristics of each bridge deck and ultimately for comparative purposes, cracking statistics were performed using the cracking frequency and width data obtained from the 2019 and 2020 field investigations. It was noted during the field inspections that cracks in traffic lanes further from the controlled lane (inspected lane) were more difficult to visual assess and would not be reliable for analysis and comparative studies. Thus, although the crack maps in Appendix A. show cracks in multiple lanes, only the cracks within the controlled traffic lane were counted in the statistics and analyses. From the crack maps, the number of cracks and total crack length were determined, and the crack density (the total crack length divided by the surveyed area) and the crack severity (the average crack width multiplied by the total crack length divided by the surveyed area) were calculated. The cracking data for each bridge is summarized by placement and presented in Table 5 through Table 15 for both 2019 and 2020 inspections. In the tables for deck topside only, the crack density and crack severity values are color coded using the same color scale (shown in Table 4) across the bridges to assist with relative comparisons between placements within the same bridge as well as between different bridges.

At Bonner Bridge Phase 1, the crack density and severity obtained in 2020 were slightly higher than those obtained in 2019. At the other bridges, a comparative assessment between the 2019 and 2020 inspections is not available because in the 2019 inspection crack mapping surveys were performed from the topside of the decks while in the 2020 inspection crack surveys were performed from the underside. It was also previously noted that at several bridges a new overlay was installed at a time between the two inspections, which altered exposure conditions of those decks and prevented mapping of the cracks.

Table 4. Color codes for crack density and crack severity for deck topside data

Color Scale	Crack density (ft/ft2)	Crack Severity (mil*ft/ft2)
	≤ 0.1	≤1
	0.1 to 0.2	1 to 3
	> 0.2	> 3

Table 5. Crack Data Summary - Russell Street Bridge - Phase I (NB) Topside - 2019 inspection

Placement #	Survey Length (ft)	Survey Width (ft)	Total Crack Length (ft)	Average Crack Width (mil)	Crack Density (ft/ft^2)	Crack Severity (mil*ft/ft^2)
1	90	12	291.3	25.8	0.27	6.95
2	81	12	221.0	29.1	0.23	6.62
3	90	12	229.1	16.4	0.21	3.48
4	94	12	316.6	14.2	0.28	3.99
5	94	12	340.8	12.0	0.30	3.63
All	**449**	**12**	**1398.8**	**19.1**	**0.26**	**4.88**

Table 6. Crack Data Summary - Russell Street Bridge - Phase I (NB) Underside - 2020 inspection

Placement #	Survey Length (ft)	Survey Width (ft)	Total Crack Length (ft)	Average Crack Width (mil)	Crack Density (ft/ft2)	Crack Severity (mil*ft/ft2)
1	90	12	163.17	-	0.15	-
3	66[1]	12	81.00	-	0.10	-
4	47[1]	12	14.83	-	0.03	-
All	**203**	**12**	**259.0**	**-**	**0.11**	**-**

Notes: [1] Crack mapping performed for partial length of deck placement.

Table 7. Crack Data Summary - Russell Street Bridge - Phase II (SB) Underside - 2020 inspection

Placement #	Survey Length (ft)	Survey Width (ft)	Total Crack Length (ft)	Average Crack Width (mil)	Crack Density (ft/ft2)	Crack Severity (mil*ft/ft2)
1	90	12	35.58	-	0.03	-
3	66	12	20.67	-	0.03	-
4	47	12	71.83	-	0.13	-
All	**203**	**12**	**128.1**	**-**	**0.05**	**-**

Table 8. Crack Data Summary - Capitol Cedar Bridge - Phase I (NB) Topside - 2019 inspection

Placement #	Survey Length (ft)	Survey Width (ft)	Total Crack Length (ft)	Average Crack Width (mil)	Crack Density (ft/ft2)	Crack Severity (mil*ft/ft2)
3	104	12	194.2	20.2	0.16	3.15
5	108	12	195.6	17.5	0.15	2.64
All	**212**	**12**	**389.8**	**18.8**	**0.15**	**2.89**

Table 9. Crack Data Summary - Capitol Cedar Bridge - Phase II (NB) Topside - 2019 inspection

Placement #	Survey Length (ft)	Survey Width (ft)	Total Crack Length (ft)	Average Crack Width (mil)	Crack Density (ft/ft2)	Crack Severity (mil*ft/ft2)
2	104	12	241.3	20.0	0.19	3.87
5	108	12	181.6	17.5	0.14	2.45
All	**212**	**12**	**422.8**	**18.7**	**0.17**	**3.15**

Table 10. Crack Data Summary - Bonner Bridge - Phase I (EB) Topside - 2019 inspection

Placement #	Survey Length (ft)	Survey Width (ft)	Total Crack Length (ft)	Average Crack Width (mil)	Crack Density (ft/ft2)	Crack Severity (mil*ft/ft2)
1	39	12	31.5	13.33	0.07	0.90
2	88	12	90.7	16.67	0.09	1.43
3	101	12	42.8	20.00	0.04	0.71
4	122	12	277.8	19.07	0.19	3.62
5	122	12	326.5	17.71	0.22	3.95
All	**472**	**12**	**769.3**	**18.00**	**0.14**	**2.45**

Table 11. Crack Data Summary - Bonner Bridge- Phase I (EB) Topside - 2020 inspection

Placement #	Survey Length (ft)	Survey Width (ft)	Total Crack Length (ft)	Average Crack Width (mil)	Crack Density (ft/ft2)	Crack Severity (mil*ft/ft2)
1	39	12	61.75	14.3	0.13	1.88
2	88	12	62.75	18.2	0.06	1.08
3	101	12	59.25	17.1	0.05	0.84
4	122	12	463.50	16.9	0.32	5.35
5	122	12	370.83	17.3	0.25	4.39
All	**472**	**12**	**1018.1**	**17.0**	**0.18**	**3.05**

Table 12. Crack Data Summary - Phase II - Bonner Bridge (WB) Topside - 2019 inspection

Placement #	Survey Length (ft)	Survey Width (ft)	Total Crack Length (ft)	Average Crack Width (mil)	Crack Density (ft/ft2)	Crack Severity (mil*ft/ft2)
1	73	12	17.6	5.0	0.04	0.19
2	154	12	41.0	5.0	0.04	0.19
3	130	12	40.8	5.0	0.03	0.17
4	122	12	29.0	5.0	0.02	0.10
5	122	12	68.8	5.0	0.05	0.23
All	**601**	**12**	**197.2**	**5.0**	**0.03**	**0.17**

Table 13. Crack Data Summary - West Laurel Bridge - Phase I (EB) Topside - 2019 inspection

Placement #	Survey Length (ft)	Survey Width (ft)	Total Crack Length (ft)	Average Crack Width (mil)	Crack Density (ft/ft2)	Crack Severity (mil*ft/ft2)
1	124	12	152.5	--	0.11	--
2	109	12	283.7	--	0.23	--
3	119	12	118.7	--	0.08	--
4	113	12	9.6	--	0.02	--
5	84	12	121.6	--	0.03	--
All	**549**	**12**	**686.1**	**--**	**0.10**	**--**

Note: Field inspection not performed by WJE for West Laurel Bridge. Cracking evaluated based on ortho mosaic photos provided by MDT. No crack width data is available.

Table 14. Crack Data Summary - West Laurel Bridge - Phase I (EB) Underside - 2020 inspection

Placement #	Survey Length (ft)	Survey Width (ft)	Total Crack Length (ft)	Average Crack Width (mil)	Crack Density (ft/ft2)	Crack Severity (mil*ft/ft2)
2	109	12	486.47	-	0.37	-

Table 15. Crack Data Summary - Rarus/Silver Bow Creek Bridge D Underside - 2020 inspection

Placement #	Survey Length (ft)	Survey Width (ft)	Total Crack Length (ft)	Average Crack Width (mil)	Crack Density (ft/ft2)	Crack Severity (mil*ft/ft2)
1	90	6	38.25	-	0.04	-
2	85	11	44.92	-	0.04	-
3	85	17	102.67	-	0.10	-
4	90	0	0.00	-	0.00	-
5	80	0	0.00	-	0.00	-
6	80	7	45.25	-	0.05	-
7	80	3	18.63	-	0.02	-
All	**590**	**44**	**249.7**	**-**	**0.03**	**-**

Analyses and Discussion

In this section, effects of a number of construction and design factors on deck cracking are analyzed and discussed based on the project records and crack data obtained from topside surveys during the 2019 field inspections. This analysis is not intended to elicit statistically valid conclusions related to the various possible factors, since sufficient data is not available, but to provide an indication of what factors might be most probable and to focus further analysis and research. Crack data from the 2020 field inspections was excluded from the analyses because the crack mapping was mostly performed from the underside. The factors examined include:

- Construction factors:
  - Deck placement time (Month)
  - Ambient and concrete temperatures
- Design factors:
  - Deck thickness
  - Bridge bearing type
  - Span length
  - Span bearing type
  - Placement location
  - Placement length

Effects of Deck Placement Time (Month)

Crack density and crack severity data was summarized by placement time (month) in Table 16, and presented graphically in Figure 52 and Figure 53. Based on these table and figures, placement time appears to have an impact on deck cracking. Decks placed in colder weather (March) exhibited more severe cracking than those placed in warmer weather (June, August, and September). Possible causes for the more severe cracking at the March placements (all Russell Street bridges) include the low ambient temperatures, the use of heating hoses, heating from the top, removal of heating, or the combined effect. This is discussed in the next section.

Table 16. Crack Data Summarized by Deck Placement Time

Placement Time (Month)	Crack Density (ft/ft^2)			Crack Severity (mil*ft/ft^2)		
	Average	Standard Deviation	No. of placements	Average	Standard Deviation	No. of placements
Mar	0.26	0.04	5	4.93	1.70	5
Jun	0.09	0.08	5	-	-	-
Aug	0.15	0.00	2	2.89	0.36	2
Sep	0.04	0.01	5	0.18	0.05	5
Oct	0.12	0.08	5	2.12	1.55	5

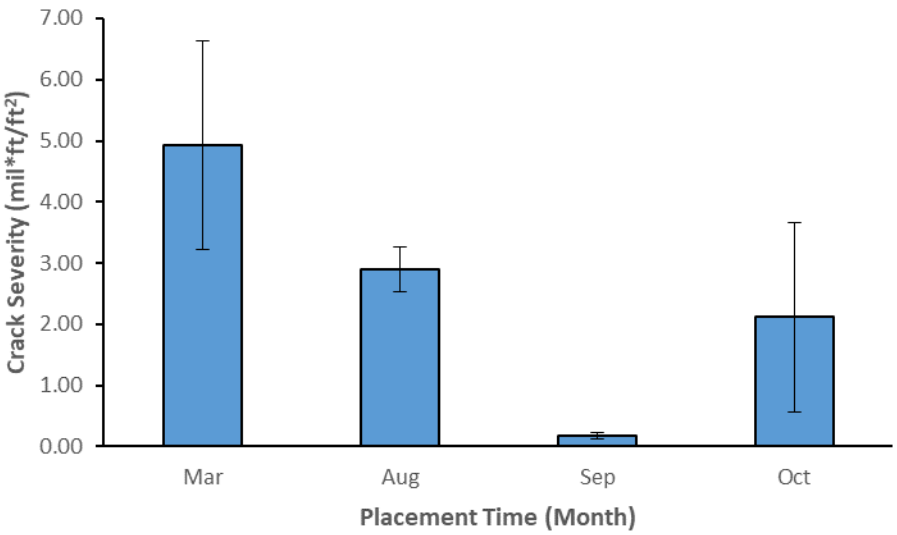

Figure 52. Deck placement time vs crack density. Each error bar indicates ±one standard deviation.

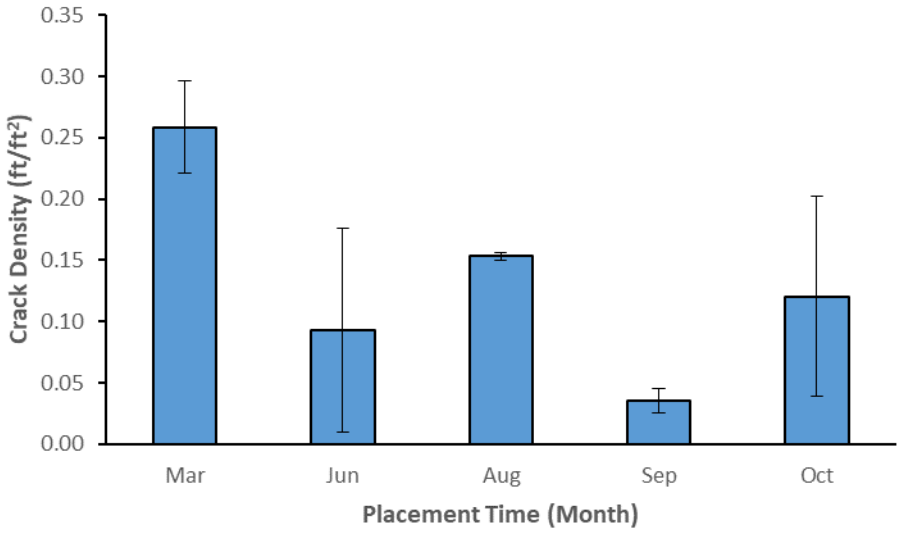

Figure 53. Deck placement time vs crack severity. Each error bar indicates ±one standard deviation.

Effects of Heating, Ambient and Concrete Temperatures During Curing

WJE performed a limited analysis of the temperature data provided by MDT at select bridges. The project records indicate that four temperature sensors were installed at each deck location, including one sensor measuring the ambient temperature and three measuring concrete temperatures at the top and bottom reinforcement mats and at mid-height of deck. The four temperature sensors were installed at up to three locations longitudinally along each deck placement.

Examples of concrete and ambient temperature data at decks without heating and with heating during concrete curing are presented in Figure 54 and Figure 55, respectively. At the deck without heating, the three concrete temperature profiles were almost identical throughout curing. At the deck with heating hoses placed on top of concrete (Russell Street Bridge Phase I, Placement 1), temperatures of one concrete sensor was unusually higher than the other two concrete sensors, and the peak concrete temperatures were much higher than the ambient temperature. As mentioned in the Field Inspections section, this deck was placed in March 2019, with heater hoses and insulation blankets placed on top of the deck the same day of concrete casting whereas the underside of the deck was not heated or insulated from the low ambient temperatures other than by the deck formwork. This may be the cause for the significant temperature differences among the three concrete sensors; the sensor with highest temperatures was likely at the top mat of deck reinforcement and heated up more than the other sensors below.

For each sensor location, the difference between the average concrete temperature (average of 3 sensors) and the ambient temperature, ΔT_{ca}, and the difference between the highest and lowest concrete temperatures among the three concrete sensors, ΔT_{cc}, were calculated at the time of peak hydration temperature. Results from the different locations within each placement were averaged. Data of ΔT_{ca}, ΔT_{cc}, crack density and crack severity are summarized in Table 17. Plots of ΔT_{ca} and ΔT_{cc} versus the two cracking indicators are presented in Figure 56 and Figure 57.

Based on these table and figures, more severe cracking appeared to occur in deck placements that had greater ΔT_{ca} and ΔT_{cc}. It is worth noting that the most severe cracking occurred at the Russel Street Bridge Phase I where the larger differences in concrete temperatures, particularly Placement 1, was possibly due to the early installation of heating hoses on top of the deck as discussed above. It is possible that the concrete temperature gradients over the deck thickness due to uneven heating during curing resulted in early-age cracks (see Field Inspections section for reported cracking after curing materials were removed), and those cracks have widened due to subsequent thermal and shrinkage movements.

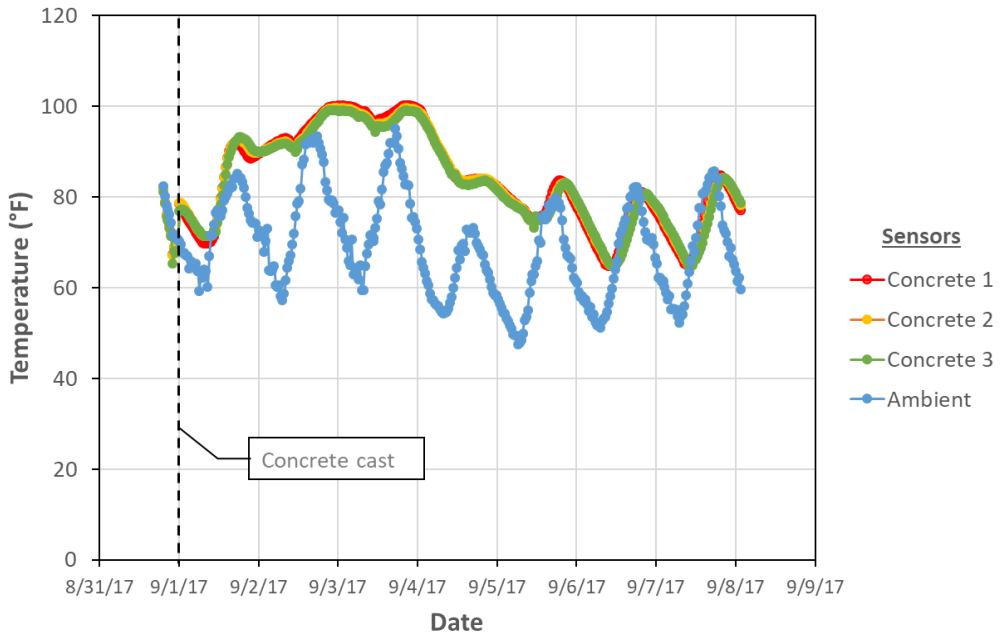

Figure 54. Curing temperature data without heating. Capitol-Cedar Bridge Phase II (SB), Placement 5, south sensor location

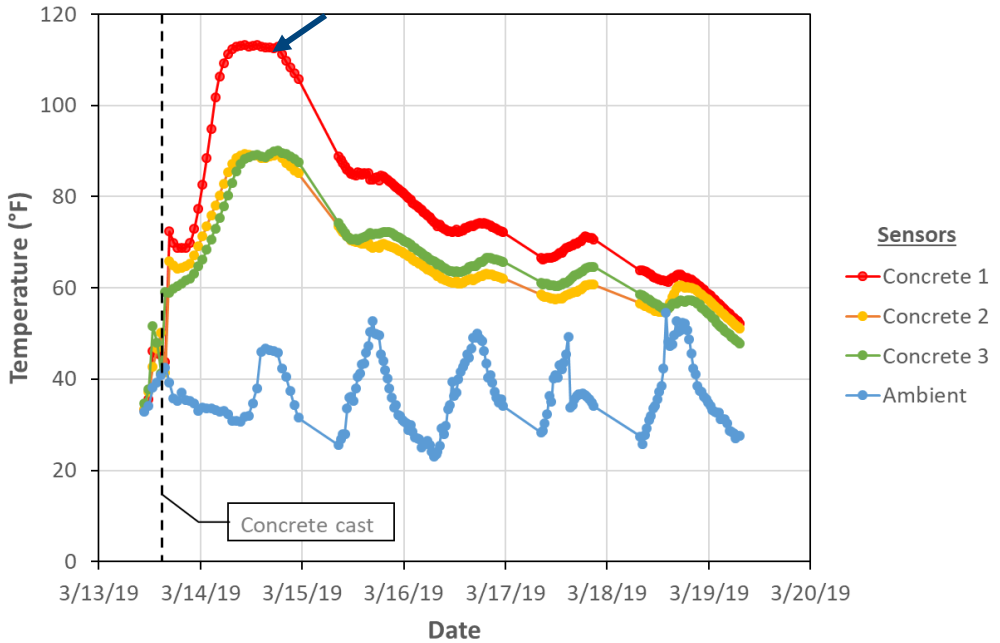

Figure 55. Curing temperature data with heating hoses on top of concrete. Russell Street Bridge Phase I (NB), Placement 1, sensor location 3. Arrow indicates unusually high temperatures in one concrete sensor, possibly due to uneven heating.

Table 17. Cracking and Temperature Data by Deck Placement

Bridge	Placement	Crack Density (ft/ft2)	Crack Severity (mil*ft/ft2)	ΔT_{ca} (°F)	ΔT_{cc} (°F)
Capitol-Cedar Phase II (SB)	2	0.16	3.15	9.0	3.7
Capitol-Cedar Phase II (SB)	5	0.15	2.64	5.1	2.9
Russell St - Phase 1	1	0.27	6.95	58.7	18.6
Russell St - Phase 1	2	0.23	6.62	43.1	3.5
Russell St - Phase 1	3	0.21	3.48	46.5	2.3
Russell St - Phase 1	4	0.28	3.99	55.7	1.3
Russell St - Phase 1	5	0.30	3.63	-	-
West Laurel - Phase I	1	0.11	-	31.5	4.5
West Laurel - Phase I	2	0.23	-	30.7	3.4
West Laurel - Phase I	3	0.08	-	30.9	3.5
West Laurel - Phase I	4	0.02	-	16.4	2.8
West Laurel - Phase I	5	0.03	-	31.0	5.6

ΔT_{ca} = difference between the highest concrete temperature and ambient temperature at peak concrete temperature

ΔT_{cc} = difference between the highest and lowest concrete temperatures among the three concrete sensors at peak concrete temperature

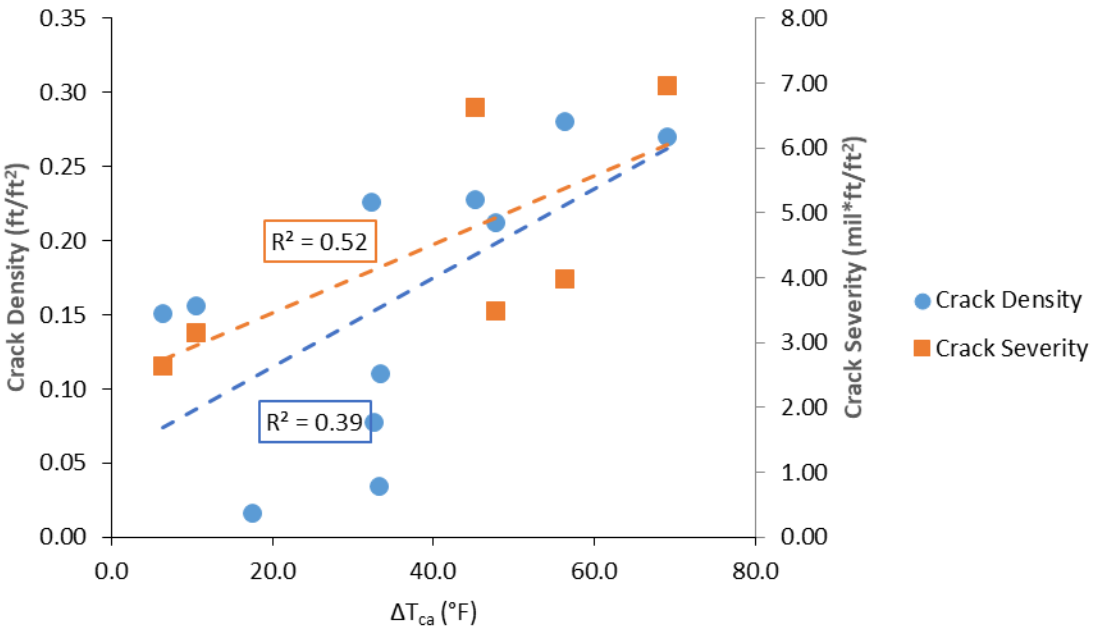

Figure 56. ΔT_{ca} vs Crack Density/Severity.

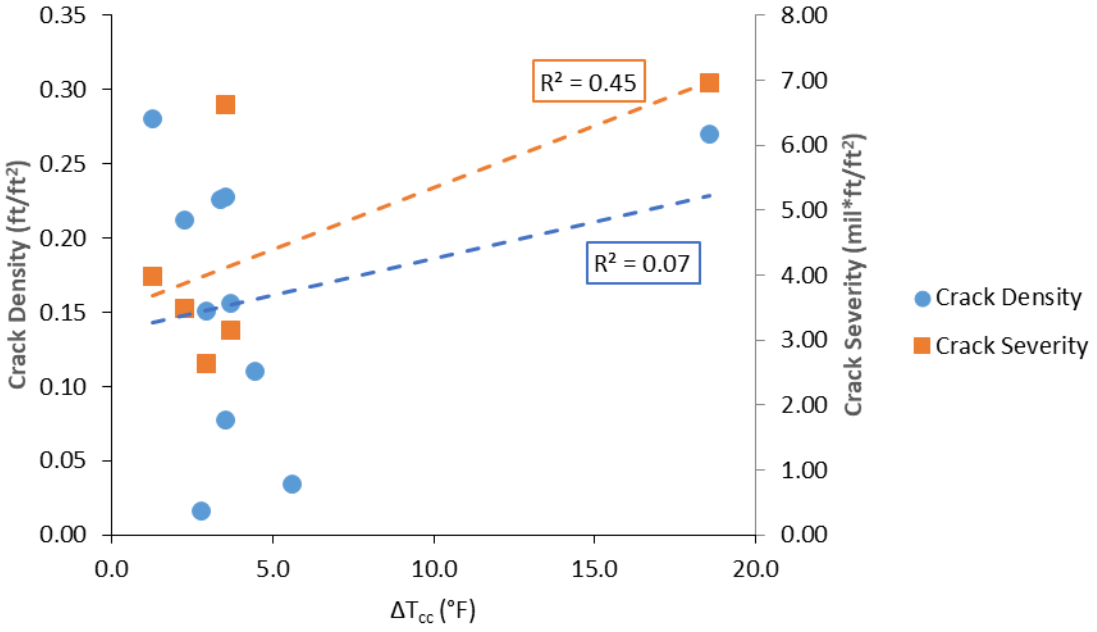

Figure 57. ΔT_{cc} vs Crack Density/Severity.

Effects of Deck Thickness and Bridge Bearing Type

At the bridges where crack mapping was performed, the superstructures consist of continuous steel girders. In the longitudinal direction, each bridge has one or more fixed bearings in addition to expansions bearings. The fixed bearings restrain longitudinal movements of the girders, which could affect stress conditions in the concrete deck under thermal, creep, and shrinkage deformations. Crack data, deck thickness and the number of fixed bearings for each bridge are summarized in Table 18.

Plots of deck thickness versus crack density and crack severity are presented in Figure 58 and Figure 59. Based on these figures, thinner decks appear to exhibit more severe cracking.

Plots of the number of fixed bearings versus crack density and crack severity are presented in Figure 60 and Figure 61. Based on these figures, the number of fixed bearings appears to have no effect on cracking.

Table 18. Summary of Crack Data for Each Bridge

Bridge Short Name	No. of Fixed Bearings	Nominal Deck Thickness (in)	Crack Density (ft/ft^2)	Crack Severity ($mil*ft/ft^2$)
Capitol-Cedar Bridge - Phase I (NB)	1	8 1/2	0.17	3.15
Capitol-Cedar Bridge - Phase II (SB)	1	8 1/2	0.15	2.89
West Laurel Bridge - Phase 1 (EB)	2	8 1/4	0.10	-
Russell Street Bridge - Phase I (NB)	2	8 1/4	0.26	4.88
Bonner Bridge - Phase I (EB)	2	9 1/2	0.14	2.45
Bonner Bridge - Phase II (WB)	2	9 1/2	0.03	0.17

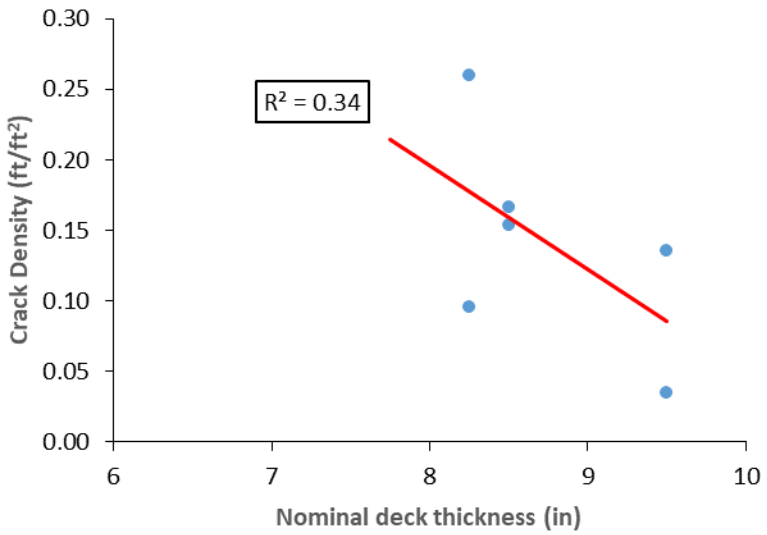

Figure 58. Deck Thickness vs Crack Density. Each data point represents one bridge.

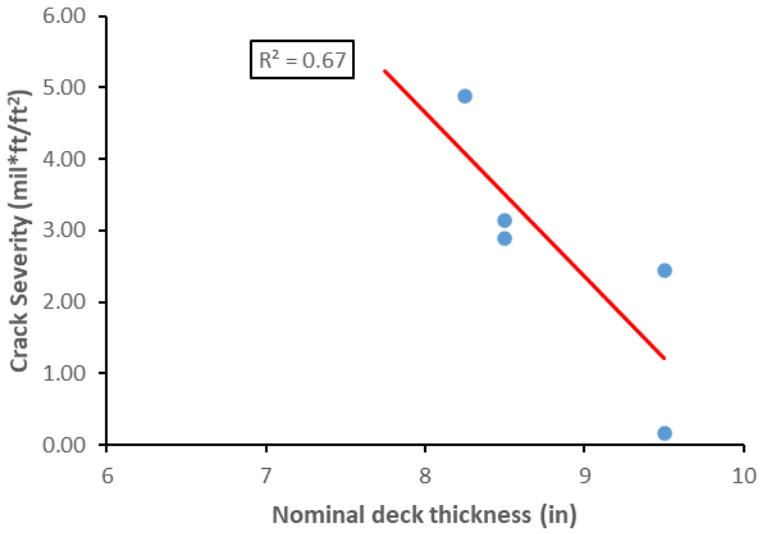

Figure 59. Deck Thickness vs Crack Severity. Each data point represents one bridge.

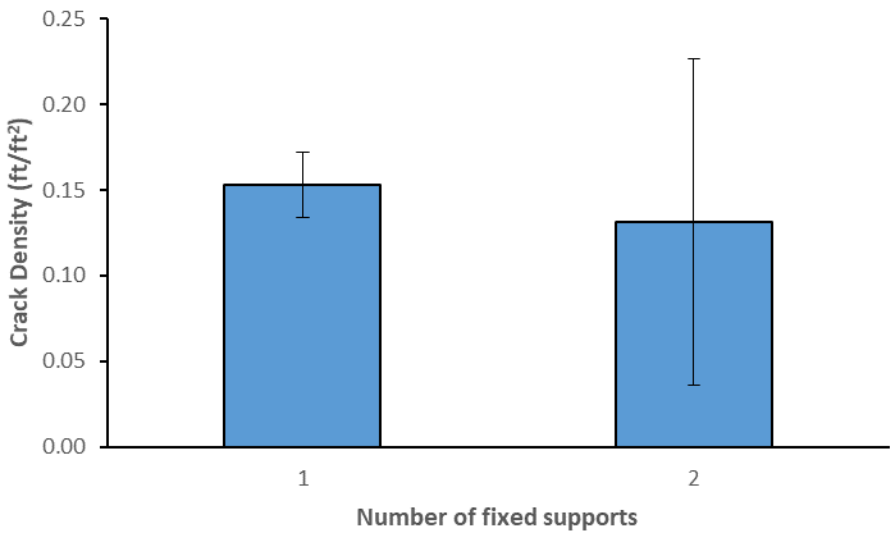

Figure 60. Number of fixed bearings vs Crack Density. Each error bar indicate ±one standard deviation.

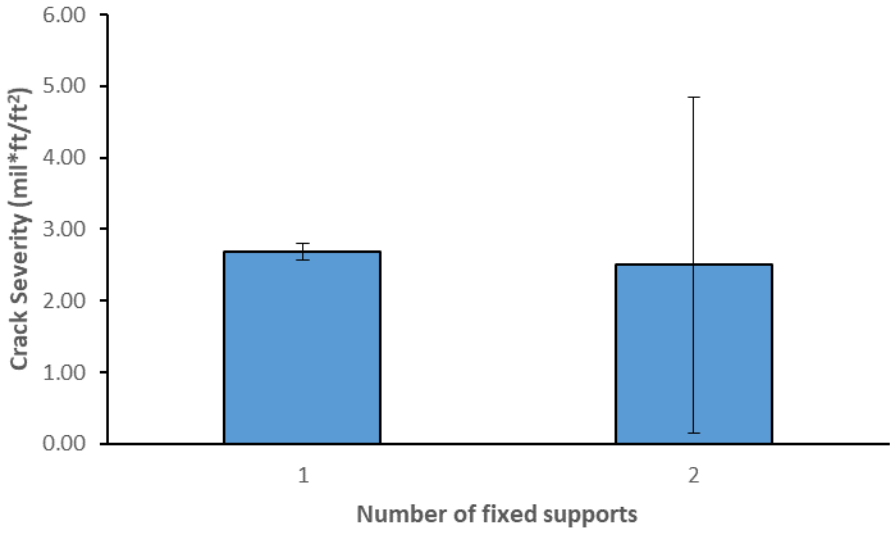

Figure 61. Number of fixed bearings vs Crack Severity. Each error bar indicate ±one standard deviation.

Effects of Span Length and Span Bearing Type

In the longitudinal direction, each span has two bearings which could be of fixed or expansion type. As mentioned above, fixed bearings restrain longitudinal movements of the girders, which could affect stress conditions in the concrete deck under thermal, creep and shrinkage deformations. Crack density and crack severity were determined for each span of the bridges and summarized by the type of bearing in Table 19 and presented graphically in Figure 62 and Figure 63. Based on these table and figures, no relationship between crack condition and span bearing type is observed.

Plots of crack density and crack severity versus span length are presented in Figure 64 and Figure 65. Based on these figures, no relationship between crack condition and span length is observed.

Table 19. Crack Data Summary by Bearing Type

Bearing Types	Crack Density (ft/ft^2)			Crack Severity ($mil*ft/ft^2$)		
	Average	Standard Deviation	No. of Spans	Average	Standard Deviation	No. of Spans
Fixed-Expansion	0.14	0.07	10	2.48	1.51	10
Fixed-Fixed	0.12	0.10	3	2.69	2.75	3

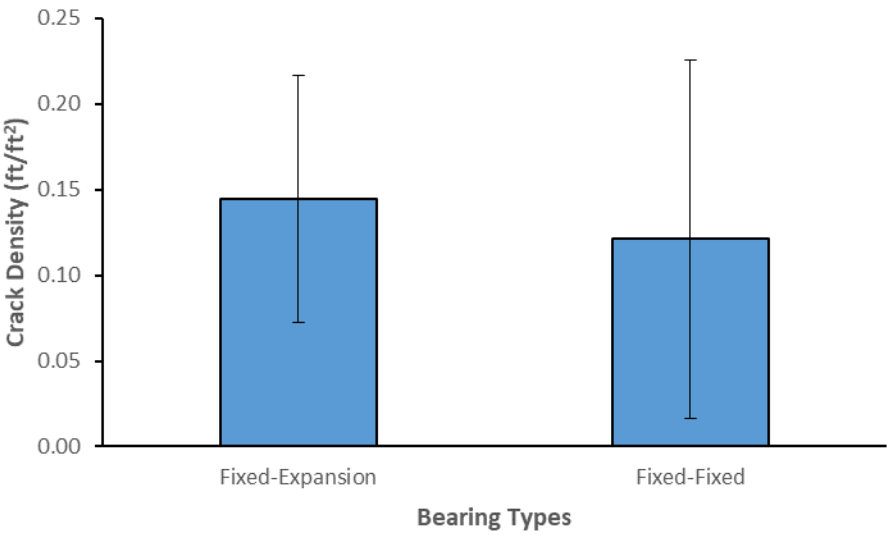

Figure 62. Span Support Condition vs Crack Density. Each error bar indicate ±one standard deviation.

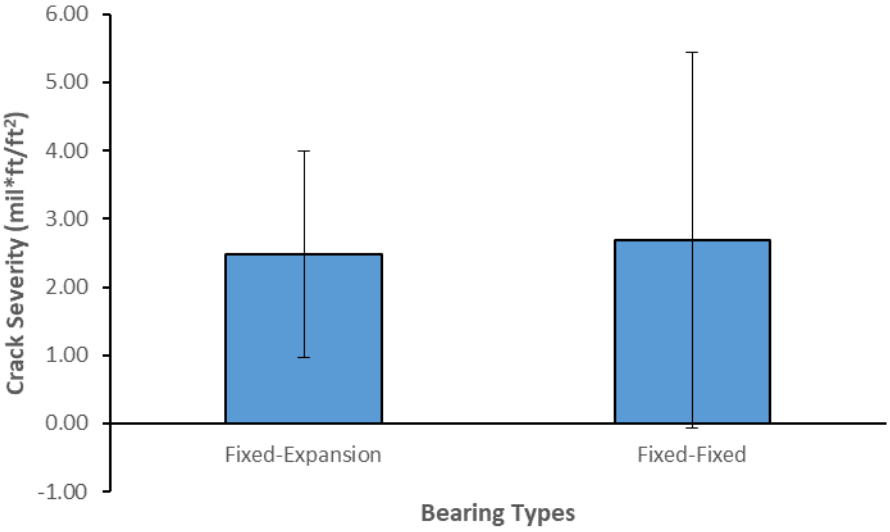

Figure 63. Span Support Condition vs Crack Severity. Each error bar indicate ±one standard deviation.

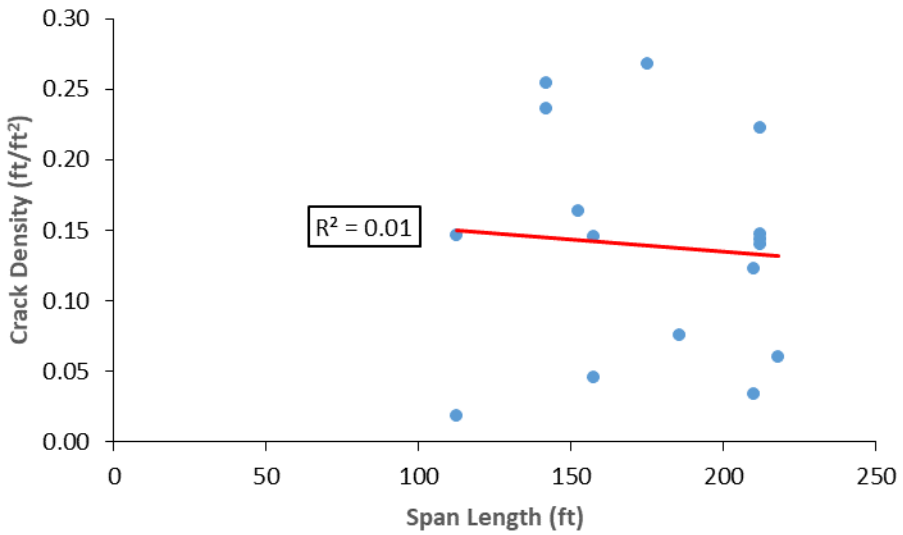

Figure 64. Span Length vs Crack Density. Each error bar indicate ±one standard deviation.

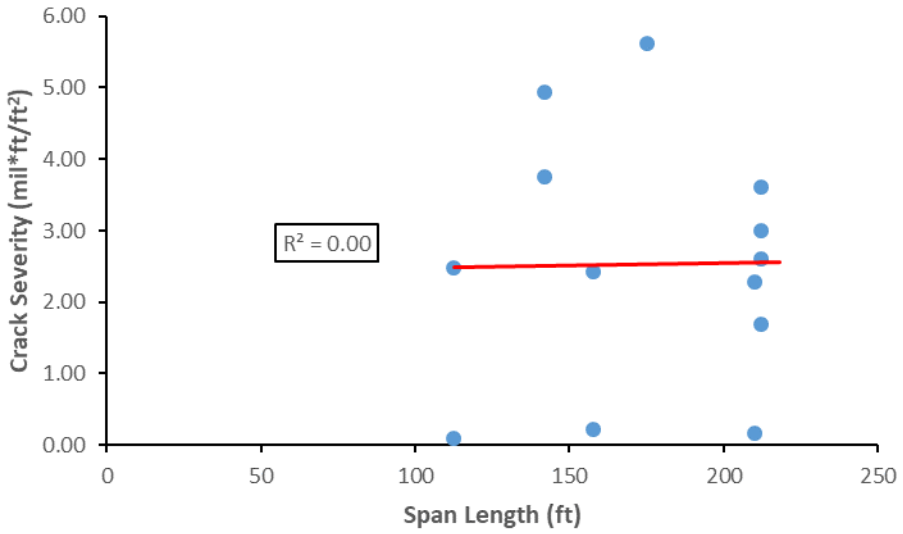

Figure 65. Span Length vs Crack Severity. Each error bar indicate ±one standard deviation.

Effects of Deck Placement Location and Placement Length

Crack density and crack severity data was summarized by placement location in Table 20, and presented graphically in Figure 66 and Figure 67. Based on these table and figures, no relationship is observed between cracking condition and placement location. While the placement location does not have consistent effect across different bridges, certain bridges have placements with both high and low crack density values, suggesting that practices related to placement may have some impact on cracking.

Plots of crack density and crack severity versus placement length are presented in Figure 68 and Figure 69. Based on these figures, no relationship is observed between cracking condition and the placement length.

Table 20. Crack Data Summary by Deck Placement Location

Placement Location	Crack Density (ft/ft^2)			Crack Severity ($mil*ft/ft^2$)		
	Average	Standard Deviation	No. of Placements	Average	Standard Deviation	No. of Placements
Exterior span	0.13	0.09	8	2.19	2.63	6
Interior span	0.12	0.08	6	2.90	2.60	5
Over Pier	0.14	0.11	10	2.58	1.59	8

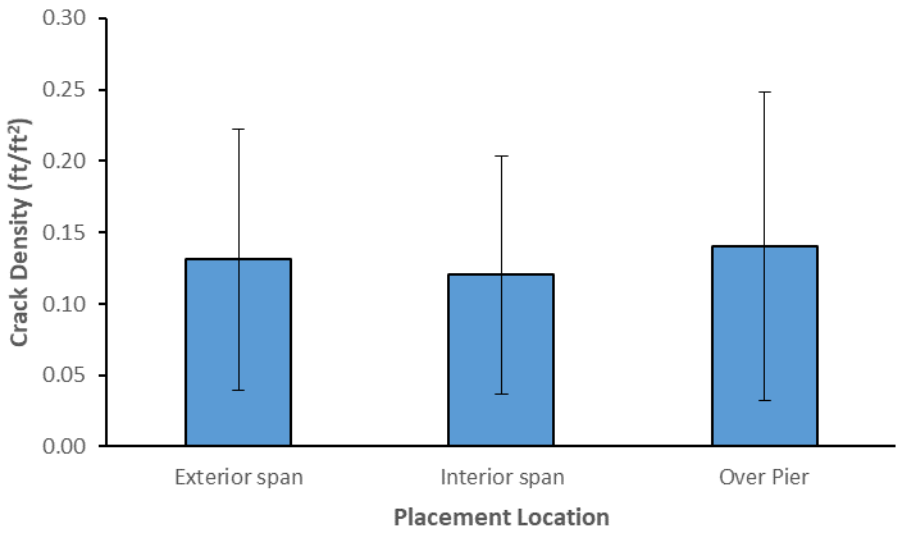

Figure 66. Deck Placement Location vs Crack Density. Each error bar indicate ±one standard deviation.

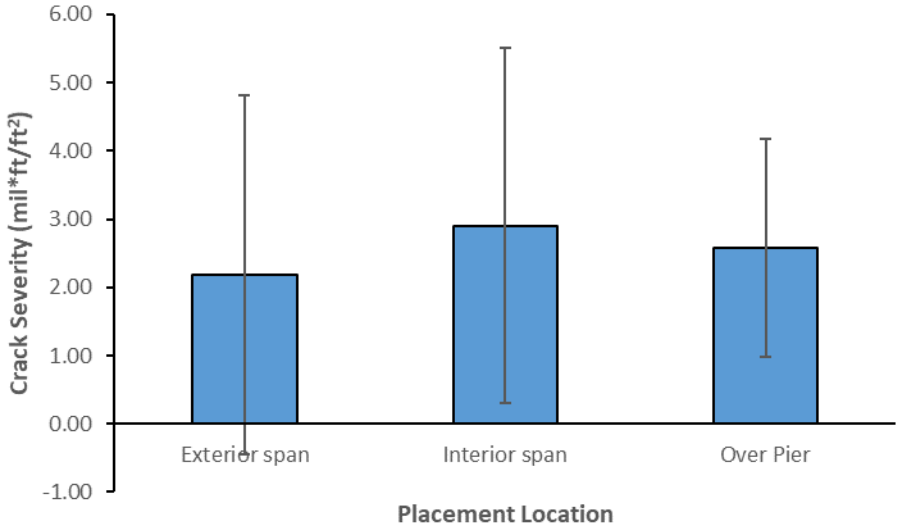

Figure 67. Deck Placement Location vs Crack Severity. Each error bar indicate ±one standard deviation.

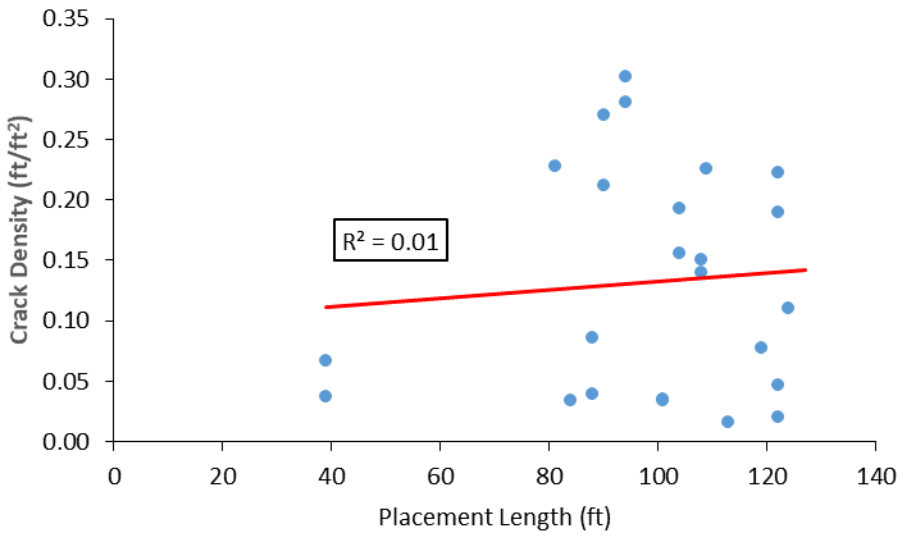

Figure 68. Deck Placement Length vs Crack Density. Each error bar indicate ±one standard deviation.

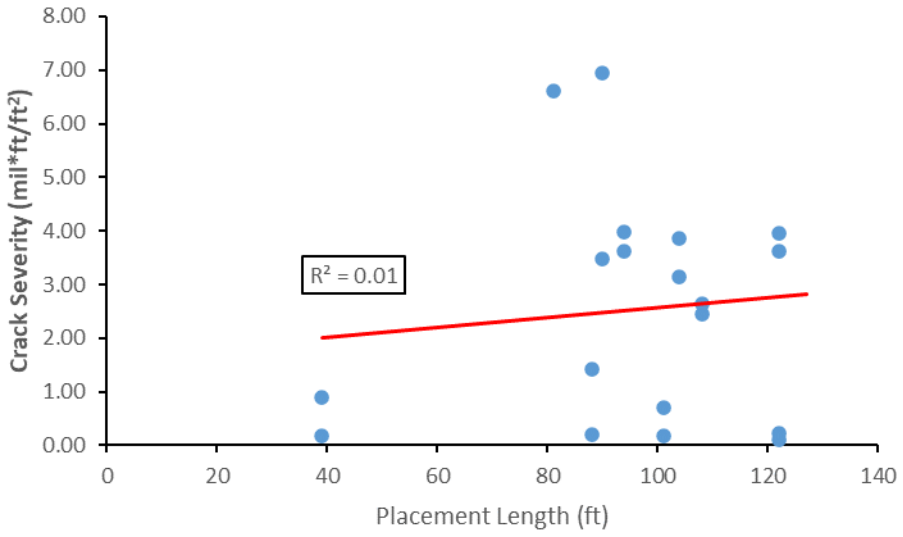

Figure 69. Deck Placement Length vs Crack Severity. Each error bar indicate ±one standard deviation.

Summary of Field Inspection and Cracking Data Analyses

The overall visual rating and cracking condition of all the bridges inspected are summarized in Table 21 and notable observations are as follows:

- GPR surveys at crack locations on the topside of four bridge decks indicate that the transverse cracks were generally in line with the transverse (topmost) deck reinforcement.
- Transverse "jump" cracks were observed at both northbound and southbound Capitol-Cedar bridges. Location of the "jump" part relative to the steel girders appears to be consistent with observations in WJE previous investigations in which it was hypothesized that the transverse cracks originated from the girders where the restraint is the greatest, then propagated away from the girders with time, and finally bent towards each other, resulting in the "jump".
- Based on observations from both the deck topside and underside, it appears that the majority of transverse cracks are through the deck thickness.
- Short, hairline, closely spaced longitudinal cracks were observed along transverse cracks on the deck underside at several bridges. In some cases, the longitudinal cracks extend across several transverse cracks, resulting in intersecting cracking patterns. It appears that these longitudinal cracks were not through the deck thickness. While the origin of these cracks is not well understood, one possible cause is a rapid loss of moisture from the concrete surface (e.g., when the bottom formwork was removed, and the deck underside was exposed to the air with low humidity).
- Differences in cracking condition between spans and placements within the same bridge were observed; however, the trend is not consistent. At some bridges, placements over piers have more severe cracking than those near mid-spans while at other bridges the trend was reversed or there was no trend between the two groups of placements.
- For cold weather placements (e.g., Russell Street bridge Phase I), early installation of heating hoses on top of deck during curing can lead to overheating and uneven heating of concrete, which possibly causes early-age cracks that become more severe with time.
- Cracking appears to be less severe in decks with greater thicknesses, consistent with literature and findings from WJE's previous investigations.
- Cracking conditions in 2019 and 2020 were generally similar at most of the bridges. At several bridges, a polymer concrete overlay was placed between the two inspections, which prevented observations of the original deck topside in the 2020 inspection and altered exposure condition of the decks. While no cracking was noted in the overlays at the time of inspection, conditions of the overlays should be monitored to assess their effectiveness.

Table 21. Summary of Overall Visual Rating and Cracking Condition

Bridge ID	Bridge Short Name	Overall Visual Rating[1]	Deck Cracking Condition
07006	Russell Street Bridge - Phase I (NB)	3.0	A lot of transverse cracks, with crack spacing of 2 to 4 feet and crack widths typically from 15 to 25 mils.
07006	Russell Street Bridge - Phase II (SB)	1.5	Transverse cracking present but milder than the Phase I bridge.
06253	Garrison Bridge	1.0	Very good condition with very few transverse cracks noted. Transverse crack spacing was generally 8 to 10 feet.
05943	Whitehall Bridge	1.0	Very good condition with very minimal transverse cracks noted.
01642	Capitol-Cedar Bridge - Phase I (NB)	4.0	Severe transverse cracking throughout, with many characteristic "jump" cracks. Transverse crack spacing was typically 2 to 6 feet and crack widths from 15 to 20 mils.
01641	Capitol-Cedar Bridge - Phase II (SB)	3.0	Significant cracking, but slightly less than the Phase I bridge. Transverse crack spacing is typically 4 to 5 feet and crack widths from 10 to 20 mils.
01434	Bonner Bridge - Phase I (EB)	1.5	Overall good condition. Transverse crack spacing was as close as 3 to 5 feet at a few sections in the two placements over piers, and generally more than 8 feet in the other placements. Crack widths from 15 to 20 mils.
01435	Bonner Bridge - Phase II (WB)	1.0	Very good condition with few transverse cracks with crack widths of 5 mils or less.
01741	West Laurel Bridge - Phase 1 - (EB)	3.0	Significant transverse cracking in the two placements at end spans with crack spacing as close as 2 to 5 feet. Minimal cracking in other placements.
01742	West Laurel Bridge - Phase 2 - (WB)	1.5 (2020 only)	Good condition, with minimal transverse cracking noted.
01104	Rarus-Silver Bow Creek - Phase I - Bridge A	1.0 (2019) 1.5 (2020)	Good condition, with minimal transverse cracking noted. Overlay placed between two inspections.
01105	Rarus-Silver Bow Creek - Phase II - Bridge B	1.0 (2020 only)	Good underside condition, with minimal transverse cracking noted. Overlay placed before 2020 inspection.
01106	Rarus-Silver Bow Creek - Phase I - Bridge C	1.5	Good condition, with minimal transverse cracking noted. Overlay placed between two inspections.
01107	Rarus-Silver Bow Creek - Phase II - Bridge D	1.5 (2020 only)	Good condition, with minimal transverse cracking noted. Overlay placed before 2020 inspection.

[1] Same ratings in 2019 and 2020 unless otherwise noted.

ITEM 4.4B - INSTRUMENTATION OF BRIDGE DECKS

To achieve a better understanding of internal temperatures and relative humidity and associated strains in Montana bridge decks, WJE instrumented a new bridge deck with thermocouples, relative humidity probes and strain gages. In addition, the data collected from the instrumentation was used to validate the finite element modeling performed in Item 4.5b (page 122).

Rarus/Silver Bow Creek Structure, Bridge D, was selected for the instrumentation plan and consists of a four-span bridge (134, 165, 165, and 134 feet) spanning a total of 598 feet. The bridge deck is approximately 40 feet wide and supported by five steel plate girders spaced approximately 8′ 6″ on center. The concrete deck thickness is 7.75 inches and is reinforced with stainless steel reinforcement. The bridge deck was a replacement deck with the existing substructure remaining in place. Sletten Construction, Inc. served as the general contractor for the bridge construction with concrete being provided by Pioneer Concrete (Butte, MT). Previously constructed Rarus bridge decks over the Silver Bow Creek (Bridges A and C) were constructed within the 14 months of this deck (Bridge D) during October and December of 2018, respectively. Bridge B was reportedly constructed within a month after the completion of Bridge D. The general condition of Bridge A and Bridge C decks were noted as good, with minimal transverse cracking, based on visual observations performed during WJE's bridge inspections as part of Item 4.4a.

Instrumentation Plan

Prior to field instrumentation, WJE submitted an instrumentation plan (dated November 21, 2019) to MDT for review and approval. The plan was approved for instrumentation installation in Placement 7 of Bridge D (Figure 70). Prior to field installation, preparation of the instrumentation was performed in the WJE's laboratory in Northbrook, Illinois: including verification of the relative humidity probes, thermocouples, and strain gages; pre-assembling of instrumentation trees; and trial run of the data acquisition and remote monitoring system. During the week of November 25th and December 1st, 2019, WJE instrumented four locations on Placement No. 7 of Bridge D with locations at the beginning and end of the concrete placement including interior, edge, and perimeter conditions. The instrumentation locations are illustrated in Figure 70 and Figure 71. At each location, WJE embedded five thermocouples and three relative humidity probes at varying depths of the deck to obtain the temperature and relative humidity profiles. WJE also embedded three vibrating wire strain gages (VWSGs) [39] at each section; two near the top and bottom surfaces and one at mid-depth. VWSGs were chosen for this purpose due to their successful track record when embedded in concrete after WJE used similar setups in new bridge deck construction projects.

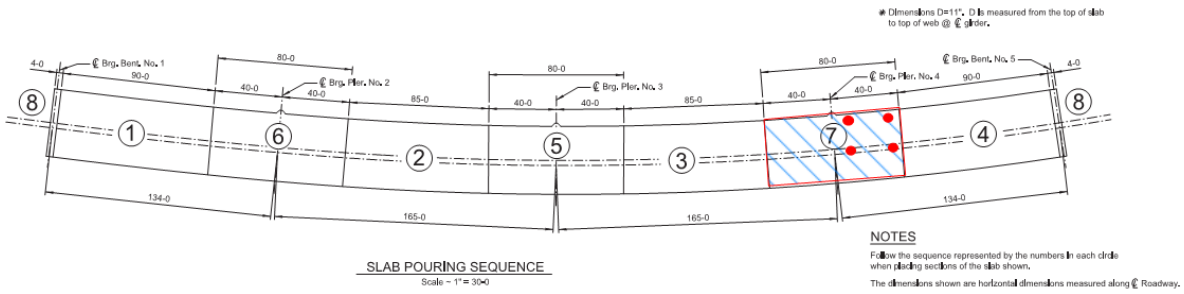

Figure 70. Placement Sequence (Placement 7 highlighted).

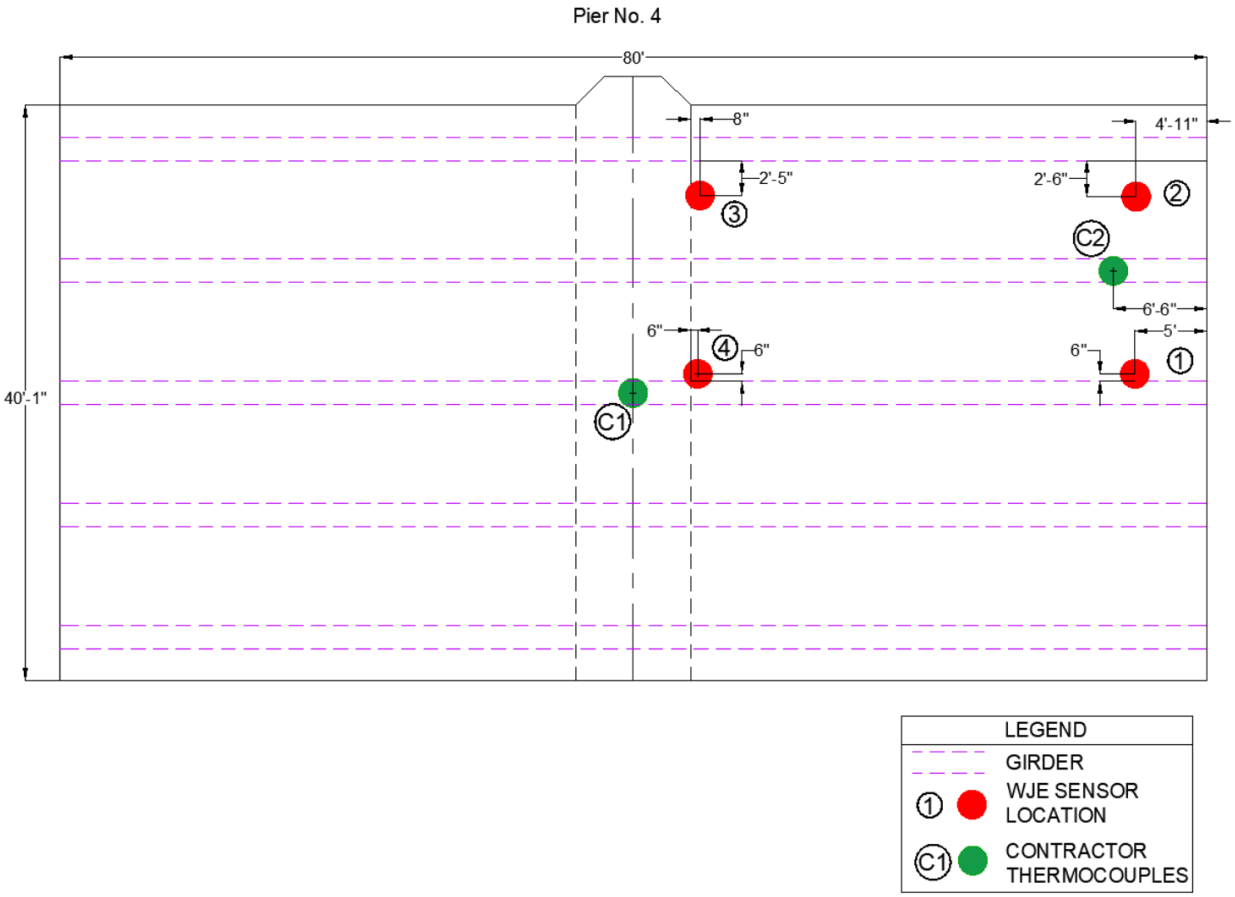

Figure 71. Placement 7, four instrumentation locations as indicated by dots.

Table 22 presents the as-built locations of each sensor and Figure 72 through Figure 74 show the typical instrumentation at each monitoring location.

Table 22. The As-Built Depths of Each Installed Sensor

	WJE Sensor Location *			
Sensor Type	Location No.			
	1	2	3	4
T1	1/2"	1/2"	1/2"	1/2"
T2	1 3/8"	1 1/4"	1 1/4"	**
T3	3 5/8"	3 5/8"	3 5/8"	3 7/8"
T4	6 7/8"	6 5/8"	6 3/4"	6 3/4"
T5	7"	7"	7 1/2"	7 1/4"
RH1	1/2"	1/2"	1/2"	1/2"
RH2	3 1/2"	3 5/8"	3 5/8"	3 7/8"
RH3	7"	7"	7 1/4"	7 1/4"
S1	1/2"	3/4"	1/2"	1/2"
S2	3 5/8"	3 5/8"	3 5/8"	3 5/8"
S3	6 3/4"	7"	6 3/4"	7"
*depth from bottom of the slab				
** 4-T2 thermocouple changed to bottom side of girder				
T - Thermocouple				
RH - Relative Humidity				
S - Strain gage				

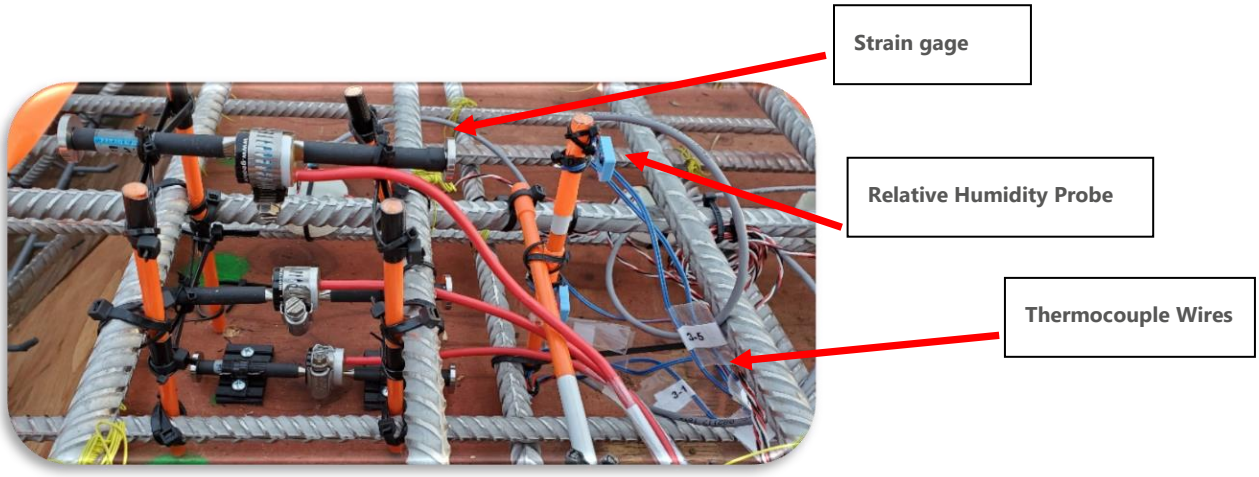

Figure 72. Typical instrumentation at each monitoring location.

Figure 73. Elevation view of installed vibrating wire strain gages at three depths.

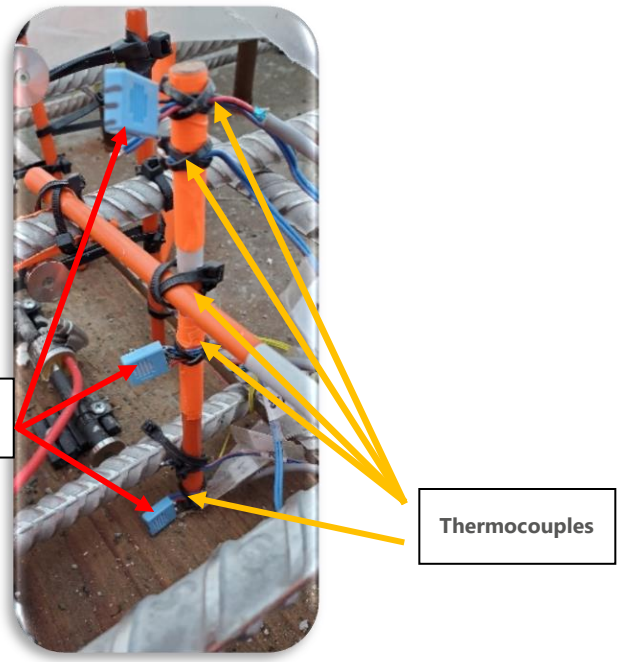

Figure 74. Elevation view of installed relative humidity probes and thermocouples.

In addition to the embedded sensors, WJE installed a weather station to monitor the ambient temperature, relative humidity, solar radiation, and wind speed during the monitoring period. This weather station was powered by solar panels and two batteries with the intent to monitor for a minimum of 6 months.

All instruments were connected through multiplexers to two Campbell Scientific data loggers [40] that were recording data at five minute intervals. The specific data logging systems were purchased in order to operate at the very low temperatures anticipated for the winter months in Montana. The systems include a communication device (cellular modem) for remote connectivity, which can be accessed by MDT and WJE personnel at any time. All instrumentation data is transmitted to and backed up on WJE's cloud server.

Concrete Placement

The concrete placement (Placement No. 7) was performed on December 5th, 2019. Mr. Robert Schulman and Todd Nelson (both of WJE) were present to make general observations of the concrete placement and to ensure that the instrumentation was operational and not disturbed during concrete deposition and finishing operations. Due to cold weather, the concrete deck forms were being heated from below by tarping around the perimeter of the bridge underside and blowing direct heat to the underside, with the temperatures in this heated space varying from 65 to 80°F (18 to 27°C) (based on temperatures measured at various locations under the deck by WJE during the installation of the instrumentation). The reinforcing steel of the deck was covered with plastic sheeting to protect it from snow and rain prior to concrete placement. On the day of the placement, ambient temperatures ranged from 23 to 26°F (-5 to -3°C) with little to no wind and a relative humidity between 75 and 85 percent. The deck was formed by removable

plywood. Light watering of plywood forms was performed by the contractor prior to concrete placement. The contractor installed three sets of thermocouples (Figure 71) with one contractor location (C1) close to WJE Sensor Location 4.

Concrete was being pumped up (approximately 60 feet) from the access road below the bridge, and the first concrete was placed on the deck at 10:08 AM. The construction joint (keyed joint) between the north end of Placement No. 7 and the existing south end of Placement No. 3 was rubbed with concrete paste prior to concrete placement. Concrete placement was performed from north to south, and concrete consolidation procedures were very good and consistent during the entire placement. The contractor made a conscious effort to protect and avoid damaging the WJE sensor locations (Figure 75) during concrete deposition, and WJE also monitored each location during the concrete placement.

Concrete plastic testing was performed by others on concrete sampled from the end of the pump as reported in Table 23.

Table 23. Concrete Plastic Testing Data

Truck No.	Concrete Temp (°F)	Slump (in.)	Air Content (%)
1	67	5.75	4.6
2	70	3.75	4.2
3	62	4.75	5.7
6	67	4.25	4.8
9	70	4.0	4.8

Note: Concrete plastic measurements taken on samples from the deck

The concrete was finished with a Bidwell finishing machine containing an auger, two rollers, and two floats with a broom finish immediately behind (Figure 76). WJE observed that the surface of the concrete was not closing well (Figure 77), leaving small voids on the near surface. No fogging was performed prior to placement of wet-burlap. Wet-burlap was typically placed within 30 to 40 minutes after concrete placement followed by plastic sheeting (typically within 90 minutes of the wet-burlap placement). Cold weather insulation was placed on top of the plastic sheeting within 150 minutes of concrete placement.

Field cured concrete cylinders were used to determine timing of removal of the winter protection (heating from below and insulation blankets). The contractor was required to achieve 4,000 psi prior to removal of heat and insulation. Typically, based on strength development of previous placements, it takes 8-9 days to achieve to 4,000 psi. Based on feedback from MDT, the concrete obtained 4,000 psi, and the heating and insulation was removed on December 16th, 2020, after about 11 days.

Based on delivery tickets, Sletten used Pioneer Ready Mix company and a mix identified as "Mix MDT 1.5 DECK2" (Table 24). This mix has 1 1/2-in. top size coarse aggregate with a blend of three coarse aggregate sizes. The mix has a total cementitious content of 564 lb./yd^3 (20 percent slag cement and 5 percent silica fume replacement) with a water to cementitious ratio of 0.42. Concrete sampling was performed after pumping by a third party and by MDT. WJE has not received the strength results nor the internal concrete temperature data (from the contractor) from this placement.

Table 24. Concrete Mixture Proportions - Pioneer Ready Mix Designation "Mix MDT 1.5 DECK2"

Constituent	Quantity (lb./yd^3)
Cement - Type IL - Lafarge (Richmond)	426
Slag Cement - Grade 100 - Lafarge (Seattle)	113
Silica Fume - Euclid SF	25
Coarse Aggregate 1 - 1 1/2"	690
Coarse Aggregate 2 - 3/4"	500
Mixed Aggregate 1 - 1/2"	650
Fine Aggregate 1	1230
Water	237
Air Entrainer (Eucon AEA 92 S)	2.5 oz/cwt
Mid-Range Water Reducer (Eucon 91)	6.0 oz/cwt
Superplasticizer (Eucon MR)	12.0 oz/cwt

Figure 75. Concrete being deposited around WJE sensor location and sampling.

Figure 76. Concrete placement, finishing, and curing procedures.

Figure 77. The finished surface of the concrete showing some surface voids, and difficulty closing of the surface.

Instrumentation Data to Date

At the time of concrete placement and as of the date of this report, all sensors were being measured and recorded. The vibrating wire strain gages were zeroed within the first 2 hours of concrete placement to establish a baseline of zero strain. The instrumentation data collected to date is illustrated in the figures in Appendix C. It should be noted that the relative humidity measurements when the ambient temperature is near and below freezing temperature cannot be relied upon. Note that thermocouple 4-2 was installed at the bottom of a steel girder. External heat was removed from the underside of the bridge on December 16th, 2019. The bridge was open to traffic on January 27, 2020. MDT has reported on two occasions (immediately after removal of the curing protection and on March 4th, 2020) that no transverse cracking has been observed on this bridge deck. A PPC overlay was installed on the bridge deck in July 2020; the exact date of the installation is unknown. Due to the presence of the PPC overlay, a cracking survey could not be performed from the topside of the deck and was performed from the underside of the bridge by Robert Frazier on 8/27/2020. Minimal transverse cracking was observed from the underside, and none of the transverse cracking occurred near sensor locations. Refer to Item 4.4a for a more detailed description of the deck inspection results.

Summary and Discussion

The following relevant findings were observed in the collected data:

1. None of the 12 installed strain gages showed any indication of cracking (sudden change in strain). This is consistent with the field inspection performed by WJE that showed minimal transverse cracking (or any cracking) on the underside of this deck with no cracking observed to be near any of the installed gages. MDT reported to WJE on multiple occasions that no observed transverse cracking was apparent in the first couple months after construction.
2. No tensile strains developed during the winter wet-curing methods (first 11 days). Compressive strains did develop in the deck immediately after removal of the winter curing procedures (insulation and heating). For this bridge, this early age compression likely provided benefits to negate net tensile stress gain during the summer months. Over the summer months, the compressive strains dissipated with the warmer temperatures and drying of the deck, with the top of the deck eventually developing tensile strains, although not large enough to cause cracking.
3. Large daily ambient temperature changes were observed with associated temperature gradients within the deck, with changes being most pronounced during the summer and early fall months. For example, in early September of 2020, ambient temperature increases and decreases of 55 to 60°F (30 to 33°C) were observed (see Figure 78). In this chart, the internal deck temperatures were measured at five depths through the concrete deck at location No. 4, with 4-5 being at the top of the deck and 4-1 being at the bottom of the deck (4-4 and 4-3 are middle of the deck). These large ambient temperature changes create temperature gradients within the concrete deck, primarily during the heating of the top side of the deck. This time period is an example of a relatively extreme event; however, ambient temperature variations during the summer and fall months are commonly 35 to 45°F (19 to 25°C). The implications of these large ambient temperature variations are further discussed and analyzed in the finite elemental modeling section.

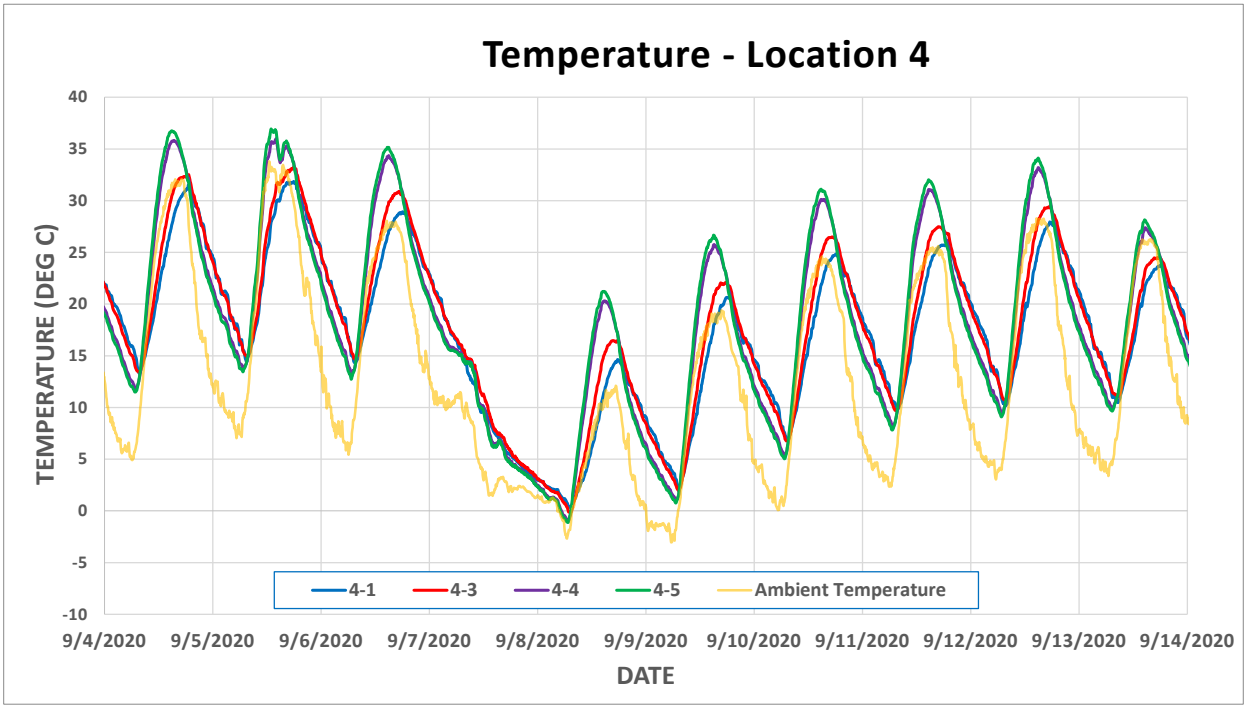

Figure 78. Ambient and internal deck concrete temperatures measured at Location No. 4, early September of 2020.

4. Large daily ambient relative humidity changes were observed, particularly in the spring and summer months, with associated large relative humidity changes and gradients within the deck concrete. For example, in early June 2020 (See Figure 79), the ambient relative humidity increased from approximately 20 to 100 percent within a 24-hour period, during a reported rain event. In this graph, the internal concrete deck relative humidity measurements are plotted at location No. 4. The measurement 4-3 represents the internal concrete relative humidity near the top of the deck; 4-2 mid-depth; and 4-1 near the bottom of the deck. This rain event created a relative humidity gradient, from top surface to bottom surface of the deck concrete, of approximately 25 to 30 percent. Prior to this rain event, the ambient relative humidity was generally low, and the concrete surface relative humidity dropped below the mid-depth relative humidity, and an approximate 5 to 10 percent relative humidity gradient was measured between the top and bottom of the deck. After the rain event, the surface of the deck went to 100 percent relative humidity and the bottom increased to 70 to 75 percent relative humidity.

   This particular rain event was one of the more extreme examples of ambient relative humidity changes observed in the data; but daily ambient relative humidity changes of 40 to 50 percent during the spring and summer months were common. The implications of these high daily relative humidity changes are further analyzed in Item 4.5b (page 122).

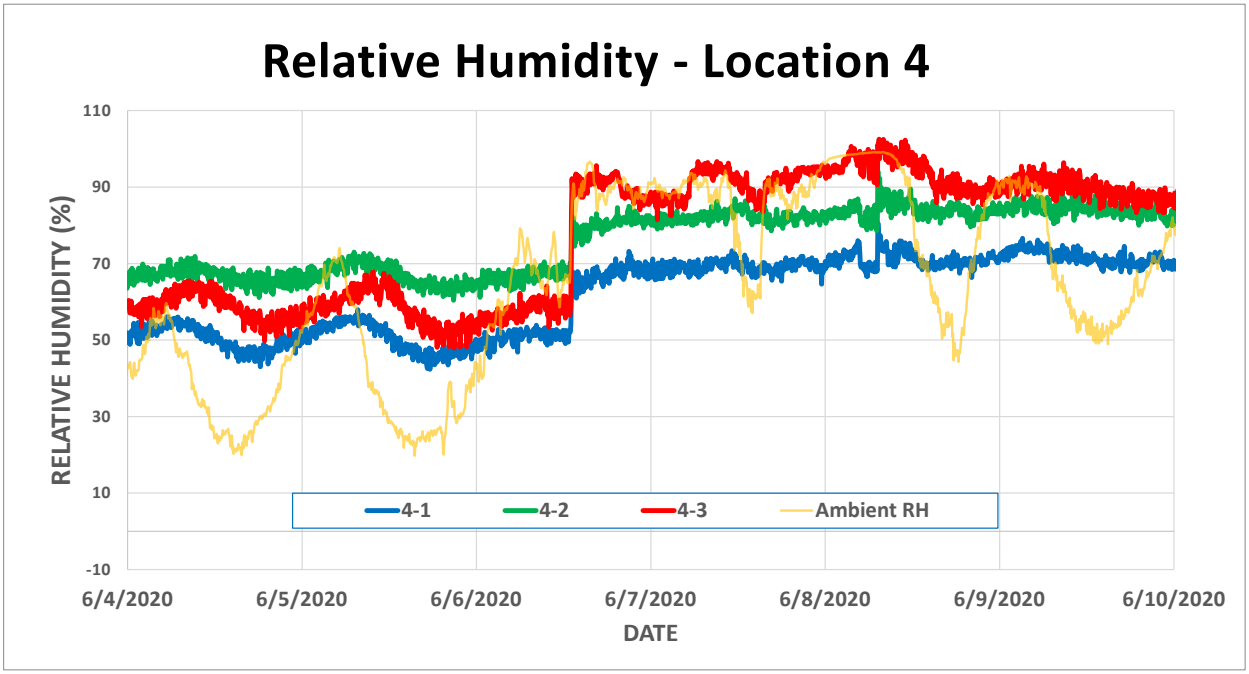

Figure 79. Graph shows the ambient and internal concrete relative humidity measurements at Location 4 during early June.

ITEM 4.5A - LABORATORY EVALUATIONS

Laboratory evaluations were performed on mix identification "MDT 1.5 DECK2" (as presented in Table 24, in Item 4.4b), which was used for the concrete placements of Bridge D of the Rarus/Silver Bow Creek Structures (instrumented bridge deck). The primary goal of the laboratory evaluations was to measure physical properties of the concrete in order to accurately model stresses and strains in the bridge deck and to assess physical properties of the mix related to the potential development of cracking. Raw materials (cement, slag cement, coarse aggregate, fine aggregate, and chemical admixtures) used in this mix design were obtained by MDT and sent to WJE. Concrete was batched in WJE's Northbrook, Illinois laboratory (adjusting weights appropriately for aggregate moisture contents) targeting the plastic properties, and test samples were fabricated in accordance with ASTM C192, *Standard Practice for Making and Curing Concrete Test Specimens in the Laboratory*. The following testing was performed on this laboratory batched concrete and implemented in the finite element (FE) modeling (detailed in Item 4.5b, page 122).

Plastic Concrete Testing Results

To fabricate the quantity of physical test samples needed, two concrete batches (2 cubic feet) were needed to achieve sufficient volume of concrete. On both of the batches, the concrete slump (AASHTO T 119), air content (AASHTO T 152), unit weight (AASHTO T 121), and temperature (AASHTO T 309) were measured, and the results are presented in Table 25. The designed mix ("MDT 1.5 DECK2") targets were 4,000 psi at 28-days, 4 inches of slump and 6.0 percent air, with a theoretical unit weight of 142.7 pounds per cubic feet (lb/ft^3). Companion specimens were sampled from both batches to perform the physical testing detailed in the following paragraphs.

Table 25. Concrete Plastic Properties

Property	Batch 1	Batch 2
Slump (in.)	4.0	4.0
Air Content (%)	7.4	7.0
Unit Weight (lb/ft^3)	139.6	141.5
Temperature (F)	71.0	71.2

Strength and Maturity

The compressive strength (AASHTO T22), splitting tensile strength (AASHTO T198), and modulus of elasticity (ASTM C469) were measured at 1, 2, 5, 21, 28 and 90 days after fabrication (Table 26, Figure 80, Figure 81). Testing at 1, 2, and 5 days was performed to capture the early age strength and modulus of elasticity development during the deck wet-curing that are difficult to estimate without testing. All test samples were moist cured until time of testing. The concrete maturity was measured on two cylinders (one from each batch) cured in the same environment as the strength specimens, and maturity equations were developed utilizing ASTM C1074, *Standard Practice for Estimating Concrete Strength by Maturity Method*. As a function of maturity, the FE model can accurately account for early- and late-age strength and modulus development.

Table 26. Strength Properties and Maturity

Test Age	Compressive Strength (psi)*	Splitting Tensile Strength (psi)*	Modulus of Elasticity (x10^6 psi)*	Maturity (°F*Hours)*
1	1,480	200	2.48	938
2	3,100	350	2.90	2951
5	3,530	355	3.32	4996
21	5,070	NT	4.00	21175
28	5,380	580	4.40	28402
90	6,400	590	4.58	92134

**Average of two cylinders, NT = Not Tested*

Figure 80. Compressive Strength and Modulus of Elasticity versus Age.

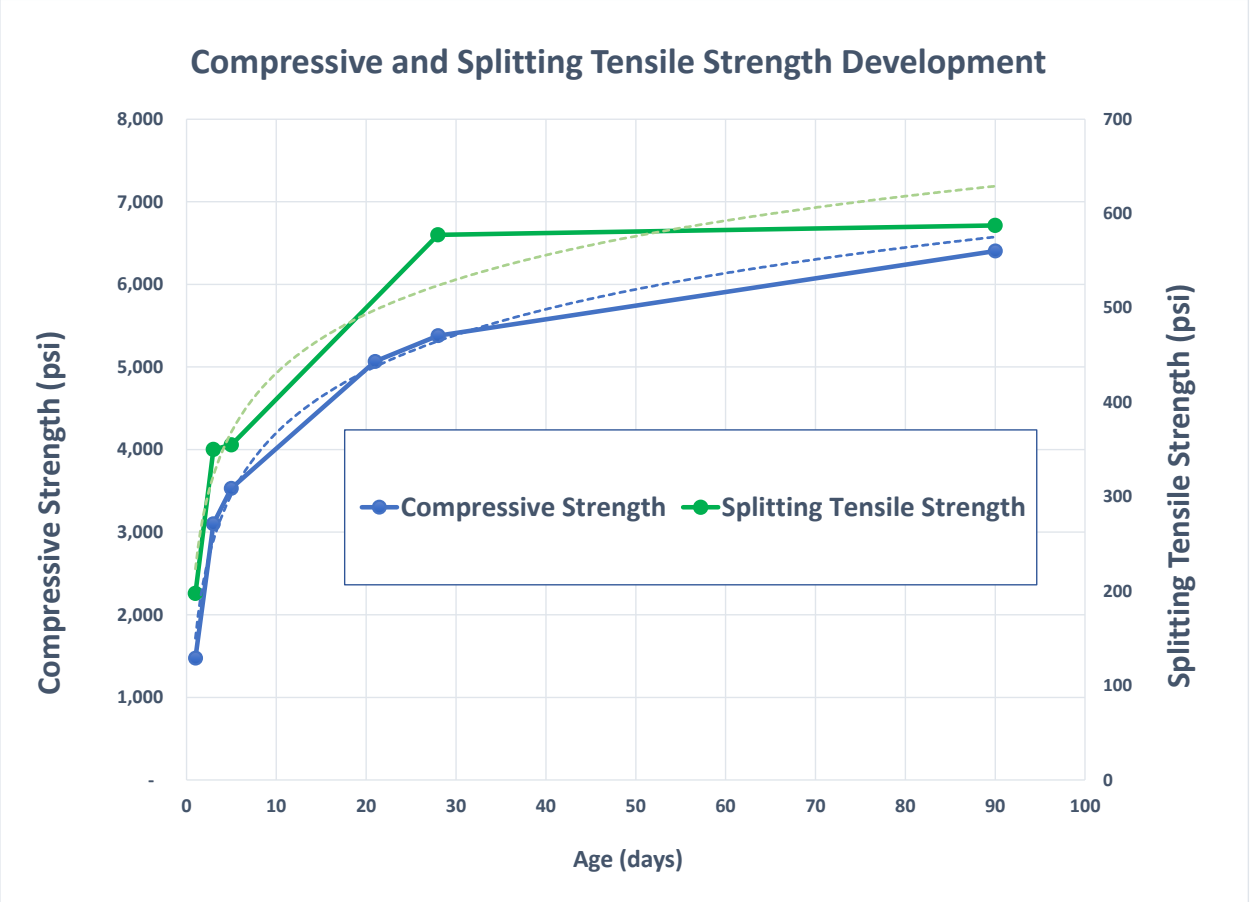

Figure 81. Compressive and Splitting Tensile Strength versus Age.

Drying Shrinkage

The concrete drying shrinkage strain was measured in general accordance with ASTM C157, *Standard Test Method for Length Change of Hardened Hydraulic-Cement Mortar and Concrete*. Three concrete prisms, measuring 3 x 3 x 11-in., were fabricated for two curing regimens: moist curing for 5 and 14 days followed by drying, consistent with the initiation of drying using WJE's previous recommended field curing procedures and with MDT's previous wet curing procedures, respectively. Each set of drying shrinkage prisms were fabricated from both batches of concrete to minimize possible variations from the separate batches. The drying shrinkage measurements were used to calculate the ultimate shrinkage value for both curing regimes and implemented in the FE modeling to calculate strains associated with drying shrinkage and relative humidity gradients (further discussed in Item 4.5b, page 122) (Table 27, Figure 82).

Table 27. Drying Shrinkage Measurements

Days of Drying	5-Day Moist Cure (µstrain)	14-Day Moist Cure (µstrain)
1	80	20
4	220	110
7	300	200
14	390	240
28	470	340
56	550	390
90	560	380
180	570	410
365	620	470

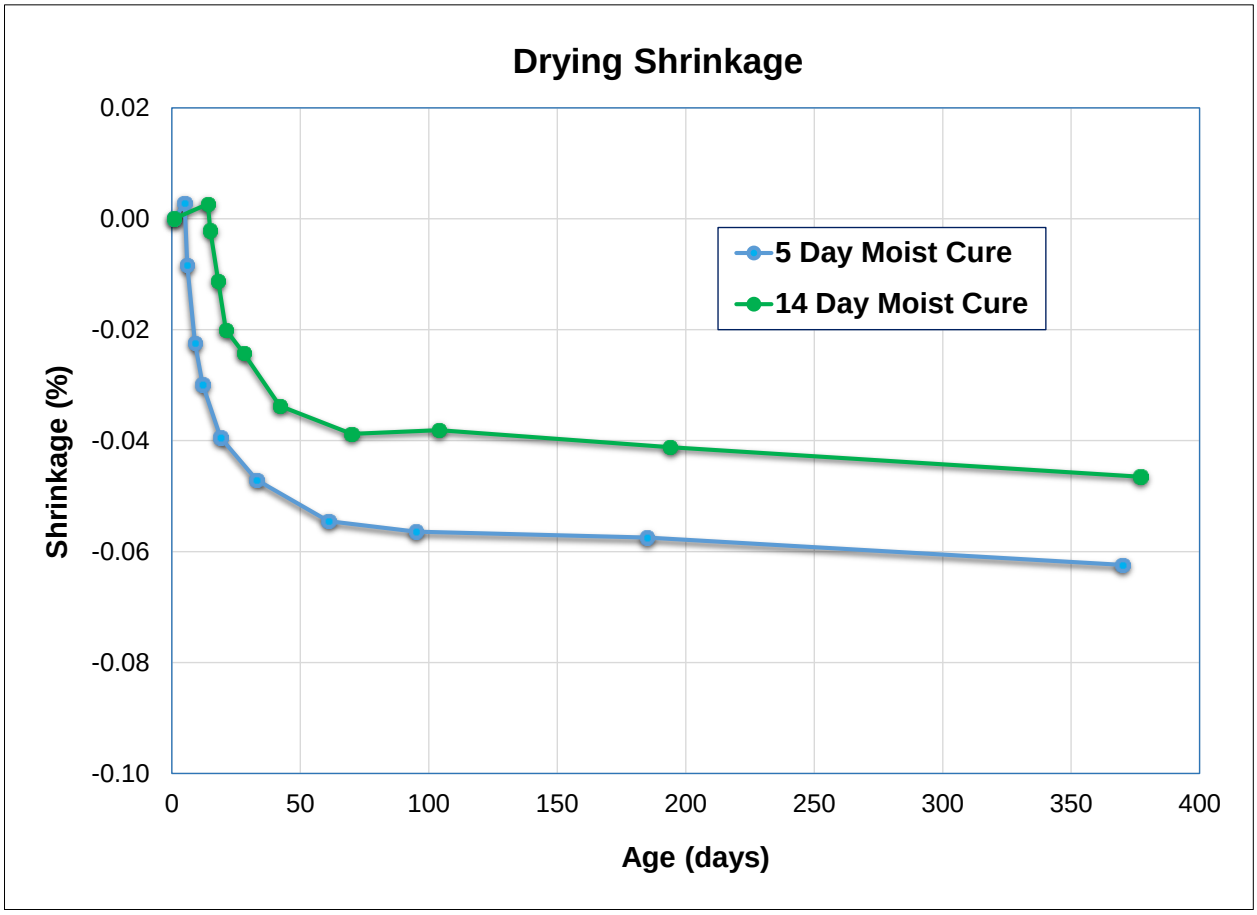

Figure 82. Drying shrinkage measurements after 5- and 14-days of moist cure (ASTM C157).

Concrete Creep

The creep characteristics of the concrete were measured in the unsealed condition (drying) after 5, 28 and 90 days of moist curing in accordance with ASTM C512, *Standard Test Method for Creep of Concrete in Compression*. The concrete creep characteristics were measured at these ages to capture both the early age and long term creep characteristics. After moist curing, creep testing was performed by loading and maintaining this load on three cylinders to 40 percent of the measured ultimate compressive strength at each age. During this loading, the cylinders were stored in standard drying room conditions: 73 ± 3.4°F (23°C ± 1.9°C) and 50 ± 4 percent relative humidity. The deformation of the cylinders under the sustained 40 percent load was then measured over the duration of the test. To account for the length change of the cylinders due to drying shrinkage, three additional unloaded cylinders (control) were measured for drying shrinkage over the duration of the test. This drying shrinkage was subtracted from the deformation measurements to get the net creep. Specific creep was then calculated by dividing the net creep of the cylinders by the loading stress (40 percent of the ultimate). This data was then used in the FE model to account for reduction in early and late age stresses due to creep characteristics (Figure 83, Figure 84).

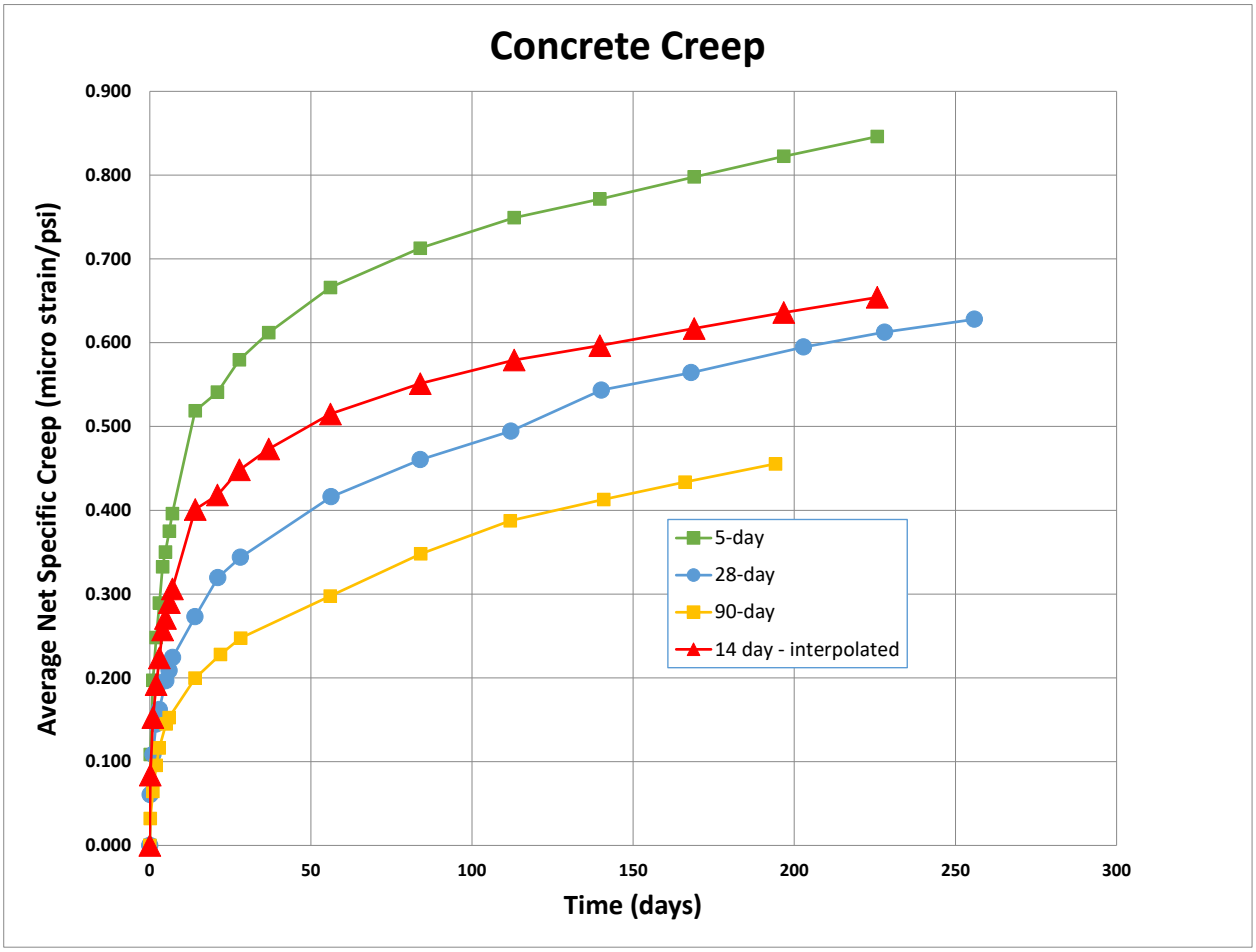

Figure 83. Concrete specific creep measured under unsealed conditions after loading at 5, 28 and 90 days. 14-day specific creep was interpolated and shown on this graph, with the need to use this data in the FE modeling.

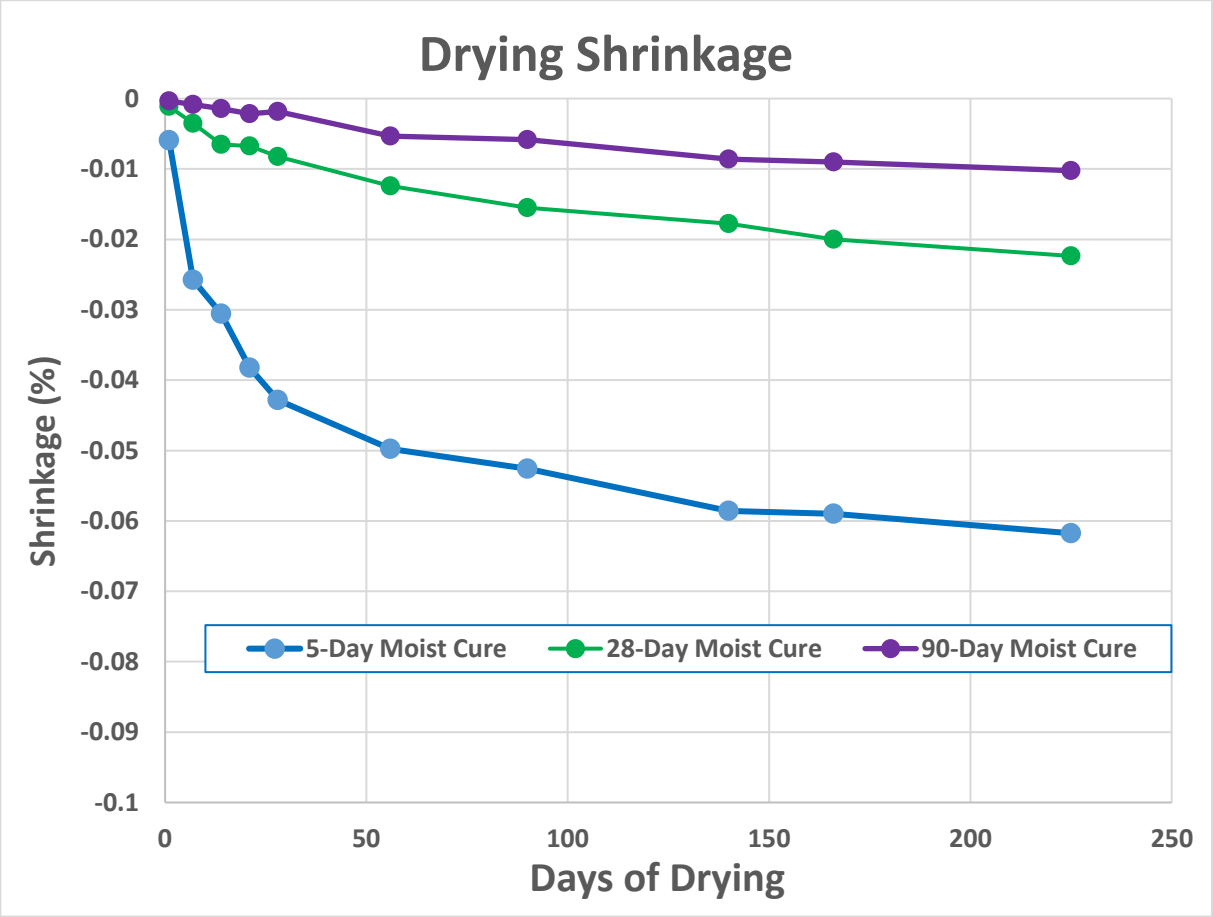

Figure 84. Drying shrinkage measured on companion cylinders (control) for creep testing (ASTM C512).

Coefficient of Thermal Expansion

The coefficient of thermal expansion was measured on two concrete cylinders (4 x 8-in.) at 5 and 28 days of age in accordance with AASHTO T336, *Standard Test Method for Thermal Coefficient of Thermal Expansion of Hydraulic Cement Concrete*. The CTE was measured in a saturated condition over a temperature range of 50 to 120°F (10 to 49°C), and resulted in average CTE of 4.10 X 10^{-6} and 4.14 x 10^{-6} in/in/°F at 5 and 28 days, respectively. These values were implemented in the FE modeling to account for volume changes associated with temperature changes.

Summary

The compressive strength testing performed by WJE was consistent with the 4,000 psi design strength and consistent with the submitted mix design performance. With respect to the compressive strength, the modulus of elasticity (MoE) development at early ages was slightly higher than anticipated with the splitting tensile strength development slightly lower than anticipated. At later ages, the MoE and splitting tensile strength were measured to be more consistent with respect to the compressive strength.

A significant reduction in drying shrinkage (and ultimate shrinkage) was noted in the ASTM C157 testing when the wet-curing was increased from 5 to 14 days, with an approximate 25 percent reduction. The shrinkage measured on the 5 day creep samples (control) was similar to the ASTM C157 specimens wet-

cured for 5 days. The drying shrinkage (and ultimate shrinkage) have a significant impact on the stresses that may develop in the bridge deck and potential for transverse deck cracking (further discussed and analyzed in Item 4.5b, page 122).

As anticipated, the creep characteristics of the concrete are much greater when loaded at earlier ages compared to later ages. For comparison, the creep at 90 days is reduced by approximately 35 percent when increasing the wet-cure, i.e. age of loading, from 5 to 28 days. This would imply that strains applied at earlier ages would creep to a greater extent than if applied at later ages. When assessing the significance of creep and age of loading on the potential for cracking, the early age benefits of creep have to be evaluated relative to the volume changes, modulus of elasticity (MoE), and tensile strength of the concrete. All of these variables effect the cracking potential of the concrete deck, and all change with concrete age. The volume change due to drying shrinkage applied to early age concrete (shorter curing period) may be larger than if applied at later ages (longer curing period); therefore, potentially negating some of the benefits of early age creep. The MoE increases with time, so for any given strain applied at early ages will have lower associated stresses than applied at later ages. However, the concrete deck will also gain tensile strength over time, so larger stresses can be resisted by the concrete prior to cracking. Therefore, the interaction between these variables is quite complex and should be assessed uniquely with each mix design and curing conditions.

The coefficient of thermal expansion (CTE) of the concrete was slightly lower than anticipated and did not change significantly from 5 to 28 days of testing. It should be noted that the measured concrete CTE (4.14 x 10^{-6} in/in/°F) is less than the CTE of the supporting steel girders (5.7 x 10^{-6} in/in/°F), as utilized in the finite element modeling (Item 4.5b, page 122).

ITEM 4.5B - FINITE ELEMENT MODELING

Introduction

Nonlinear finite element (FE) simulations were conducted to help gain further insight into the effect of environmental factors on concrete deck stresses that can cause transverse deck cracking and to further refine the WJE crack-mitigation recommendations To investigate the deck performance, a three-dimensional (3D) finite element model of Rarus/Silver Bow Creek - Bridge D located in Butte, Montana was constructed and analyzed in the general-purpose FE program Abaqus v2020. This deck is a 4-span bridge composed of a five steel plate girder superstructure and a 7.75 inch thick composite concrete deck. The nonlinear FE model consisted of the full-length deck geometry, girders and lateral braces.

The finite element modeling effort was divided into two broad categories: (1) those related to the early-age concrete deck (short-term) performance and (2) those corresponding to aged concrete typically after 90 days of placement (long-term). The objective of the FE modeling was to identify the factors that have the greatest impact on the maximum tensile stresses within the concrete deck at early or later ages that pose the greatest risk to transverse cracking.

Several factors were investigated including nonlinear temperature and moisture gradients through the deck thickness, curing, concrete creep and shrinkage effects, deck thickness effect, and the degree of restraint provided by the steel girders. To study the temperature effects, several temperature histories

based on deck placement time, type of curing and insulation, and extreme diurnal temperature increase and decrease were considered. In terms of moisture effect, an extreme moisture gradient corresponding to after and before a rain event was considered based on data collected from the instrumented bridge deck (See Item 4.4b). Most concrete properties used in the FE model were measured by laboratory testing, as detailed in Item 4.5a. Concrete creep properties were calibrated based on WJE's in-house laboratory testing at different ages. A sensitivity study was carried on the tensile stress in the concrete deck to variations in physical model parameters; such as degree of restraint and deck thickness.

The results of the different loading scenarios were analyzed to identify deck placement times for different environmental conditions that were best at limiting the developed tensile stresses in the concrete deck. Also, analyzing the results provided insight into the deck performance under different temperature and moisture gradient conditions. Identifying scenarios and parameters that reduce the tensile stresses within the deck will reduce the potential for early- and late-age transverse cracking thereby increasing the service life of bridge decks.

Model Geometry and Mesh

Rarus/Silver Bow Creek - Bridge D is a 4-span bridge with approach span lengths of 134-ft. and intermediate spans of 165-ft. placed on existing substructure. The bridge superstructure is oriented approximately North-South. The deck is 40-ft. wide and 7.75-in. thick that is made composite with five steel plate girders using shear studs. Girders are continuous and curved with 5.3-ft. deep web plates spaced at 8.5-ft. Girders are laterally braced by cross frames spaced at about 17-ft. and 18-ft. in approach and intermediate spans, respectively. Figure 85 shows a drawing excerpt of the bridge cross-section at mid-span and near pier.

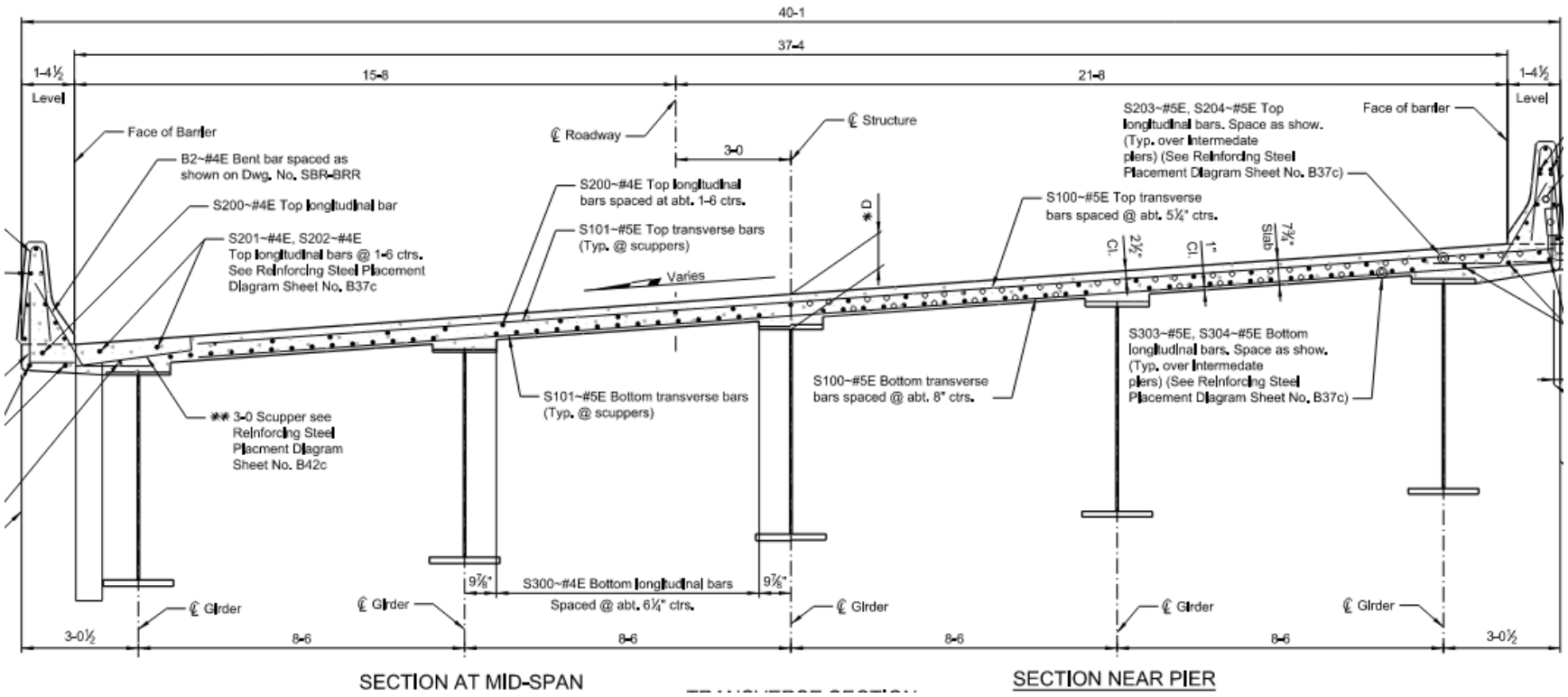

Figure 85. Modeled bridge cross-section, an excerpt from Drawing No. 23386.

Steel Girders

Eight-noded shell elements with reduced integration (S8R in Abaqus terminology) were used to model plate girders' webs and flanges. Shell elements had five through-thickness integration points. Bearing stiffener and web stiffener plates were also modeled using shell elements. The existing curve in the girders was modeled to match the radii given in the design drawings. Beam (frame) elements (B31 in Abaqus terminology) were utilized to model support and intermediate cross bracings. Figure 86 shows the plan view excerpt and modeled girders in the FE model. Figure 87 shows a snapshot of the FE mesh of the girders and beams.

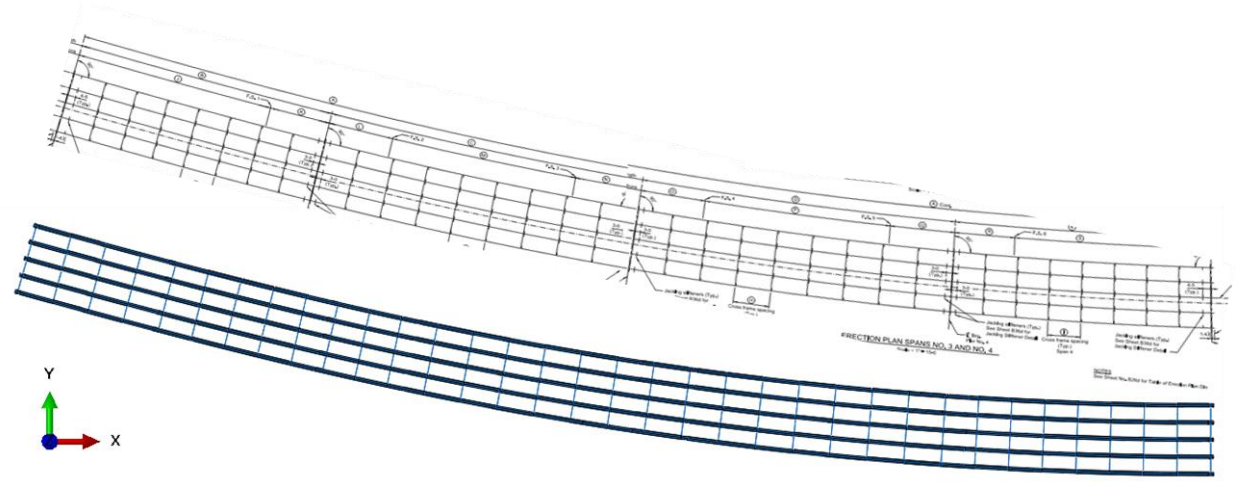

Figure 86. Framing plan excerpt from Drawing No. 23371 (top) and framing plan in the FE model (bottom).

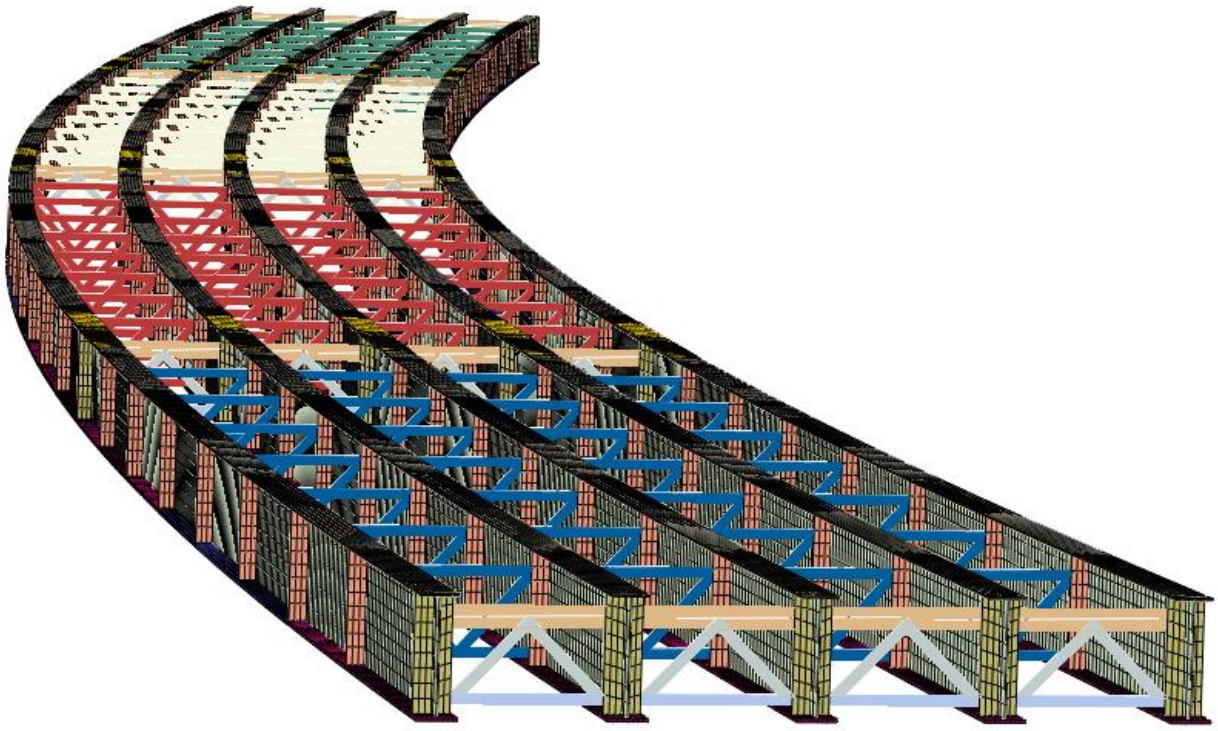

Figure 87. Finite element mesh of the girders modeled with shell elements and cross framings modeled with beam elements.

Concrete Deck and Reinforcement

Eight-noded solid elements with reduced integration (C3D8R in Abaqus terminology) were used to model the entire concrete deck. The deck is modeled continuously throughout. Per the design drawings, the bridge deck is cast in seven placements as shown in Figure 70 of Item 4.4b. Placements No. 1 to 4 correspond to near abutments or mid-span regions (positive moment regions) and Placements No. 5 to 7 were at pier locations (negative moment regions). WJE's site instrumentations were all embedded in Placement No. 7 (Pour 7); therefore, the FE analysis effort was particularly focused on this section of the deck. At Pour 7, the deck model was refined with 8 finite elements through the deck thickness that transitioned into 4 elements away from this region. Through-thickness elements were created such that there is always an element node in close proximity to an embedded sensor to facilitate post-processing results. A total of about 100 elements were used across the deck width at Pour 7 region that reduced to about 50 elements elsewhere. Element size was selected to balance accuracy with computation time. A total of 350,000 solid elements were used to model the bridge deck. Deck top and bottom reinforcement were discretely modeled only at Pour 7 region. Reinforcing steel was modeled using truss elements (T3D2 in Abaqus terminology).

For simplicity, the deck transverse slope, barriers, and deck haunches were not included in the model. Figure 88 shows the deck finite element mesh, and Figure 89 shows the reinforcing steel used in Pour 7.

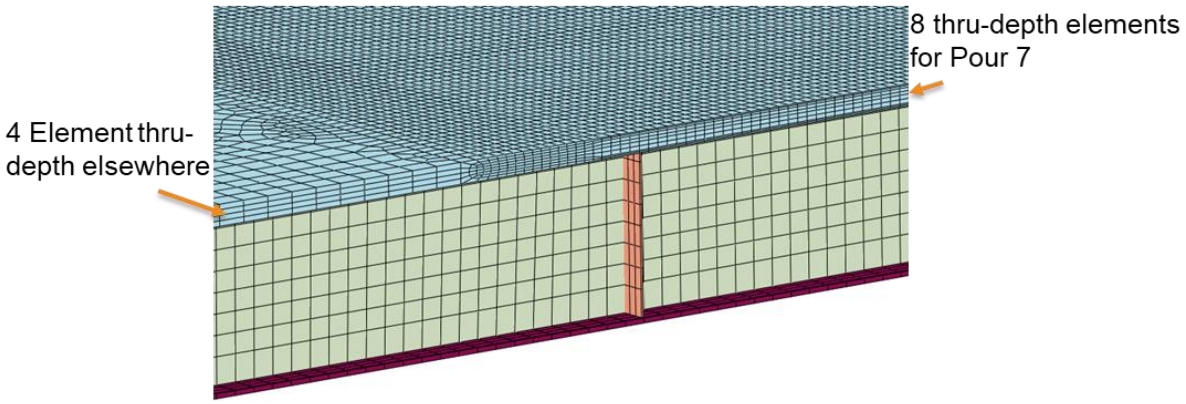

Figure 88. Finite element mesh of the bridge deck and girder, refined mesh at Pour 7 region with transition to coarse mesh elsewhere.

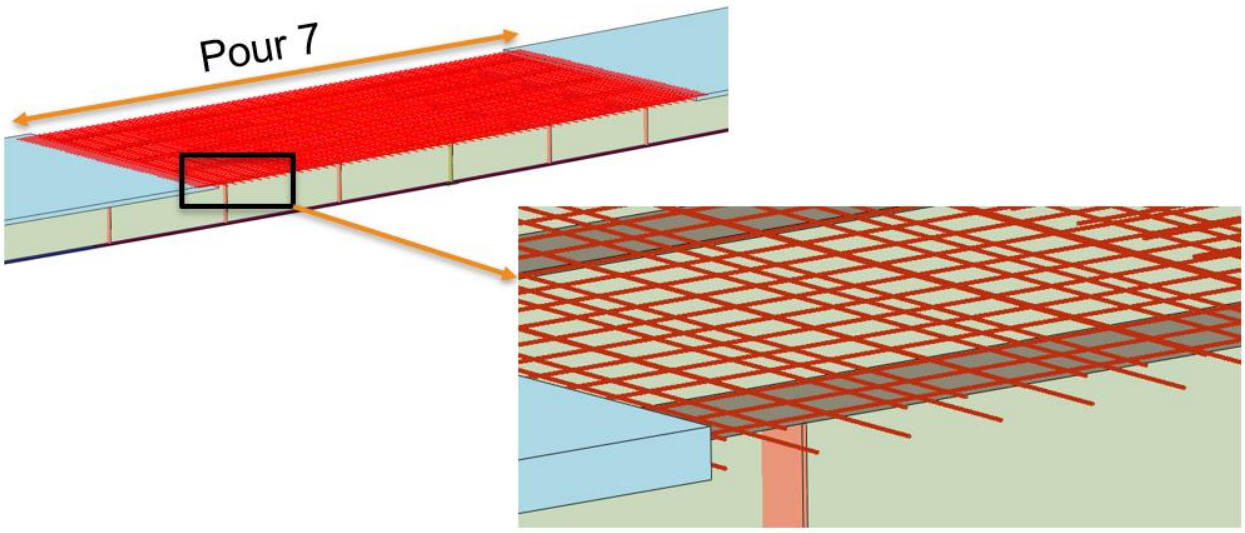

Figure 89. Reinforcing steel modeled with truss elements only in Pour 7.

Boundary Conditions

According to bridge design drawings, the bridge superstructure is free to expand at Bents No. 1 and 5 and is fixed at intermediate piers. However, at piers No. 2 and 4, the bearing and support configuration is such that the girders can partially expand for about one inch (in the direction tangent to bridge curvature) until they bear against the side plates. Figure 90 represents the drawing excerpts of support configuration at bents and piers. In the FE model, the support at Pier No. 3 was modeled as a fixed (pin) boundary condition, and the other 4 supports were modeled as a roller boundary condition. The translation transverse to bridge curvature was always fixed. The boundary conditions were applied using Abaqus kinematic coupling to a reference point at each girder support location. It is noted that this set of boundary conditions resulted in better agreement with measured strains in the field that is further discussed in the model calibration section. Figure 91 summarizes the FE model boundary conditions.

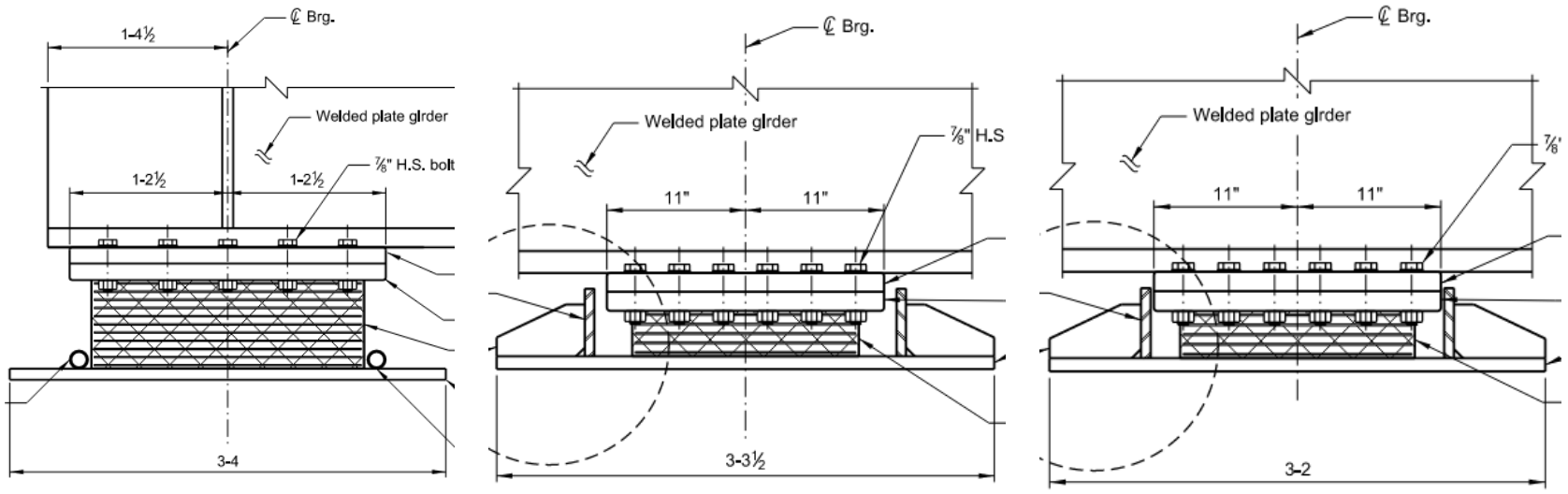

Figure 90. Excerpts from Drawing No. 23368, 23369, and 23370 show bearing details at Bents No. 1 and 5 (left), Pier No. 2 and 4 (center), and Pier No. 3 (right).

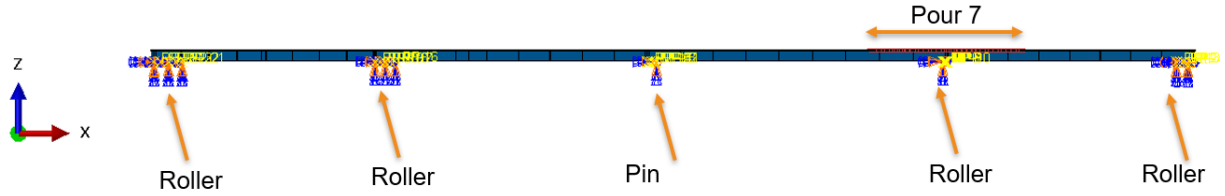

Figure 91. Side-view of the FE model boundary conditions showing pin and roller conditions at bents and piers.

Model Interactions

Steel reinforcing elements in Pour 7 were connected to the concrete solid elements using Abaqus's embedded constraint definition. Generally, the embedded constraint can be described as tying the displacement degrees of freedom in the steel truss element nodes to the solid concrete element where each respective node is located.

Concrete deck and steel girders are designed to act as one composite member. According to design drawings, the composite action is controlled by using shear studs and existing friction between steel and concrete that allow for shear transfer. In the FE model, due to simplicity, the shear studs were not included individually but it was assumed that the resulting shear force was fully transferred via rough friction (no sliding) between the deck soffit and the steel top flange. In Abaqus, a contact setting with no separation and rough friction properties was used to capture the full composite behavior of the deck and steel girders. Later in the sensitivity analysis section, the friction parameter of the interface was modified to allow for some sliding (or partial composite action) to investigate the effect of restraint provided by steel girders.

Material Properties

Basic Properties

Steel girders and reinforcing steel were modeled as linear elastic material. The concrete deck was modeled as an age-dependent viscoelastic material. No plasticity or damage-related material properties for concrete were included in this analysis. While elastic analysis cannot predict stresses after cracking, it can indicate if cracking will occur, with higher elastic stresses predicting more extensive cracking. In terms of the concrete basic properties, concrete compressive strength, splitting tensile strength, modulus of elasticity (MoE), and coefficient of thermal expansion (CTE) were measured at WJE's laboratory at different ages versus maturity (See Item 4.5a). In this analysis, the as-measured age-dependent MoE was used to capture the elastic portion of the concrete deck response. Age-dependent MoE is especially important in modeling early-age behavior. As previously shown in the laboratory evaluation section, the concrete MoE reached almost an asymptote after 90 days, as a result, for late-age analysis the MoE at 90 days was considered fixed. Table 28 summarizes the basic properties used in the FE model. When there were multiple measurements of a property, the average value of all specimens was used. The lab results showed only a slight change of CTE with respect to specimen age, as a result, an average value of CTE at 28 days was utilized in all ages of concrete considered in the model. It is also noted that the splitting tensile strength was not explicitly used in the FE model, but rather was an indicator of when concrete cracking was expected by comparing to predicted tensile stresses of the deck.

Table 28. Basic Concrete Properties Used in the FE Model

Age (days)	Modulus of Elasticity (x10^6 psi)	Splitting Tensile Strength (psi)	Coefficient of Thermal Expansion (x10^{-6} /˚F (/˚C))	Poisson's Ratio
1	1,480	200	4.14 (7.45)	0.2
3	3,100	350	4.14 (7.45)	0.2
5	3,530	355	4.14 (7.45)	0.2
21	5,070	Not available	4.14 (7.45)	0.2
28	5,380	580	4.14 (7.45)	0.2
90	6,400	590	4.14 (7.45)	0.2

Calibrating Creep Properties

The stress relaxation of the concrete deck is important for accurately accounting for thermal and shrinkage stresses of concrete decks. The stress relaxation of the concrete deck due to creep was modeled using a built-in viscoelastic model in Abaqus. The instantaneous response was captured by inputting the modulus of elasticity at different concrete ages. The time and age-dependent portion of the viscoelastic response was modeled using a time-hardening power-law model of creep [41]. This creep model was selected because it fit well to the WJE's laboratory measured creep data and because the model parameters could be made age-dependent which was crucial in early-age modeling when the material properties are changing more significantly. The age dependency was achieved by using an additional field variable accounting for the age of the concrete deck. Equation (2) shows the creep law model used in this study:

$$\dot{\overline{\varepsilon_{cr}}} = Aq^n t^m \quad (2)$$

Where, $\overline{\varepsilon_{cr}}$ is the uniaxial equivalent creep strain, q is the uniaxial equivalent deviatoric stress, t is the creep time, and A, n, and m are material properties that can be defined as a function of concrete age. As discussed in the Laboratory Evaluations section (Item 4.5a), the concrete creep was measured after 5, 28, and 90 days of moisture-curing in accordance with ASTM C512. The creep model was calibrated against the measured creep compliance at different ages and results were summarized in Table 29. Figure 92 shows the calibrated creep compliance against the measured creep data.

Table 29. Calibrated Creep Model Material Parameters

Age (days)	Power law multiplier (A) (1/ksi)	Equivalent Stress Order (n)	Time Order (m)
5	3.45E-05	1.0	-0.8
28	1.51E-05	1.0	-0.70
90	9.70E-06	1.0	-0.67

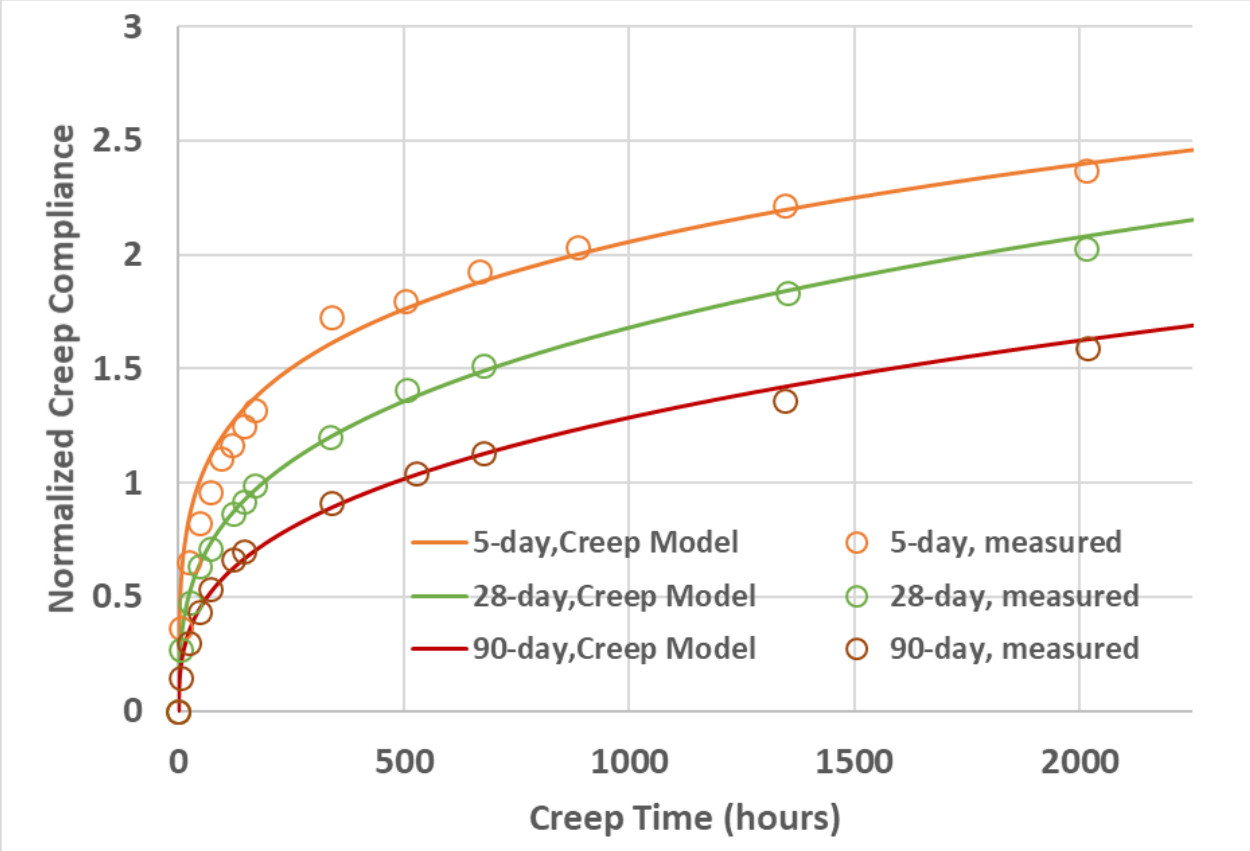

Figure 92. Calibrated creep compliance in the Abaqus model at different concrete ages.

Load Application

This section describes all the loads and how they were applied in the FE model. The dead load due to steel girders and deck self-weight was applied in several steps to mimic the staged-construction. In the first step, the self-weight of girders was applied without the concrete deck. In the next steps, unhardened concrete weight was applied utilizing the "Model Change" feature in Abaqus based on the pour casting sequence shown in the design drawing. Analysis of staged construction self-weight resulted in insignificant stresses in the concrete deck and will not be included in the future sections of this report. Live loads and any additional dead loads such as concrete barriers were not included in the FE analysis.

Temperature Induced Loads

A nonlinear temperature gradient in the concrete deck was used in the FE model. The through-depth temperature profiles for various environmental (loading) conditions were obtained by the 4C-Temp&Stress simulation tool [42]. 4C-Temp&Stress determines temperature variation over a cross-section by solving the heat equation numerically. It includes the concrete heat of hydration, ambient wind, temperature, type of formwork, and insulation. The 4C-Temp&Stress thermal models were calibrated against the measured field temperature (as measured and recorded with field instrumentation) before

producing early-age and long-term temperature scenarios. The temperature outputs from 4C-Temp&Stress were used as inputs for Abaqus FE Model to predict the temperature-induced stresses.

Drying Shrinkage and Moisture Induced Loads

One of the important issues to be considered in the FE analysis is the consequence of drying shrinkage over time and moisture-induced spatial deformations due to the local gradient of concrete humidity. In the FE model, the time-dependent shrinkage strain and moisture-gradient strains were prescribed using the concept of equivalent temperature. Shrinkage and moisture gradient induced strains were divided by concrete coefficient of thermal expansion to obtain an equivalent temperature difference that causes an equal amount of strain. According to ACI 209.2R-08 [43], the shrinkage strain at age of concrete t (days), measured from the start of drying at t_c (days), is calculated by Equation (3):

$$\varepsilon_{sh}(t, t_c) = \frac{(t-t_c)^a}{f+(t-t_c)^a} \cdot \varepsilon_{shu} \quad (3)$$

In the FE model, the laboratory-measured ultimate shrinkage strain was corrected to account for initial curing time, ambient relative humidity (RH), shape, and size effect, which will be further discussed in the next section. It is well known that shrinkage of concrete decks does not occur uniformly through-thickness and there exists a nonuniform moisture gradient that affects the drying shrinkage at various depths. Various mathematical relationships have been used to relate moisture-gradient strains to concrete internal RH. The most commonly used formula is shown in Equation (4) [26]:

$$shrinkage \propto 1 - RH^b \quad (4)$$

Where b ranges from 1 to 4. Researchers have found that $b = 3$ agrees well with shrinkage and humidity measurements in concrete specimens of different sizes [44] and many other researchers have used the equation $1 - RH^3$ to estimate RH-gradient strains [45]. In this study, the shrinkage strain obtained from Equation (3) was adjusted by Equation (4) to incorporate the existing RH gradient through deck thickness.

FE Model Validation

The full-scale FE model of the deck and girders was first validated against the measured field strain gauges of the Rarus/Silver Bow Structure, Bridge D. A 36-hour time frame after the deck concrete has reached the 28 days strength and before the bridge was opened to traffic was selected for validation. Figure 93 shows the temperature readings of this time frame at four different locations in Pour 7. The horizontal axis on these figures represents the time in days after placement. At the start of this time frame (4:00 AM, January 19th, 2020), the top and bottom of the deck temperature were around 25˚F (-4˚C) with the middle section slightly warmer, the ambient temperature was around 23˚F (-5˚C). It then cooled to 17°F (-8°C) before it warmed up to about 58˚F (14.5˚C). At about 3:00 PM, the ambient thermometer recorded the warmest time of the day at 38˚F (3.5˚C). During the night hours, it cooled down again reaching the minimum temperature of 10˚F (-12.8˚C) (ΔT=-28˚F (-16.3˚C)) in the next morning at 5:00 AM. The top thermocouple (1-5) which was located 0.75-in. below the surface follows the ambient temperature with the smallest lag, whereas, the bottom thermocouple (1-1) located 0.5-in. from the soffit lags the ambient by a few hours. Girder temperature was recorded only in one location (location 4-2) at the bottom of the top flange of the middle girder. Thermocouple recordings at each location were averaged to input in the FE model. All the thermocouples at the same depth were averaged to represent the temperature at that depth. In this case, there were five locations through the deck thickness with thermal readings corresponding to five

thermocouples. Then, these average thru-depth temperatures were used to obtain nodal temperature inputs for the FE model. The following assumptions were made when generating the nodal temperature inputs:

- Nodal inputs were calculated by interpolation of the averaged recorded data based on the vertical distance to the closest thermocouple locations.
- Nodal temperature inputs of the top and bottom surfaces were extrapolated using the two nearest thermocouple readings.
- All girders were assumed to have the same temperature changes (based on the only thermocouple reading available).

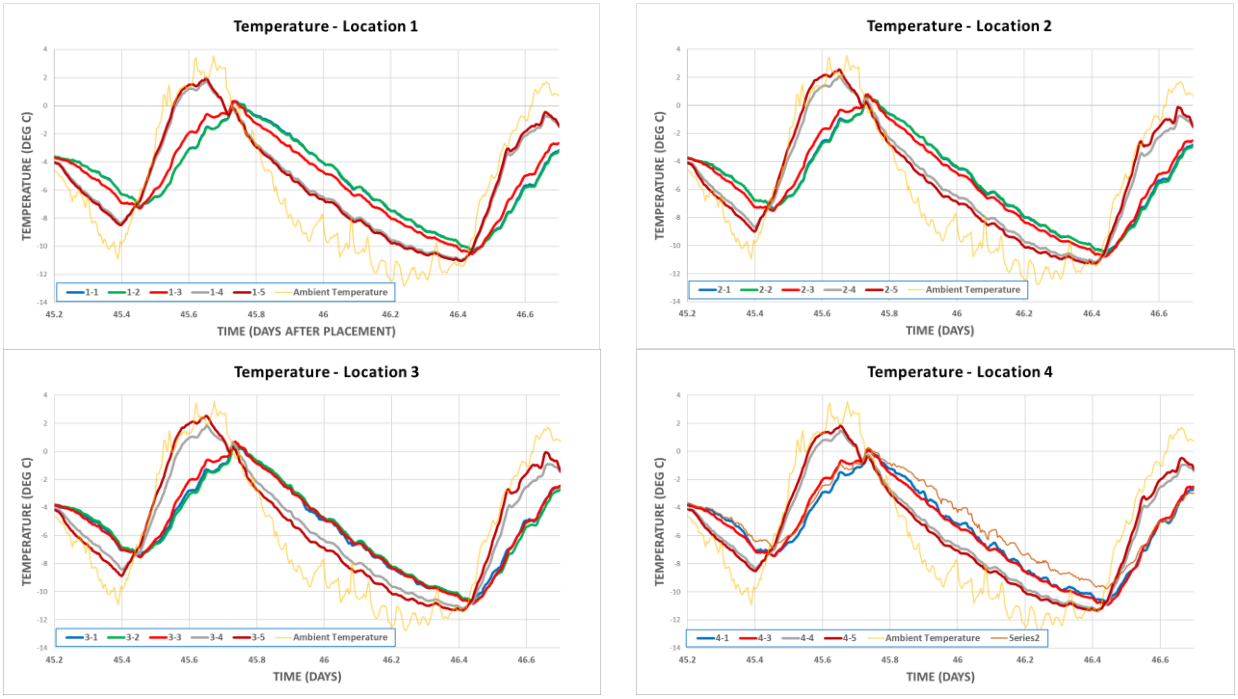

Figure 93. 36-hour time-frame showing through-thickness concrete and ambient temperature recordings at four locations in placement No. 7 to be used in FE model validation.

Figure 94 compares the average strain gauge measurements (measured in bridge longitudinal direction) at 4 locations with the FE predictions. The vertical axis of this figure represents the strain difference due to temperature changes. The strain difference at the beginning of the time frame was set to zero. The negative strain difference means compressive strains and the positive represents tensile strains. The strain figure provides further insight into the deck performance under the given diurnal temperature history. When subjected to a positive temperature difference, the deck strains tend to change from compressive to tensile. The maximum tensile and compressive strains experienced by the concrete deck lagged the ambient temperature and were coincident with the time when the steel girder reached the maximum and minimum temperatures, respectively. The FE predictions reasonably agreed with the measured strain magnitudes and matched the change in strain modes when the deck alternated between tension and compression.

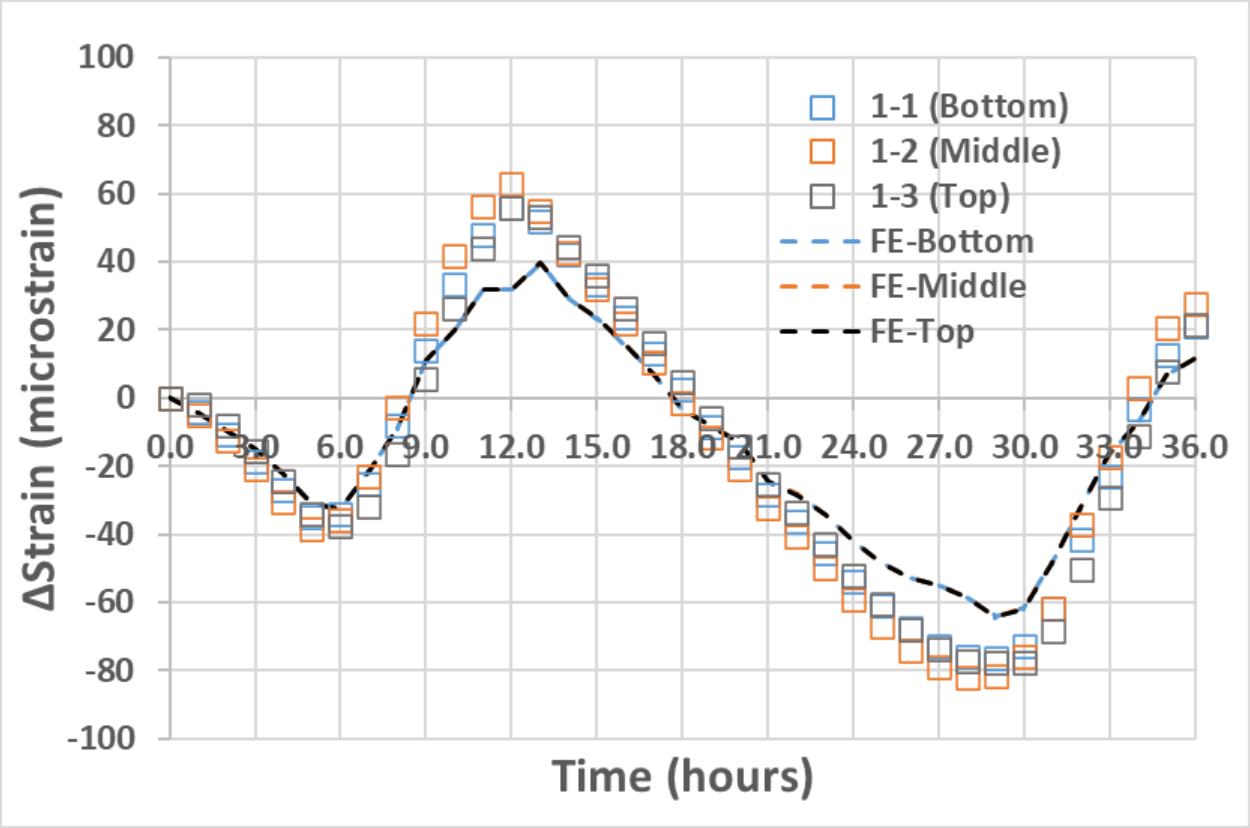

Figure 94. Thermal strain difference calculated by FE model compared with average field strain gauge readings (Gages 1-1, 1-2, and 1-3), tensile is positive.

Later-Age Analysis Scenarios

The later-age analysis scenarios were defined to identify potential causes of elevated tensile stresses and transverse cracking potential after the deck concrete has gained at least the 90-day strength level. At this age, the concrete modulus of elasticity has almost reached an asymptote and is not expected to increase much. Several diurnal temperature profiles corresponding to normal and extreme temperature rises and drops and one extreme moisture gradient profile corresponding to before and after a rain event were investigated. In all the long-term load cases, the concrete elasticity and creep properties at 90 days were used. Table 30 lists all the load cases considered for the long-term analysis. Cases 1 to 4 exclude drying shrinkage strains and are only focused on thermal stresses. Case 5 aims to predict stresses due to uniform drying shrinkage strains only, and Case 6 considers nonuniform moisture gradient and drying shrinkage across the deck cross-section. Case 7 combines the effect of nonuniform moisture gradient and diurnal temperature changes. For Cases 1 through 4, 6 and 7, the extreme temperature changes and moisture gradients were obtained from actual field measurements from the instrumented bridge deck.

Table 30. Load Cases Considered in Long-Term Analysis

Load Case No.	Load Case Name	Note
1	Temperature Drop, Normal	ΔT=-50˚F (28˚C)
2	Temperature Drop, Extreme	ΔT=-65˚F (36˚C)
3	Temperature Rise, Normal	ΔT=+55˚F (30˚C)
4	Temperature Rise, Extreme	ΔT=+70˚F (39˚C)
5	Uniform Shrinkage	Uniform shrinkage strain across deck cross-section, up to 5 months
6	NonuniformNonuniformMoisture Gradient	Ambient RH rise and drop ~ 80%
7	Combined nonuniformnonuniformMoisture and temperature Gradient	Ambient RH rise and drop ~ 80% Concrete Temperature drop and rise 55˚F (30˚C)

Temperature History Focused on Temperature Drops

The first load case corresponds to the maximum observed temperature drop of about 50˚F (28˚C) at the Rarus/Silver Bow Creek, Bridge D, site that occurred in early September. The observed concrete temperatures dropped approximately 45 to 50˚F (25 to 28˚C) in 24 hours, depending on the sensor location. The second load case was for the same period assuming that the low temperature was less than the temperature that was measured, resulting in a more extreme but practical temperature drop of 65˚F (36˚C). Figure 95 illustrates the cross-sectional temperature histories of the first two cases. The horizontal axis represents time in hours. The first 36 hours of both cases were identical representing typical diurnal cycles followed by 50˚F and 65˚F (28 to 36˚C) temperature drops, respectively for Case 1 and Case 2. Curves A to G correspond to deck top to bottom surfaces, respectively. The procedure to prepare the cross-sectional temperature inputs for the FE model was the same as previously discussed.

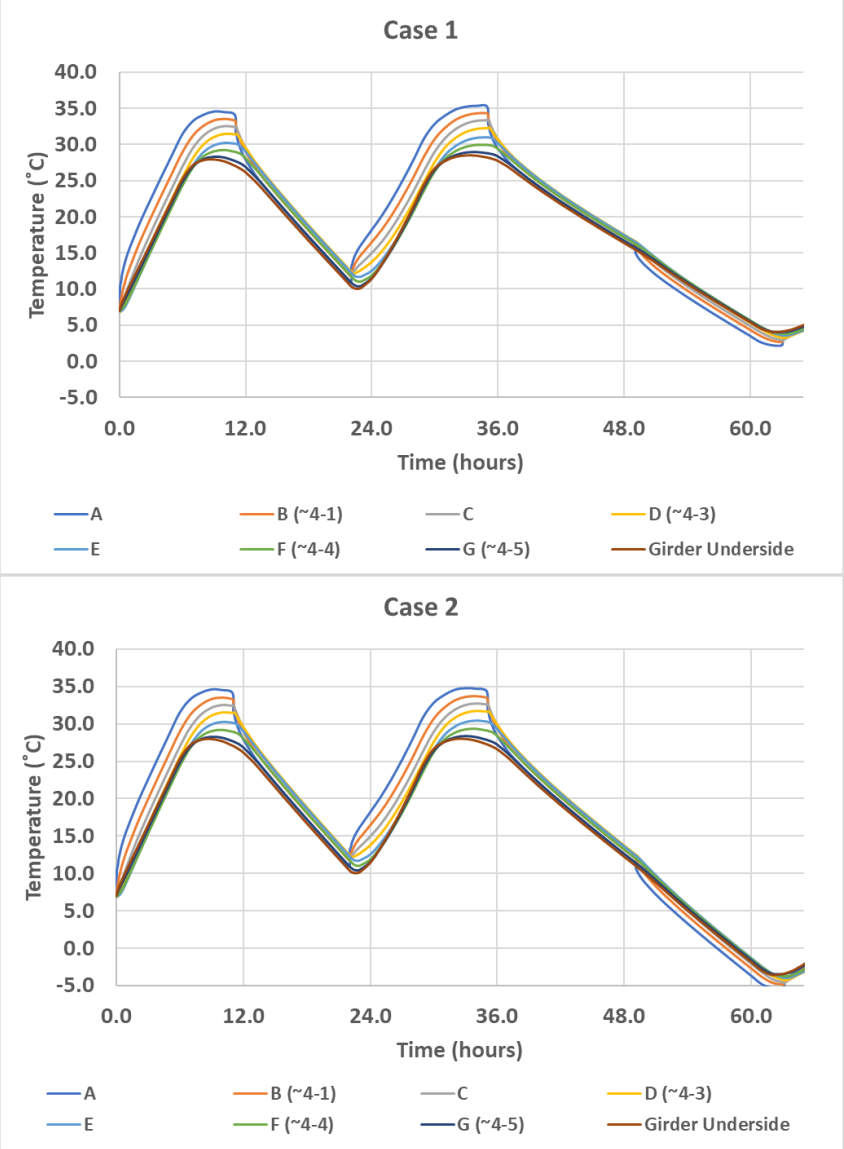

Figure 95. Case 1 and Case 2 diurnal temperature cycles focusing on effects due to maximum temperature drop. A to G represent deck top to bottom, respectively.

Figure 96 shows deck top and bottom surface longitudinal stress contours in the Pour 7 region after 35 hours. The steel girders were not shown in this view. Pour 7 is centered on Pier No. 4 which extends 40-ft. each way (left and right in the figures below). The stress unit is ksi (1,000 lbs/sq. in.) with positive stress representing tension. The longitudinal stress distribution is of primary importance since if elevated, it can lead to transverse cracking typically found on bridge decks. At the time of 35 hours (corresponding to the warmer afternoon hours), the deck cross-section from top to bottom was under tension with bottom layers experiencing more tensile stresses. The elevated tensile stresses at the bottom of the deck were due to the difference in the coefficient of thermal expansion (CTE) between steel girders and the deck. Steel girders tend to expand more than the concrete deck does because of a higher CTE, causing the deck to undergo tension. The tensile stresses were more pronounced at the girder top flange footprints due to the

tied interface definition in the FE model. This figure also shows that the stresses were locally higher at the pier centerline.

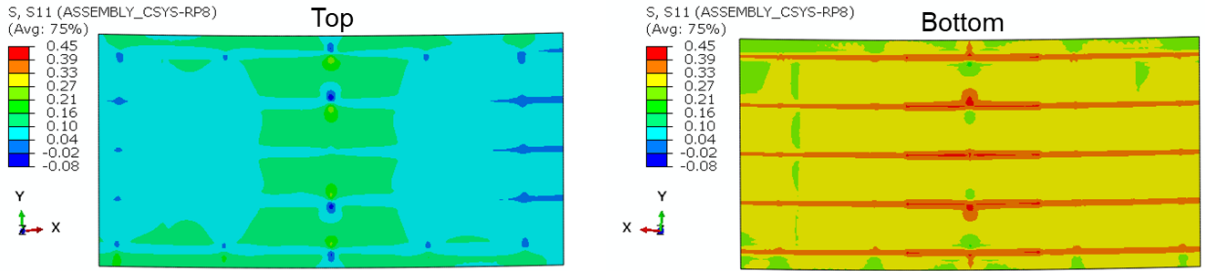

Figure 96. Longitudinal stress contours are shown for Pour 7 at 35 hours at the warmest afternoon times. The stress unit is ksi with positive indicating tensile stress.

Figure 97 compares the deck top and bottom surface longitudinal stresses after the bridge has cooled down at 60 hours (corresponding to late-night hours). These figures show that a more uniform drop in temperature resulted in more compressive stresses in the deck, as Case 2 top and bottom surfaces showed higher compressive stresses compared to the top and bottom deck in Case 1. When the ambient cools down, steel girders with higher CTE tend to contract more than the concrete deck does, causing compression in the deck cross-section. These compressive stresses decreased from the bottom of the deck to the top. Figure 97 also showed that the compressive stresses at the bottom were higher around the pier centerline.

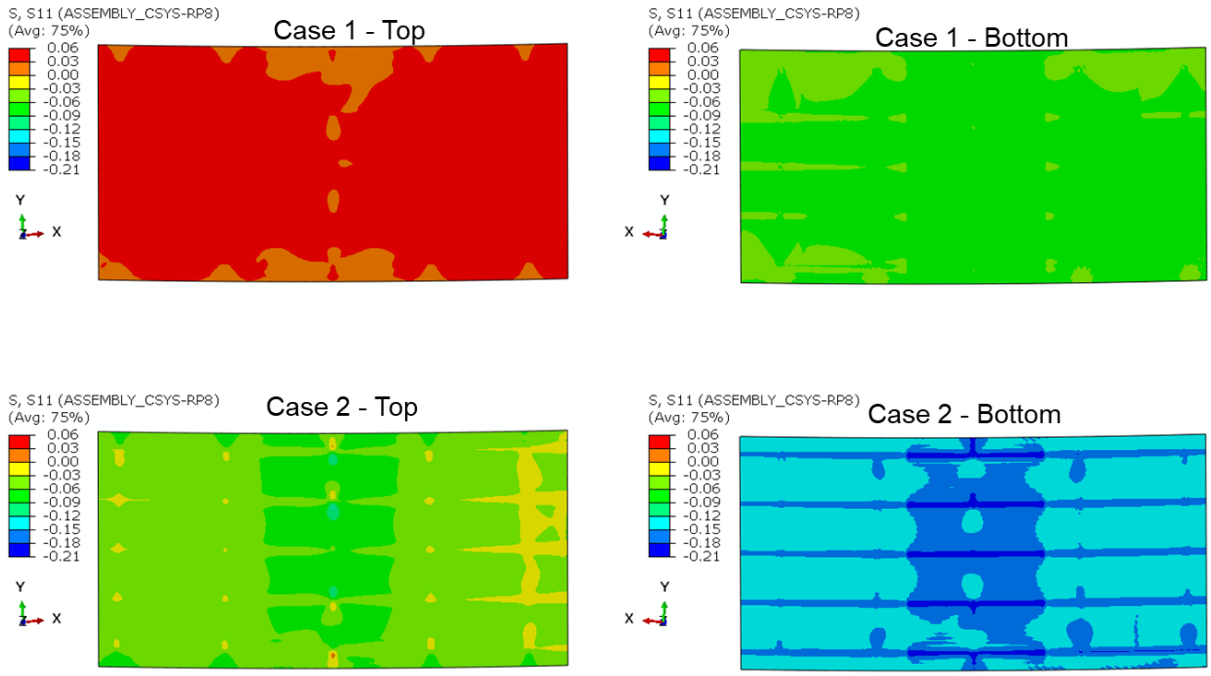

Figure 97. Longitudinal stress contours are shown for Pour 7 at 60 hours at the coldest night times. The stress unit is ksi with positive indicating tensile stress.

The longitudinal stresses were averaged across the pier centerline and compared in Figure 98 for top, center, and bottom of the deck cross-section. Several elements were selected near girders and between girders to capture the higher and lower stress regions in the averaging. It is noteworthy to mention that

from time 24 to 36 hours the deck top and bottom warmed up 45 and 40°F (25 and 20˚C)causing Δσ=+450psi and Δσ=+250psi, respectively. Then from time 36 to 60 hours the top and bottom surfaces cooled down 60 and 45°F (33 and 25˚C) causing Δσ=-300psi and Δσ=-400psi in Case 1 and Δσ=-500psi and Δσ=-400psi in Case 2, respectively.

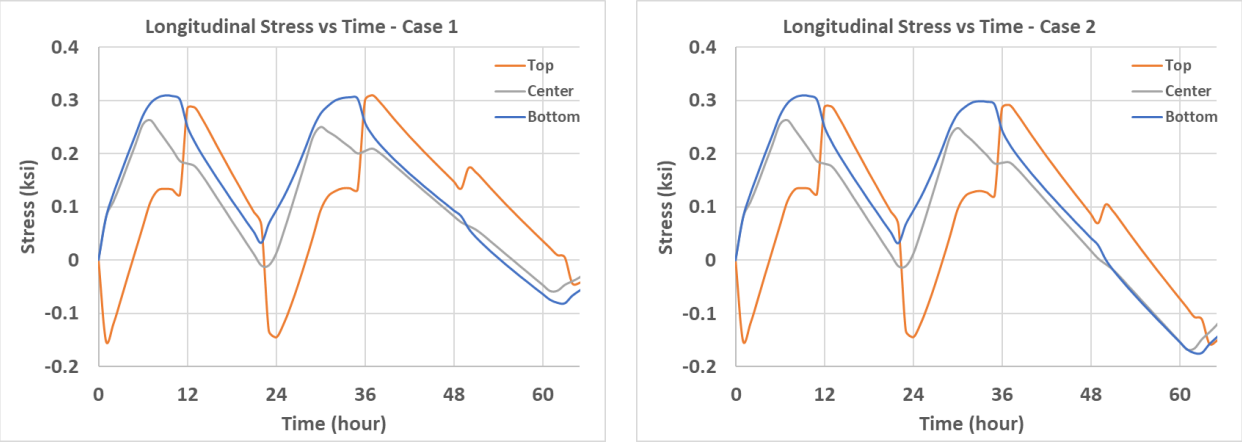

Figure 98. Average cross-sectional longitudinal stress is shown for Case 1 and Case 2. The stress unit is ksi with positive indicating tensile stress.

Temperature History Focused on Temperature Rises

The third load case corresponds to the maximum observed temperature rise of about 55˚F (31˚C) at the Rarus/Silver Bow Creek, Bridge D, site that occurred in early May. The observed concrete temperatures rose between 35 and 50˚F (19 to 28˚C) in 24 hours, depending on the sensor location. The fourth load case was for the same period assuming that the high temperature was higher than the temperature that was measured, resulting in a more extreme temperature rise of 70˚F (39˚C). Figure 99 illustrates the cross-sectional temperature histories of these two cases. The horizontal axis represents time in hours. Curves A to G correspond to deck top to bottom surfaces, respectively. The procedure to prepare the cross-sectional temperature inputs for the FE model was the same as previously discussed.

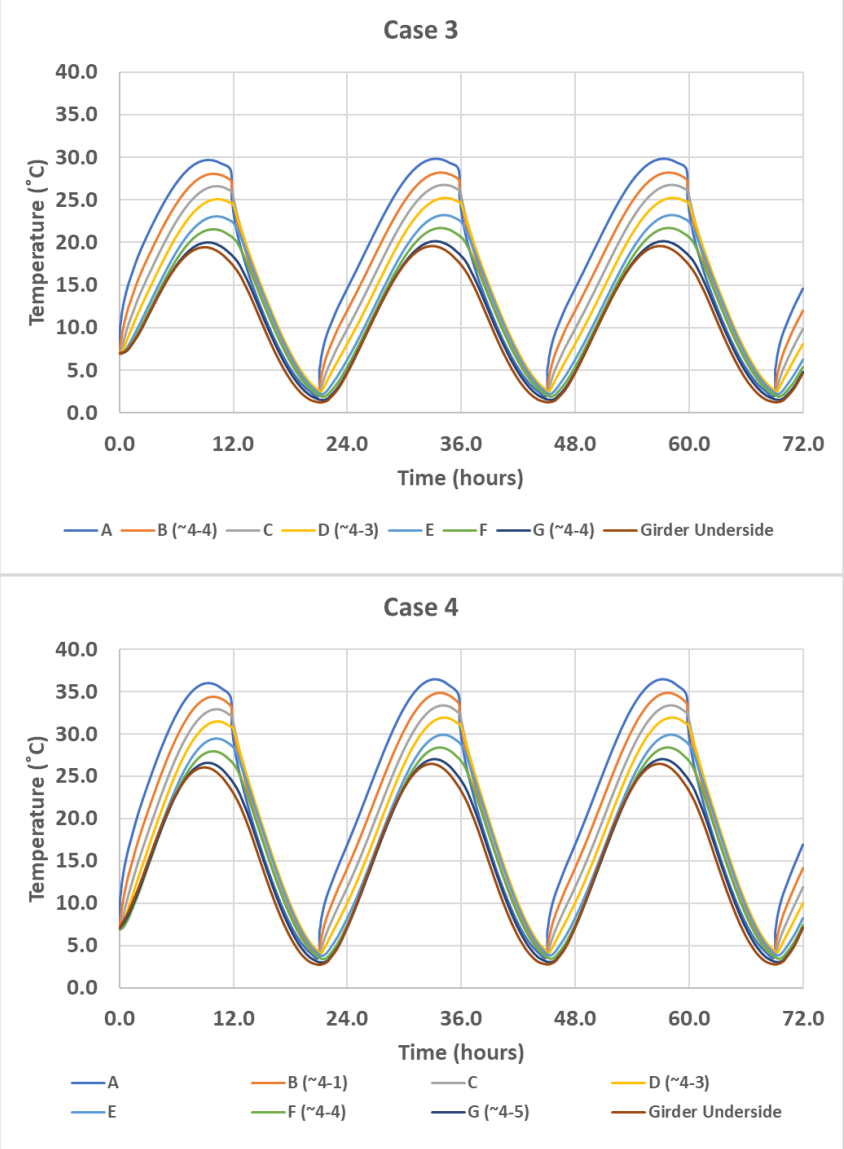

Figure 99. Case 3 and Case 4 diurnal temperature cycles focusing on effects due to maximum temperature rise. A to G represent deck top to bottom, respectively.

Figure 100 shows deck top and bottom surface longitudinal stress contours in the Pour 7 region at t=45 hours. The steel girders were suppressed from the view. At t= 45 hours (corresponding to the coldest morning hours), the deck cross-section from top to bottom was under compression with bottom layers experiencing more compressive stresses. The elevated compressive stresses at the bottom of the deck were due to the difference in the coefficient of thermal expansion (CTE) between steel girders and the deck. Steel girders with higher CTE tend to contract more than the concrete deck does, causing the deck to undergo compression. The compressive stresses were more pronounced at the girder top flange footprints due to the tie interface definition in the FE model. This figure also shows that the compressive stresses were locally higher at the pier center line and tend to reduce towards the mid-span.

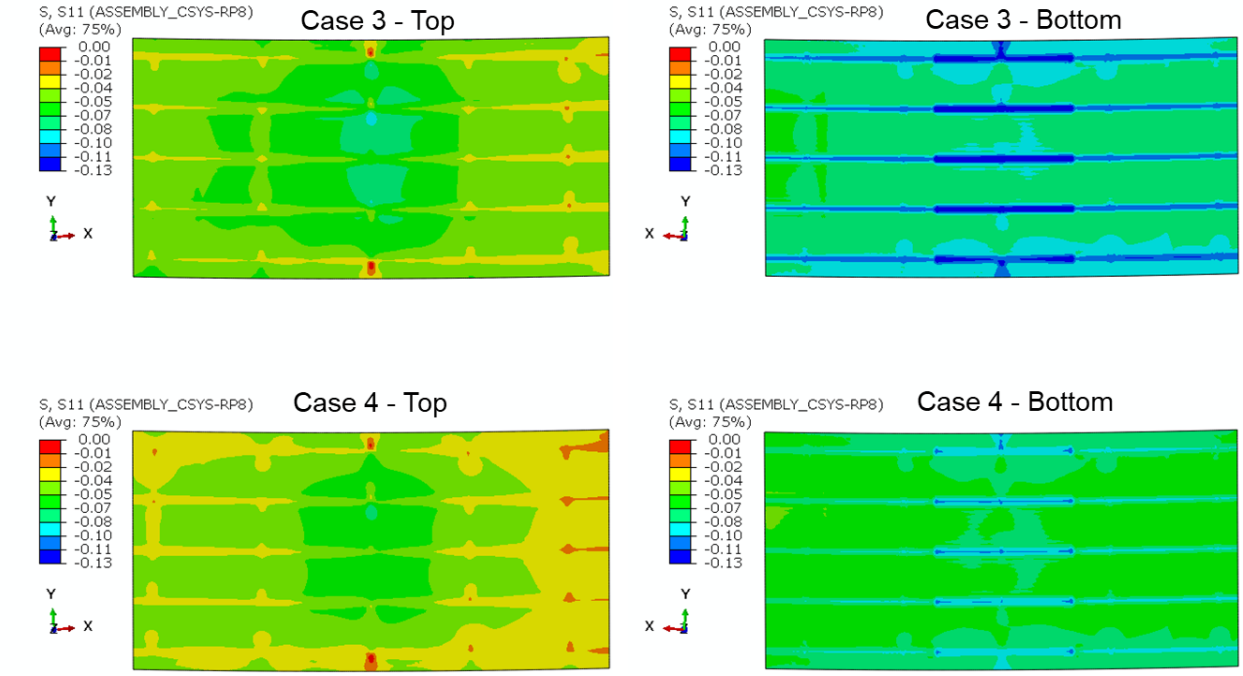

Figure 100. Longitudinal stress contours are shown for Pour 7 at 45 hours at the coldest morning hours. The stress unit is ksi with negative indicating compressive stress.

Figure 101 compares the deck top and bottom surface longitudinal stresses after the bridge has warmed up at t=60 hours (corresponding to late evening hours). These figures show that temperature rise resulted in more tensile stresses in the deck, as in Case 4 top and bottom surfaces showed higher tensile stresses compared to the top and bottom deck in Case 3. When the ambient warmed up, steel girders with higher CTE tend to expand more than the concrete deck does, causing tension in the deck cross-section. These tensile stresses decreased from the bottom of the deck to the top. Figure 101 also showed that the tensile stresses at the bottom were higher at the pier center line and near the girder lateral bracing locations.

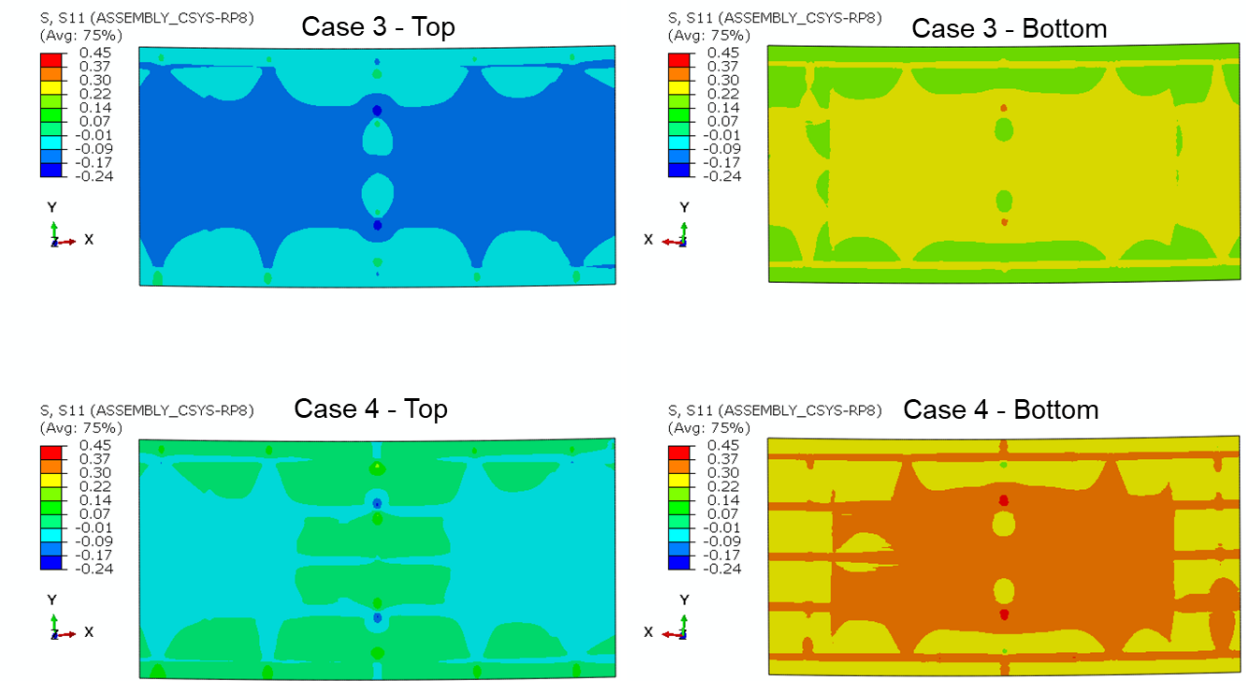

Figure 101. Longitudinal stress contours are shown for Pour 7 at 58 hours at the warmest afternoon times. The stress unit is ksi with positive indicating tensile stress.

The longitudinal stresses were averaged across the pier centerline and compared in Figure 102 for top, center, and bottom of the deck cross-section. Several elements were selected near girders and between girders to capture the higher and lower stress regions in the averaging. This figure showed that from t=48 hours to t=58 hours there was a positive stress range (Δσ) increase in the top surface stress with a second jump from t=58 hours to t=61 hours. The second jump was due to the nonuniform temperature gradient that existed within the deck at this time frame. The top surface temperature dropped about 20°F (11˚C) in just 3 hours, which was twice as high as the bottom surface temperature drop. In this case, the top surface must contract more than bottom layers that now act as restraint causing an additional jump in tensile stresses at the top surface. The highest predicted tensile Δσ in Case 3 and 4 from t=48 to t=61 hours were 420 and 510 psi at the top surface, respectively.

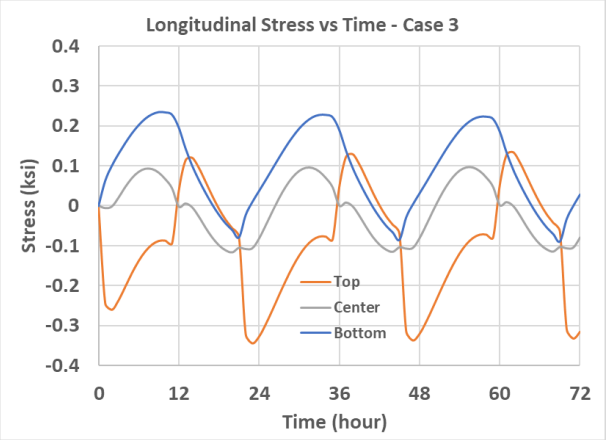

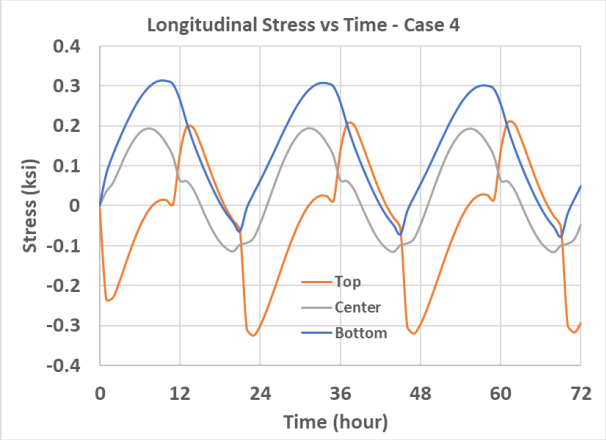

Figure 102. Average cross-sectional longitudinal stress shown for Case 3 and Case 4. Stress unit is ksi with positive indicating tensile stress.

Uniform Drying Shrinkage

Restraint of drying shrinkage of concrete leads to internal tensile stress development. The differential humidity (RH) between concrete and the ambient air is the driving force for drying shrinkage. ACI and many other design codes provide equations to estimate concrete shrinkage strain at different ages, many of which require the estimation of ultimate shrinkage strain. As part of the laboratory evaluations in Item 4.5a the concrete drying shrinkage strain was measured in accordance with ASTM C157 and the ultimate drying shrinkage was calculated using the equations in ACI 209.2R-08 [43]. Table 31 summarizes the parameters and correction factors used to estimate the deck shrinkage strain.

Table 31. Summary of Parameters Used to Estimate Drying Shrinkage Strain Per ACI 209

Parameter	Magnitude
Ultimate Shrinkage Strain by ASTM C157, ε_{shu}	420 μ strain
Annual Ambient Relative Humidity, RH	60%
Initial Curing Time, t_c	14 days
Volume to Surface Ratio, V/S	3.81 in
Shape and Size Factor, f	102.6 days
Time order, α	1.0
Initial Moist Curing Coefficient, $\gamma_{sh,tc}$	0.93
Ambient Relative Humidity Coefficient, $\gamma_{sh,RH}$	0.88
Size Coefficient, $\gamma_{sh,vs}$	0.76

Figure 103 shows the estimated shrinkage strain with time for the concrete deck up to 150 days after placement. In the FE model input, the shrinkage strain was converted to equivalent temperature, shown on the right vertical axis in Figure 103.

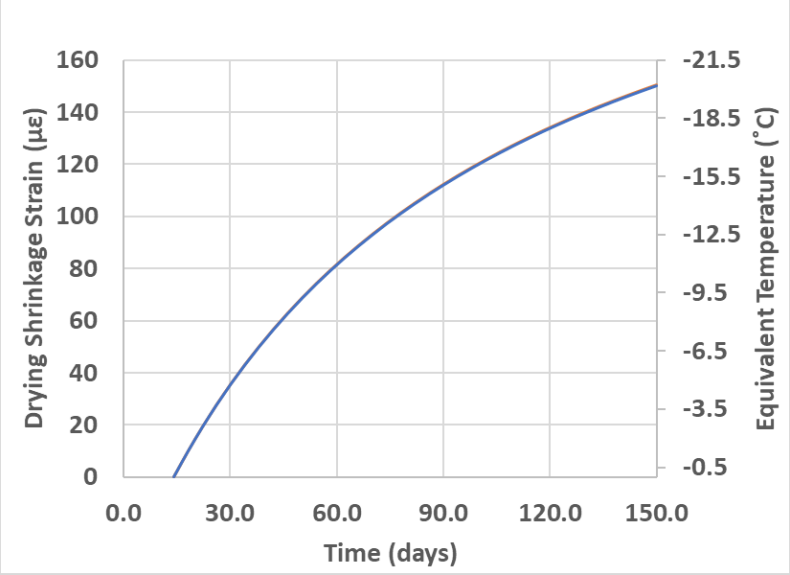

Figure 103. Estimated drying shrinkage strain profile of the bridge deck converted to equivalent temperature to be used in the FE model.

Figure 104 shows deck top and bottom surface longitudinal stress contours in the Pour 7 region at t=150 days. The steel girders were suppressed from the view. At this time, the deck cross-section from top to bottom was under tension with bottom layers experiencing more tensile stresses. The elevated tensile stresses at the bottom of the deck were due to the restraining effect of the steel girders that are highest at the bottom of the deck. The tensile stresses were more pronounced at the girder top flange footprints due to the tie interface definition in the FE model. This figure also shows that the tensile stresses were locally higher at the pier center line and tend to reduce towards the mid-span. At the top of the deck, tensile stresses were higher in between the girder lines. The magnitude of the tensile stresses was not high enough to cause cracking. According to the lab data, the concrete specimen had a 90-day splitting tensile strength of 588 psi.

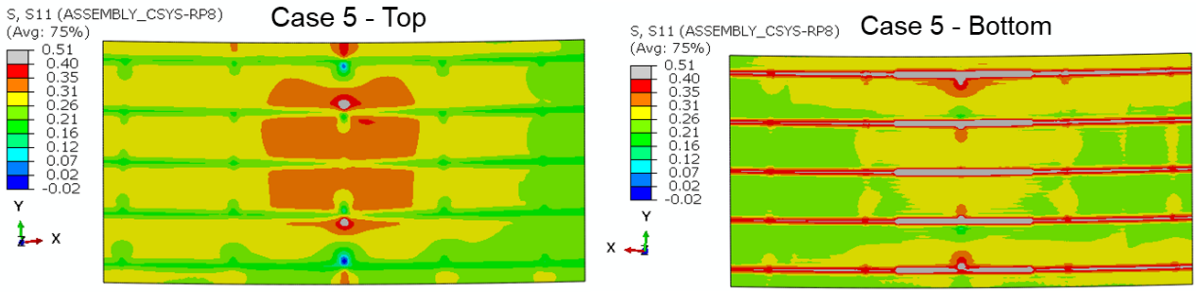

Figure 104. Longitudinal stress contours are shown for Pour 7 after simulating 150 days of drying shrinkage. The stress unit is ksi with positive indicating tensile stress.

The longitudinal stresses were averaged across the pier centerline and compared in Figure 105 for top, center, and bottom of the deck cross-section. Several elements were selected near girders and between girders to capture the higher and lower stress regions in the averaging. The FE model prediction showed that after 150 days the tensile stress as high as 300 psi can develop across the deck cross-section with

bottom layers undergoing slightly higher tensile stress. Age-dependent creep behavior was included in this analysis case to capture stress relaxation with time.

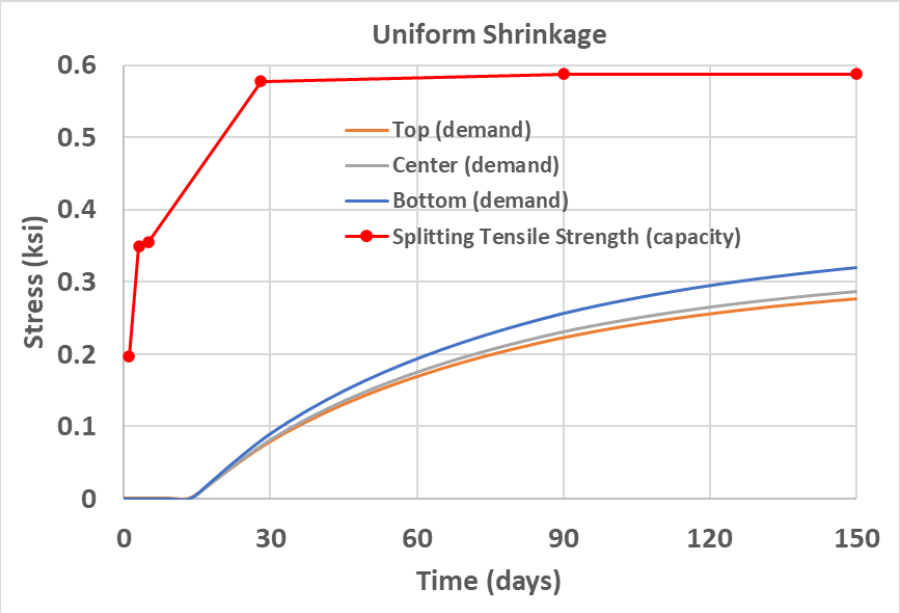

Figure 105. Predicted average longitudinal stress is shown for the uniform shrinkage load case (Case 5). The stress unit is ksi with positive indicating tensile stress.

Moisture Gradient

Since the bridge decks are exposed to ambient air on the top and bottom sides, water movement takes place due to surface evaporation and moisture diffusion causing nonuniform cross-sectional moisture distribution, which in turn results in differential drying shrinkage. It is known that concrete subjected to daily cycling of RH in the field can approach the same shrinkage level as that caused by completed drying at a constant RH level. Therefore, the magnitude of differential shrinkage due to nonuniform RH distribution can become significantly greater than the thermal strains. In this case, if external restraints to the nonuniform volume change are added, it can lead to significant tensile stresses and cracking.

To investigate the nonuniform moisture gradient effect, a two-week time frame was selected from June 1st, 2020 where two rain events were observed causing significant ambient and concrete RH changes based on data collected from field instrumentation. Figure 106 shows the measured ambient and concrete RH with time for this time frame. Since the field instrumentation measured the in-place RH approximately 1/2 inch from the top and bottom surface of the deck, the top and bottom concrete RH profiles were estimated by assuming a factor of 1.05 at the peaks and 0.95 at the valleys of RH readings at the nearest RH gauge. As shown, before the rain event, the mid-section RH sensor (4-2) had always higher RH with respect to the top and bottom sensors (4-3 and 4-1) when the ambient RH was low (dry condition), indicating the deck had lost more moisture from the top and bottom. After the first rain event, the ambient RH reached 100 percent RH from 25 percent in about 36 hours. Consequently, the top RH sensor located near the top surface measured a concrete RH of 100 percent, whereas the bottom RH sensor recorded 75 percent indicating at least 25 percent RH difference from top to bottom.

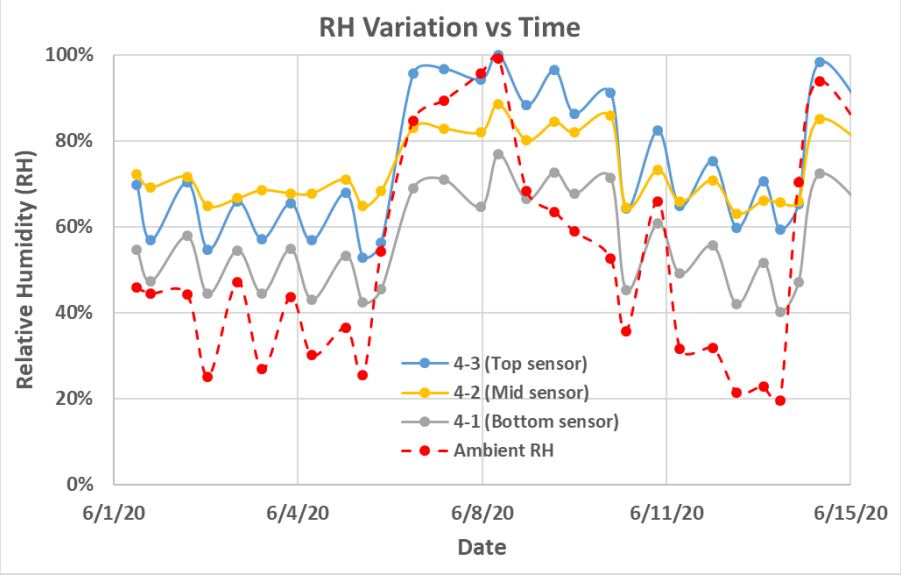

Figure 106. Deck cross-sectional and ambient RH variation recorded in early June 2020.

To translate the RH data to FE model input, the cross-sectional RH measurements from top to bottom were first converted to shrinkage strain forms using Equations (3) and (4) then to equivalent temperatures by dividing to the CTE of concrete. Figure 107 shows the longitudinal stress contours on the bridge deck top and bottom in Pour 7 due to nonuniform RH gradient before and after the rain event discussed above. Before the rain event, the concrete RH difference between the top and bottom was relatively small in the range of 10 to 13 percent. After the ambient RH rose to 100 percent due to rain, the top surface RH also rose to 100 percent (a 53 percent increase). The bottom surface on the other hand reached 74 percent RH level, leaving a significant 26 percent RH difference between the top and bottom of the deck. As a result, higher shrinkage strains were expected to occur at the bottom rather than the top, leading to a substantial increase in tensile stresses at the deck soffit as shown in Figure 107. This is analogous to bottom layers cooling down with a higher rate relative to top layers of the deck that would lead to a similar conclusion. It is noted that no thermal strains were included in this particular load case and only the effect of cross-sectional RH gradient was studied. The thermal strains effect can be additive or subtractive which is discussed next. The tensile stresses observed at the bottom of the deck tend to be higher than concrete tensile strength particularly near the pier center line and at the lateral bracing locations solely from the moisture gradient observed that could lead to crack initiations in these regions.

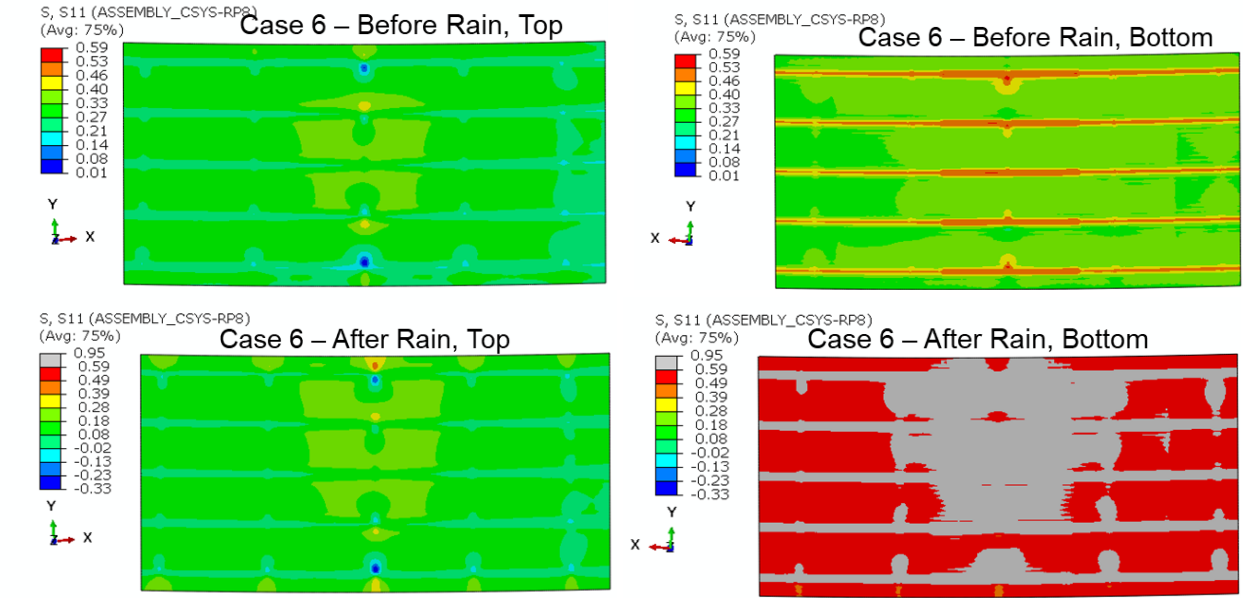

Figure 107. Longitudinal stress contours are shown for Pour 7 before and after a rain event. The stress unit is ksi with positive indicating tensile stress.

The longitudinal stresses were averaged across the pier centerline and compared in Figure 108 for top, center, and bottom of the deck cross-section. Several elements were selected near girders and between girders to capture the higher and lower stress regions in the averaging. The FE model prediction showed that right after the rain event (June 6th) the tensile stress as high as 700 psi can develop at the bottom layers reducing to 450 psi at the centroid. About 8 days after the rain, the ambient RH dropped back to the 20 percent range, causing the top deck to undergo more shrinkage relative to the centroid and bottom leading to $\Delta\sigma$=+200 psi in this time frame.

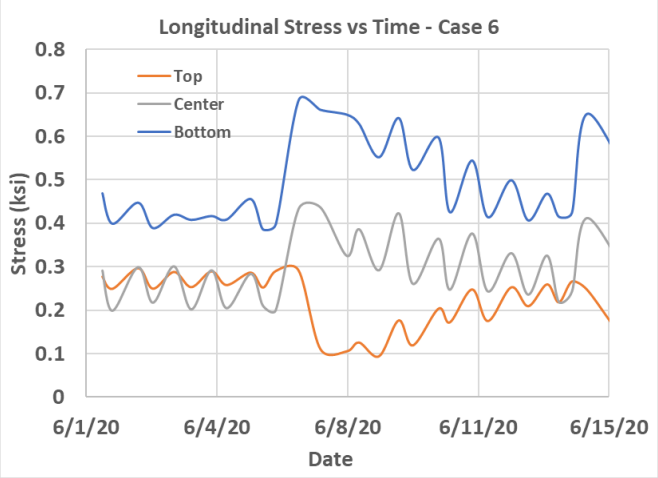

Figure 108. Predicted average longitudinal stress is shown for the nonuniform RH gradient load case (Case 6). The stress unit is ksi with positive indicating tensile stress.

Combined Moisture and Temperature Gradient

Results from the nonuniform moisture gradient case were combined with the measured temperature data of the same period to analyze the stress results from the nonuniform moisture gradient case were merged with the results from the nonuniform temperature gradient of the same period to analyze the combined effects of both actions. The starting point of this analysis case was chosen to correspond to the time when the deck mid-section had 65 percent RH and top to bottom showed an almost uniform temperature of 82˚F (28˚C). The stress state was assumed to be zero at the beginning of this analysis case to study the relative stress changes due to RH and temperature gradients. Figure 109 shows the RH (left vertical axis) and temperature (right vertical axis) variations within the same time frame. It is clear from this figure that the peaks on the temperature profile coincide with valleys on the RH profile. In other words, concrete RH was always lower at the warmest time of the day and highest at the coldest time of the day. When the rain event started on or about June 6th, 2020, there was also a substantial decrease in the ambient temperature of about 55°F (30˚C). In the previous section, it was shown that a reduction in concrete RH was analogous to concrete cooling down and an increase in concrete RH was similar to concrete heating up. As a result, it is shown that the combined effect of RH and temperature loading to be subtractive.

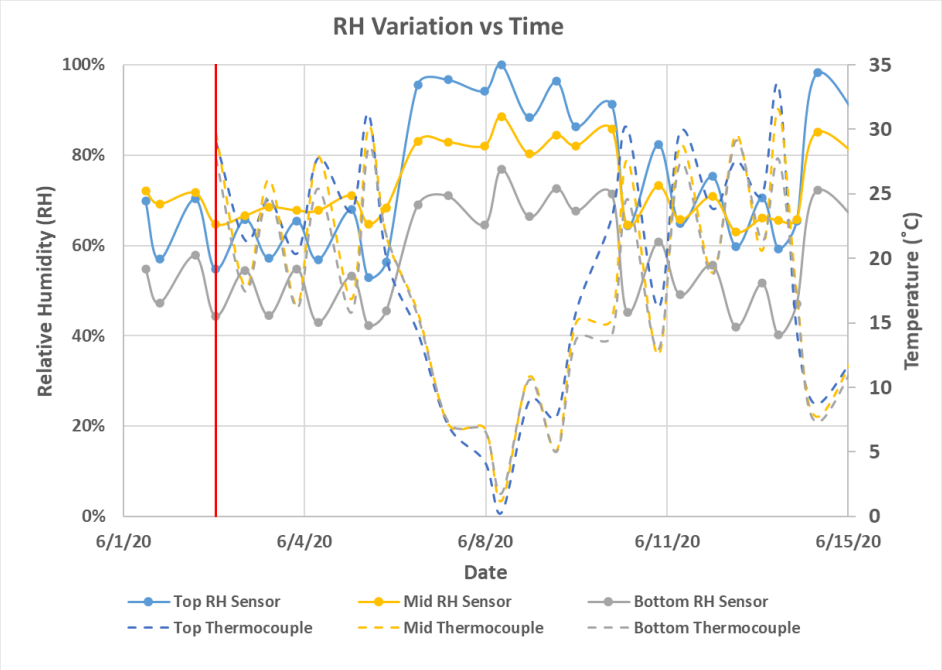

Figure 109. Deck cross-sectional RH and temperature variation recorded in early June 2020. The red line indicates the starting point of the analysis Case 7 where a zero stress state was assumed.

The longitudinal stresses were averaged across the pier centerline and compared in Figure 110 for top, center, and bottom of the deck cross-section. Several elements were selected near girders and between girders to capture the higher and lower stress regions in the averaging. The previously observed higher tensile stresses after the first rain event at the bottom and mid-section of the concrete deck have now been countered by compressive stresses that developed due to decreasing deck temperature. The FE model prediction also showed a spike in the top section tensile stress right after the rain event. This higher

tensile stress coincided with the time when concrete was cooling down from a previous peak temperature and the time when concrete RH was sharply increasing.

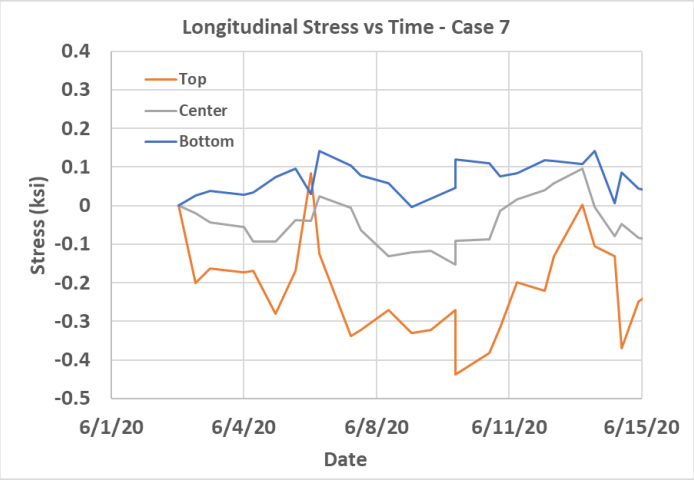

Figure 110. Predicted average longitudinal stress is shown for the combined nonuniform RH and temperature gradient load case (Case 7). The stress unit is ksi with positive indicating tensile stress.

Early-Age Analysis Scenarios

The early-age analysis scenarios were defined to identify potential causes of elevated tensile stresses within the first 14 days of the concrete deck after placement. This analysis section was focused on investigating the effectiveness of the alternative (WJE's) curing recommendations on the stress performance of the deck. The calibrated 1- to 14-day material properties; such as modulus of elasticity and creep parameters, were used to capture the early age time-dependent response of the concrete deck. Four load cases were defined related to early-age deck conditions and analyzed. The first two load cases correspond to typical summer placement with a 4-day insulation period or without insulation but with 14-day wet curing. The third load case was to simulate typical winter placement with a 14-day insulation period, similar to what was done on the instrumented bridge. The fourth load case also corresponded to winter placement with 5-day curing period. Table 32 lists the four load cases considered for the early-age analysis. Since during the early-age analysis cases the concrete deck was either insulated or wet-cured before exposure to ambient conditions, the amount of drying shrinkage was assumed negligible, and only thermal loads were included.

Table 32. Short-Term Analysis Case Details

Load Case No.	Placement Time	Insulation	Wet-Curing time	Other factors considered
1	Summer, 4 pm	Yes, 0 to 4 days	4 days	
2	Summer, 4 pm	No	14 days with plastic sheeting	
3	Winter, 4 pm	Yes, 0 to 14 days	14 days	Enclosure heated for 14 days
4	Winter, 4 pm	Yes, 0 to 5 days	5 days	Blankets and heating pipes applied from the top

Summer Placement

The first two load cases correspond to summer placement to show the benefits of WJE's curing recommendations. In Case 1, insulation was applied for up to 4 days after placement. It was assumed that the concrete placement was completed by 4 pm with an initial temperature of 75˚F (24˚C). Girder initial temperatures were assumed 62˚F (16.7˚C). The ambient temperature fluctuated between 42˚F (5.5˚C) and 80˚F (27˚C). At the end of the cure periods (4 or 14 days), it was assumed that the formwork and insulation were removed at noon. Thermal model simulations of all cases were performed using the 4C-Temp&Stress tool. Case 1 was simulated for up to 7 days. In Case 2, no insulation was included but 14 days of wet curing with plastic sheeting was considered before exposure to ambient temperature and Case 2 was simulated for up to 17 days. Other assumptions were the same as Case 1.

Figure 111 illustrates the cross-sectional temperature histories of the first two cases. The horizontal axis represents time in hours. Curves A to G correspond to deck top to bottom surfaces, respectively. The procedure to prepare the cross-sectional temperature inputs for the FE model was the same as previously discussed.

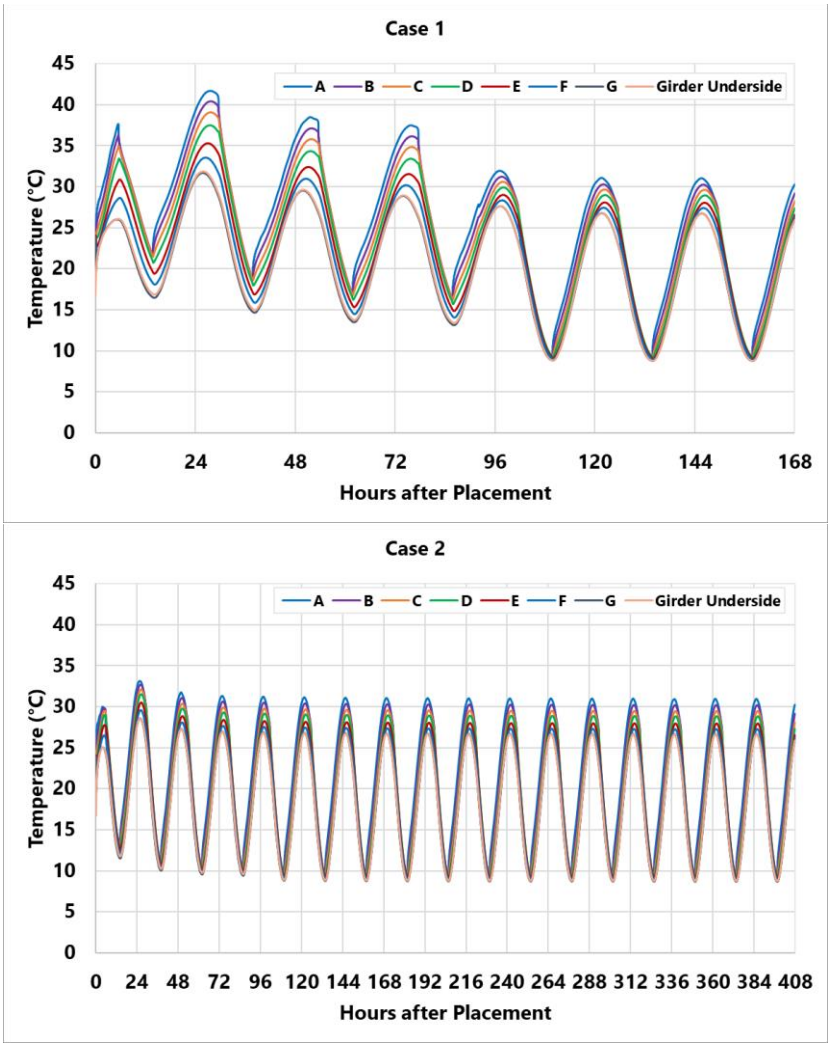

Figure 111. Case 1 and Case 2 concrete cross-sectional temperature cycles for summer placement scenarios. A to G represent deck top to bottom, respectively.

The longitudinal stresses were averaged across the pier centerline and compared in Figure 112 for the top, center, and bottom of the deck cross-section. Several elements were selected near girders and between girders to capture the higher and lower stress regions in the averaging. In the stress analysis of short-term cases, it was assumed that the first 24 hours was the zero-stress state in which no stresses could develop due to thermal straining. In Case 1, the FE model predicted little to no tensile stress within the 4-day curing period with insulation. The stress mode remained in the compression zone (negative stress) varying almost uniformly in this period with the peak to peak amplitude of about 150 psi ($\Delta\sigma_{max}$=150 psi). The average 5-day splitting tensile strength was 355 psi, so cracking would not be expected. Upon removal of insulation and exposure to ambient temperature at day 4, nonuniform stresses develop top to bottom with the top surface having a higher stress amplitude of 250 psi ($\Delta\sigma_{max}$=150 psi). The result of analysis Case 1 showed slight increase in tensile stresses after exposure to normal ambient temperatures. Analysis Case 2 on the other hand, showed a small tensile stress magnitude up to 40 psi from the first day of curing, however, the stress amplitude remained almost equal to the Case 1 result. The result of analysis Case 2 also showed no elevated tensile stresses after exposure to normal ambient temperatures.

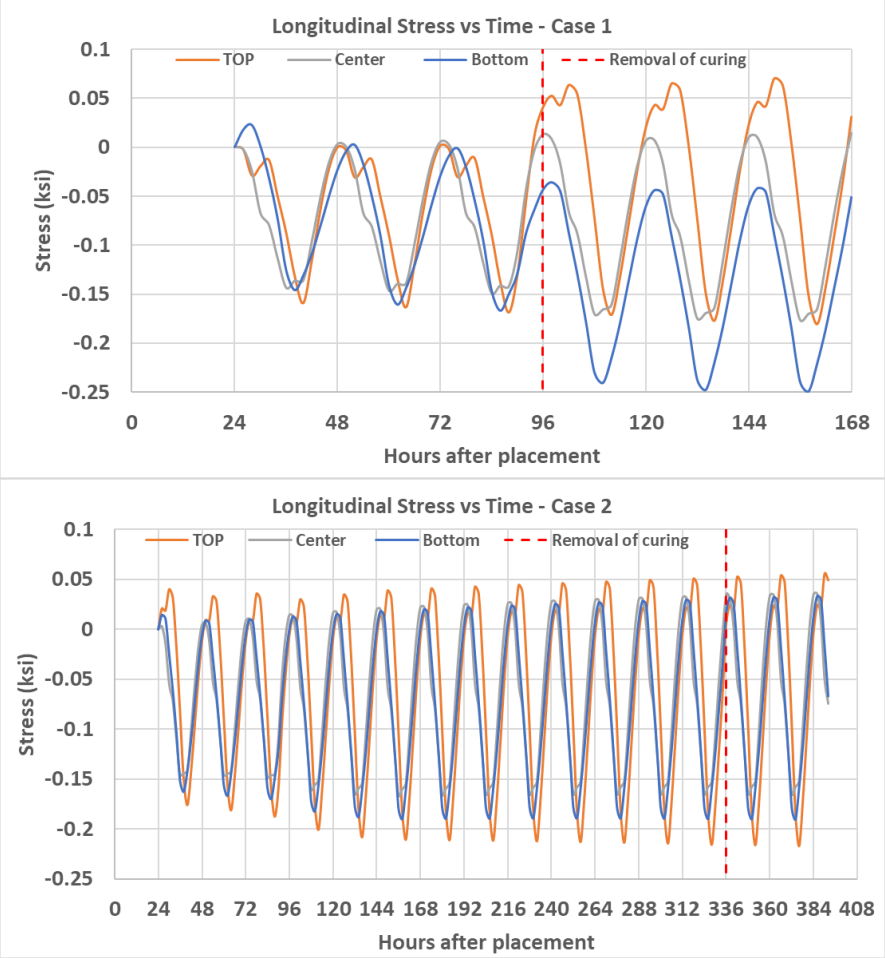

Figure 112. Average cross-sectional longitudinal stress is shown for short-term analysis Case 1 and Case 2. The stress unit is ksi with positive indicating tensile stress.

Winter Placement

The third and fourth cases correspond to winter placement. In case three, insulation and enclosure heating from the deck bottom was applied for up to 14 days after placement. It was assumed that the concrete was placed by 4 pm with an initial temperature of 67˚F (20˚C). Girder's initial temperature was assumed 77˚F (25˚C). The ambient temperature fluctuated between 12˚F (-11˚C) and 36˚F (2˚C). It was assumed that the formwork and insulation were removed at noon. The thermal model simulation was performed using the 4C-Temp&Stress tool. Case 3 was simulated for up to 16 days.

In load case four, blankets and heating pipes were applied from the top of the deck for up to 5 days after placement. It was assumed that the concrete was placed by 4 pm with an initial temperature of 67˚F (20˚C). Girder's initial temperature was 57˚F (14˚C). Girders received no heating exposure from the curing procedure, and they were assumed to fluctuate with ambient temperature. The ambient temperature fluctuated between 25˚F (-4˚C) and 52˚F (11˚C). It was assumed that the formwork and insulation were removed at night. Case 4 was simulated for up to 5 days. Figure 113 shows the cross-sectional temperature histories of the winter placement cases. The horizontal axis represents hours after placement. Curves A to G correspond to deck top to bottom surfaces, respectively. In case 3, the insulation and

enclosure heating application kept the deck temperature range between 59 and 68˚F (15 and 20˚C) for 14 days after the initial hydration heat dissipated. The procedure to prepare the cross-sectional temperature inputs for the FE model was the same as previously discussed.

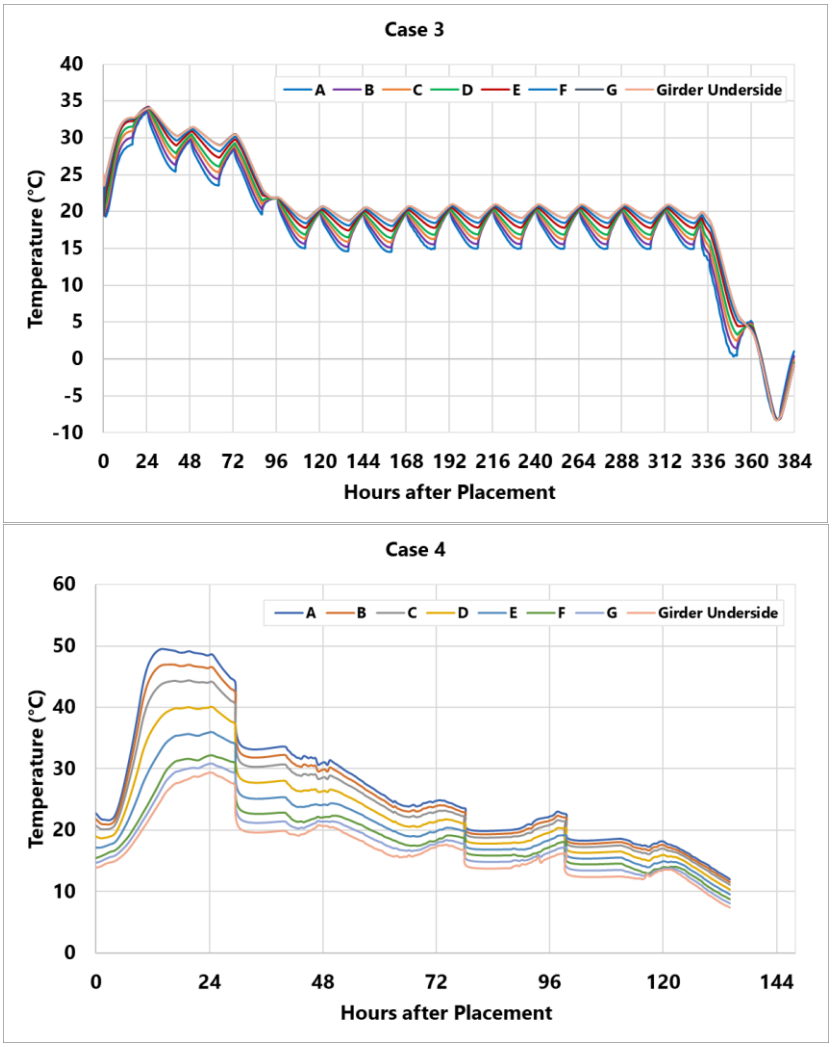

Figure 113. Case 3 (top) and Case 4 (bottom) concrete cross-sectional temperature cycles for winter placement. A to G represent deck top to bottom, respectively.

The longitudinal stresses were averaged across the pier centerline and compared in Figure 114 for top, center, and bottom of the deck cross-section. Several elements were selected near girders and between girders to capture the higher and lower stress regions in the averaging. It was assumed that the first 24 hours was the zero-stress state in which no stresses could develop due to thermal straining. In Case 3, the FE model predicted small tensile stress of 40 psi within the first 4 days of the curing period when the heat of hydration was dissipating. After that, the stress mode remained well in the compression zone (negative stress) for the 14-day insulation and enclosure heating period with the peak-to-peak amplitude of about 75 psi ($\Delta\sigma_{max}$=75 psi). Upon removal of insulation and exposure to ambient temperature at day 14, nonuniform stresses develop top to bottom; however, due to cold ambient temperatures, the cross-

sectional stresses remained in the compressive zone. Therefore, the result of analysis Case 3 showed no elevated tensile stresses after exposure to normal ambient temperatures.

In Case 4, the FE model predicted elevated tensile stress of 200 to 300 psi at the top of the deck within the first 5 days after placement. The early-age splitting tensile stress of the material ranges between 200 to 350 psi. The bottom of the deck remained in the compression zone. The elevated tensile stresses at the top of the deck can be explained by the deck being heated only from the top. At the peak of hydration heat, there was a 36°F (20˚C) temperature difference from the top of the deck to the girders. After the hydration, the concrete deck cools down at a higher rate relative to girders that are already exposed to cold ambient temperature. The contraction of the concrete deck, particularly at the top surface, is restrained by steel girders that result in the development of tensile stresses equal to splitting tensile strength.

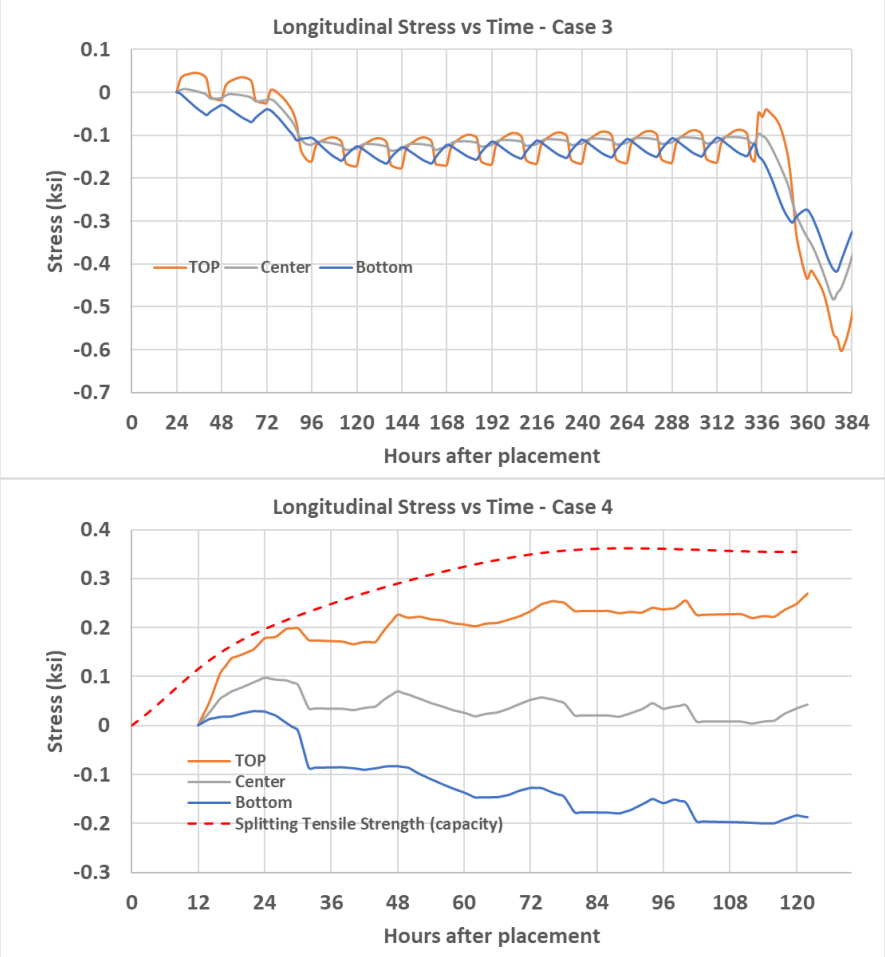

Figure 114. Average cross-sectional longitudinal stress is shown for early-age analysis Case 3. (top) and Case 4 (bottom) The stress unit is ksi with negative indicating compressive stress.

Sensitivity Study

Girder Restraint

Deck restraining can be classified into two broad categories, internal and external restraints. Internal restraints are provided by bridge reinforcement and due to nonuniform cross-sectional temperature or moisture gradients. In the composite deck system, the external restraint is predominantly provided by girders due to the presence of shear studs and friction between deck and girder top flange. The degree of restraint is defined as the ratio of actual stress resulting from volume change to the stress that would result if completely restrained. In this study, in addition to the base-line model, two other cases with different degrees of constraint were selected to investigate the girder restraining effect on deck response to thermal loads. As previously discussed, the baseline model represented a fully composite deck-girder system without any allowance for slippage of the concrete deck. Consequently, Case 2 and Case 3 represent partial composite and non-composite deck systems. To estimate the degree of restraint in each case, an average cross-sectional stress response due to a temperature change of 18°F (10˚C) was compared to a case where a concrete section was fully restrained. Table 33 lists all the cases included in

this section. The cases outlined in this table were all subjected to the same temperature profiles previously introduced as Case 3 in Figure 99.

Table 33. Cases Considered to Investigate Girder Restraint Effect on Concrete Deck Stress Response

Case No.	Case Name, Condition	Deck Slippage Allowed?	Average Degree of Restraint
1	Base-line, full composite	No	50%
2	Partial Composite	Yes, some slipage	29%
3	Non-composite	Yes, more slipage	0%

In each case, the longitudinal stresses were averaged across the pier centerline and compared in Figure 115 for top, center, and bottom of the deck cross-section. Several elements were selected near girders and between girders to capture the higher and lower stress regions in the averaging. This figure showed that with the same diurnal temperature changes, the stress amplitude (max stress - min stress) decreases with a decrease in the degree of constraint. The most reduction in stress amplitude was observed at the deck mid-section for the non-composite case. Previously, it was argued that the second jumps in the tensile stresses at the top surface (t=12, 36, 60 hours) was due to a nonuniform temperature gradient. It is shown here that the stress magnitudes after these jumps remained unchanged due to a change in the degree of restraint provided by girders. In other words, the main cause of the jumps, the internal restraint because of the temperature gradient, was unaffected. Table 34 summarizes the percent change in stress amplitude due to different degrees of constraint. It is noted that despite a reduction in stress amplitude in the non-composite deck section, it will be unfavorable to design a non-composite deck when subjected to vehicular live loads.

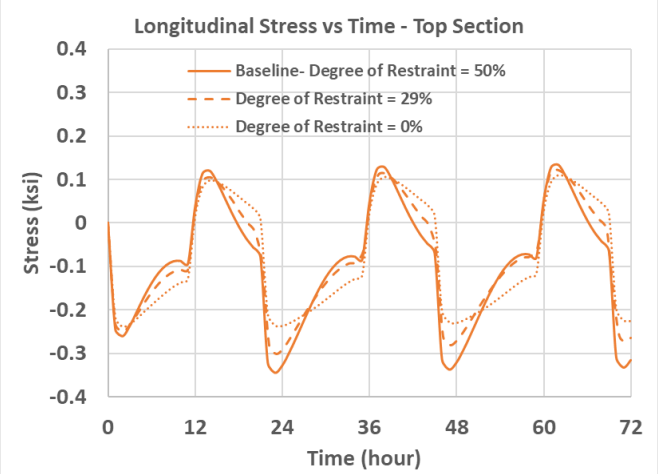

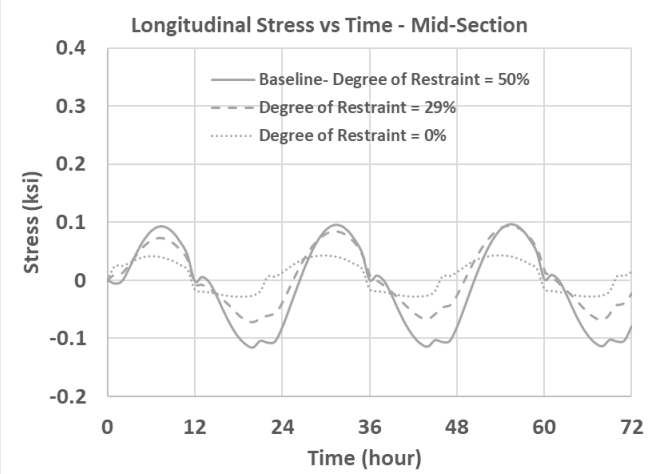

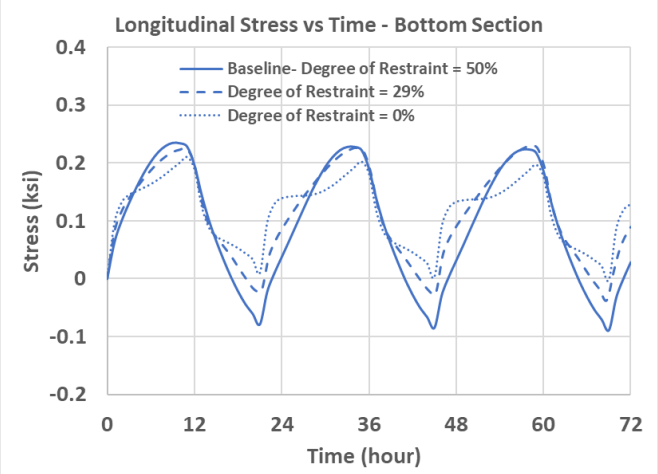

Figure 115. Average cross-sectional longitudinal stress is shown for different degree of restraints at the top, center, and bottom of deck cross section. The stress unit is ksi with positive indicating tensile stress.

Table 34. Percent Change in Average Stress Due to Varying External Degree of Constraint

Case No.	Case Name, Condition	Average Degree of Restraint	Percent change in stress amplitude		
			Top	Center	Bottom
1	Base-line, full composite	50%	-	-	-
2	Partial Composite	29%	12%	22%	17%
3	Non-composite	0%	27%	66%	34%

Deck Thickness

Since the interaction of the deck and girders in a bridge is complex, the effect of deck thickness on the development of tensile stresses due to environmental actions is not consistent. However, increasing the deck thickness is believed to decrease the thermal stresses. To investigate the relationship between deck thickness and thermal stresses, two different deck thicknesses were analyzed in addition to the base-line deck (7.75-in., 6 and 10-in. decks were subjected to identical temperature profiles that were previously introduced in Case 3 of Figure 99. First, thermal analyses were performed on different deck sizes to develop the cross-sectional temperature profiles, and the results were used to input in the FE stress model. The effect of shrinkage and moisture gradient was not considered in the deck thickness sensitivity analysis.

In each case, the longitudinal stresses were averaged across the pier centerline and compared in Figure 116 for top, center, and bottom of the deck cross-section. Several elements were selected near girders and between girders to capture the higher and lower stress regions in the averaging. The effect of deck thickness on thermal stress can be explained by two interacting phenomena, internal and external restraint. Thicker decks are more likely to develop a larger nonuniform temperature gradient that can cause elevated tensile stresses at the top surface when the deck is heating up. On the other hand, thicker decks are stiffer such that the effect of external restraint from the girders can be smaller. This translates into smaller deck movements due to girders expanding or contracting. Thinner decks tend to behave oppositely. The average thermal stress resultants shown in Figure 116 verify such perspective. At the upper layers of the deck, from t=23 to 34 hours, a positive increase in stress occurred (tensile). This tensile stress change was mainly due to the bridge deck conforming to girders expansion which is largest for the thinner deck and smallest for the thicker deck. Consequently, from t=34 to 38 hours in the same graph, a steeper positive increase in stress occurred which was mainly due to the temperature gradient developed at the warmest time of the day. This second tensile stress jump was higher in the thicker deck suggesting that there existed a larger nonuniform temperature gradient. Stress magnitudes at the lower layers of the deck were higher in the thinner deck as a result of the more pronounced girder restraint effect at these levels.

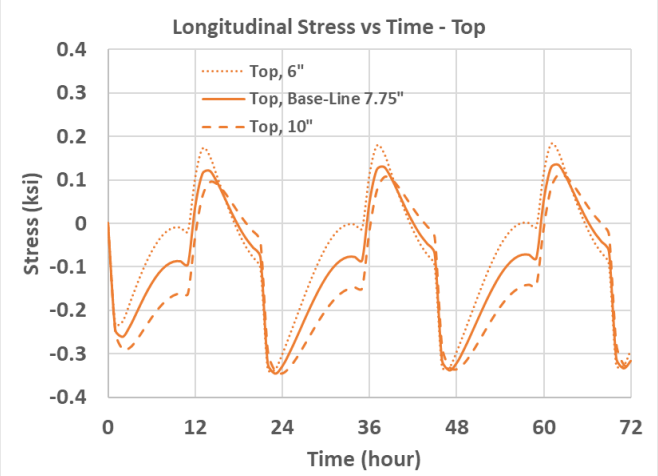

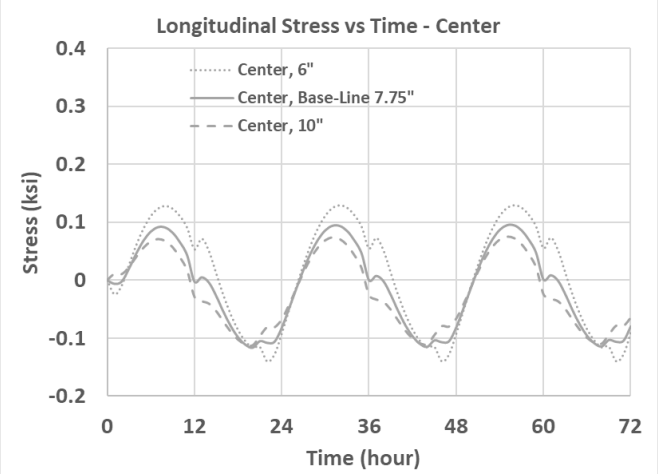

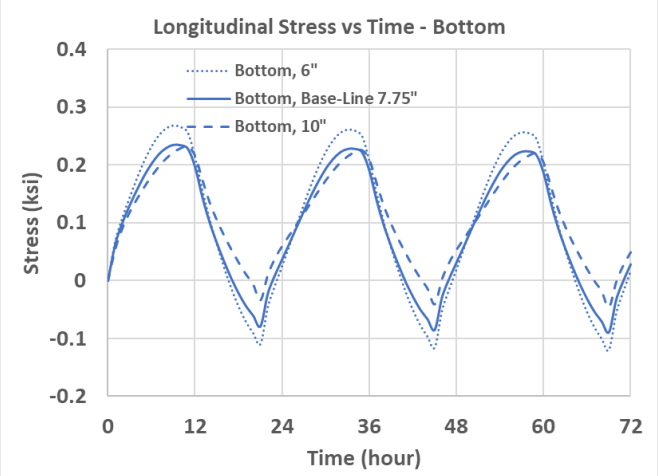

Figure 116. Average cross-sectional longitudinal stress is shown for different deck thicknesses at the top, center, and bottom of deck cross section. The stress unit is ksi with positive indicating tensile stress.

Summary and Conclusions

Nonlinear FE simulations were performed to investigate the stresses developed due to environmental actions on the concrete bridge deck on steel girders. A 3D finite element model of Rarus/Silver Bow Creek,

Bridge D, located in Butte, Montana was constructed and analyzed in Abaqus v2020. The FE model included the full-length deck geometry, girders, and lateral braces. Effects of nonuniform temperature and moisture gradients and drying shrinkage on tensile stress development were investigated on later-age concrete. Cross-sectional temperature histories were identified for diurnal summer and winter temperatures focusing on rigorous ambient temperature drops and rises. The nonuniform moisture gradient effect was investigated considering severe RH gains and losses before and after a rain event. Early-age stress analyses were conducted aiming to compare the early-age deck performance subjected to different curing methods and placement times. For early-age FE simulations, temperature histories, changing mechanical properties with age, and creep effects were included. Additionally, analyses were carried out for the sensitivity of the tensile stress in the concrete deck to variations in the degree of restraint and deck thickness.

Based on the FE analyses performed, the following conclusions are drawn:

1. Stresses in concrete deck due to restrained thermal, moisture and shrinkage are nonlinear across the depth of member.
2. In the morning and afternoon hours, the temperature gradient is generally higher. The largest cross-sectional temperature gradient is observed when the top surface of the deck is warmest. At this time, due to the effect of solar radiation, the top of the deck is always warmer than the ambient temperature.
3. During the evening and night hours, the deck starts to cool down. At the beginning of the evening hours, the top surface has a faster rate of heat loss. When the cooling rate at the upper layers becomes stable, the deck shows an almost uniform temperature drop due to lack of solar radiation until the next heating cycle begins.
4. Stress analysis at the later ages showed that with ambient ΔT=+55˚F (30˚C) a stress amplitude of 400 psi can develop at the top surface. The largest net tensile stress however was predicted to happen at the bottom of the deck. The net tensile stress magnitude due to ambient ΔT=+55 to 70˚F (30 to 39˚C) was predicted to be 250 to 300 psi.
5. At the warmest time of a summer day, there can exist a nonlinear temperature gradient of 19°F (10˚C) between the top and bottom of the concrete deck. Such a thermal gradient can create tensile stress of 200 psi in magnitude at top layers.
6. Wintertime FE simulation at a later ages showed that mostly compressive stresses can develop due to bridge cooling down. Thermal simulations showed that the cross-sectional temperature gradient on a winter night was small leading to an almost uniform temperature drop in the deck. Stress simulation predicted that compressive stress amplitudes of 400 to 500 psi can develop when the ambient temperature drops 50 to 65˚F (27 to 36˚C).
7. The development of tensile stresses in the deck due to bridge warming up or compressive stresses due to bridge cooling down is mainly attributed to the difference between the coefficient of thermal expansion of steel girders and concrete deck. In the composite deck system, steel girders have higher stiffness and thermal expansion coefficient that are prone to more expansion and contraction resulting in deck tensile and compressive stresses, respectively.

8. The FE simulation showed that the tensile stresses developed due to restraint drying shrinkage of the concrete deck can be as high as 300 psi. Shrinkage stress simulation was conducted for up to 150 days after concrete placement. The FE simulation results signify the long-term importance of the drying shrinkage effect, especially when combined with diurnal temperature changes that can result in elevated tensile stresses and increased cracking risk of the concrete deck.
9. The stress analysis of nonuniform moisture gradient suggested that there can exist a significant RH gradient throughout the deck after a rain event that can lead to higher RH at the top surface causing elevated tensile stresses at the bottom of the deck. Due to the moisture gradient alone, tensile stresses as high as 250 to 300 psi were predicted to develop at the lower depths of the concrete deck.
10. FE analysis of the combined moisture and temperature gradient showed that the effect of these two phenomena can be subtractive. Although, additional modeling would be needed to confirm that this is always the case based on seasonal changes in relative humidity and temperature. It was shown that the higher tensile stresses at the centroid and bottom of the deck due to moisture gradient were partially offset by compressive stresses that can develop as a result of the bridge cooling down during the rain event.
11. The early-age simulation results for the summer placement showed that application of insulation within the first few days after placement can effectively keep the tensile stresses low when compared to the case with no insulation. Within the two cases considered for the summer placement, no significant tensile stresses were predicted after the removal of the insulation and curing measures.
12. In general, the stress analysis of the winter placement with heating enclosure from the bottom of the deck showed a better performance in terms of the development of tensile stresses. Deck stresses due to the application of insulation from the top and heating from the bottom resulted in no tensile stresses in the concrete deck. After removal of the insulation and heat and exposure to the cold ambient temperature, concrete temperature sharply dropped which caused large compressive stresses to develop top to bottom.
13. In cold-weather placement, the application of a heating source only from the top is not effective in reducing the tensile stresses. There exists a large temperature gradient from the top of the concrete deck to the steel girders that are exposed to cold ambient temperatures. This will cause the development of tensile stresses as high as 300 psi and increased top-surface cracking risk within the first 3 days after placement.
14. Sensitivity analyses on the thicker or thinner decks show a slight decrease in tensile stresses when going from a 6 inch deck to a7.75 inch deck, but to a much lesser extent when going from 7.75 inch deck to a 10 inch deck.
15. The sensitivity analyses on the degree of restraint did not produce any practical and significant decrease in tensile stresses due to diurnal temperature cycles.

REFERENCES

[1] C. French, L. Eppers, Q. Le and J. Hajjar, "Transverse Cracking in Bridge Decks: Summary Report," Univeristy of Minnesota, Minnesota Department of Transportation, Minneapolis, 1999.

[2] R. J. Frosch, D. T. Blackman and R. D. Radabaugh, "FHWA/IN/JTRP-2002/25, Investigation of Bridge Deck Cracking in Various Bridge Superstructure Systems," Joint Transportation Research Program, West Lafayette, IN, 2003.

[3] J. Yuan, D. Darwin and J. Browning, "SM Report No. 103, Development and Construction of Low-Cracking hihg-Performance Concrete (LC-HPC) Bridge Decks: Free Shrinkage Tests, Restrained Ring Tests, Construction Experience, and Crack Survey Results," Transportation Pooled Funding Study Project Nos. TPF-5(01) and TPF-5(17), 2011.

[4] M. Saadeghvazri and R. Hadidi, Cause and Control of Transverse Cracking in Concrete Bridge Decks - FHWA NJ-2002-19, Newark, NJ: FHWA, 2002.

[5] E. Schmeckpeper and S. Lecoultre, Synthesis into the Causes of Concrete Bridge Deck Cracking and Observations on the Initial Use of High Performance Concrete in the US 95 Bridge over the SOuth Fork of the Palouse River, Moscow, Idaho, 2008.

[6] T. Van Dam, N. Duffala and J. Stempihar, Minimization of Cracking in New Concrete Bridge Decks - 530-14-803, Carson City, NV: Nevada Department of Transportation, 2016.

[7] S. Kosmatka and M. Wilson, Design and Control of Concrete Mixtures, 16th ed., Skokie, IL: Portland Cement Association, 2016.

[8] ACI Committee 318, Building Code Requirements for Structural Concrete, Framington Hills, MI: American Concrete Institute, 2019.

[9] National Climatic Data Center (www.ncdc.noaa.gov), CCD-Data - Relative Humidity 18, 2018.

[10] B. Wan, C. Foley and J. Komp, Concrete Cracking in New Bridge Decks and Overlays - WHRP 10-05, Madison, WI: Wisconsin Highway Research Board, 2010.

[11] N. Harikrishnan, O. Celik and M. Sprinkel, Reducing Cracks in Concrete Bridge Decks using Shrinkage Reducing Admixture - FHWA/VRTC 16-R13, Richmond, VA: FHWA, 2016.

[12] J. Ideker, T. Deboot and T. Fu, Internal Curing of High-Performance Concrete for Bridge Decks - SPR 711, Salem, OR: Oregon Department of Transportation Research Section, 2013.

[13] A. Al-Manaseer and A. Fayyaz, Creep and Drying Shrinkage of High Performance Concrete of the Skyway Structures of the New San Francisco-Oakland Bay Bridge and Cement Paste - CA 10-1131, San Francisco, CA: California Department of Transportation, 2011.

[14] K. Foliard and N. Berke, Properties of High-Performance Concrete Containing Shrinkage-Reducing Admixture, vol. 27, Cambridge, MA: Cement and Concrete Research, 1997.

[15] Oklahoma State University, "Tarantula Curve," [Online]. Available: www.optimizedgraded.com.

[16] D. Bentz and J. Weiss, Internal Curing: A 2010 State-of-the-Art Review - NISTIR 7765, Gaithersburg, MD: NIST, 2010.

[17] T. Barret, A. Miller and W. Weiss, Documentation of the INDOT Experience and Construction of the Bridge Decks Containing Internal Curing in 2013 - FHWA/IN/JTRP-2015/10, West Lafeyette, IN: Joint Transportation Research Program, 2015.

[18] W. Hamid, E. Steinberg, I. Khoury, A. Semendary and K. Walsh, Thermally Induced Behavior of Paired Internally Cured Concrete and Conventional Concrete Decks in Composite Bridges, vol. 26, ASCE - Journal of Bridge Engineering, 2021.

[19] C. Bank, A. Malia, M. Oliva, J. Russel, A. Bentur and A. Shapira, Specification and Design of FIber Reinforced Bridge Deck forms for Use on WIde Flange T-Girders, Madison, WI: Wisconsin Highway Research Program, 2007.

[20] M. West, D. Darwin and J. Browning, Effect of Materials and Curing Period on Shrinkage of Concrete, Lawrence, KS: Transportation Pooled Fund Program Project No. TPF-5(051), 2010.

[21] J. Yang, Q. Wang and Y. Zhou, Influence of Curing Time on the Drying Shrinkage of Concretes with Different Binders and Water-to-Binder Ratios, vol. vol. 2017, Advances in Materials Science and Engineering, 2017.

[22] P. Krauss and E. Rogalla, "NCHRP Report 380, Transverse Cracking in Newly Constructed Bridge Decks," Transportation Research Board, Washington DC, 1996.

[23] T. Van Dam, N. Duffala and J. Stempihar, "Phase I: Minimization of Cracking in New Concrete Bridge Decks, Report No. 530-14-803," Nevada Department of Transportation, Carson City, NV, 2016.

[24] A. Neville, Properties of Concrete, 5th ed., New York: Pearson, 2011.

[25] ACI Committee 207, "ACI 207.2R-07, Report on Thermal and Volume Change Effects on Cracking of Mass Concrete," American Concrete Institute, Farmington Hills, MI, 2007.

[26] ACI Committee 209, "ACI 209.1R-05, Report on Factors Affecting Shrinkage and Creep of Hardened Concrete," American Concrete Institute, Farmington Hills, MI, 2005.

[27] P. B. Bamforth, "CIRIA Report C766, Control of Cracking Caused by Restrained Deformation in Concrete," CIRIA, London, 2018.

[28] M. Shlafli and E. Bruhwiler, "Fatigue of Existing Reinforced Concrete Bridge Deck Slabs," *Engineering Structures,* vol. 20, no. 11, pp. 991-998, 1998.

[29] I. Bayane, A. Mankar, E. Bruhwiler and J. D. Sorensen, "Quantification of Traffic and Temperature Effects on the Fatigue Safety of a Reinforced-Concrete Bridge Deck based on Monitoring Data," *Engineering Structures,* vol. 196, 2019.

[30] F. Yazdani, "Damage Assessment, Characterization, and Modeling for Enhanced Design of Concrete Bridge Decks in Cold Regions," Mountain-Plains Consortium, Fargo, North Dakota, 2015.

[31] Y. Xi, B. Shing, N. Abu-Hejleh, A. Asiz, A. Suwito, Z. Xie and A. Ababneh, "CDOT-DTD-R-2003-3, Assessment of the Cracking Problem in Newly Constructed Bridge Decks in Colorado," Colorado Department of Transportation, Denver, 2003.

[32] E. R. Schmeckpeper and S. T. Lecoultre, "Report N08-05, Synthesis into the Causes of Concrete Bridge Deck Cracking and Observation on the Initial Use of High Performance Concrete in the US 95 Bridge over the South Fork of the Palouse River," Idaho Department of Transportation, Boise, 2007.

[33] Y. Deng, B. Phares and D. Harrington, "Causes of Early Cracking in Concrete Bridge Decks," *CP Road Map,* p. 6, November 2016.

[34] D. Darwin, J. Browning and W. D. Lindquist, "Control of Cracking in Bridge Decks: Observations from the Field," *Cement, Concrete, and Aggregates,* vol. 26, no. 2, 2004.

[35] D. L. Rettner, M. S. Fiegen, M. B. Snyder and K. A. MacDonald, "Report 2014-09, Analysis of Bridge Deck Cracking Data," Minnesota Department of Transportation, St. Paul, 2014.

[36] M. A. Saadeghvaziri and R. Hadidi, "FHWA-NJ-2002-19, Cause and Control of Transverse Cracking in Concrete Bridge Decks," New Jersey Department of Transportation, Newark, 2002.

[37] T. Hopper, A. Manafpour, A. Radlinska, G. Warn, F. Rajabipour, D. Morian and S. Jahangirnejad, "Bridge Deck Cracking: Effects on In-Service Performance, Prevention, and Remediation," Pennsylvania Department of Transportation, Harrisburg, 2015.

[38] B. Wan, C. Foley and J. Komp, "WHRP 10-05, Concrete Cracking in New Bridge Decks and Overlays," Wisconsin Department of Transportation, Madison, 2010.

[39] Geokon, "Vibrating Wire Strain Gages (VWSGs)," [Online]. Available: https://www.geokon.com/4200-Series.

[40] Campbell Scientific, "CR 6 Measurement and Control Datalogger," [Online]. Available: https://www.campbellsci.com/cr6.

[41] ABAQUS, 2020.

[42] *4C-Temp&Stress. Temperature and Stress Simulation During Hardening,* Evanston, IL: Germann Instruments, Inc., 1998.

[43] ACI Committee 209, "ACI 209.2R-08, Guide for Modeling and Calculating Shrinkage and Creep in Hardened Concrete," American Concrete Institute, Farmington Hills, MI, 2008.

[44] H. Kwak, S. Ha and J. Kim, "Non-structural cracking in RC walls: Part I. Finite element formulation," *Cement and Concrete Research, 36(4),* pp. 749-760, 2006.

[45] C. Ferreira, C. Sousa, R. Faria, M. Azenha and M. Pimentel, "Thermo-Hygro-Mechanical Simulation of Cracking in Thick Restrained RC Members: Application to a 50 cm Thick Slab," *Journal of Advanced Concrete Technology, Vol. 17,* pp. 489-505, 2019.

APPENDIX A. DECK CURING TEMPERATURE DATA

Russell Street Bridge Phase I (NB)

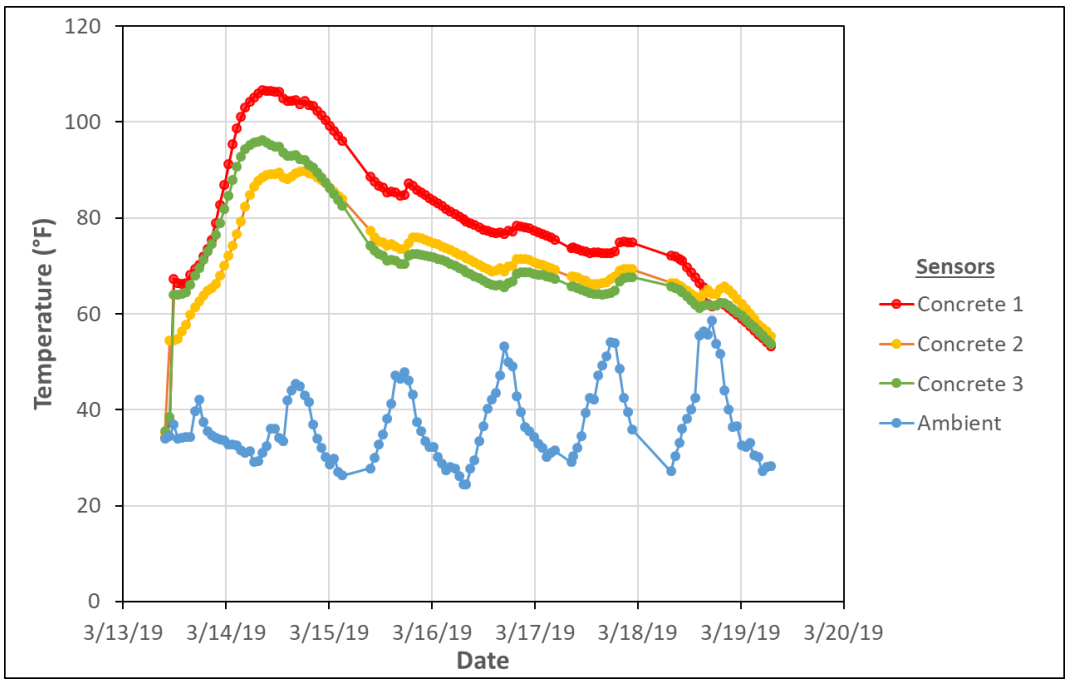

Figure A1. Temperature data - Russell Street Bridge Phase I (NB), Placement 1, Sensor Location 1

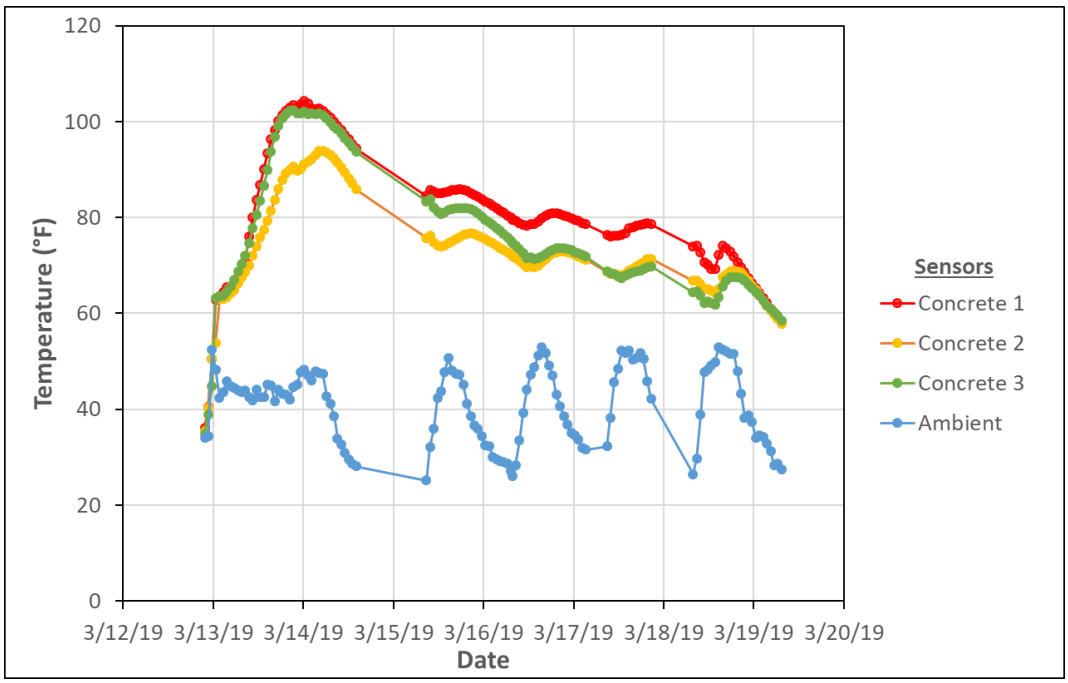

Figure A2. Temperature data - Russell Street Bridge Phase I (NB), Placement 1, Sensor Location 2

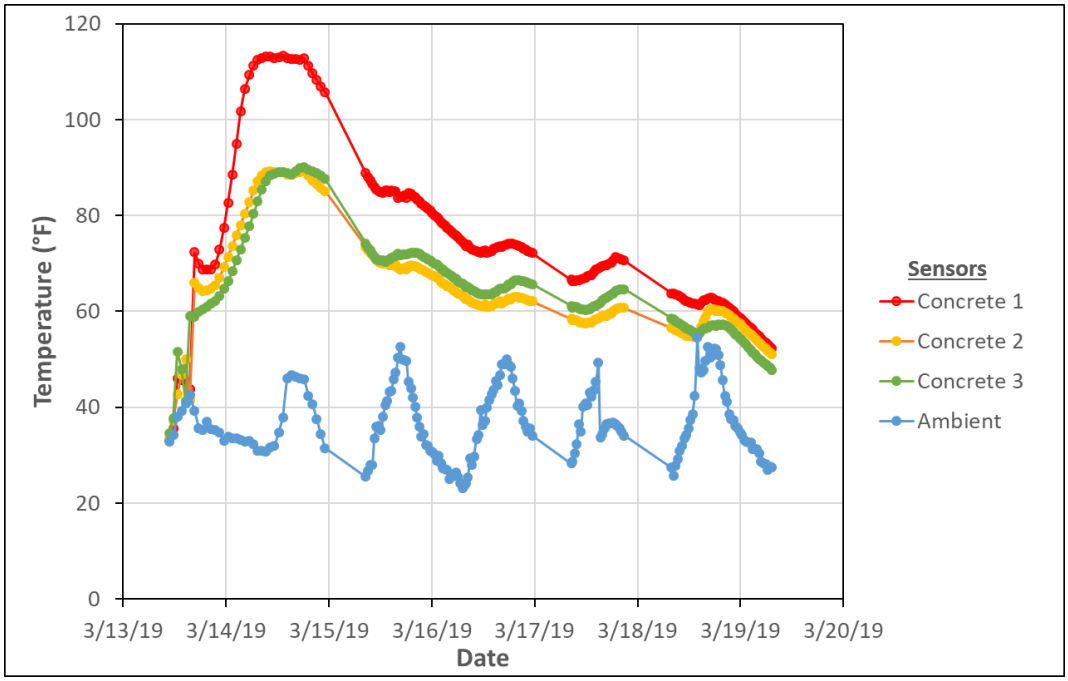

Figure A3. Temperature data - Russell Street Bridge Phase I (NB), Placement 1, Sensor Location 3

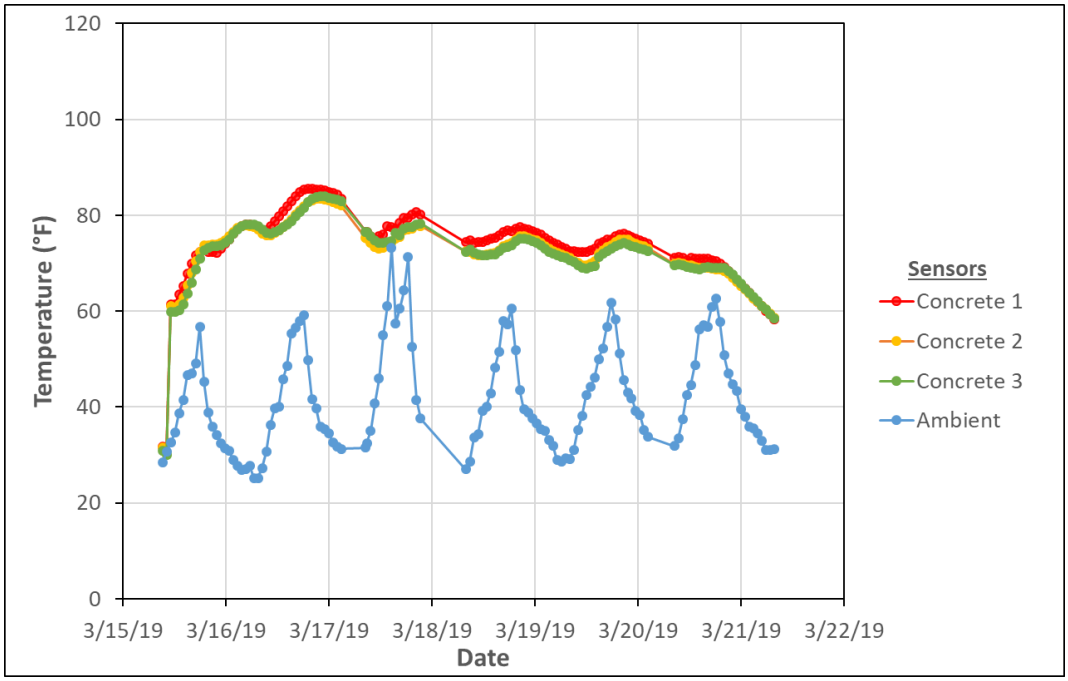

Figure A4. Temperature data - Russell Street Bridge Phase I (NB), Placement 2, Sensor Location 1

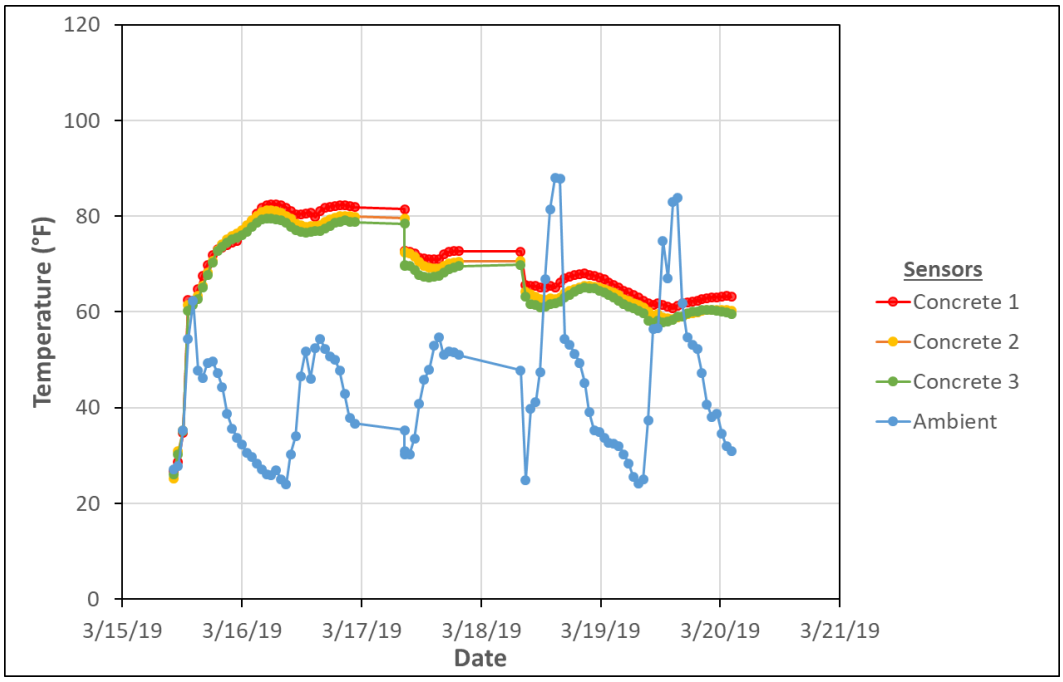

Figure A5. Temperature data - Russell Street Bridge Phase I (NB), Placement 2, Sensor Location 2

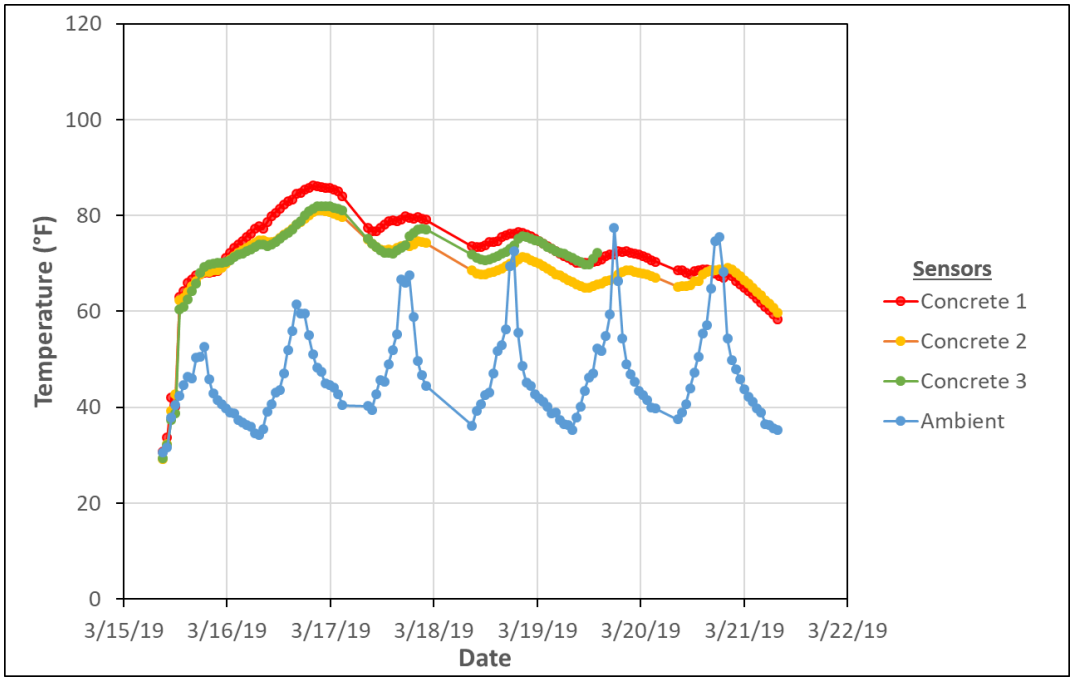

Figure A6. Temperature data - Russell Street Bridge Phase I (NB), Placement 2, Sensor Location 3

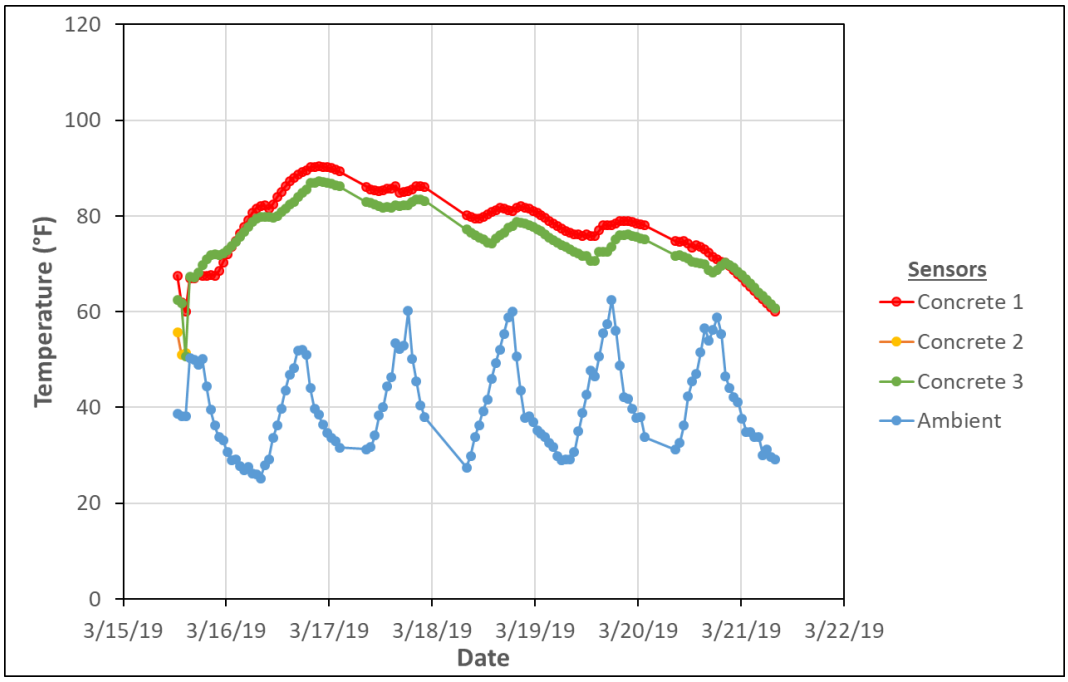

Figure A7. Temperature data - Russell Street Bridge Phase I (NB), Placement 3, Sensor Location 1

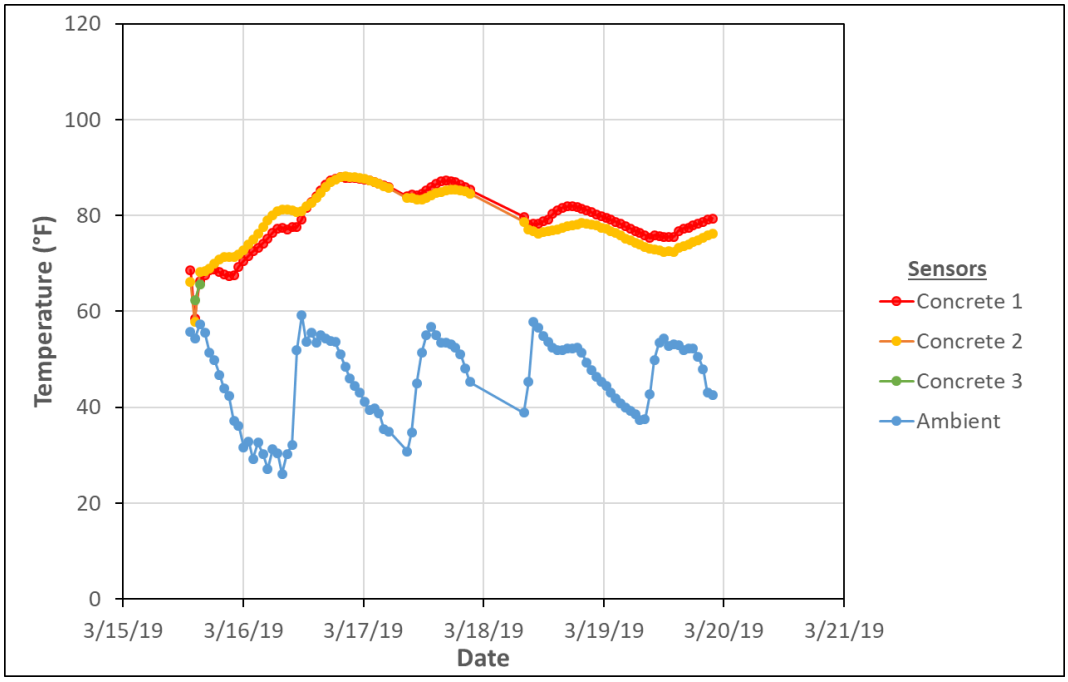

Figure A8. Temperature data - Russell Street Bridge Phase I (NB), Placement 3, Sensor Location 2

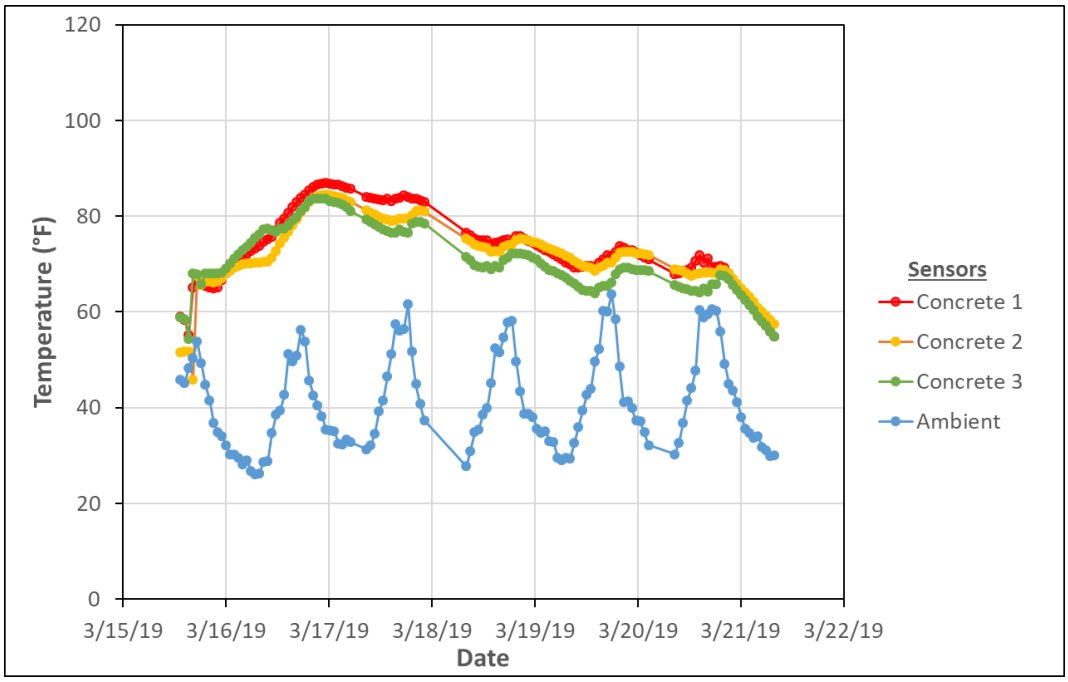

Figure A9. Temperature data - Russell Street Bridge Phase I (NB), Placement 3, Sensor Location 3

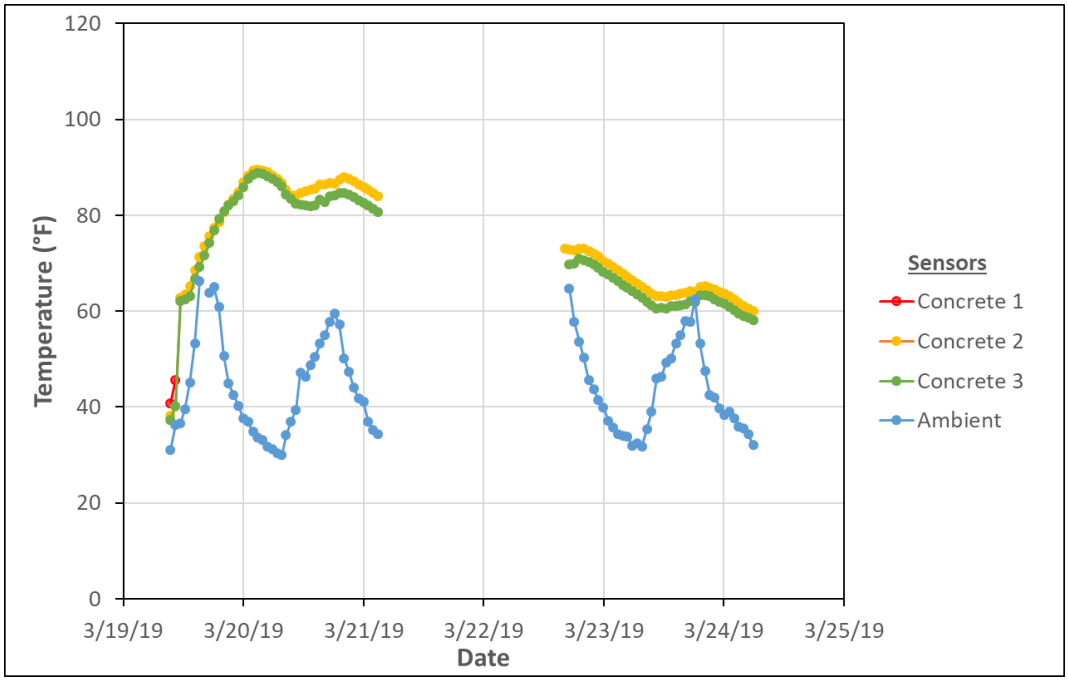

Figure A10. Temperature data - Russell Street Bridge Phase I (NB), Placement 4, Sensor Location 1

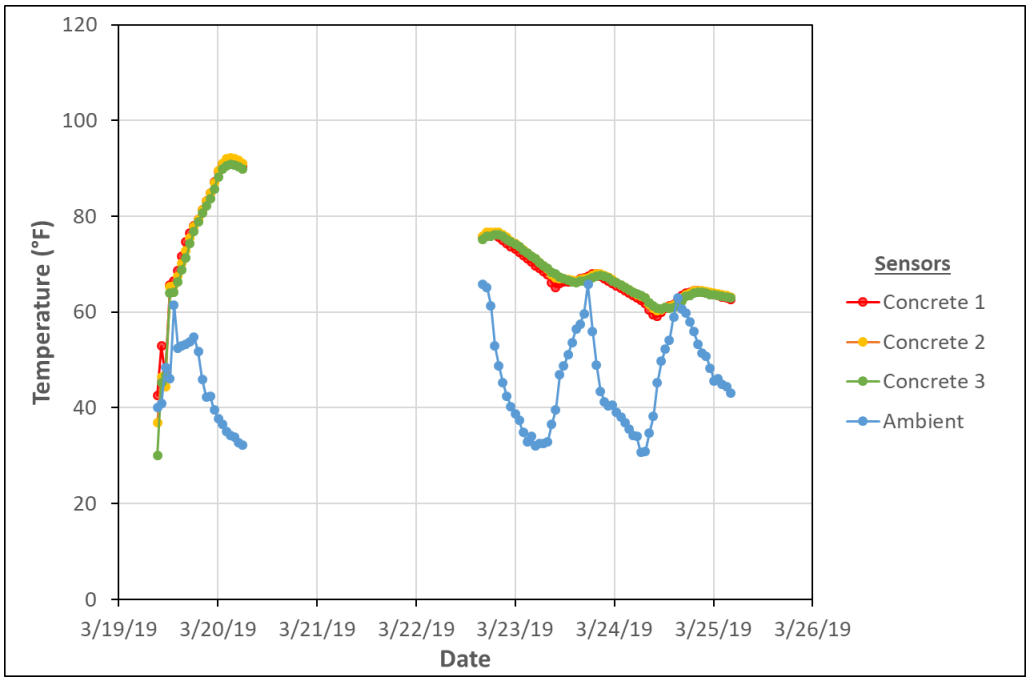

Figure A11. Temperature data - Russell Street Bridge Phase I (NB), Placement 4, Sensor Location 2

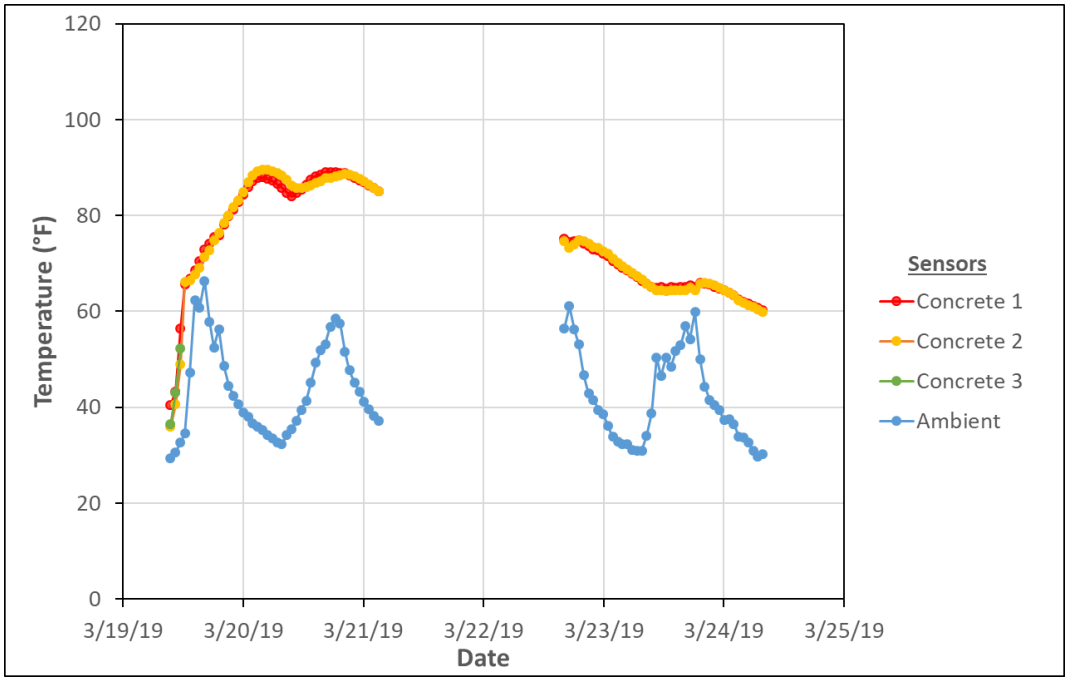

Figure A12. Temperature data - Russell Street Bridge Phase I (NB), Placement 4, Sensor Location 3

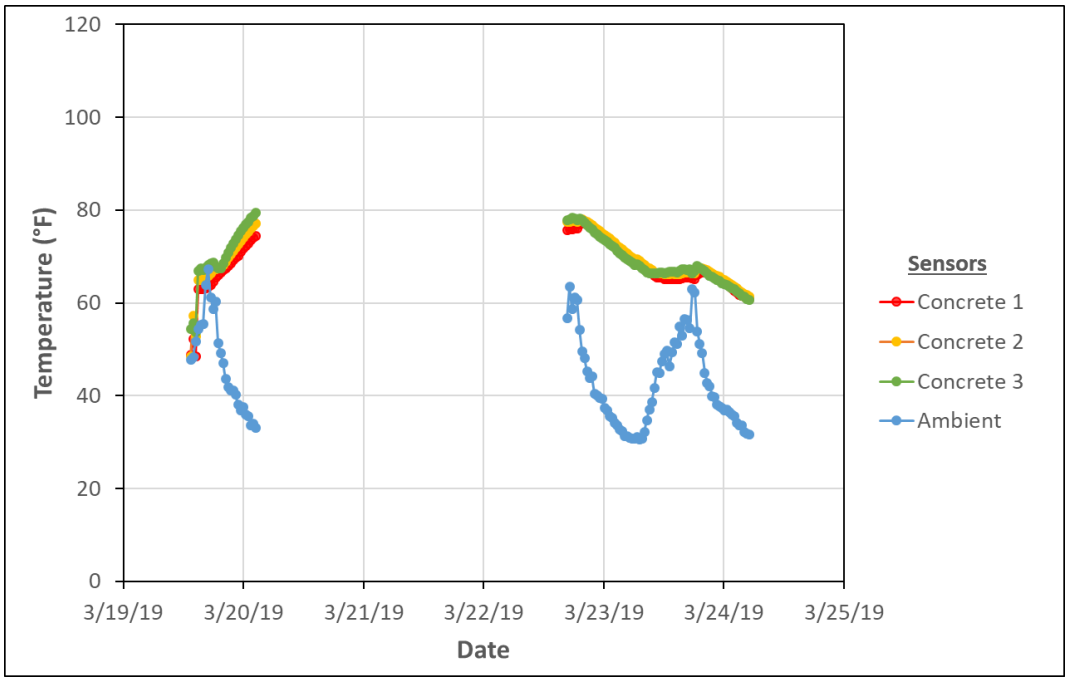

Figure A13. Temperature data - Russell Street Bridge Phase I (NB), Placement 5, Sensor Location 1

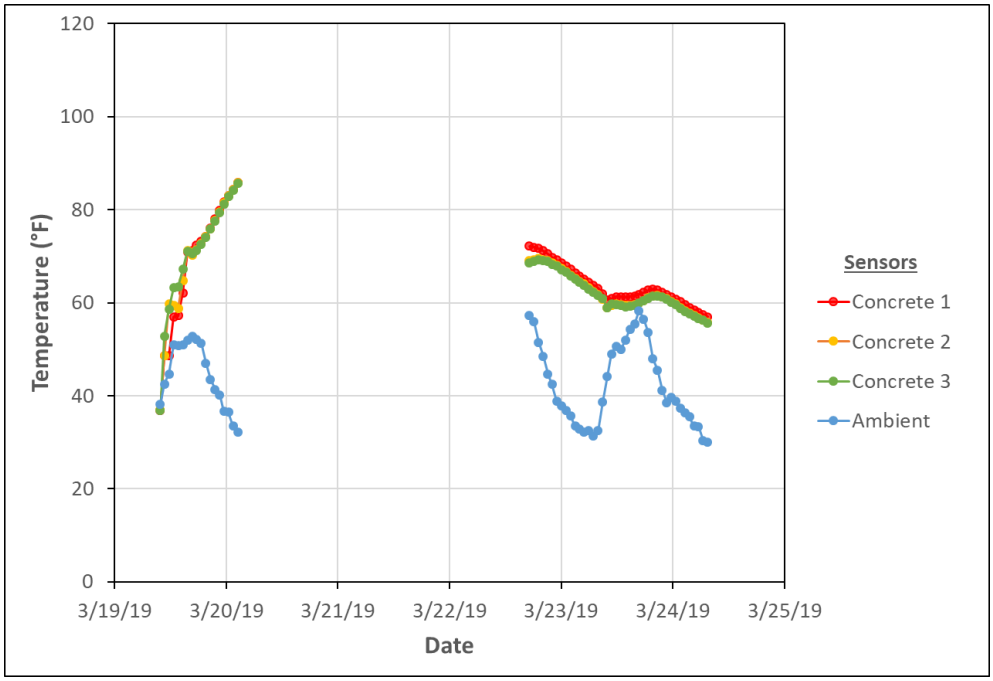

Figure A14. Temperature data - Russell Street Bridge Phase I (NB), Placement 5, Sensor Location 2

Russell Street Bridge Phase II (SB)

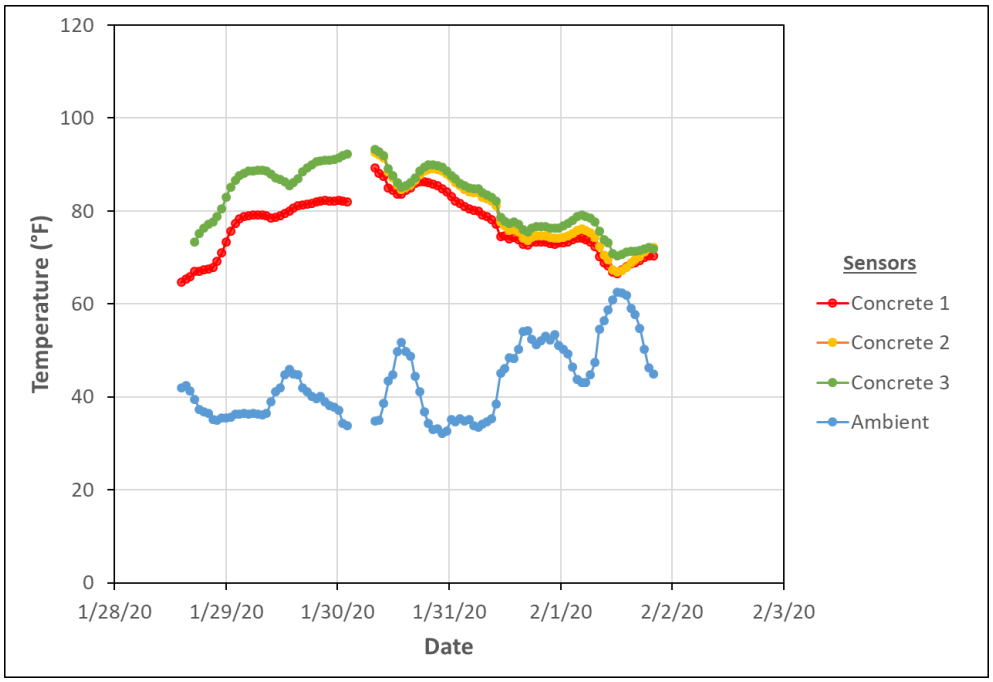

Figure A15. Temperature data - Russell Street Bridge Phase II (SB), Placement 1, Sensor Location 1b

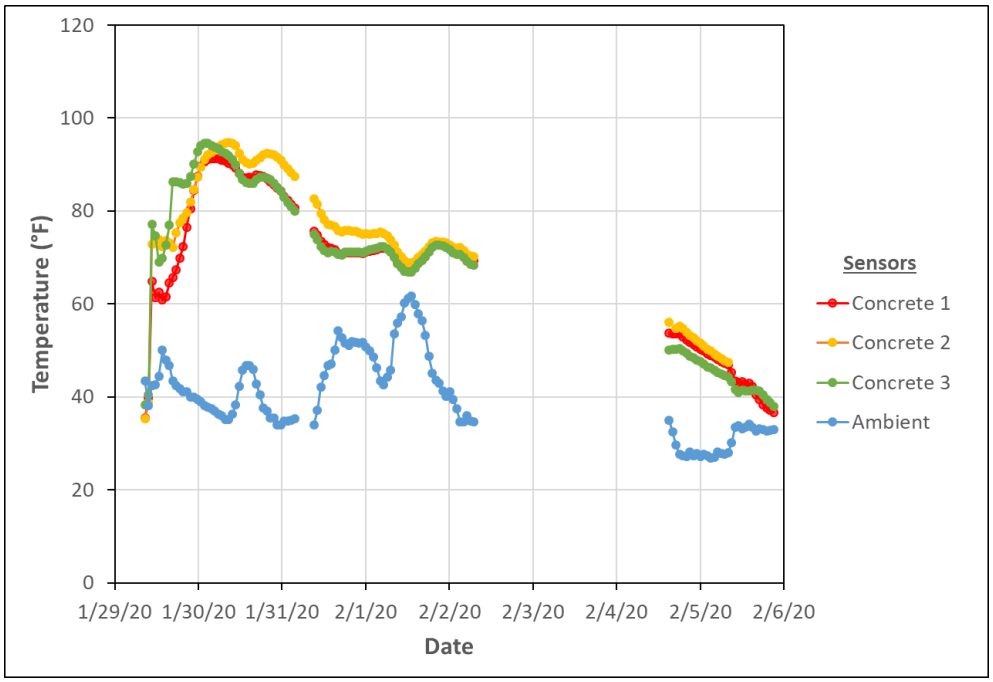

Figure A16. Temperature data - Russell Street Bridge Phase II (SB), Placement 2, Sensor Location 2

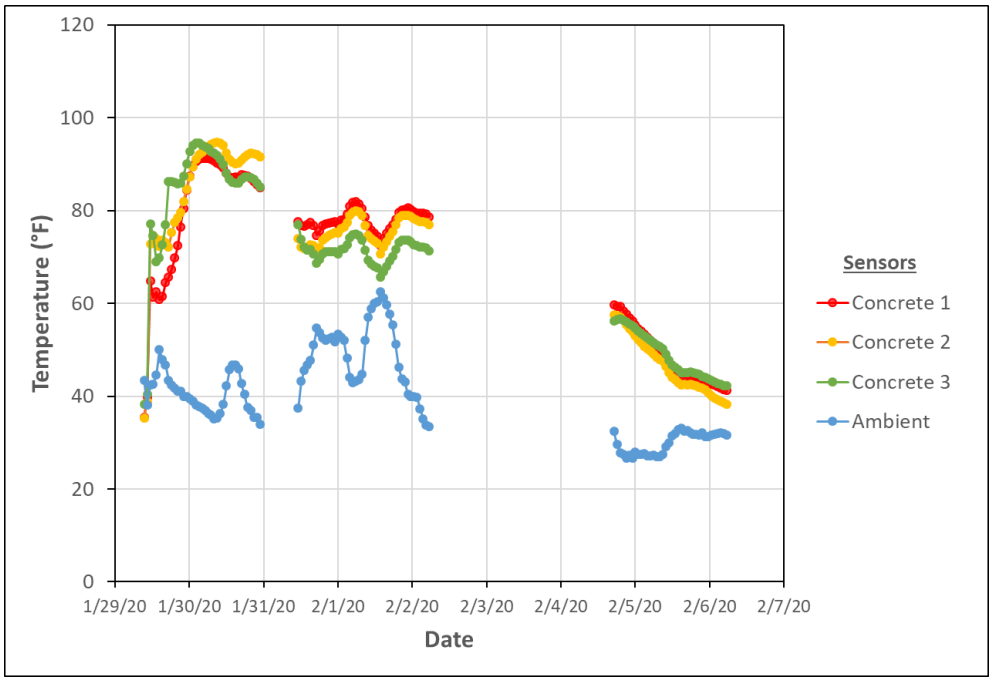

Figure A17. Temperature data - Russell Street Bridge Phase II (SB), Placement 2, Sensor Location 2a

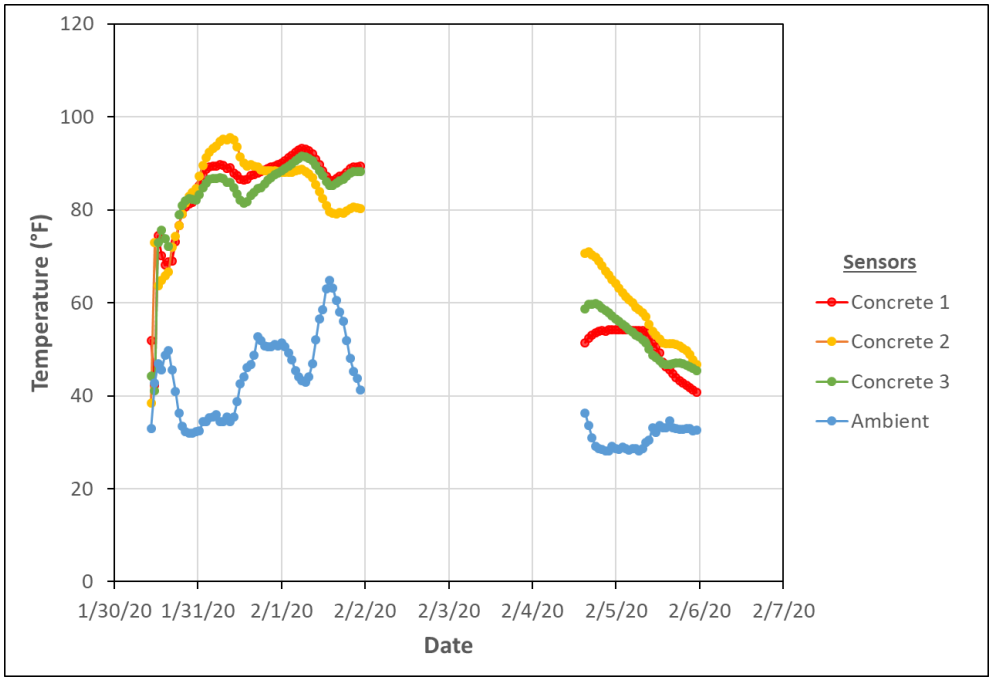

Figure A18. Temperature data - Russell Street Bridge Phase II (SB), Placement 3, Sensor Location 3/3a

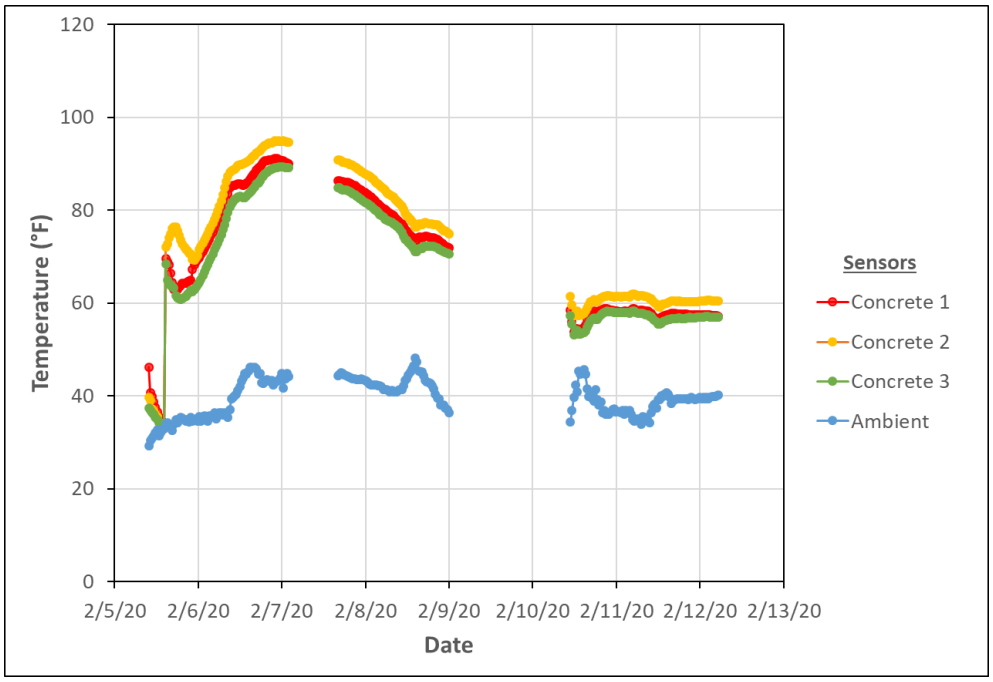

Figure A19. Temperature data - Russell Street Bridge Phase II (SB), Placement 4, Sensor Location 4

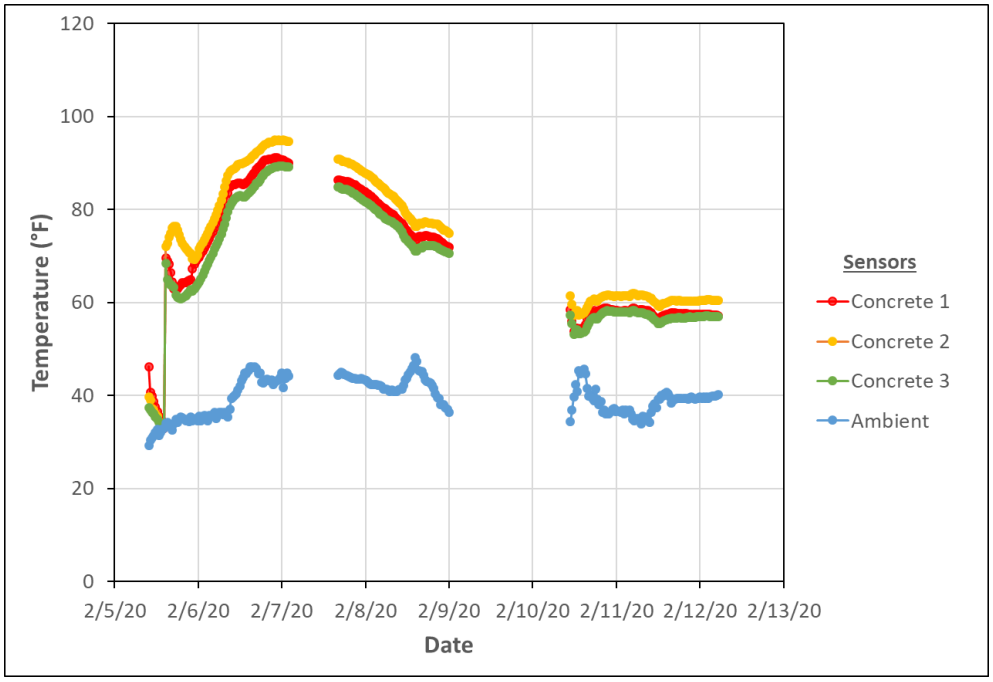

Figure A20. Temperature data - Russell Street Bridge Phase II (SB), Placement 4, Sensor Location 4b

Capitol-Cedar Bridge Phase II (NB)

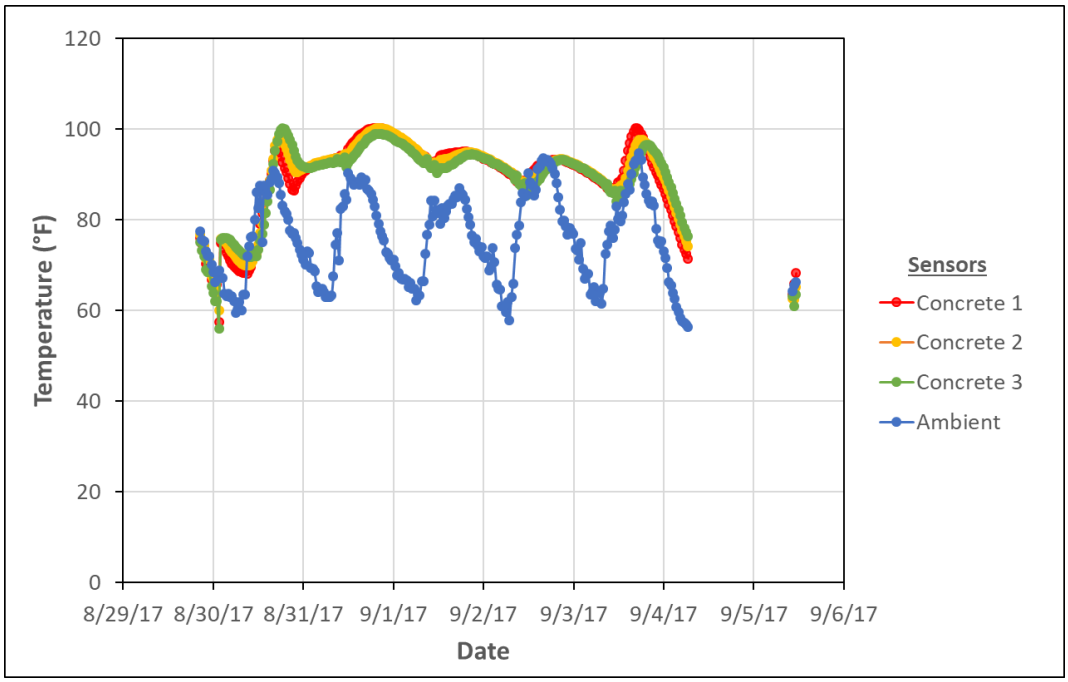

Figure A21. Temperature data - Capitol-Cedar Bridge Phase II (NB), Placement 1, Middle

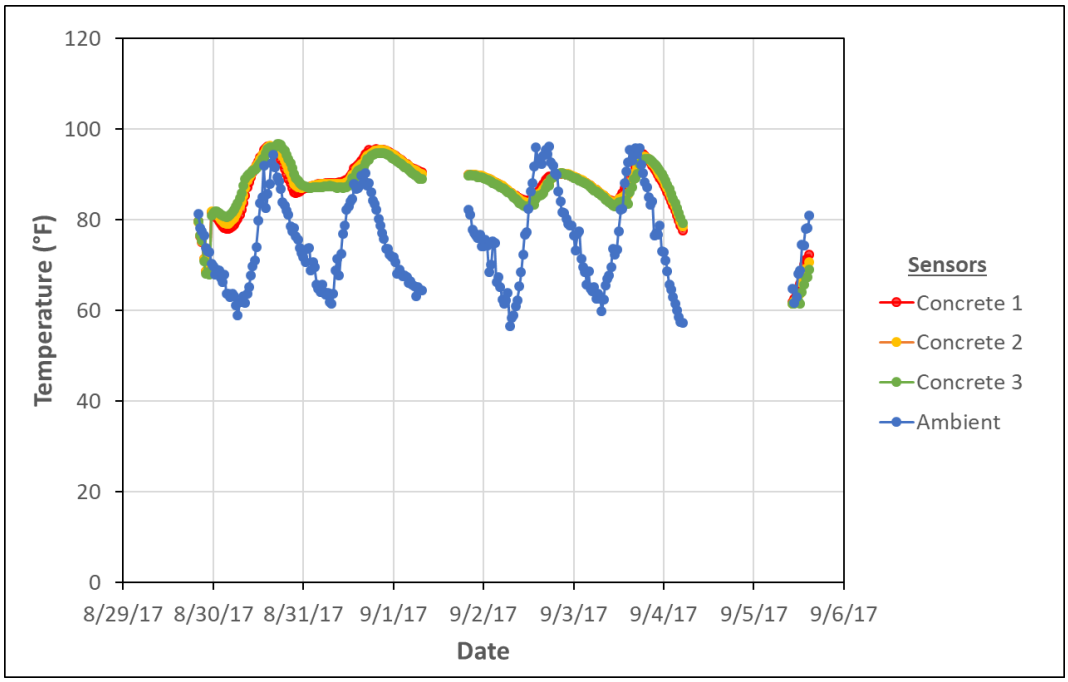

Figure A22. Temperature data - Capitol-Cedar Bridge Phase II (NB), Placement 1, North

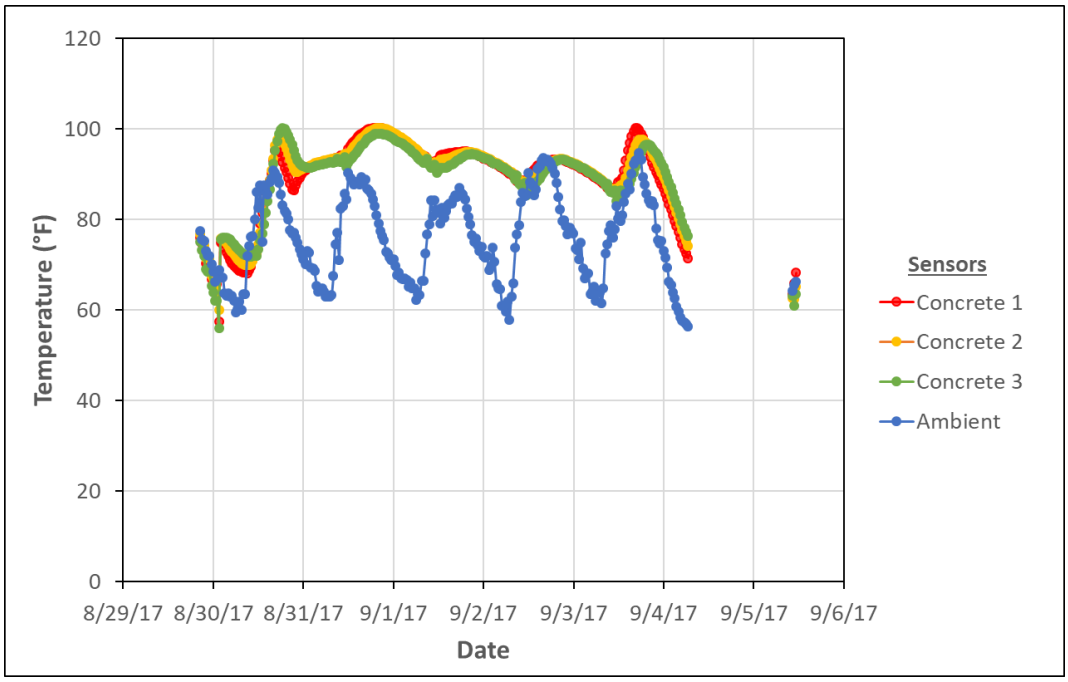

Figure A23. Temperature data - Capitol-Cedar Bridge Phase II (NB), Placement 1, Middle

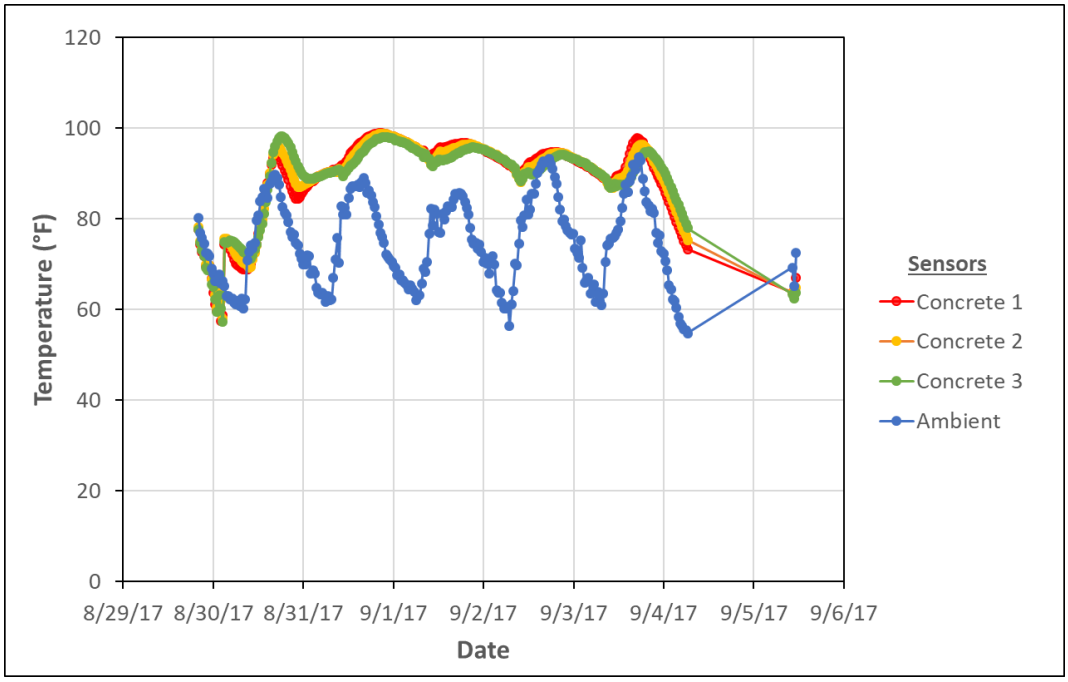

Figure A24. Temperature data - Capitol-Cedar Bridge Phase II (NB), Placement 1, South

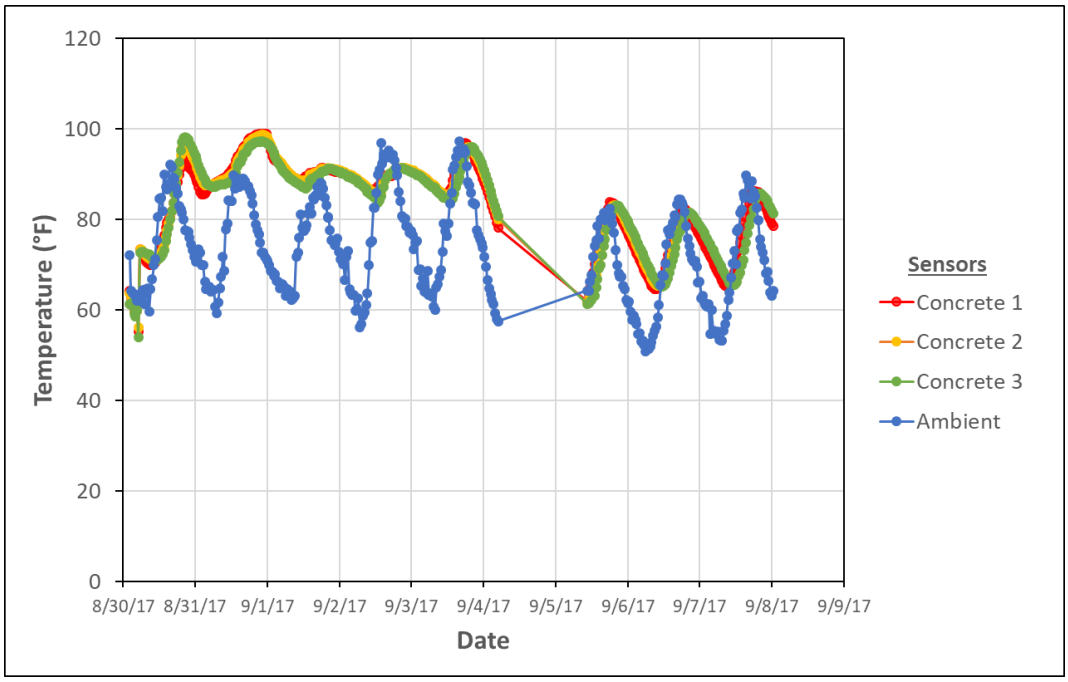

Figure A25. Temperature data - Capitol-Cedar Bridge Phase II (NB), Placement 2, North

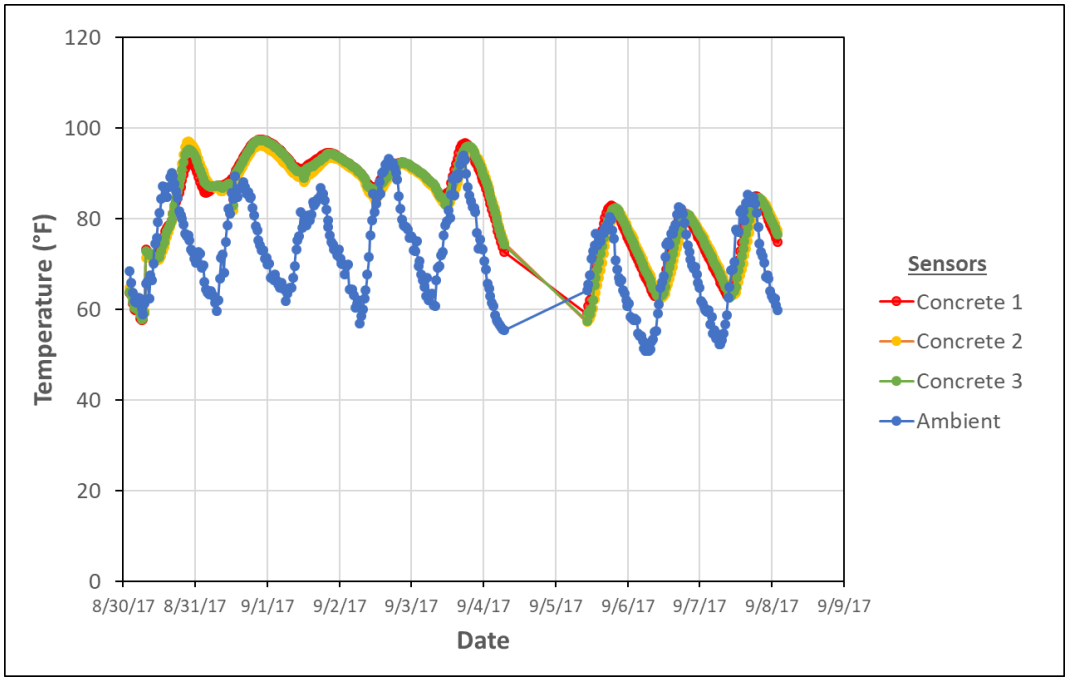

Figure A26. Temperature data - Capitol-Cedar Bridge Phase II (NB), Placement 2, Middle

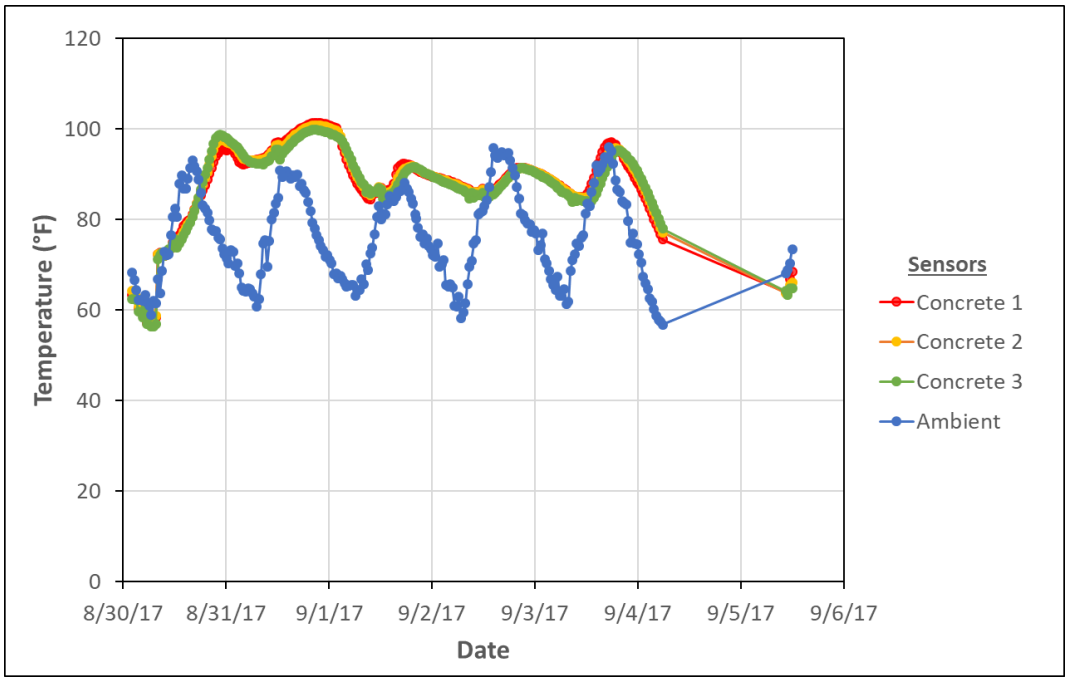

Figure A27. Temperature data - Capitol-Cedar Bridge Phase II (NB), Placement 2, South

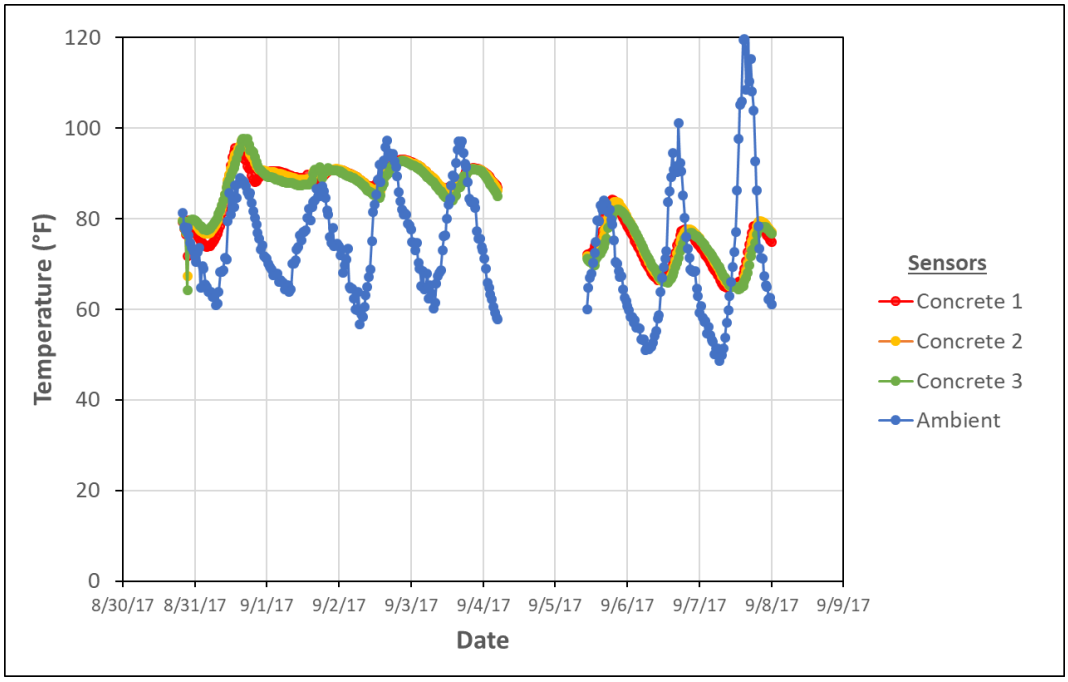

Figure A28. Temperature data - Capitol-Cedar Bridge Phase II (NB), Placement 3, North

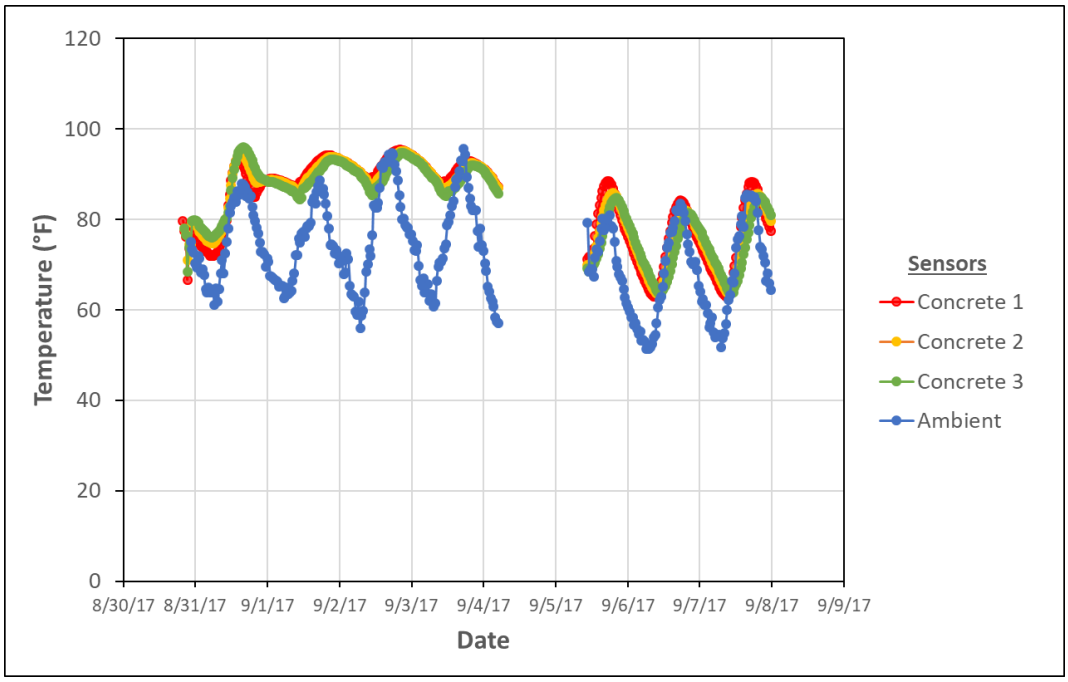

Figure A29. Temperature data - Capitol-Cedar Bridge Phase II (NB), Placement 3, Middle

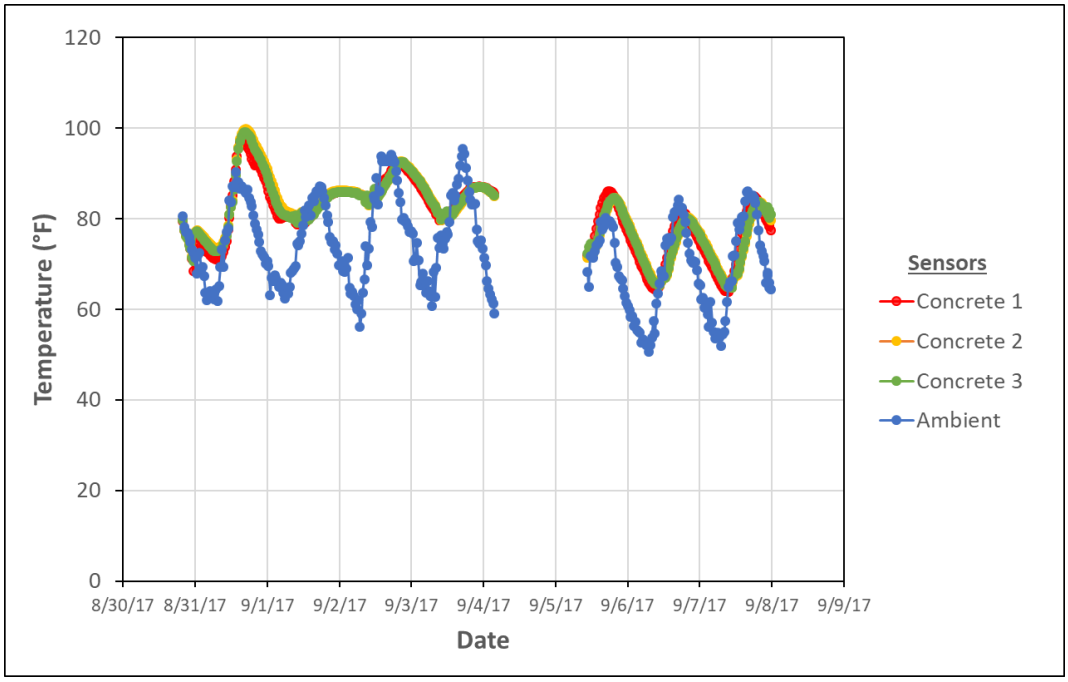

Figure A30. Temperature data - Capitol-Cedar Bridge Phase II (NB), Placement 3, South

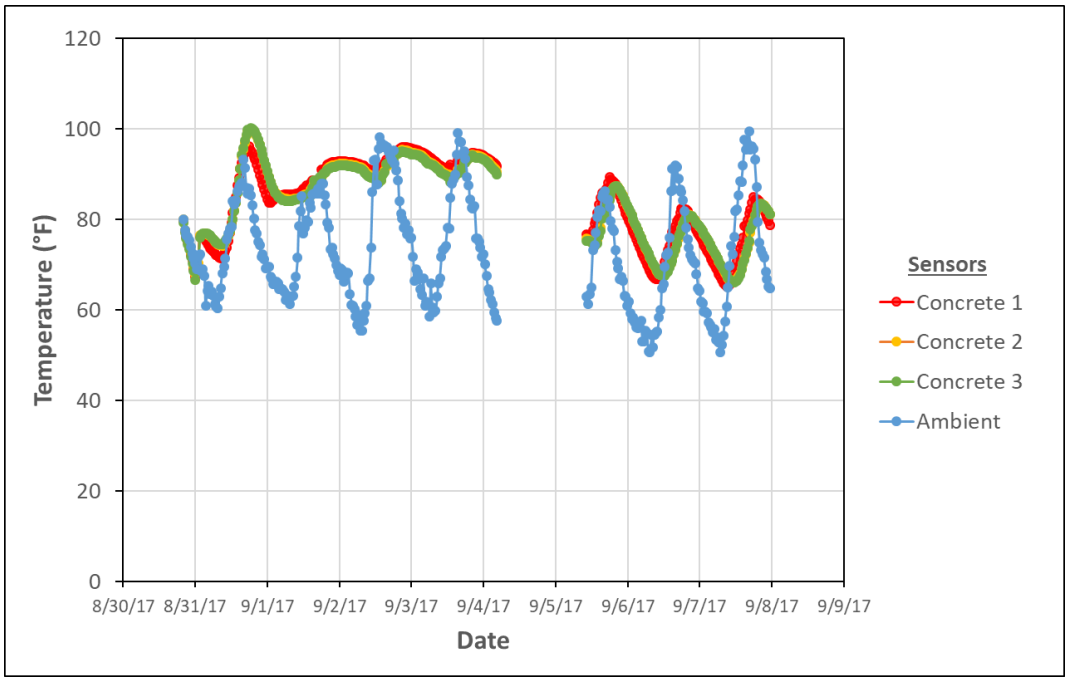

Figure A31. Temperature data - Capitol-Cedar Bridge Phase II (NB), Placement 4, North

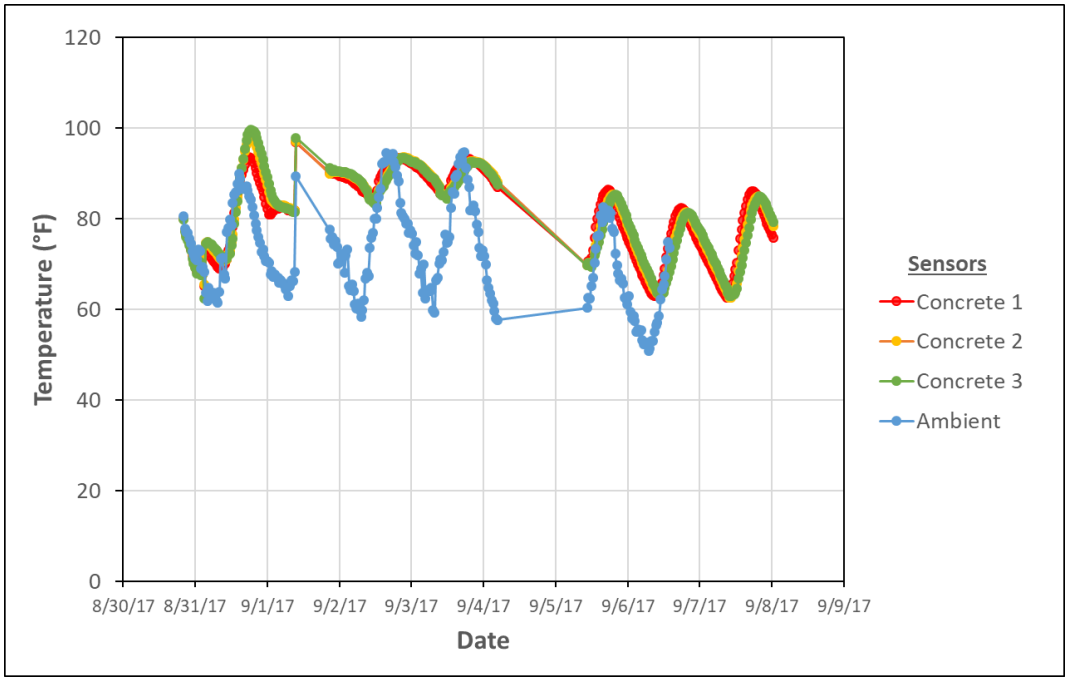

Figure A32. Temperature data - Capitol-Cedar Bridge Phase II (NB), Placement 4, Middle

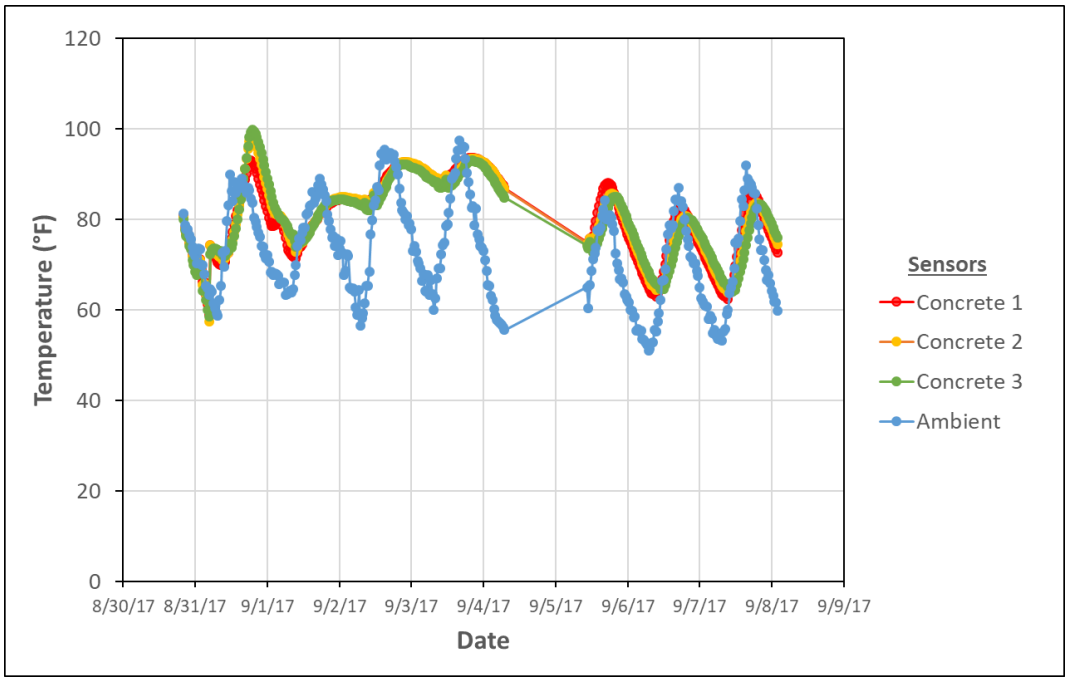

Figure A33. Temperature data - Capitol-Cedar Bridge Phase II (NB), Placement 4, South

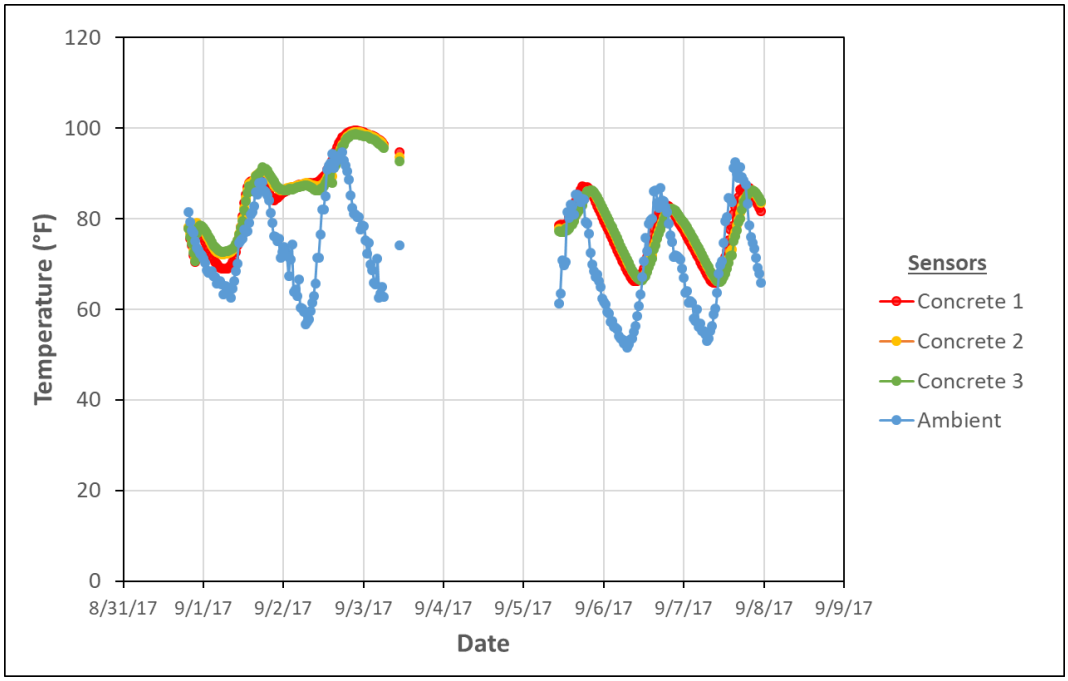

Figure A34. Temperature data - Capitol-Cedar Bridge Phase II (NB), Placement 5, North

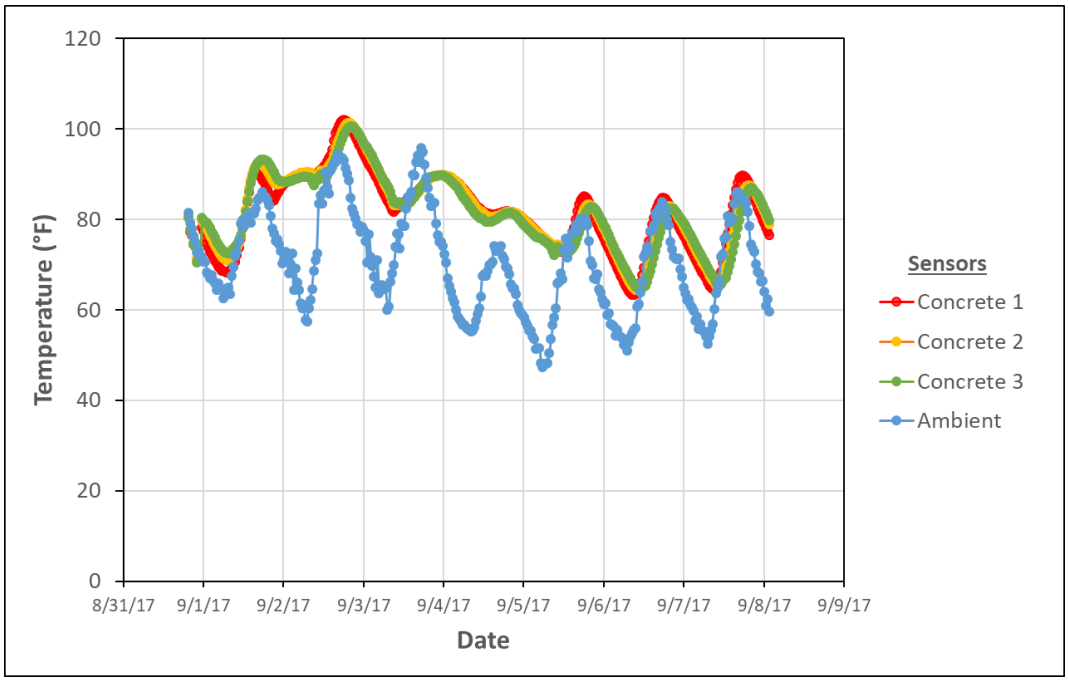

Figure A35. Temperature data - Capitol-Cedar Bridge Phase II (NB), Placement 5, Middle

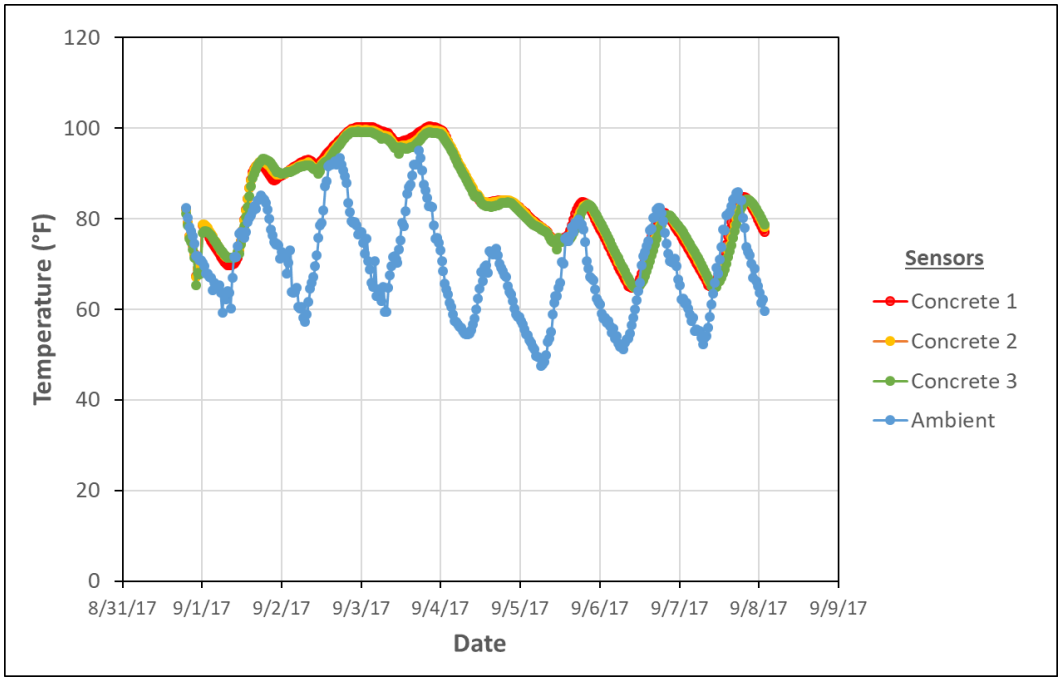

Figure A36. Temperature data - Capitol-Cedar Bridge Phase II (NB), Placement 5, South

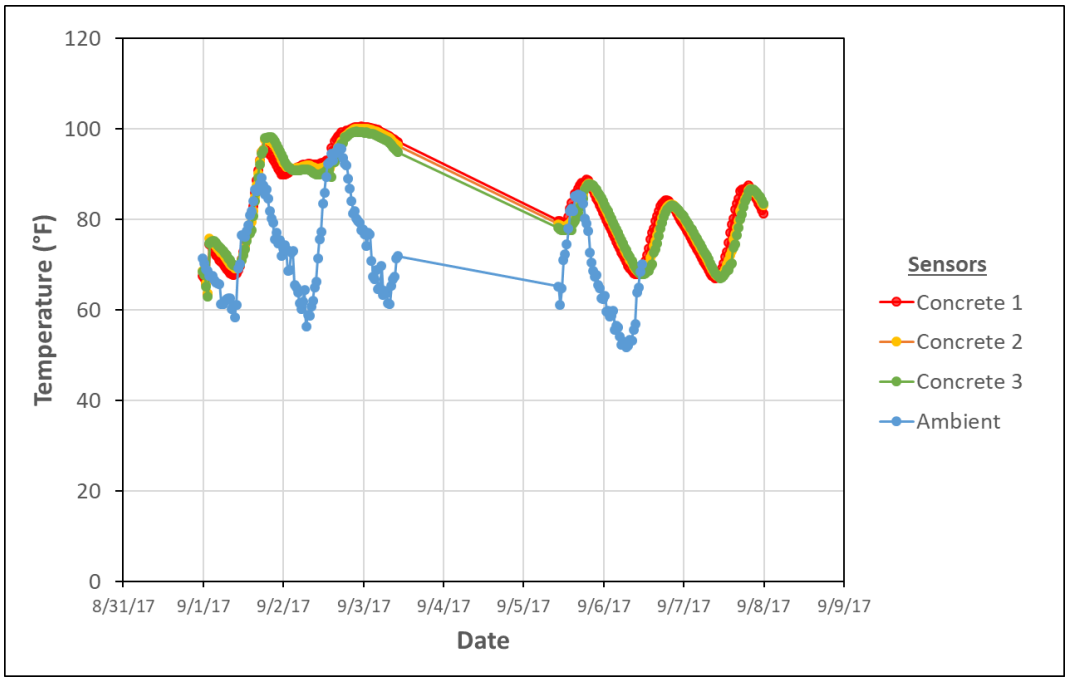

Figure A37. Temperature data - Capitol-Cedar Bridge Phase II (NB), Placement 6, North

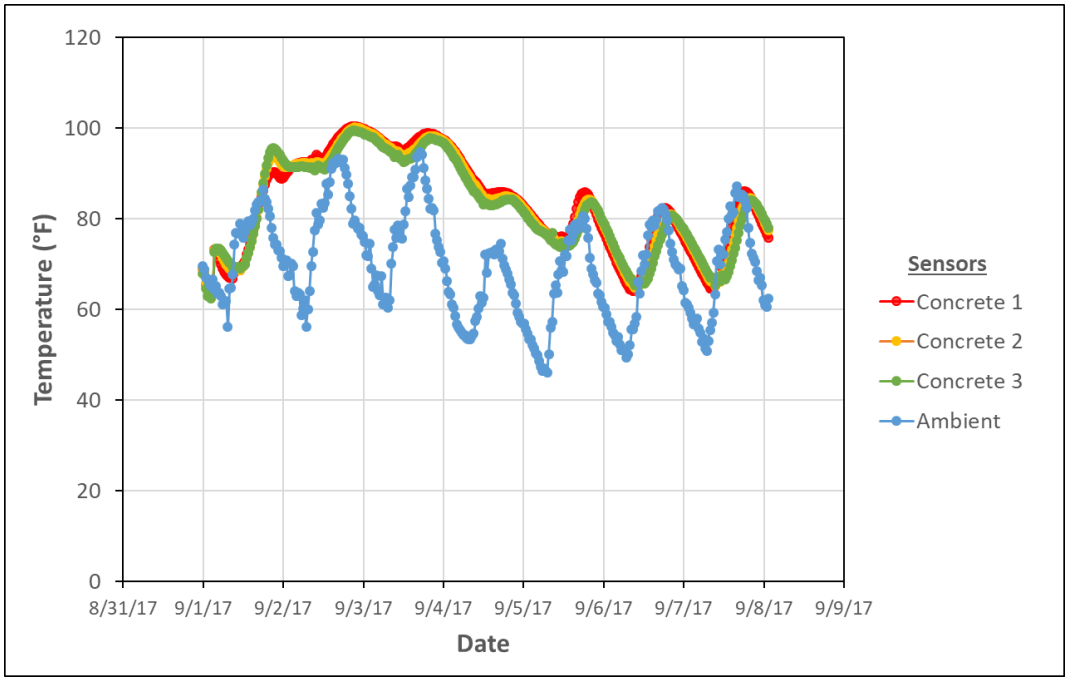

Figure A38. Temperature data - Capitol-Cedar Bridge Phase II (NB), Placement 6, Middle

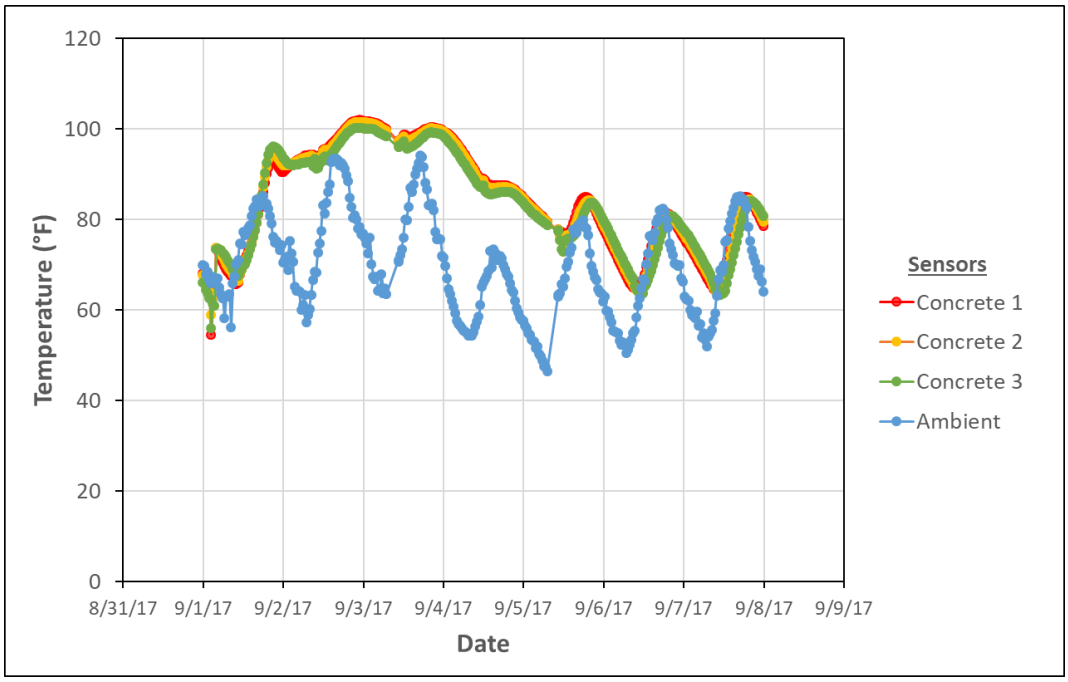

Figure A39. Temperature data - Capitol-Cedar Bridge Phase II (NB), Placement 6, South

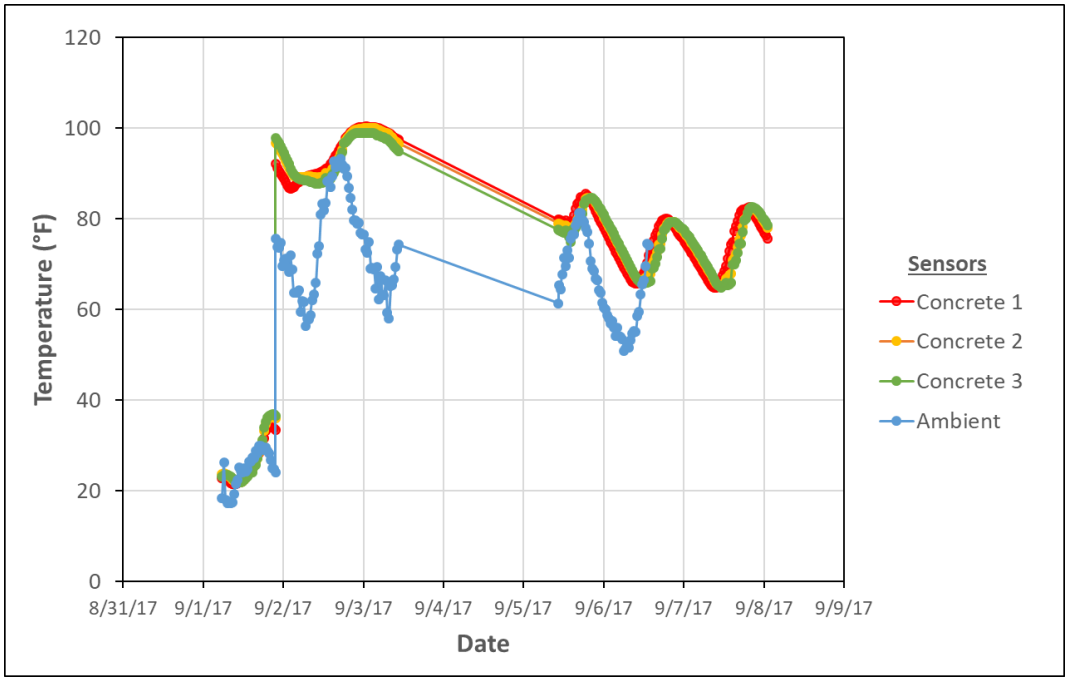

Figure A40. Temperature data - Capitol-Cedar Bridge Phase II (NB), Placement 7, North

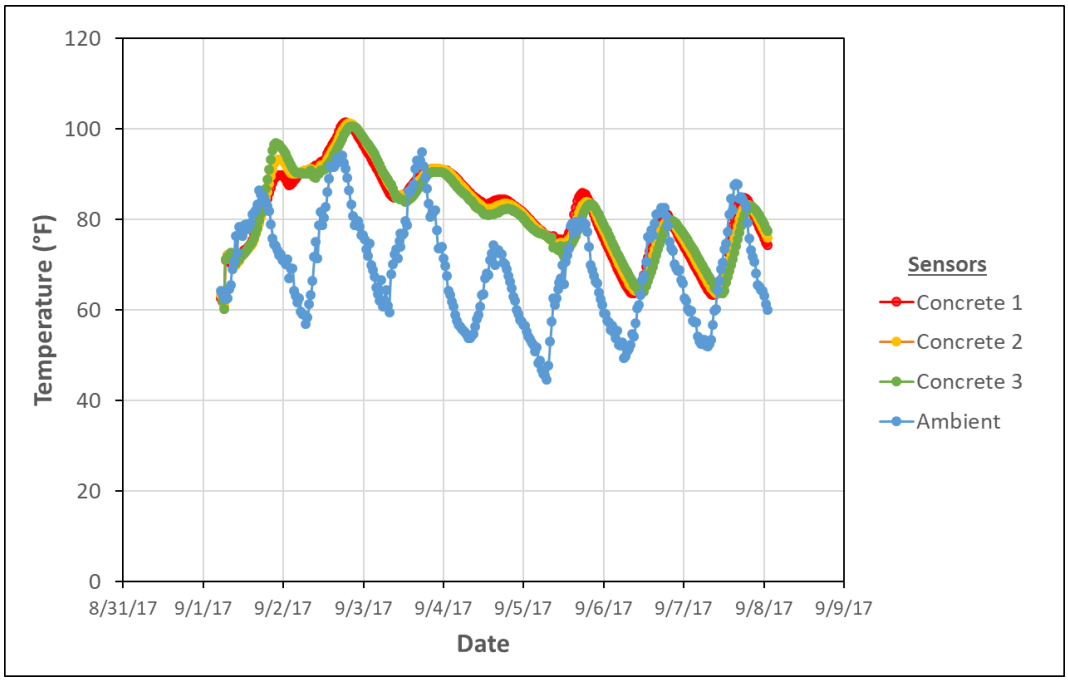

Figure A41. Temperature data - Capitol-Cedar Bridge Phase II (NB), Placement 7, Middle

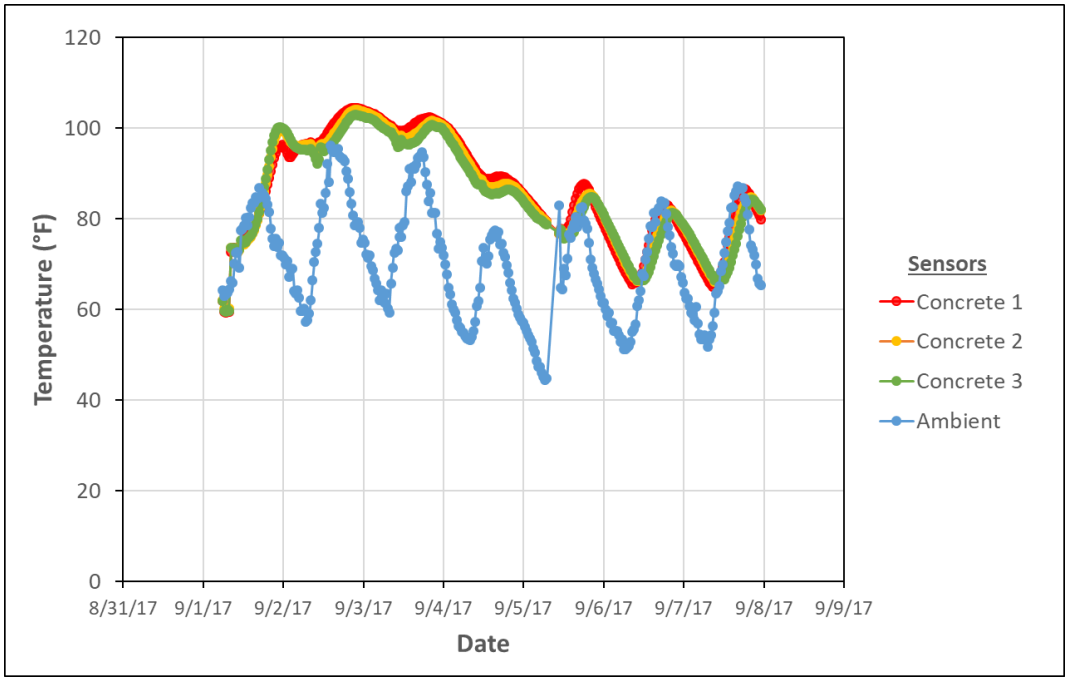

Figure A42. Temperature data - Capitol-Cedar Bridge Phase II (NB), Placement 7, South

West Laurel Bridge Phase I (EB)

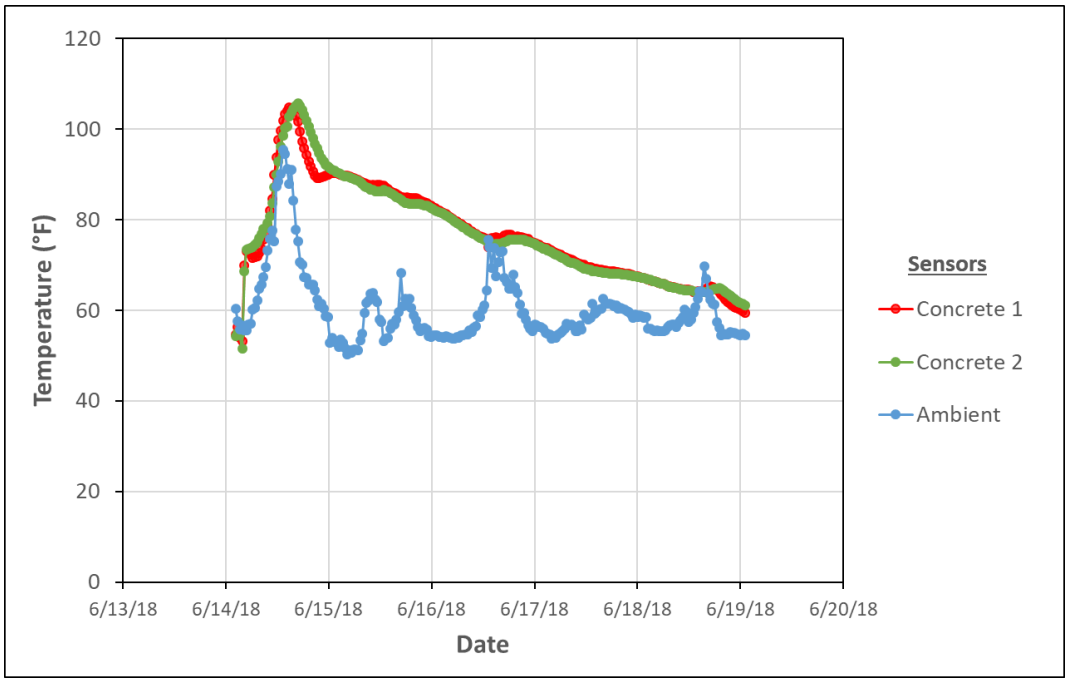

Figure A43. Temperature data - West Laurel Bridge Phase I (EB), Placement 1, Right

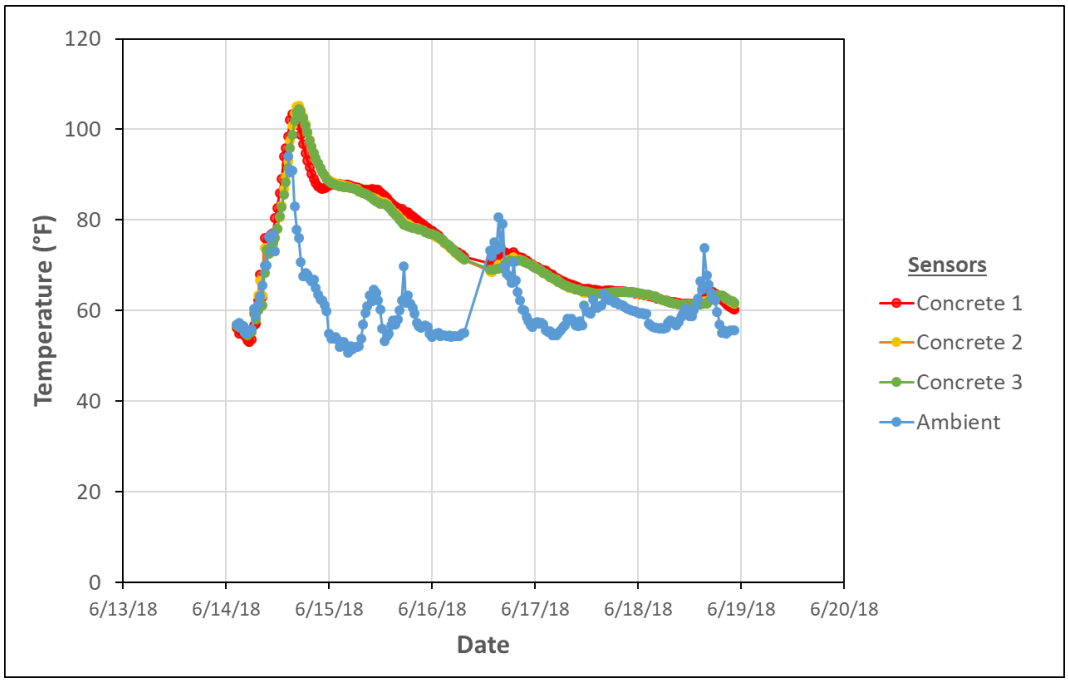

Figure A44. Temperature data - West Laurel Bridge Phase I (EB), Placement 1, Middle

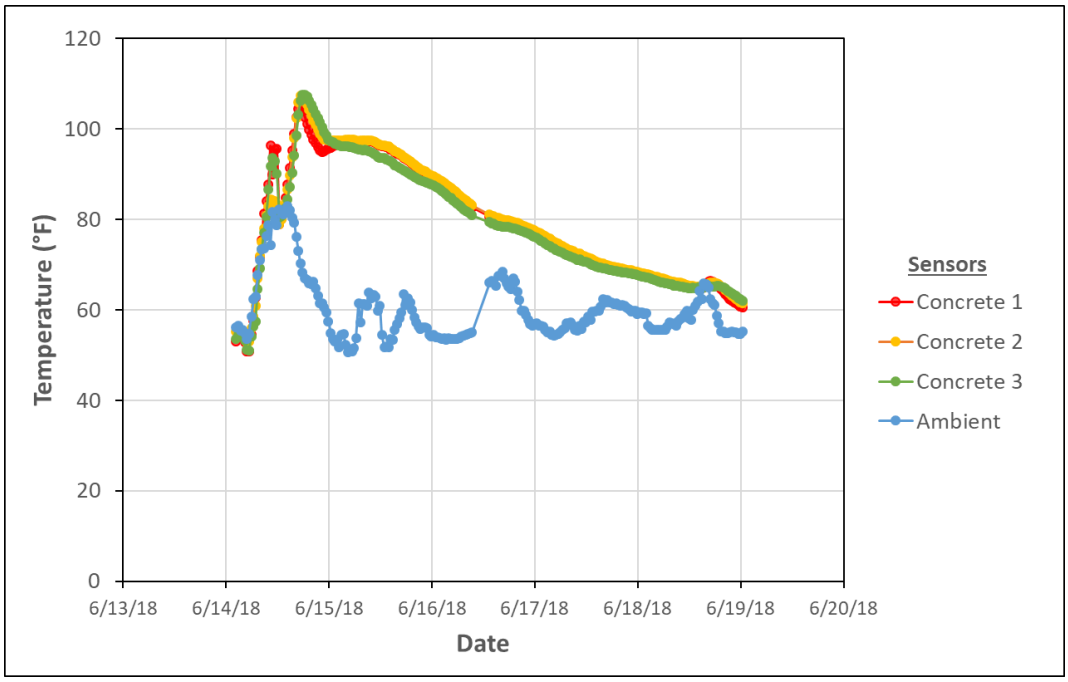

Figure A45. Temperature data - West Laurel Bridge Phase I (EB), Placement 1, Left

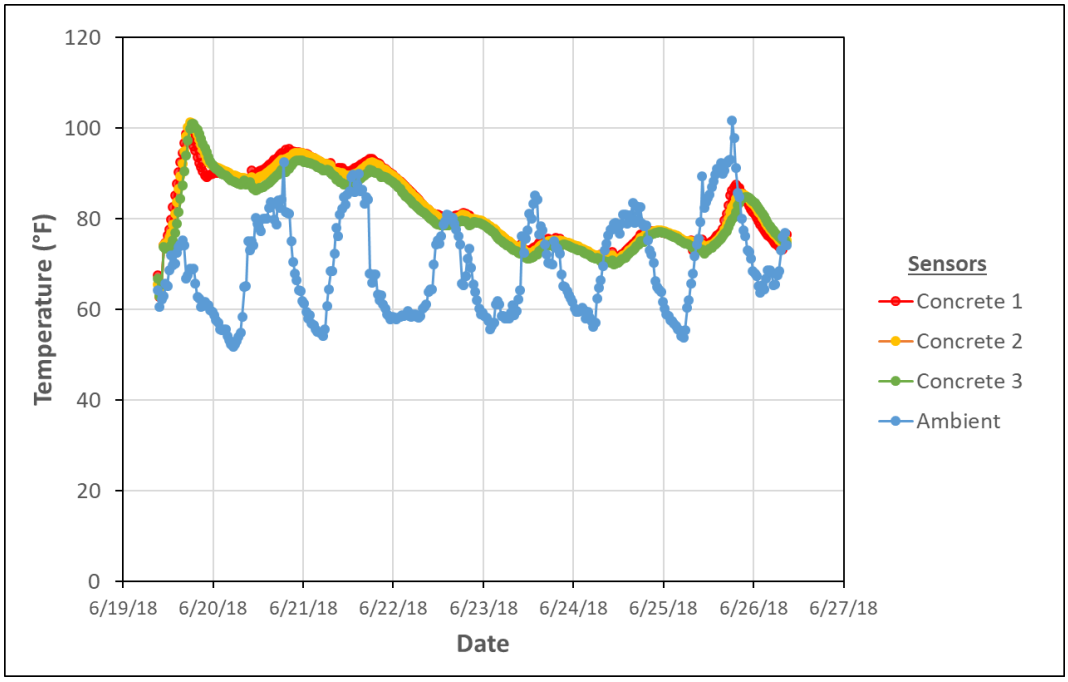

Figure A46. Temperature data - West Laurel Bridge Phase I (EB), Placement 2, Left

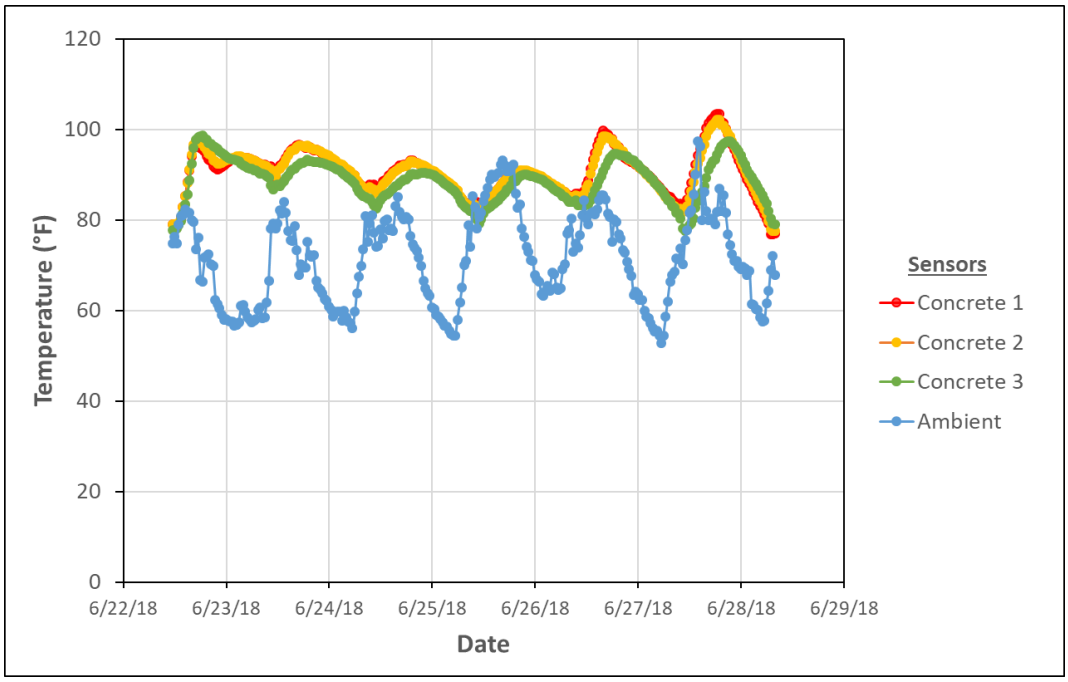

Figure A47. Temperature data - West Laurel Bridge Phase I (EB), Placement 3, Left

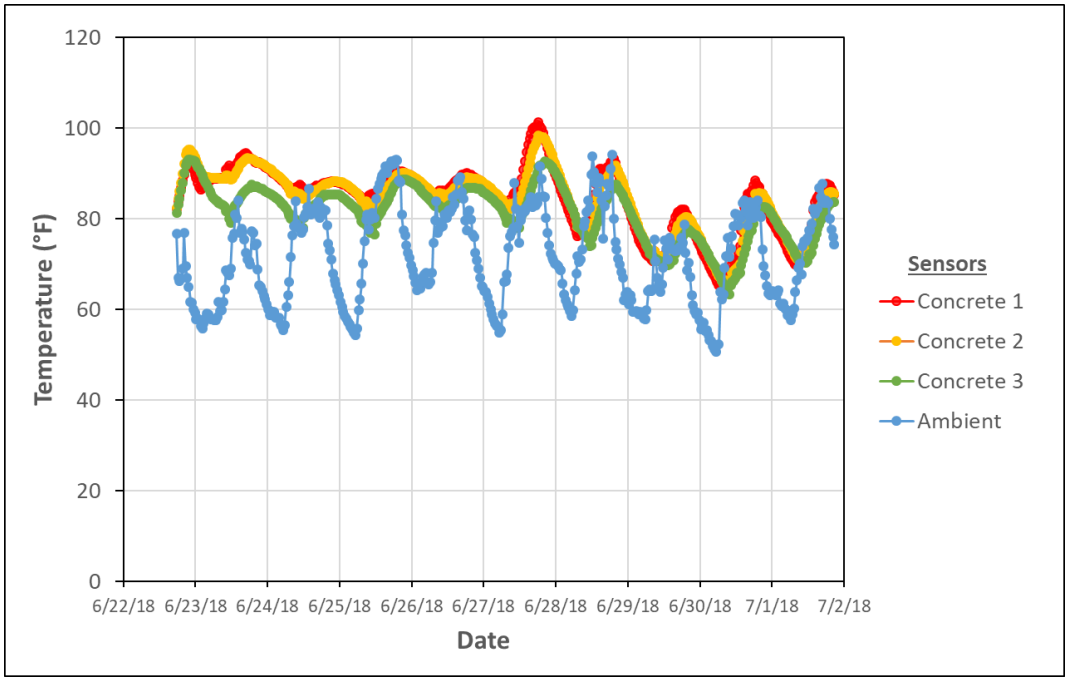

Figure A48. Temperature data - West Laurel Bridge Phase I (EB), Placement 3, Middle

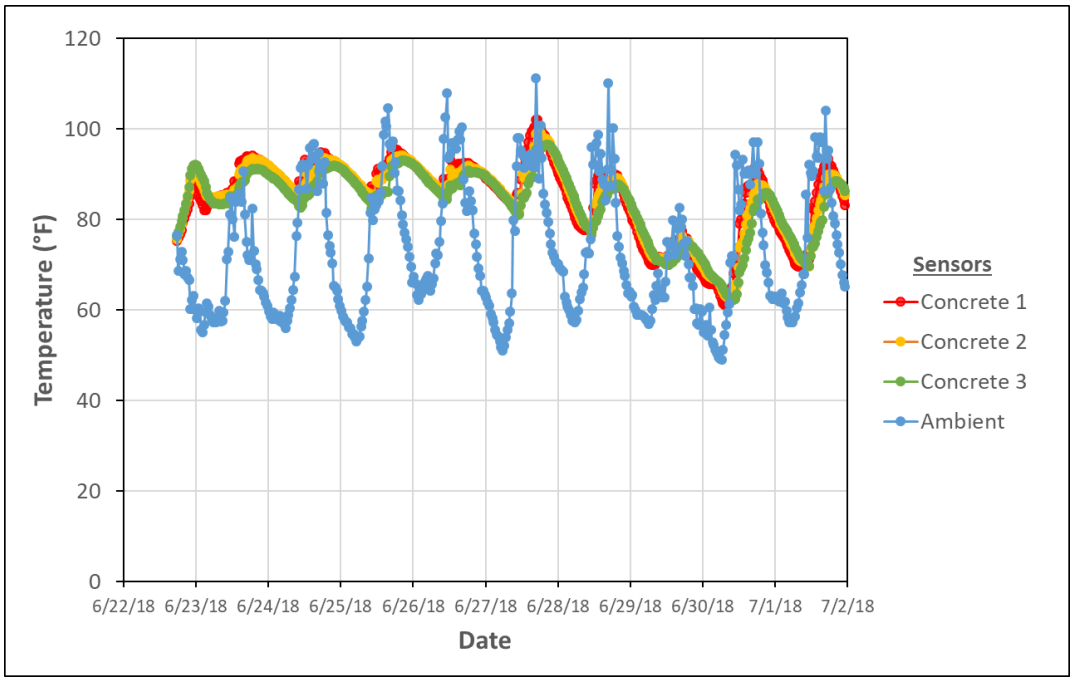

Figure A49. Temperature data - West Laurel Bridge Phase I (EB), Placement 3, Right

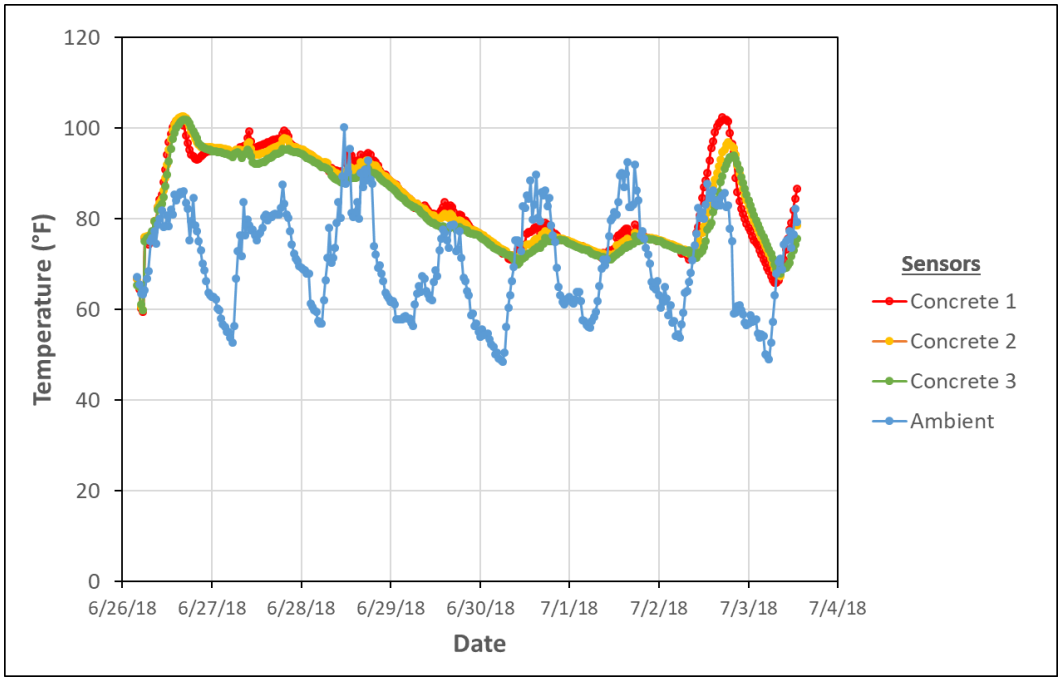

Figure A50. Temperature data - West Laurel Bridge Phase I (EB), Placement 4, Left

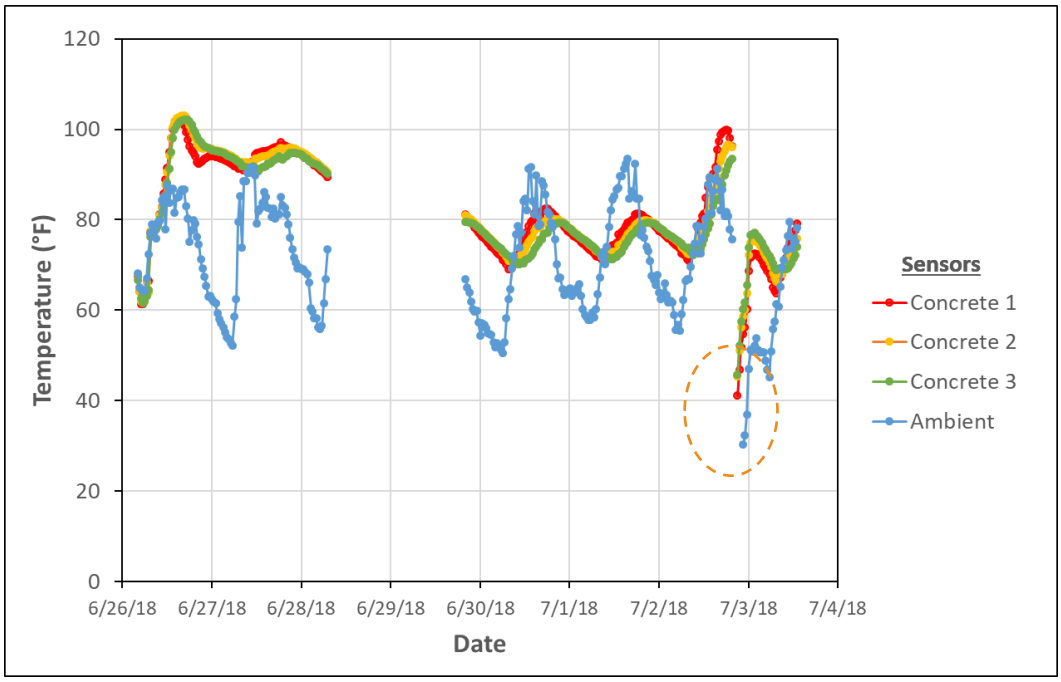

Figure A51. Temperature data - West Laurel Bridge Phase I (EB), Placement 4, Middle. Dotted ovals indicate unreliable data.

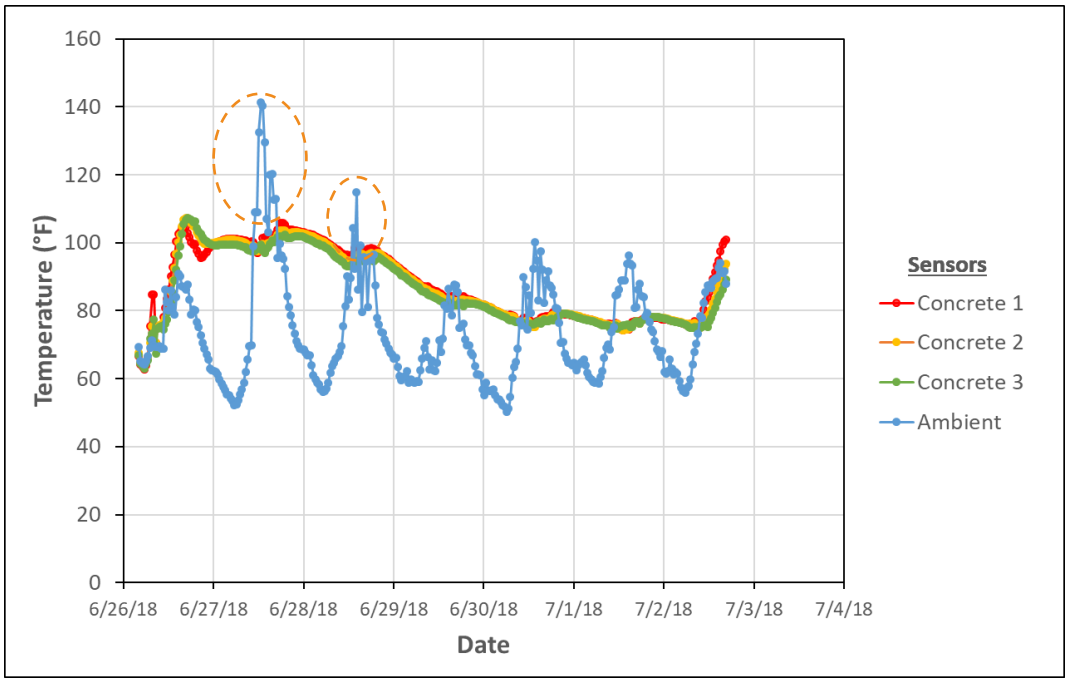

Figure A52. Temperature data - West Laurel Bridge Phase I (EB), Placement 4, Right. Dotted ovals indicate unreliable data.

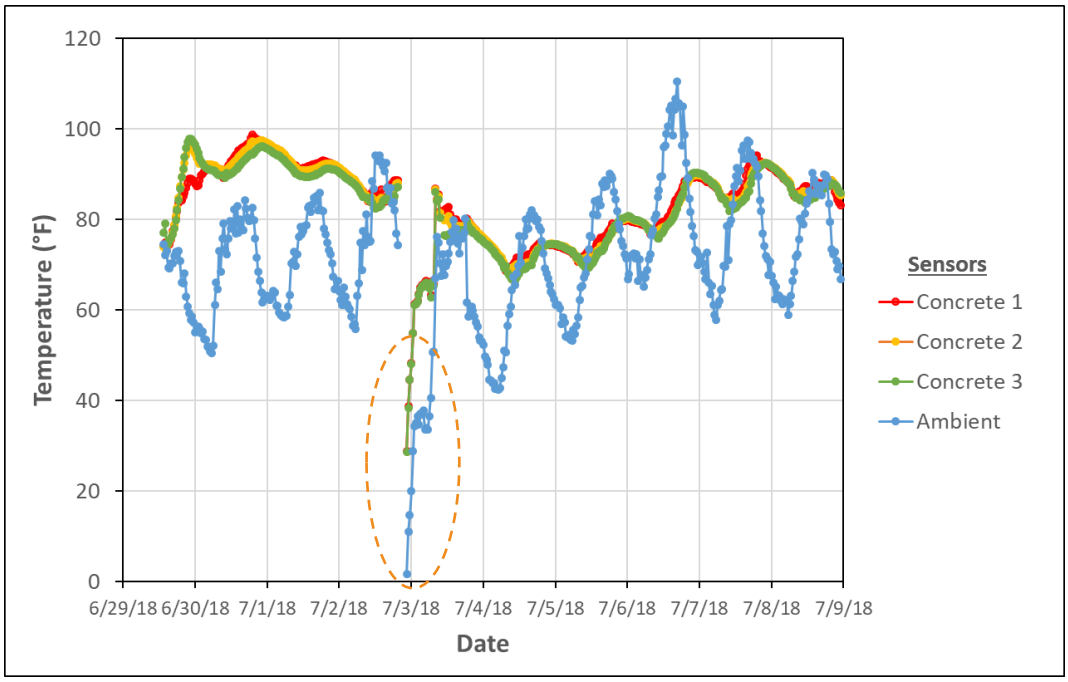

Figure A53. Temperature data - West Laurel Bridge Phase I (EB), Placement 5, LT_EE. Dotted ovals indicate unreliable data.

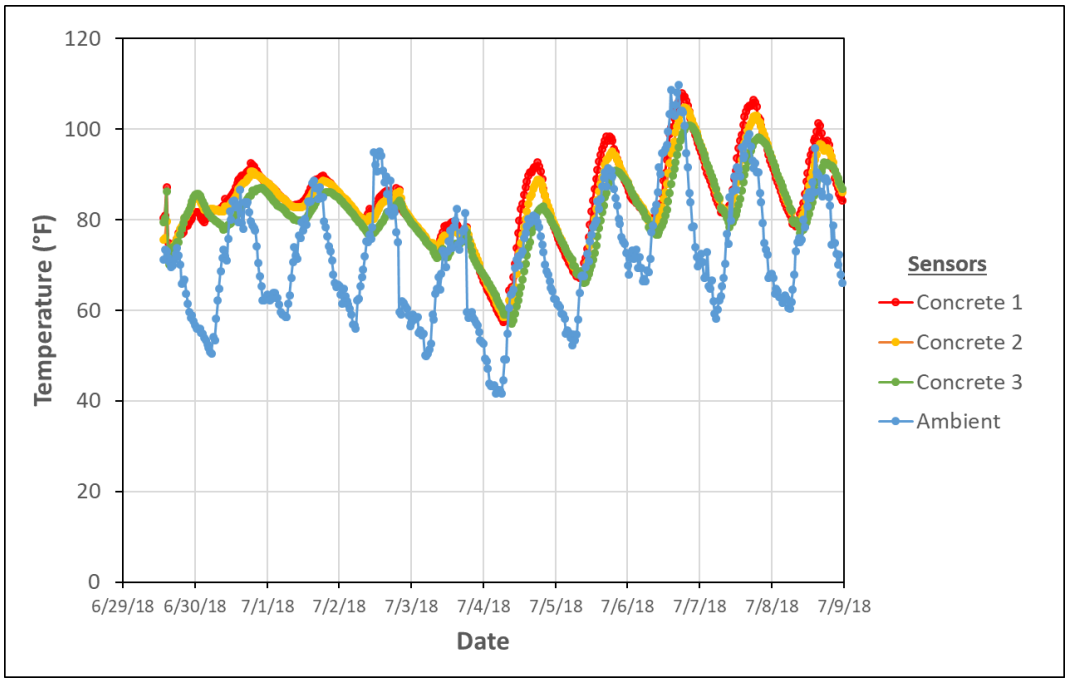

Figure A54. Temperature data - West Laurel Bridge Phase I (EB), Placement 5, LT_WE

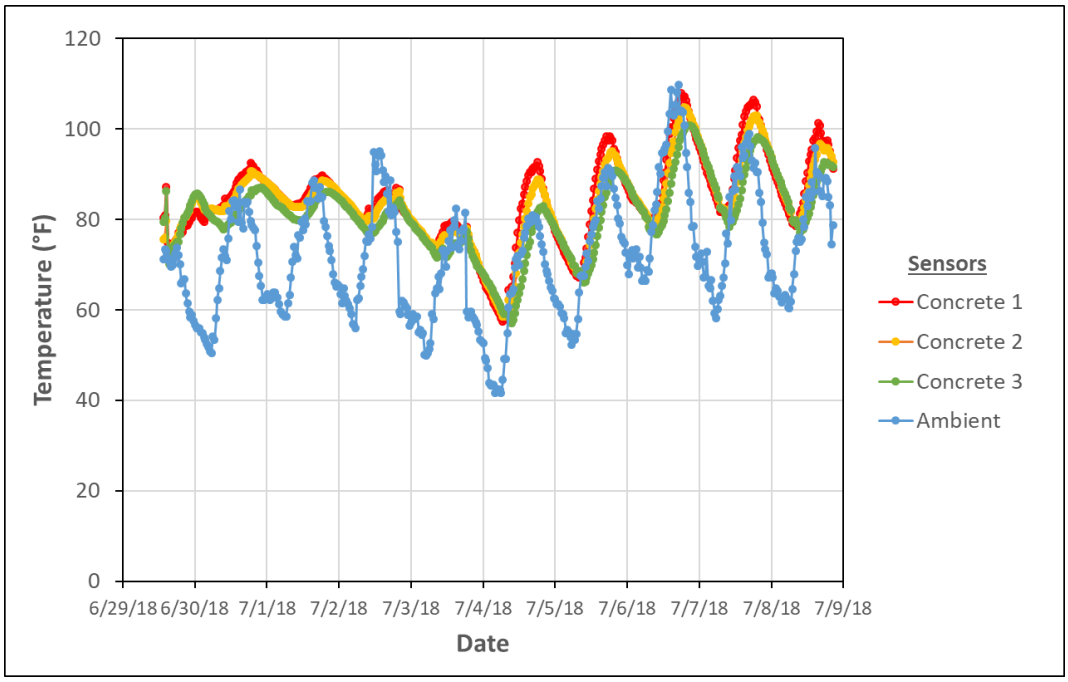

Figure A55. Temperature data - West Laurel Bridge Phase I (EB), Placement 5, RT_WE

West Laurel Bridge Phase II (WB)

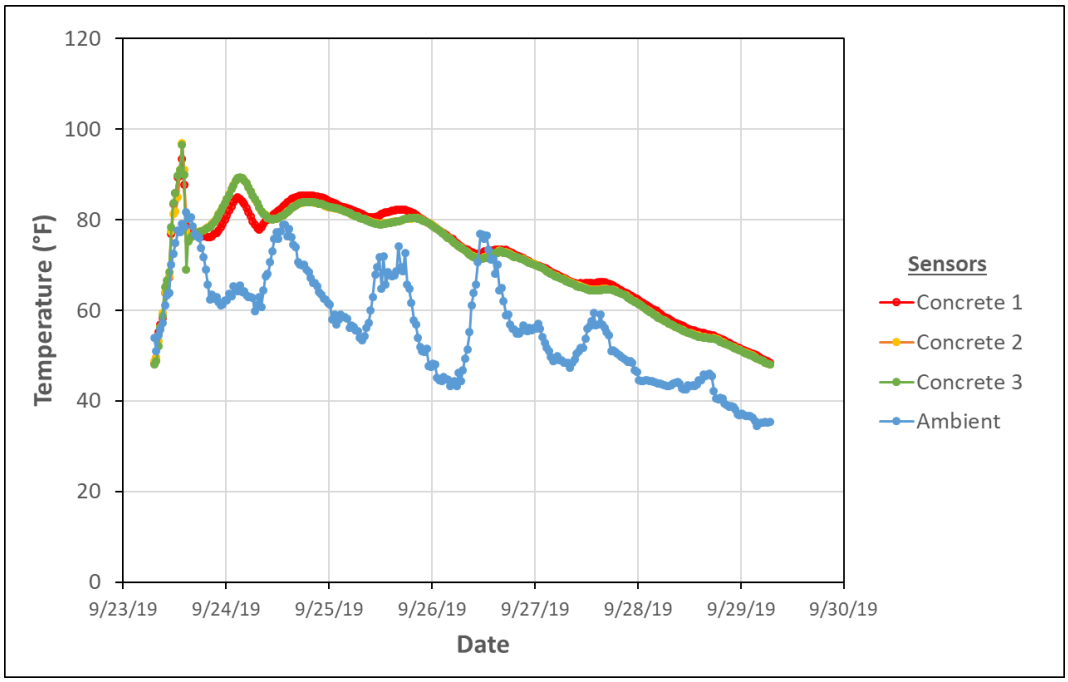

Figure A56. Temperature data - West Laurel Bridge Phase II (WB), Placement 1, North

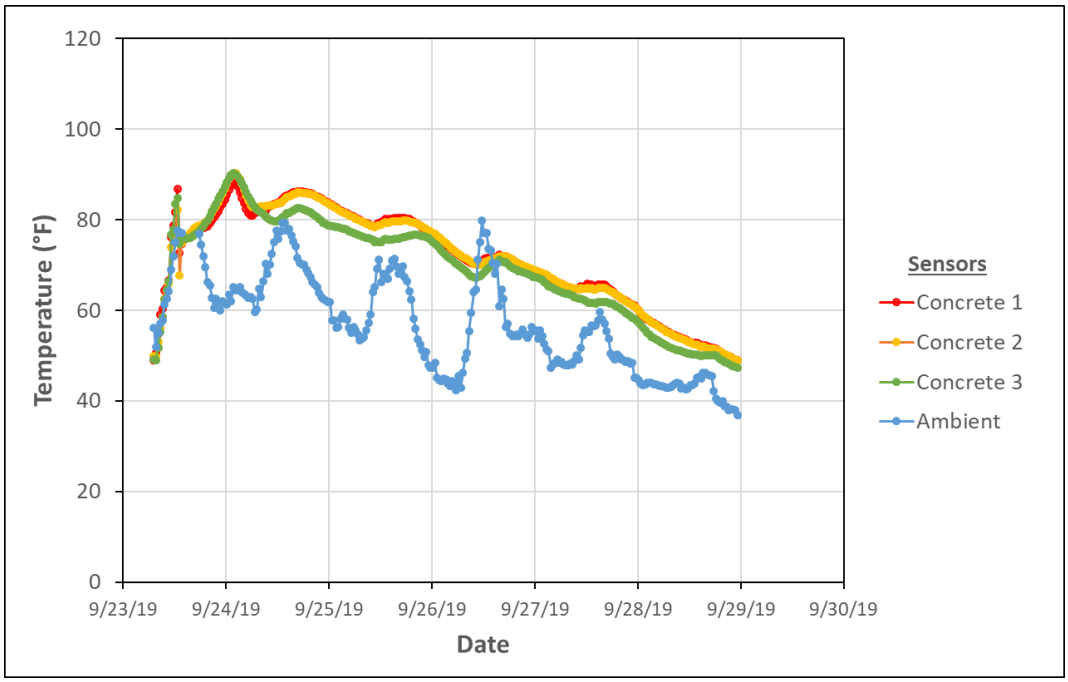

Figure A57. Temperature data - West Laurel Bridge Phase II (WB), Placement 1, Middle

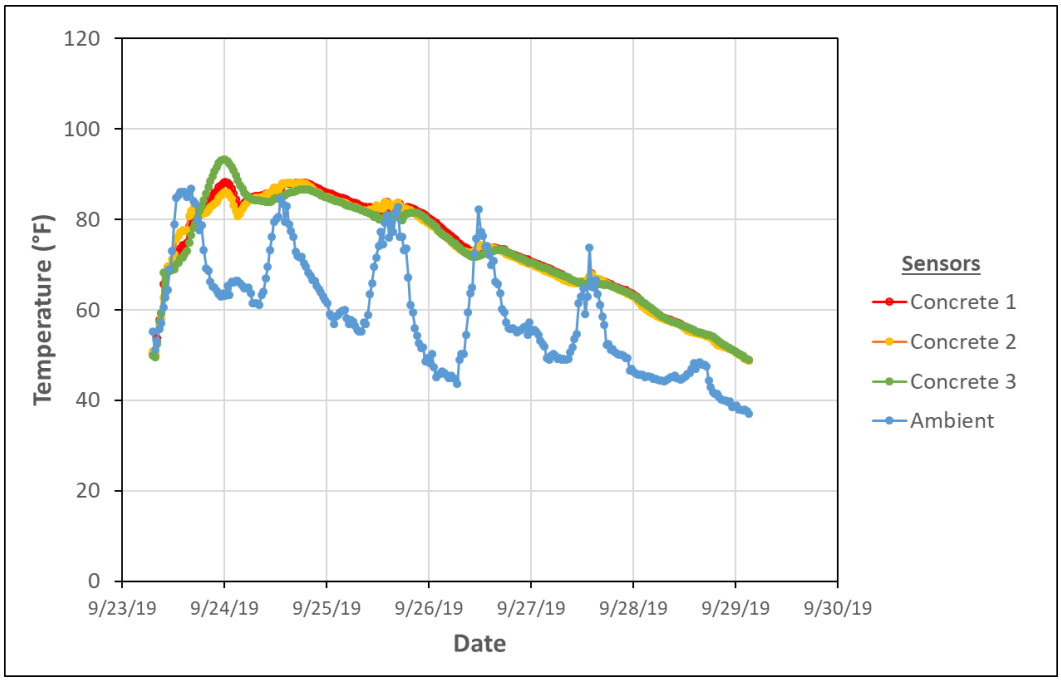

Figure A58. Temperature data - West Laurel Bridge Phase II (WB), Placement 1, South

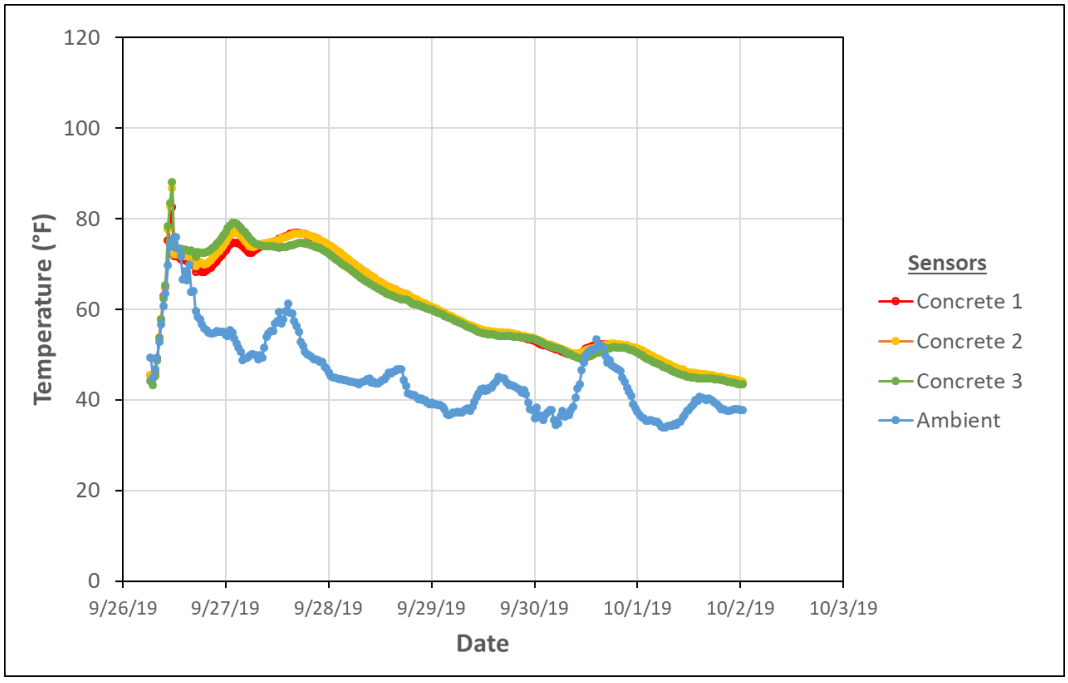

Figure A59. Temperature data - West Laurel Bridge Phase II (WB), Placement 2, North

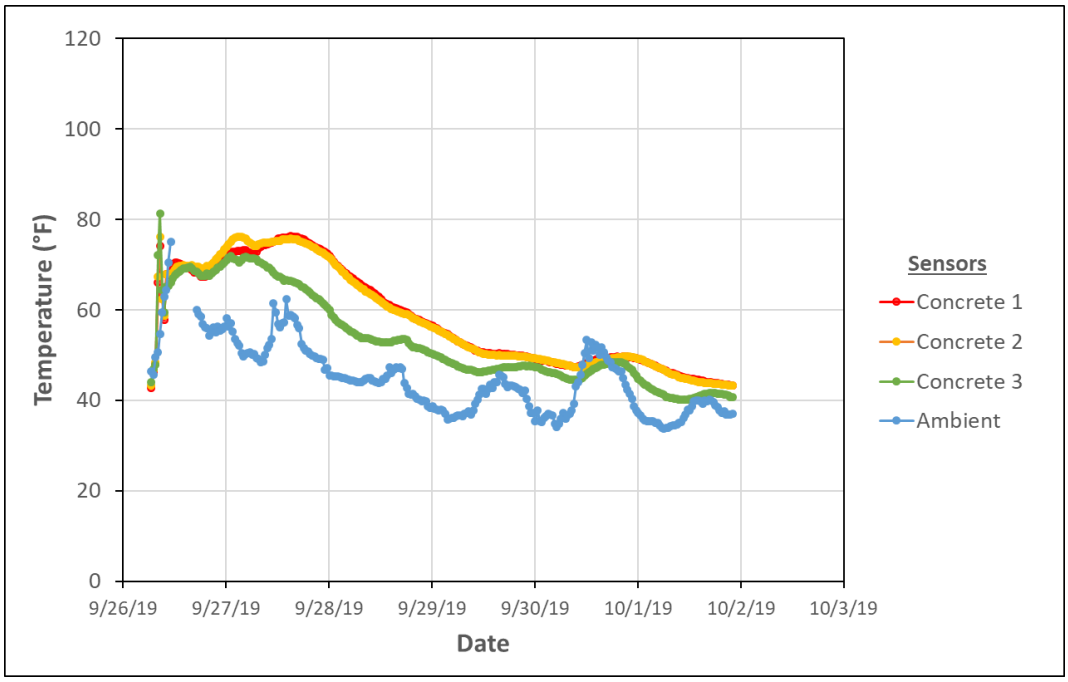

Figure A60. Temperature data - West Laurel Bridge Phase II (WB), Placement 2, Middle

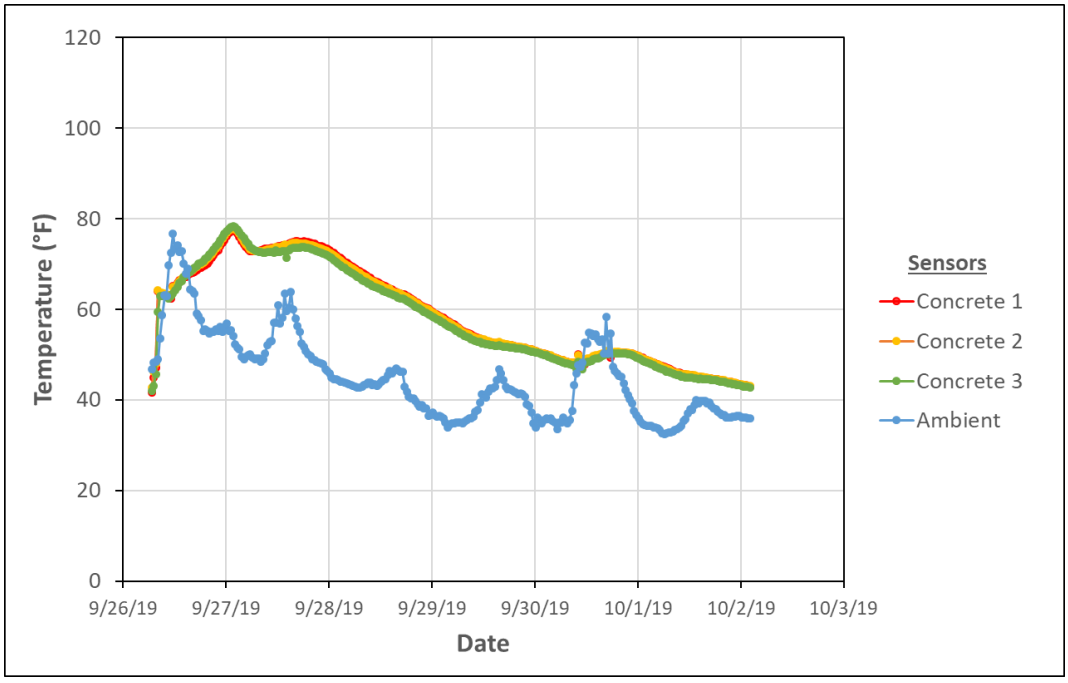

Figure A61. Temperature data - West Laurel Bridge Phase II (WB), Placement 2, South

Whitehall Bridge

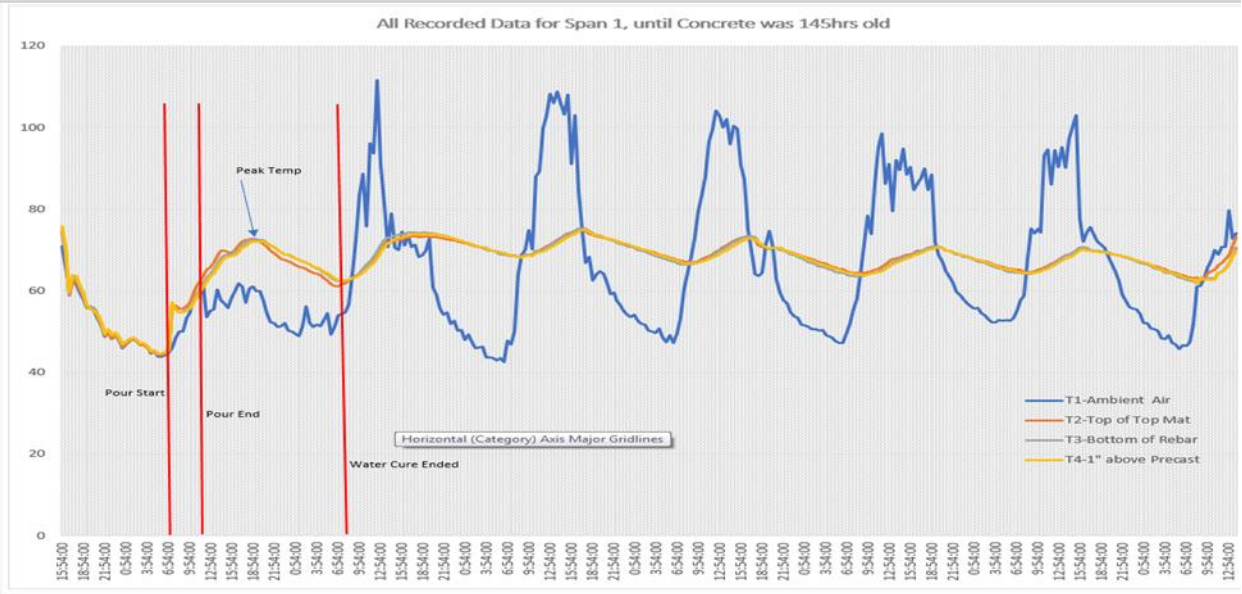

Figure A62. Temperature data - Whitehall Bridge, Span 1 - All data

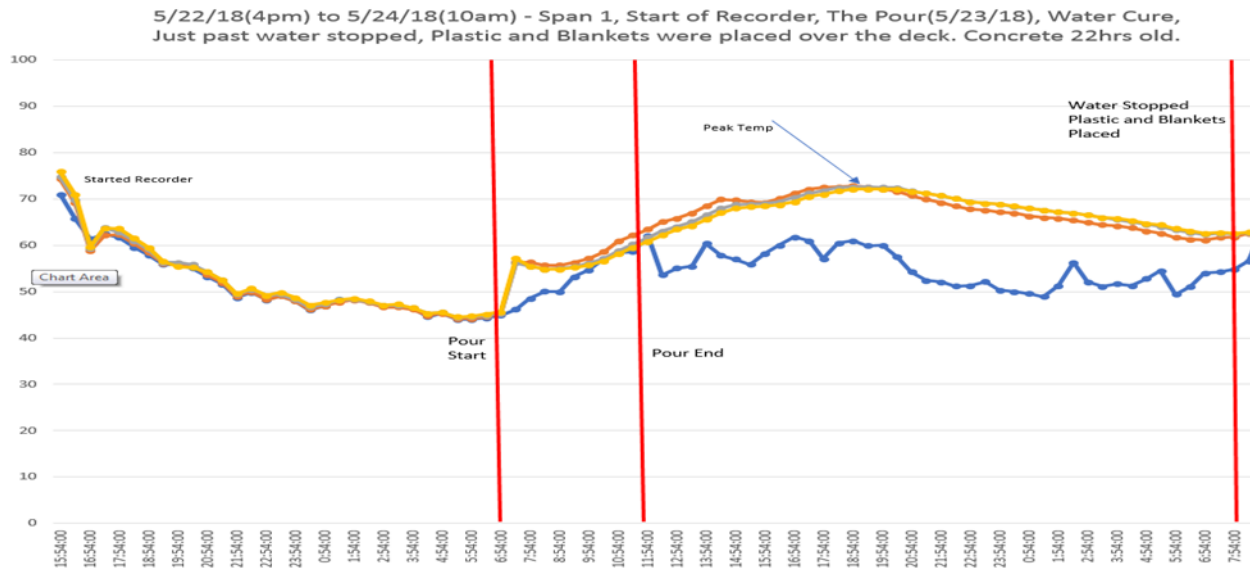

Figure A63. Temperature data - Whitehall Bridge, Span 1 - Data for the first 22 hours

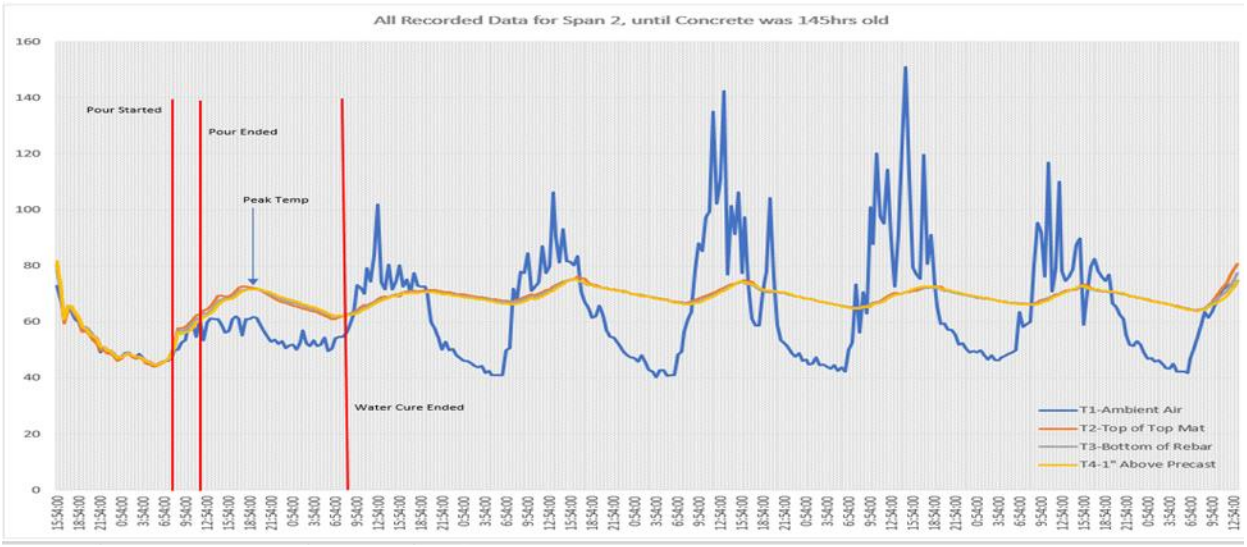

Figure A64. Temperature data - Whitehall Bridge, Span 2 - All data

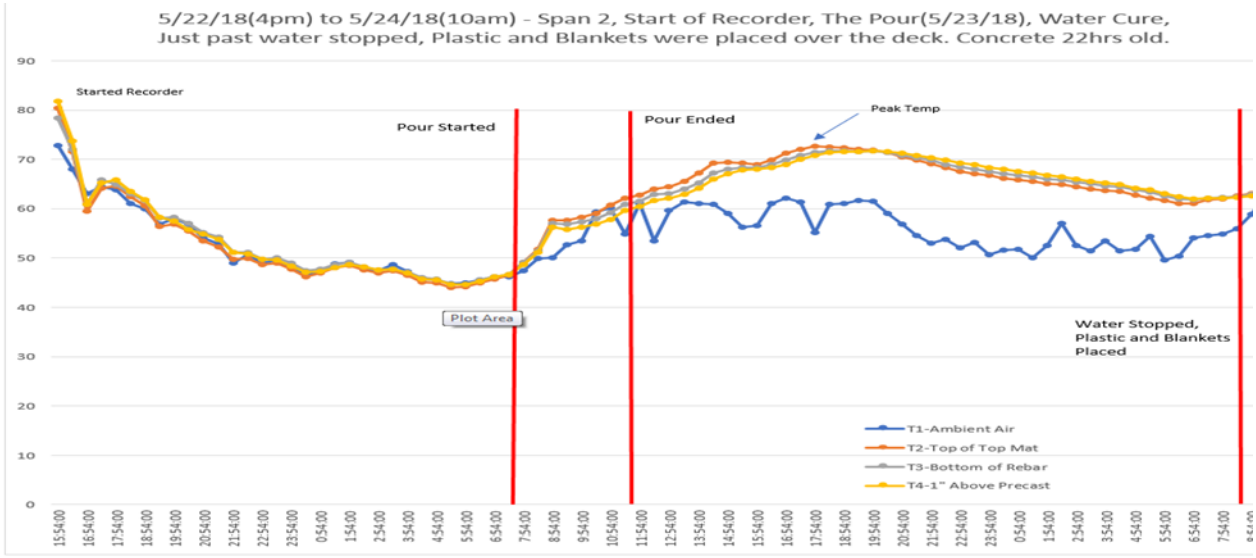

Figure A65. Temperature data - Whitehall Bridge, Span 2 - Data for the first 22 hours

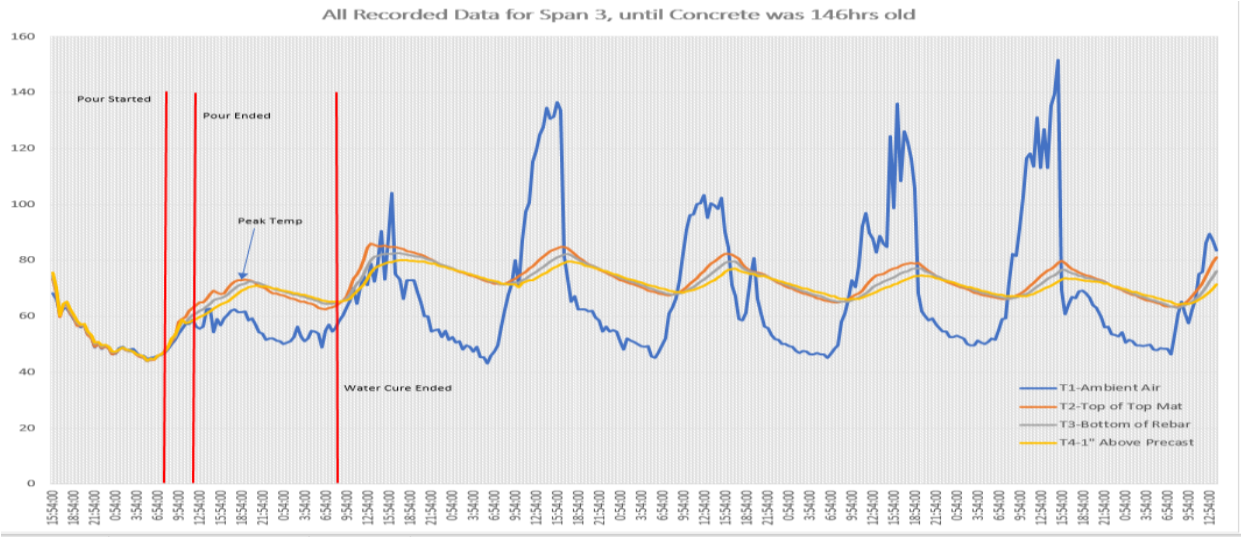

Figure A66. Temperature data - Whitehall Bridge, Span 3 - All data

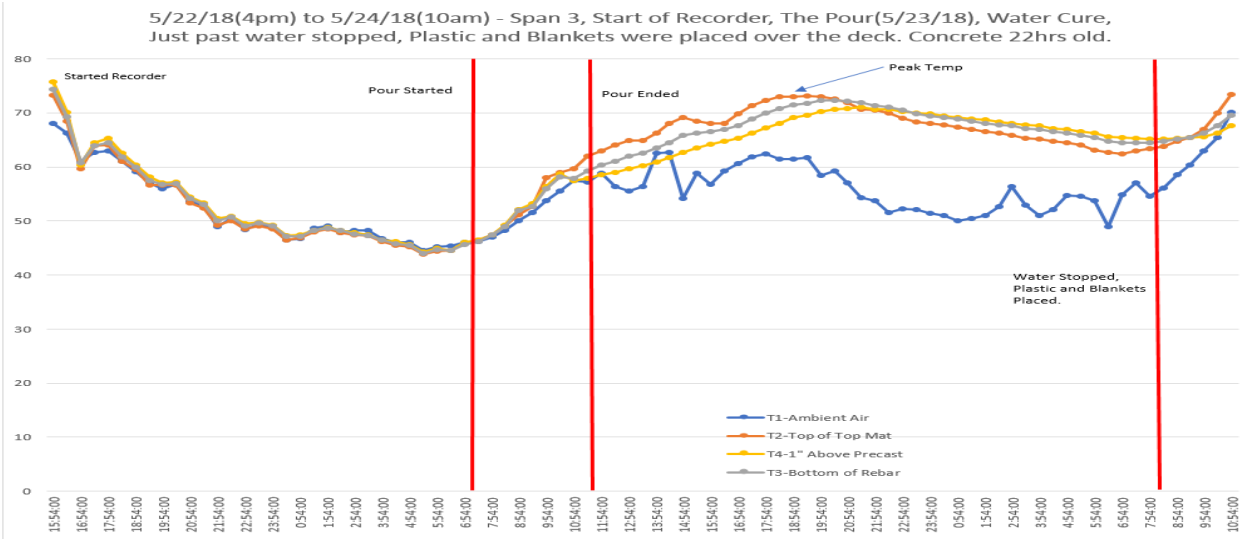

Figure A67. Temperature data - Whitehall Bridge, Span 3 - Data for the first 22 hours

Garrison Bridge

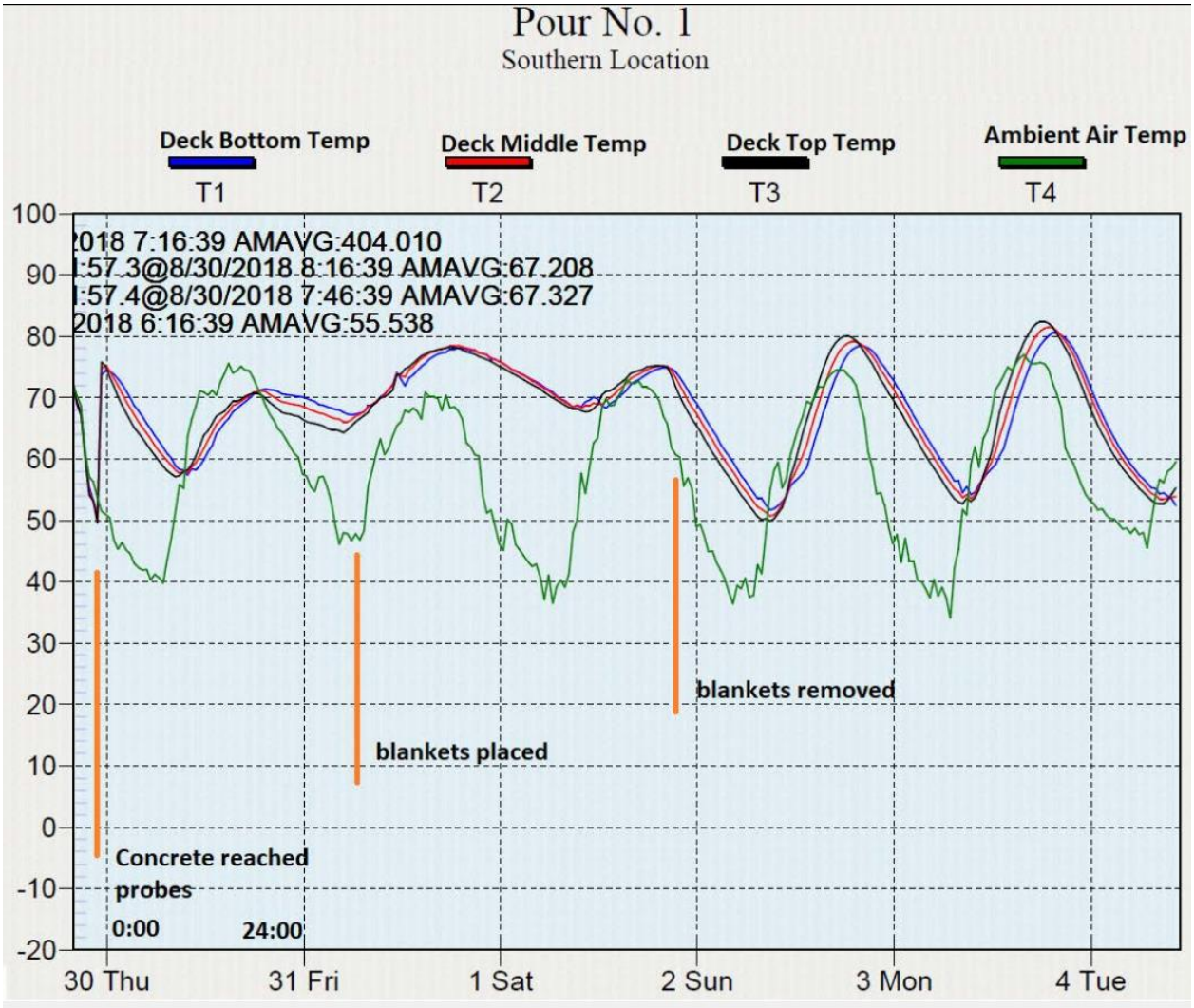

Figure A68. Temperature data - Garrison Bridge, Placement 1, Southern location. Blanket was mistakenly removed too early as noted in MDT Memorandum dated 9/25/2018.

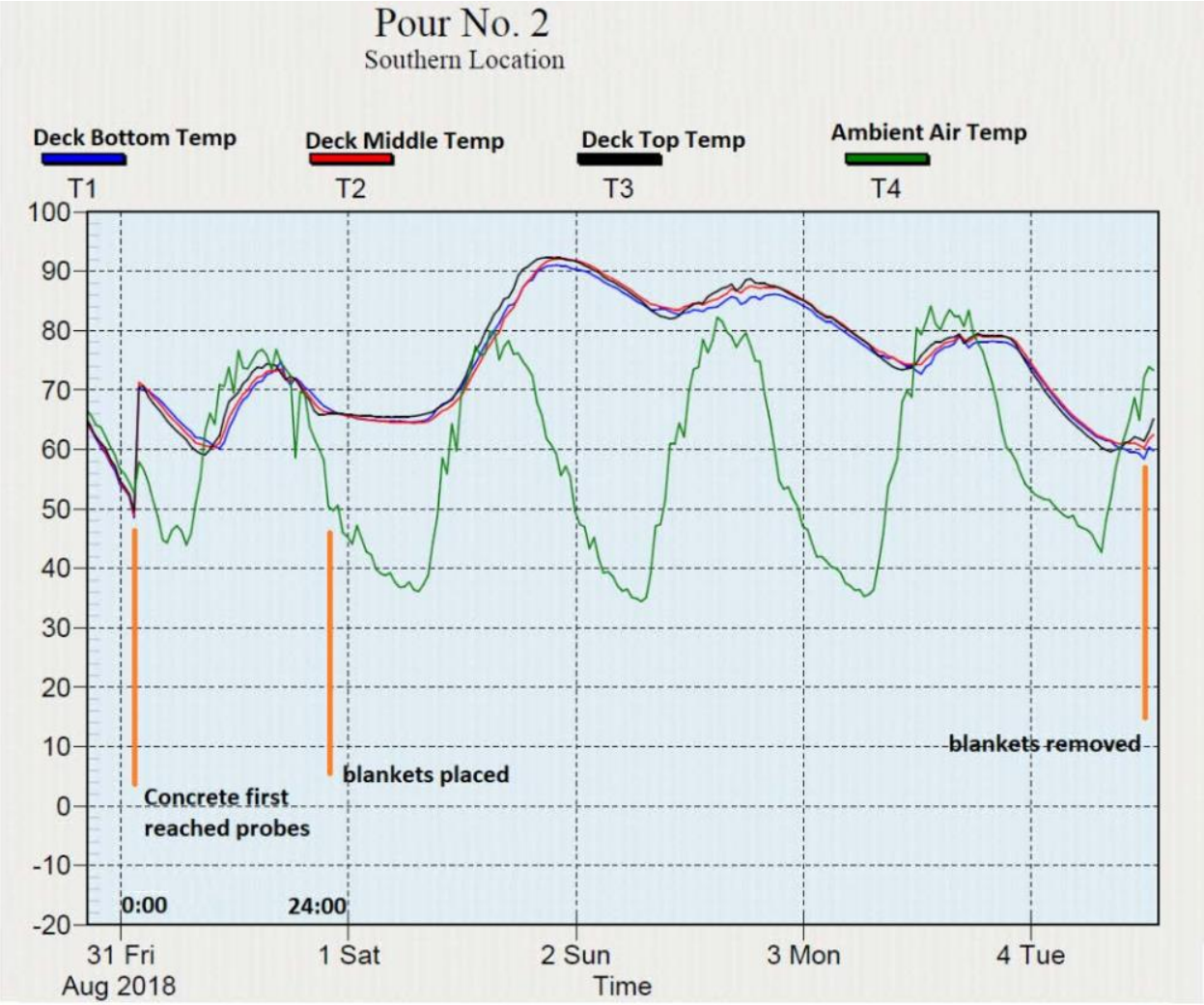

Figure A69. Temperature data - Garrison Bridge, Placement 2, Southern location

APPENDIX B. BRIDGE DECK CRACK MAPS

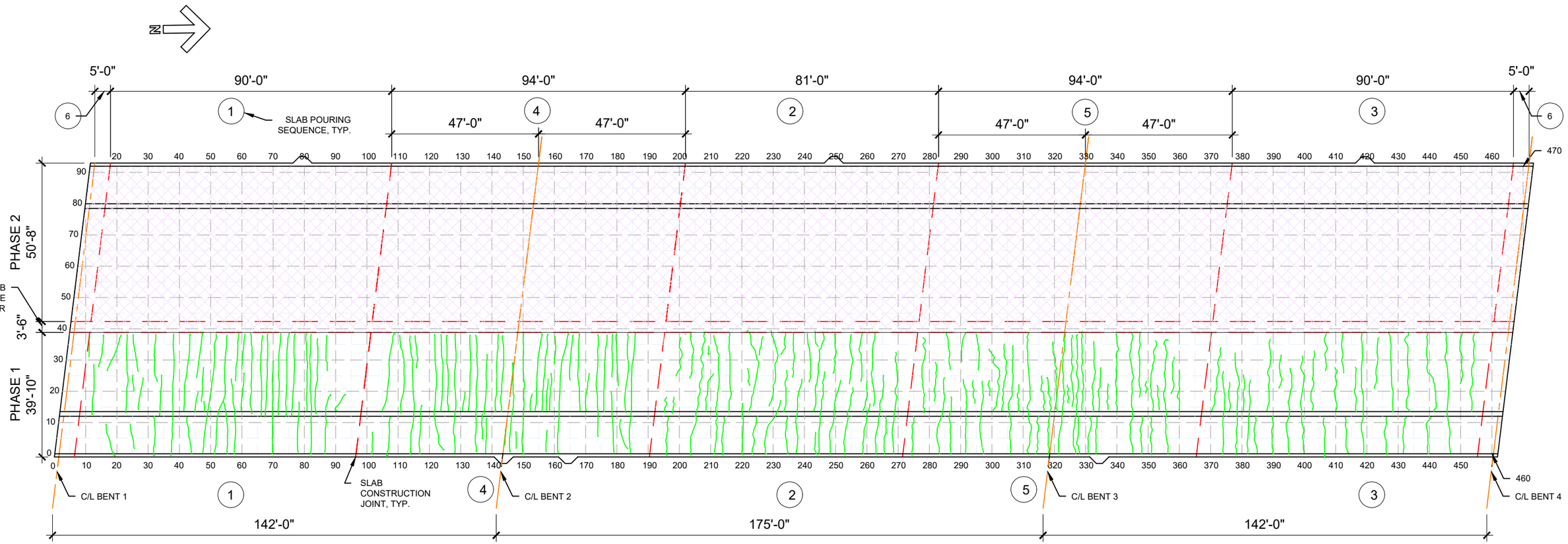

RUSSEL STREET BRIDGE OVER CLARK FORK RIVER - PHASE I - TOPSIDE - 2019 INSPECTION

1/32"= 1'-0"

WJE ENGINEERS ARCHITECTS MATERIAL SCIENTISTS
Wiss, Janney, Elstner Associates, Inc.

Russell St - Broadway to Idaho
WJE No. 2019.2214.0
Inspection dates: December 2, 2019
SCALE: AS NOTED

CRACK

CRACK SURVEY NOT PERFORMED

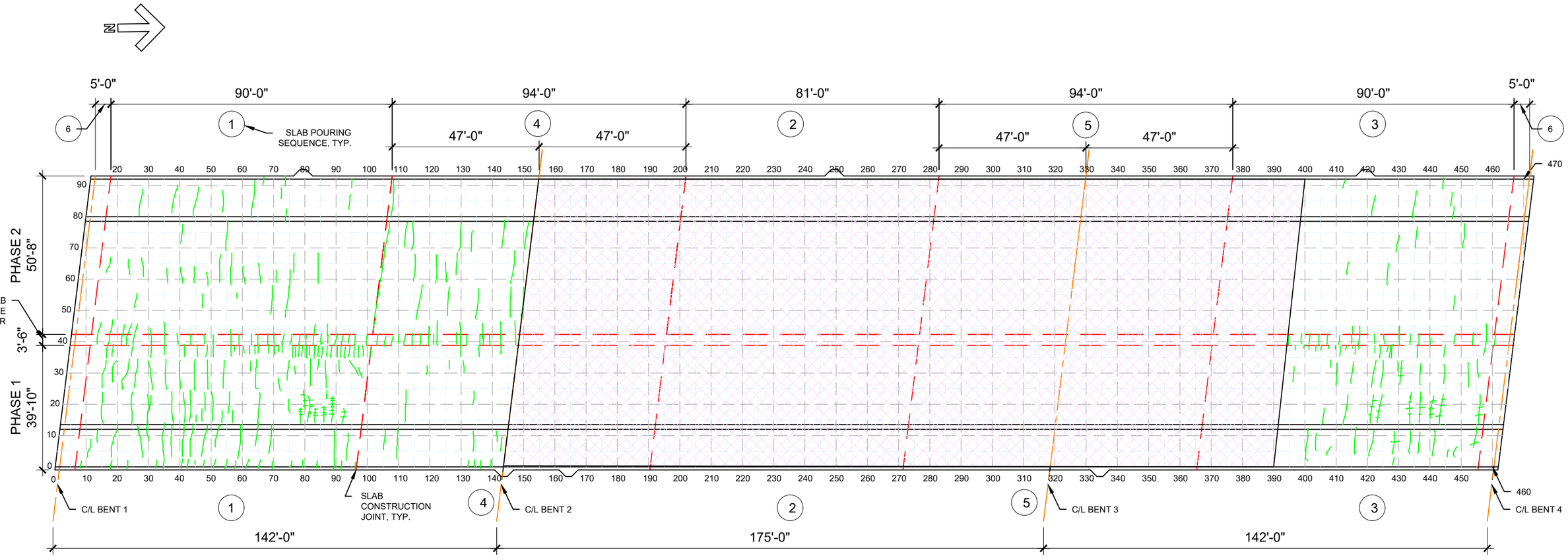

RUSSEL STREET BRIDGE OVER CLARK FORK RIVER - PHASE I & PHASE II - UNDERSIDE - 2020 INSPECTION

1/32"= 1'-0"

WJE ENGINEERS ARCHITECTS MATERIAL SCIENTISTS
Wiss, Janney, Elstner Associates, Inc.

Russell St - Broadway to Idaho
WJE No. 2019.2214.0
Inspection dates: December 2, 2019
SCALE: AS NOTED

CRACK

CRACK SURVEY NOT PERFORMED

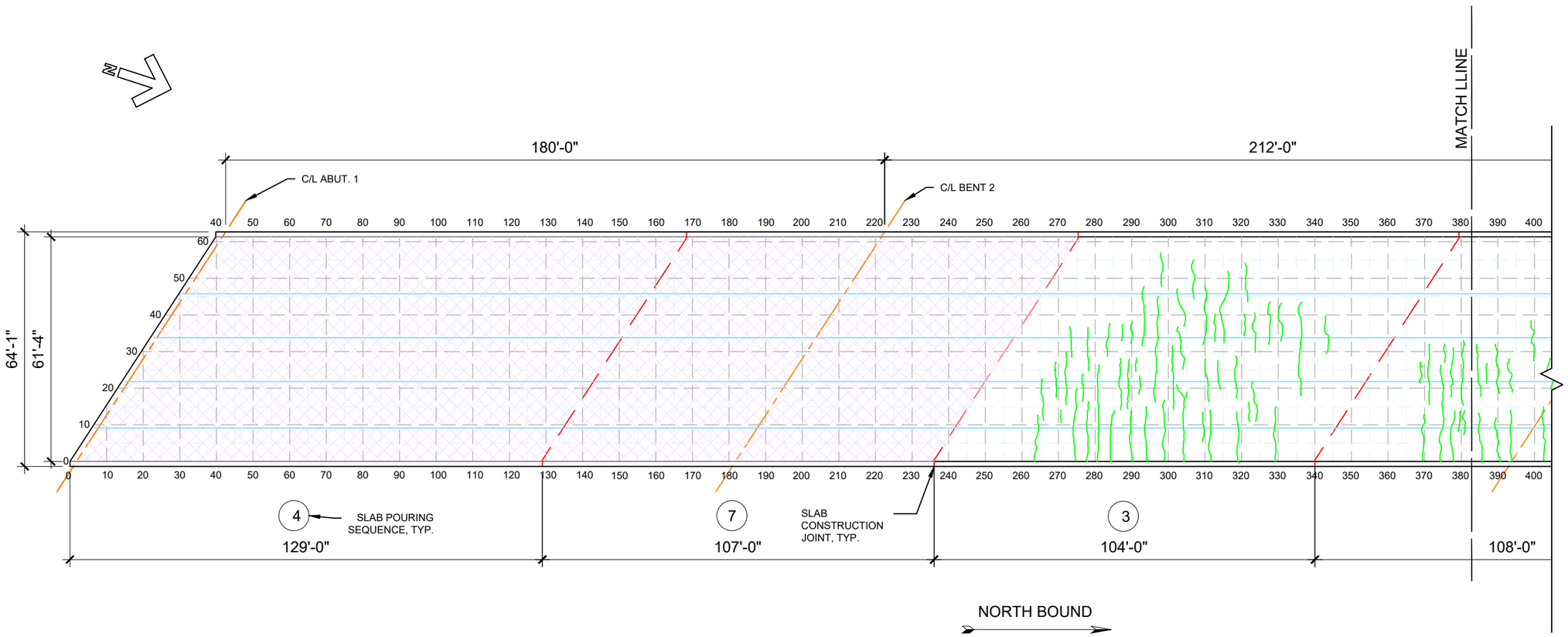

CAPITOL CEDAR BRIDGE OVER MRL - NORTH BOUND - PHASE I - TOPSIDE - 2019 INSPECTION

1/32"= 1'-0"

WJE ENGINEERS ARCHITECTS MATERIAL SCIENTISTS
Wiss, Janney, Elstner Associates, Inc.

Capitol Interchange/Cedar Interchange - Helena
WJE No. 2019.2214.0
Inspection dates: December 6, 2019
SCALE: AS NOTED

CRACK

CRACK SURVEY NOT PERFORMED

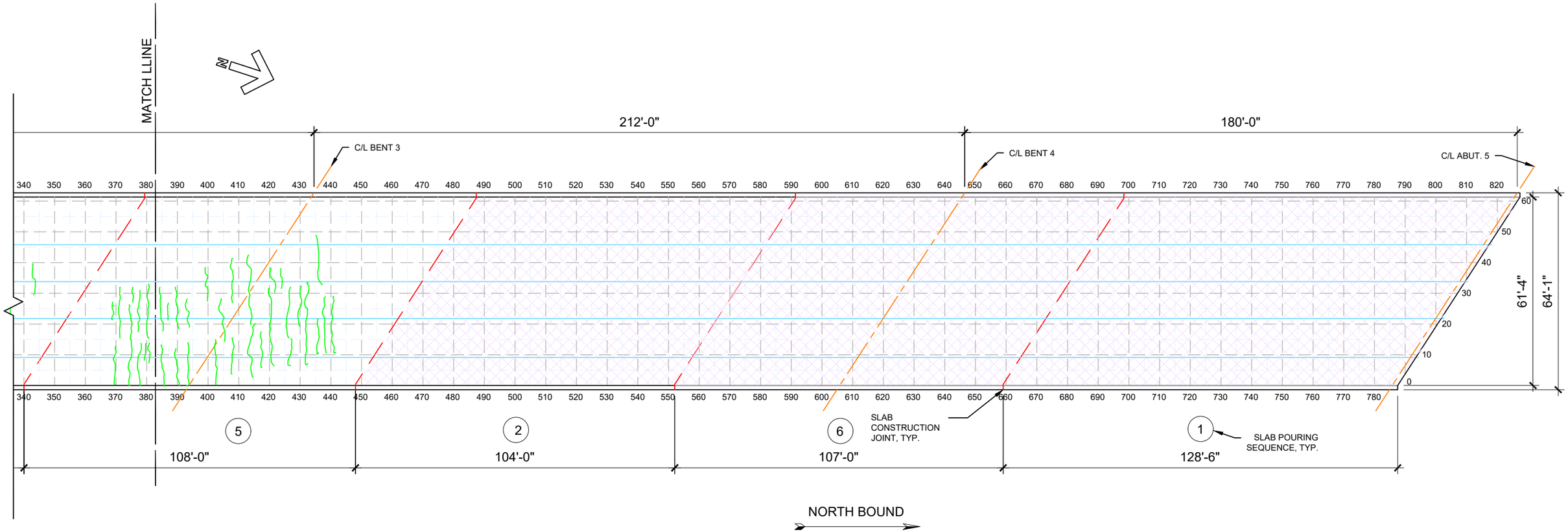

CAPITOL CEDAR BRIDGE OVER MRL - NORTH BOUND - PHASE I - TOPSIDE - 2019 INSPECTION

1/32"= 1'-0"

WJE ENGINEERS ARCHITECTS MATERIAL SCIENTISTS
Wiss, Janney, Elstner Associates, Inc.

Capitol Interchange/Cedar Interchange - Helena
WJE No. 2019.2214.0
Inspection dates: December 6, 2019
SCALE: AS NOTED

CRACK

CRACK SURVEY NOT PERFORMED

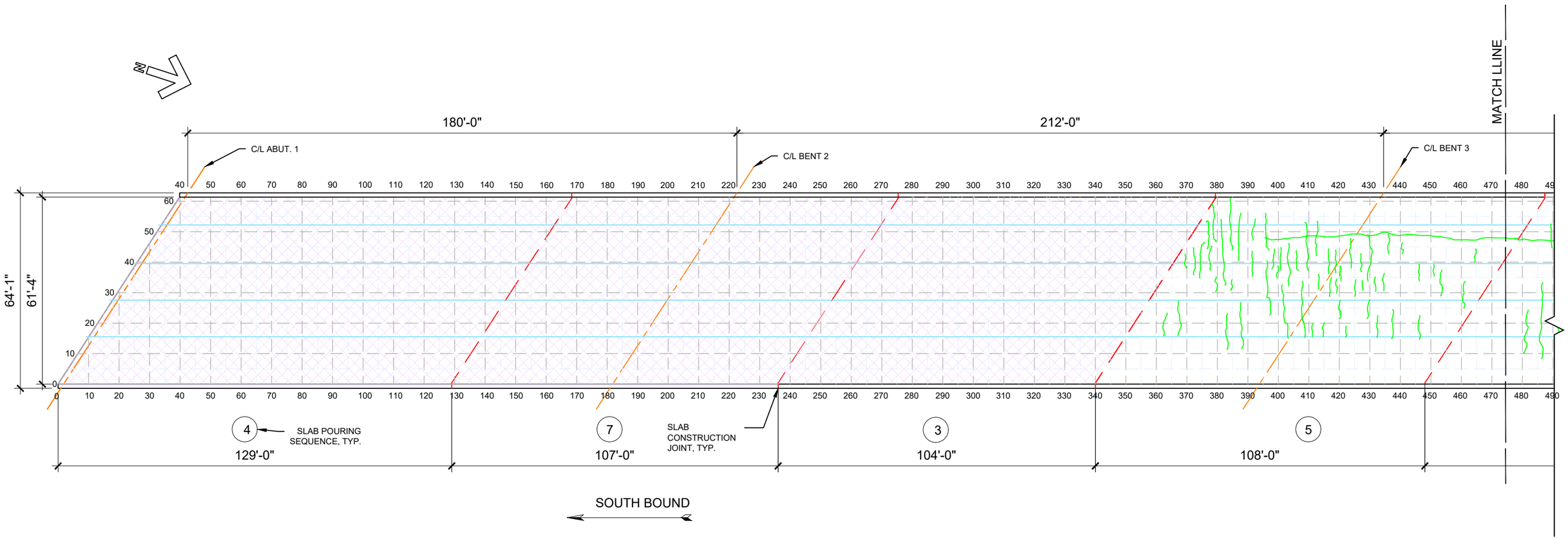

CAPITOL CEDAR BRIDGE (OVER MRL) - SOUTH BOUND - PHASE II - TOPSIDE - 2019 INSPECTION

1/32"= 1'-0"

WJE ENGINEERS ARCHITECTS MATERIAL SCIENTISTS
Wiss, Janney, Elstner Associates, Inc.

Capitol Interchange/Cedar Interchange - Helena
WJE No. 2019.2214.0
Inspection dates: December 6, 2019
SCALE: AS NOTED

CRACK

CRACK SURVEY NOT PERFORMED

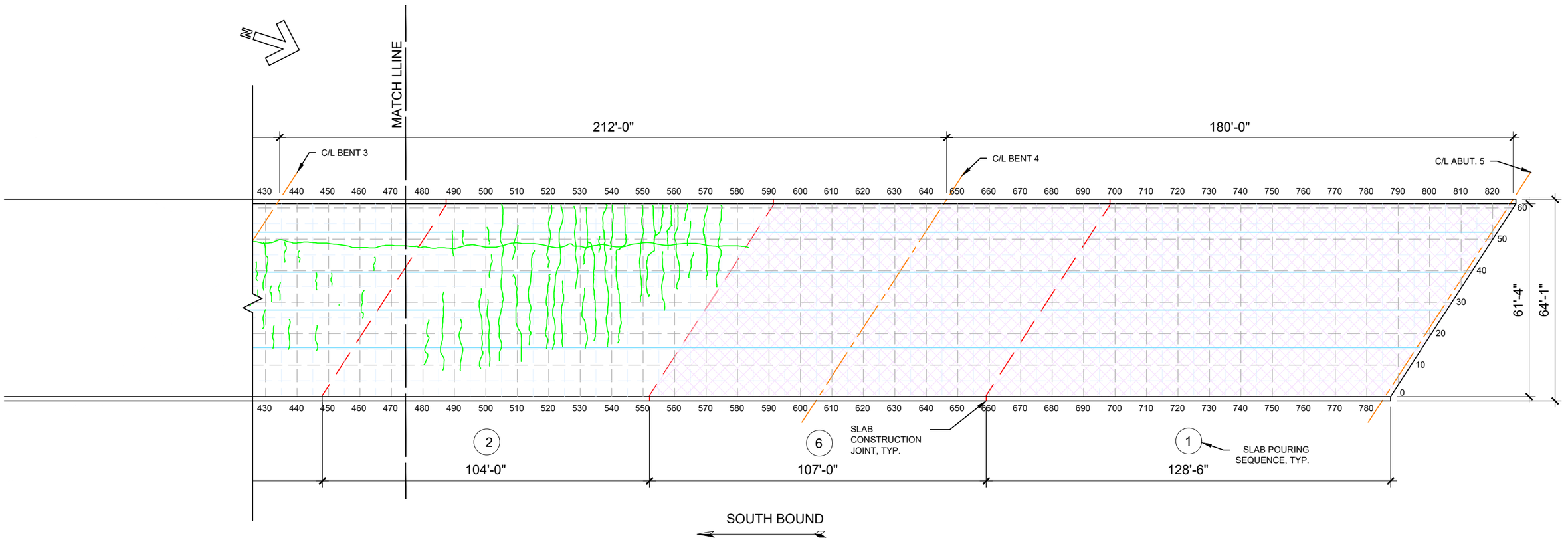

CAPITOL CEDAR BRIDGE (OVER MRL) - SOUTH BOUND - PHASE II - TOPSIDE - 2019 INSPECTION

1/32"= 1'-0"

WJE ENGINEERS ARCHITECTS MATERIAL SCIENTISTS
Wiss, Janney, Elstner Associates, Inc.

Capitol Interchange/Cedar Interchange - Helena
WJE No. 2019.2214.0
Inspection dates: December 6, 2019
SCALE: AS NOTED

CRACK

CRACK SURVEY NOT PERFORMED

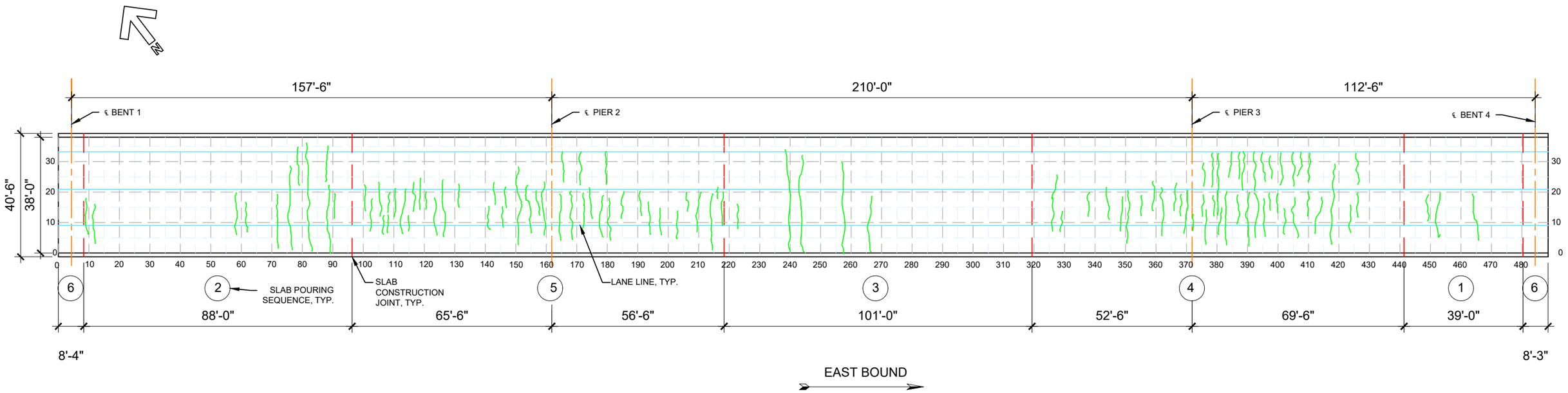

BONNER SPRING BRIDGE OVER BLACKFOOT RIVER - EAST BOUND - PHASE I - TOPSIDE - 2019 INSPECTION

1/32"= 1'-0"

WJE ENGINEERS ARCHITECTS MATERIAL SCIENTISTS
Wiss, Janney, Elstner Associates, Inc.

Bonner Spring Bridge
WJE No. 2019.2214.0
Inspection dates: December 7, 2019
SCALE: AS NOTED

CRACK

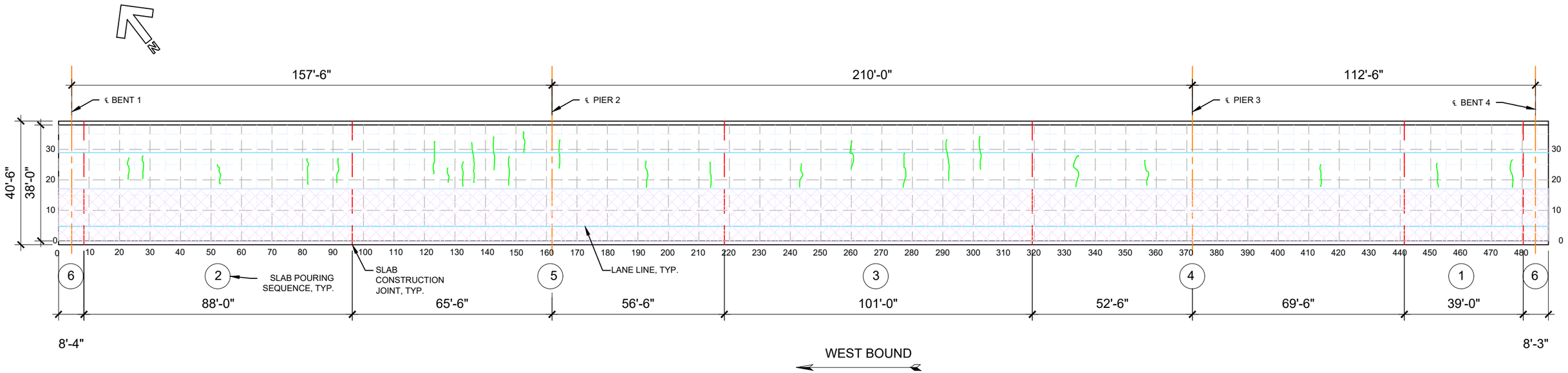

BONNER SPRING BRIDGE OVER BLACKFOOT RIVER - WEST BOUND - PHASE II - TOPSIDE - 2019 INSPECTION

1/32"= 1'-0"

WJE ENGINEERS ARCHITECTS MATERIAL SCIENTISTS
Wiss, Janney, Elstner Associates, Inc.

Bonner Spring Bridge
WJE No. 2019.2214.0
Inspection dates: December 7, 2019
SCALE: AS NOTED

CRACK

CRACK SURVEY NOT PERFORMED

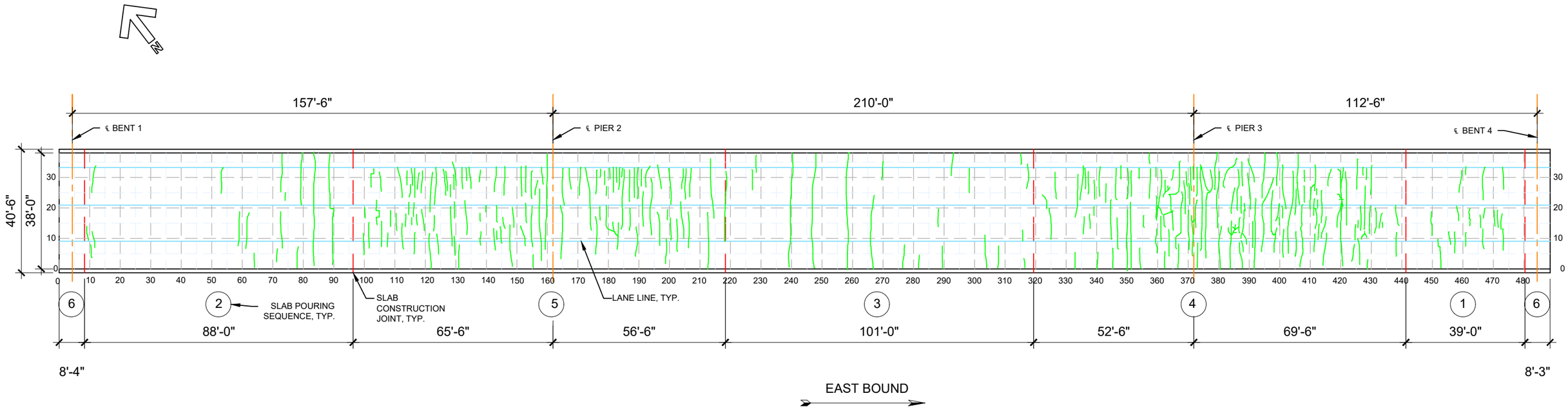

BONNER SPRING BRIDGE OVER BLACKFOOT RIVER - EAST BOUND - PHASE I - TOPSIDE - 2020 INSPECTION

1/32"= 1'-0"

WJE ENGINEERS ARCHITECTS MATERIAL SCIENTISTS
Wiss, Janney, Elstner Associates, Inc.

Bonner Spring Bridge
WJE No. 2019.2214.0
Inspection dates: August, 2019
SCALE: AS NOTED

CRACK

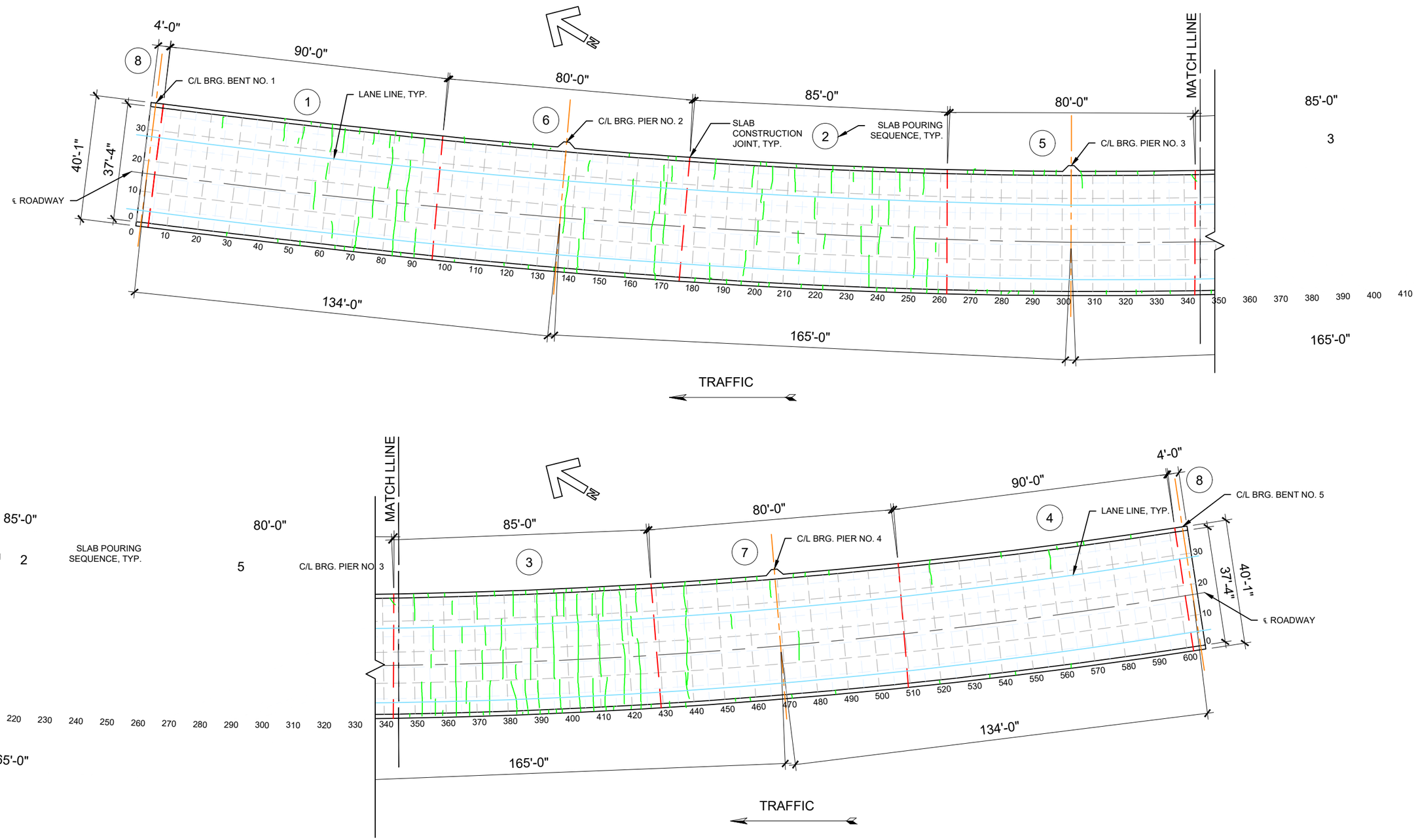

RARUS/SILVERBOW CREEK BRIDGE D - I15 SOUTH BOUND - UNDERSIDE - 2020 INSPECTION

1/32"= 1'-0"

WJE ENGINEERS ARCHITECTS MATERIAL SCIENTISTS

Wiss, Janney, Elstner Associates, Inc.

Rarus/Silverbow Creek Bridge D

WJE No. 2019.2214.0

Inspection dates: August 2020

AS NOTED

CRACK

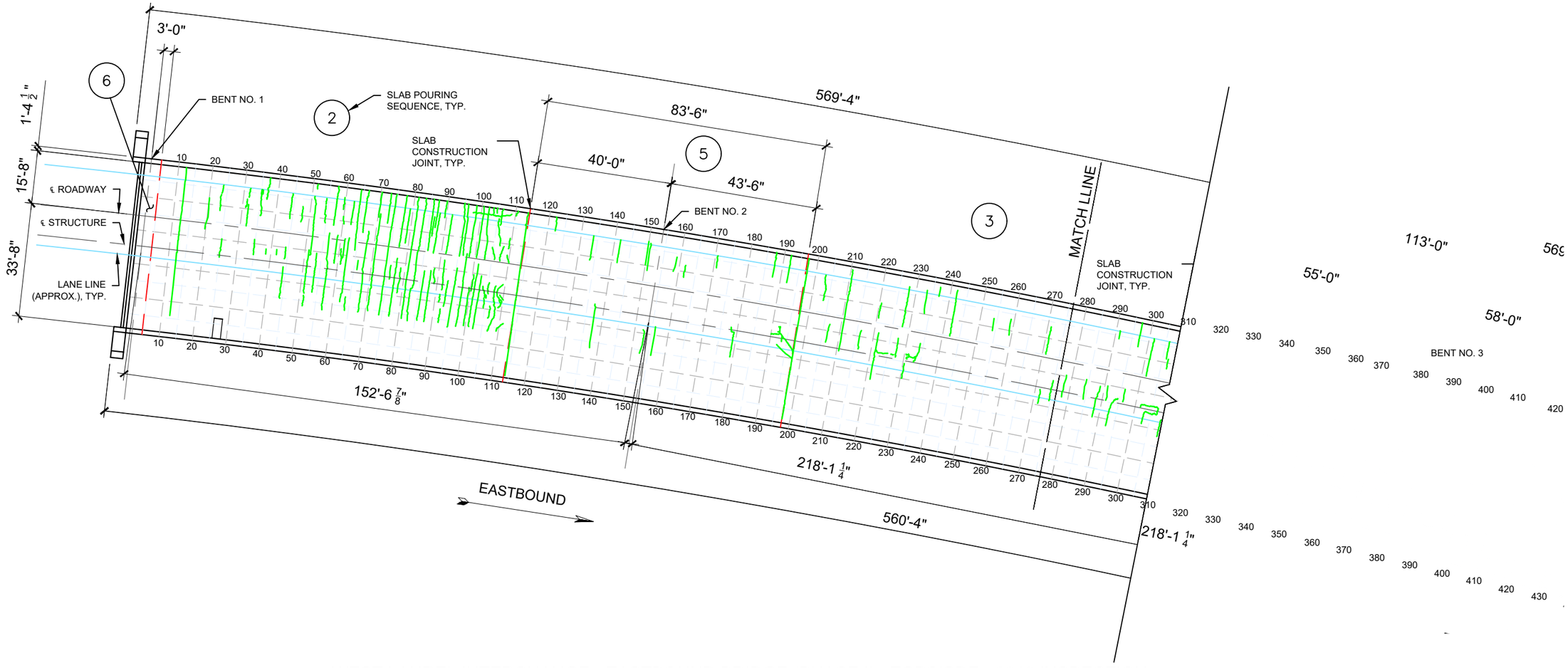

WEST LAUREL INTERCHANGE - EASTBOUND BRIDGE (PHASE I) - TOPSISDE - 2019 INSPECTION

1/32"= 1'-0"

NOTES:

CRACK MAPPING WAS BASED ON ORTHO MOSAIC PHOTOS PROVIDED BY MDT.

WJE ENGINEERS ARCHITECTS MATERIAL SCIENTISTS
Wiss, Janney, Elstner Associates, Inc.

West Laurel Interchange - West
WJE No. 2019.2214.0
Inspection dates: November 2019
SCALE: AS NOTED

CRACK

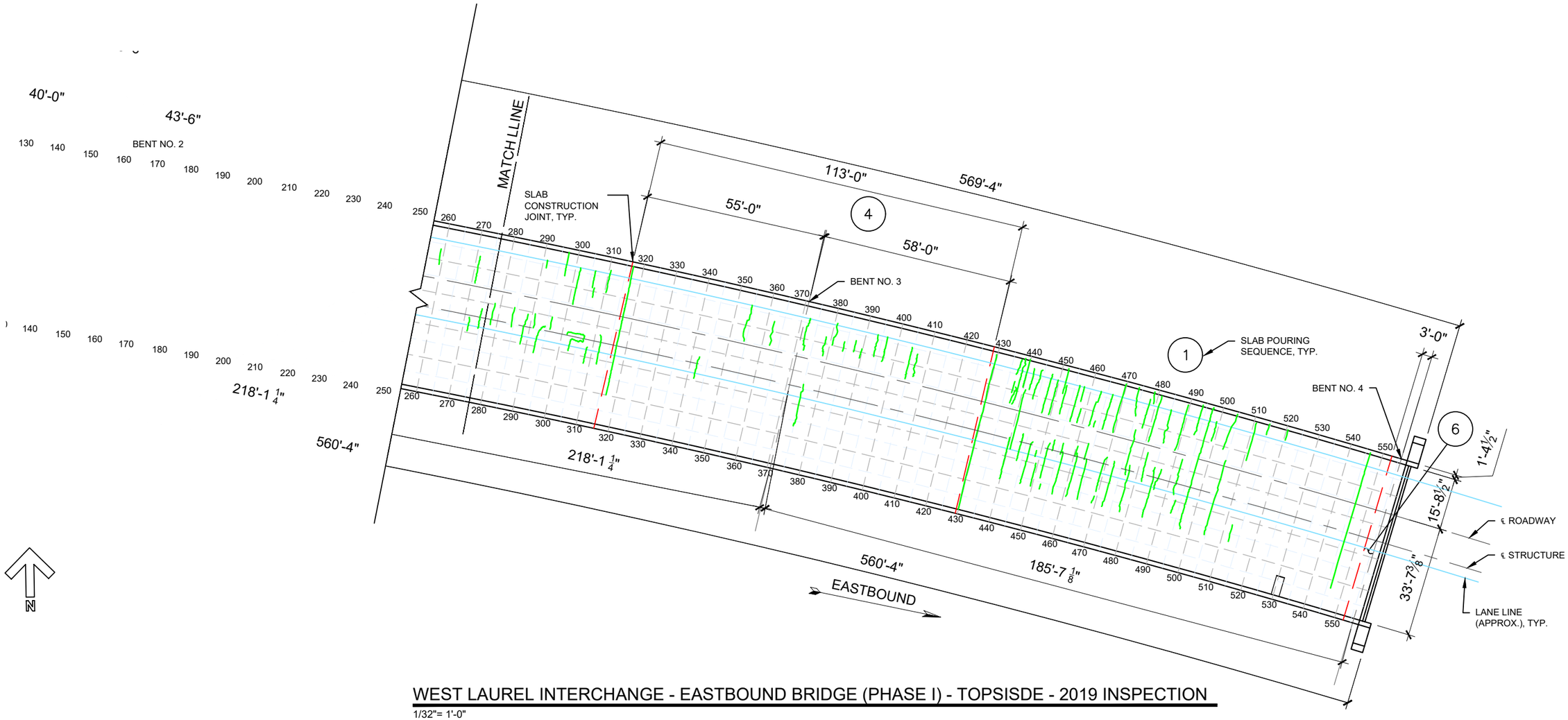

WEST LAUREL INTERCHANGE - EASTBOUND BRIDGE (PHASE I) - TOPSISDE - 2019 INSPECTION

1/32"= 1'-0"

NOTES:

CRACK MAPPING WAS BASED ON ORTHO MOSAIC PHOTOS PROVIDED BY MDT.

WJE ENGINEERS ARCHITECTS MATERIAL SCIENTISTS
Wiss, Janney, Elstner Associates, Inc.

West Laurel Interchange - West
WJE No. 2019.2214.0
Inspection dates: November 2019
SCALE: AS NOTED

CRACK

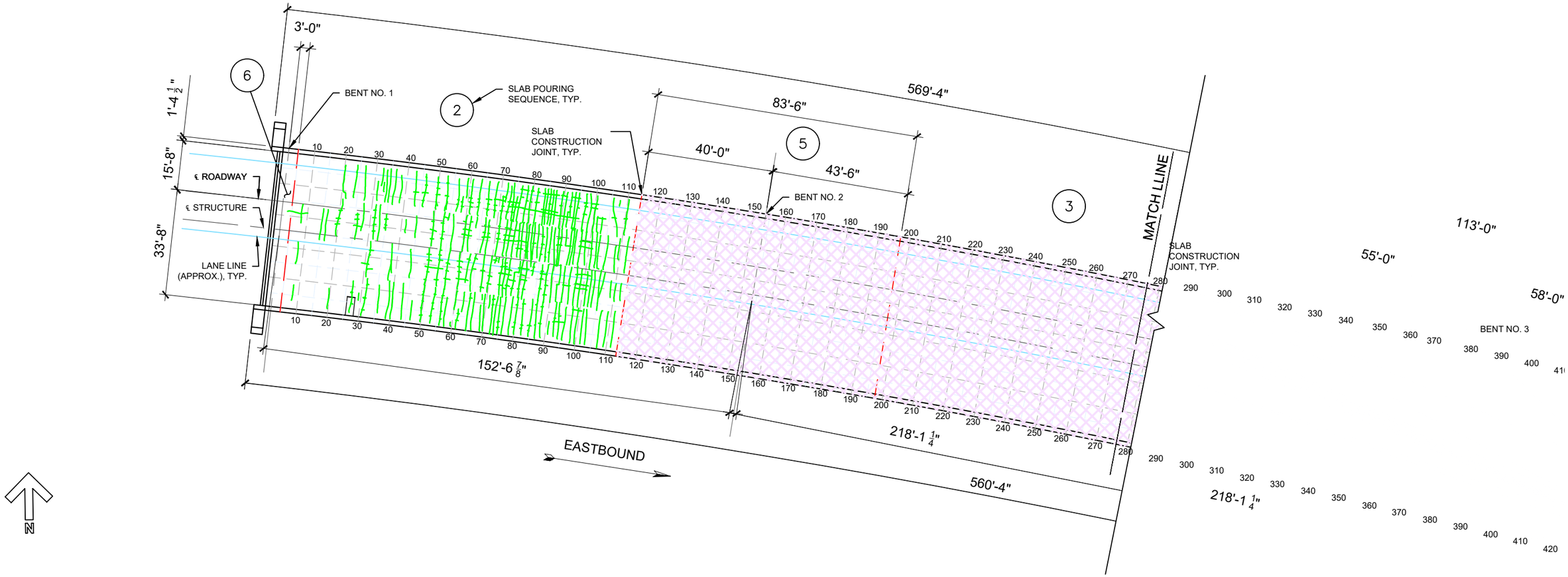

WEST LAUREL INTERCHANGE - EASTBOUND BRIDGE (PHASE I) - UNDERSIDE - 2020 INSPECTION

1/32"= 1'-0"

WJE ENGINEERS ARCHITECTS MATERIAL SCIENTISTS
Wiss, Janney, Elstner Associates, Inc.

West Laurel Interchange - West
WJE No. 2019.2214.0
Inspection dates: August 2020
SCALE: AS NOTED

CRACK

CRACK SURVEY NOT PERFORMED

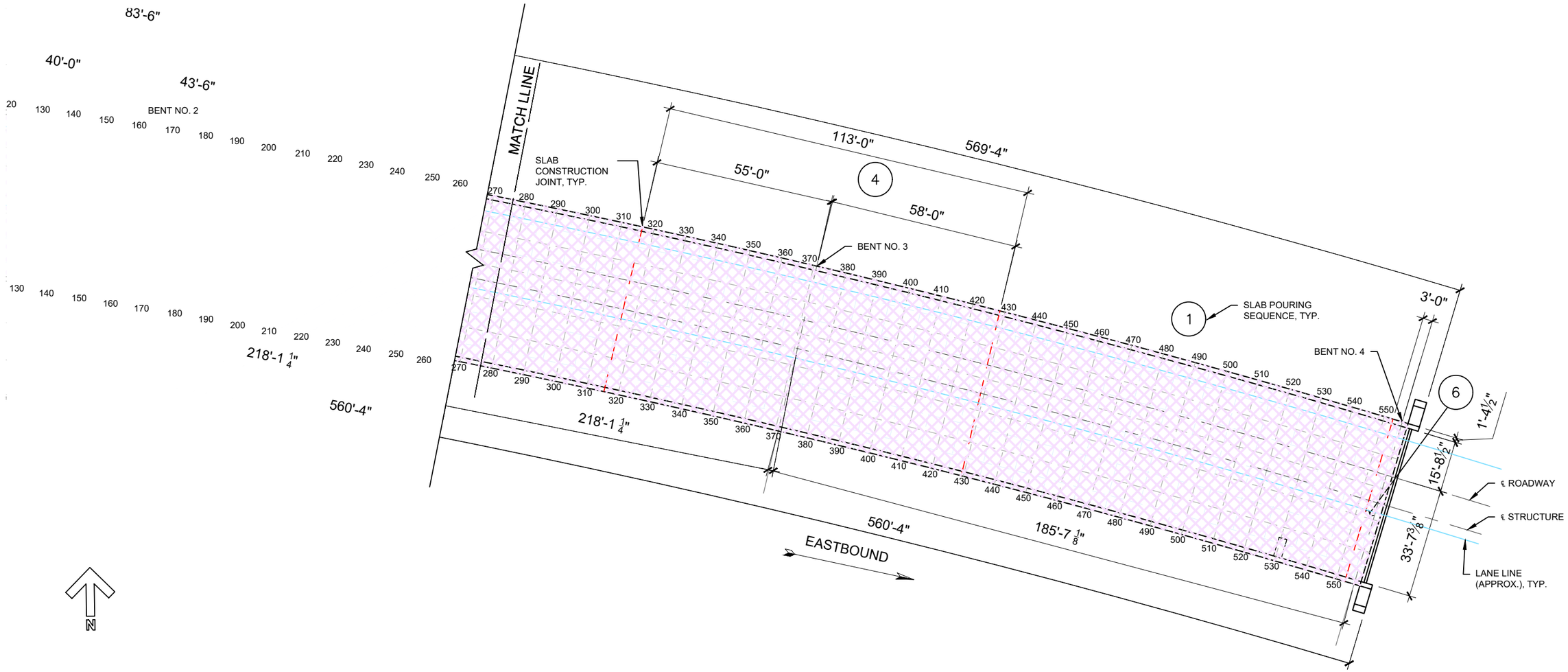

WEST LAUREL INTERCHANGE - EASTBOUND BRIDGE (PHASE I) - UNDERSIDE - 2020 INSPECTION

1/32"= 1'-0"

WJE ENGINEERS ARCHITECTS MATERIAL SCIENTISTS
Wiss, Janney, Elstner Associates, Inc.

West Laurel Interchange - West
WJE No. 2019.2214.0
Inspection dates: August 2020
SCALE: AS NOTED

CRACK

CRACK SURVEY NOT PERFORMED

APPENDIX C. INSTRUMENTATION DATA

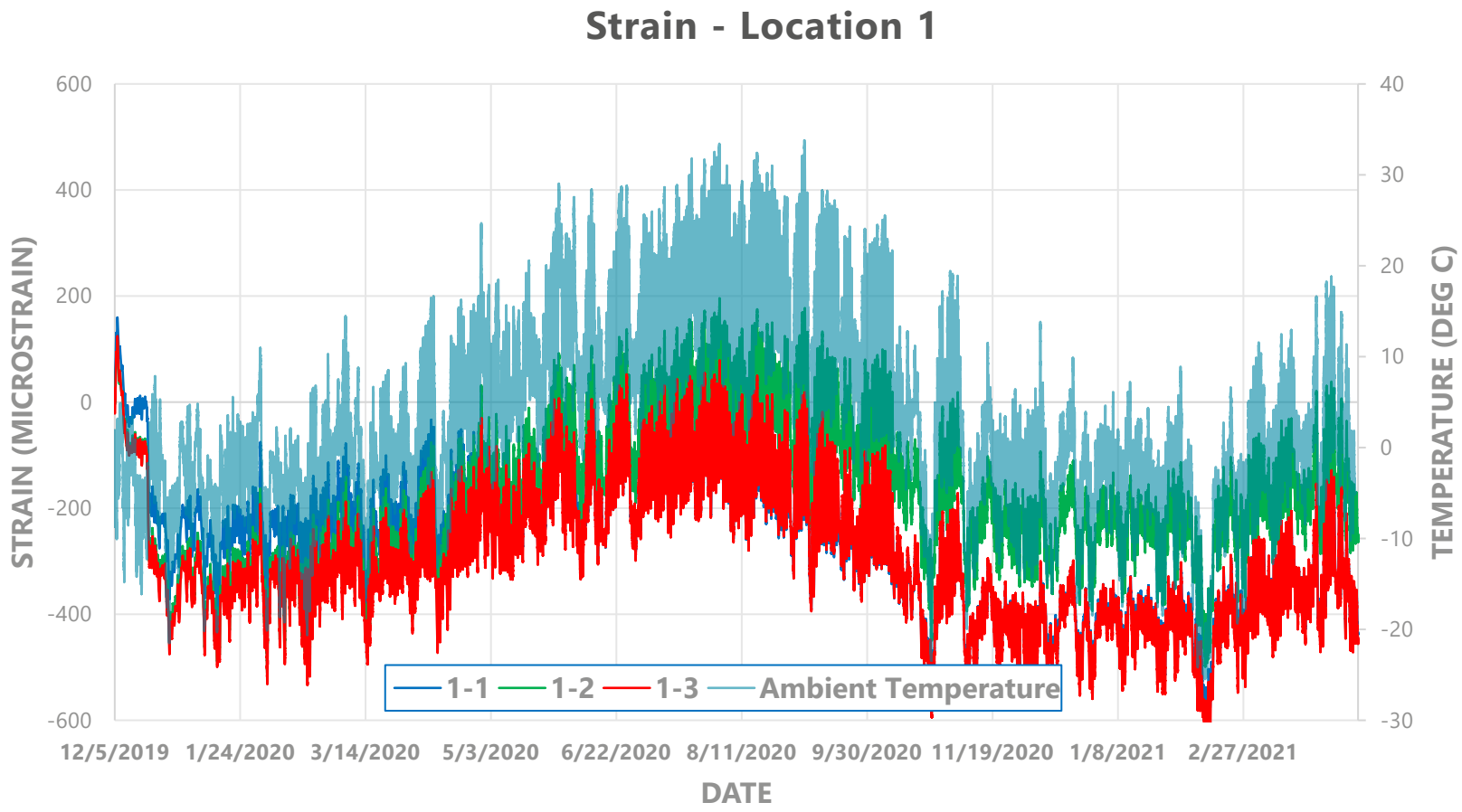
Strain - Location 1
STRAIN (MICROSTRAIN)
600
400
200
0
-200
-400
-600
TEMPERATURE (DEG C)
40
30
20
10
0
-10
-20
-30
1-1
1-2
1-3
Ambient Temperature
12/5/2019
1/24/2020
3/14/2020
5/3/2020
6/22/2020
8/11/2020
9/30/2020
11/19/2020
1/8/2021
2/27/2021
DATE

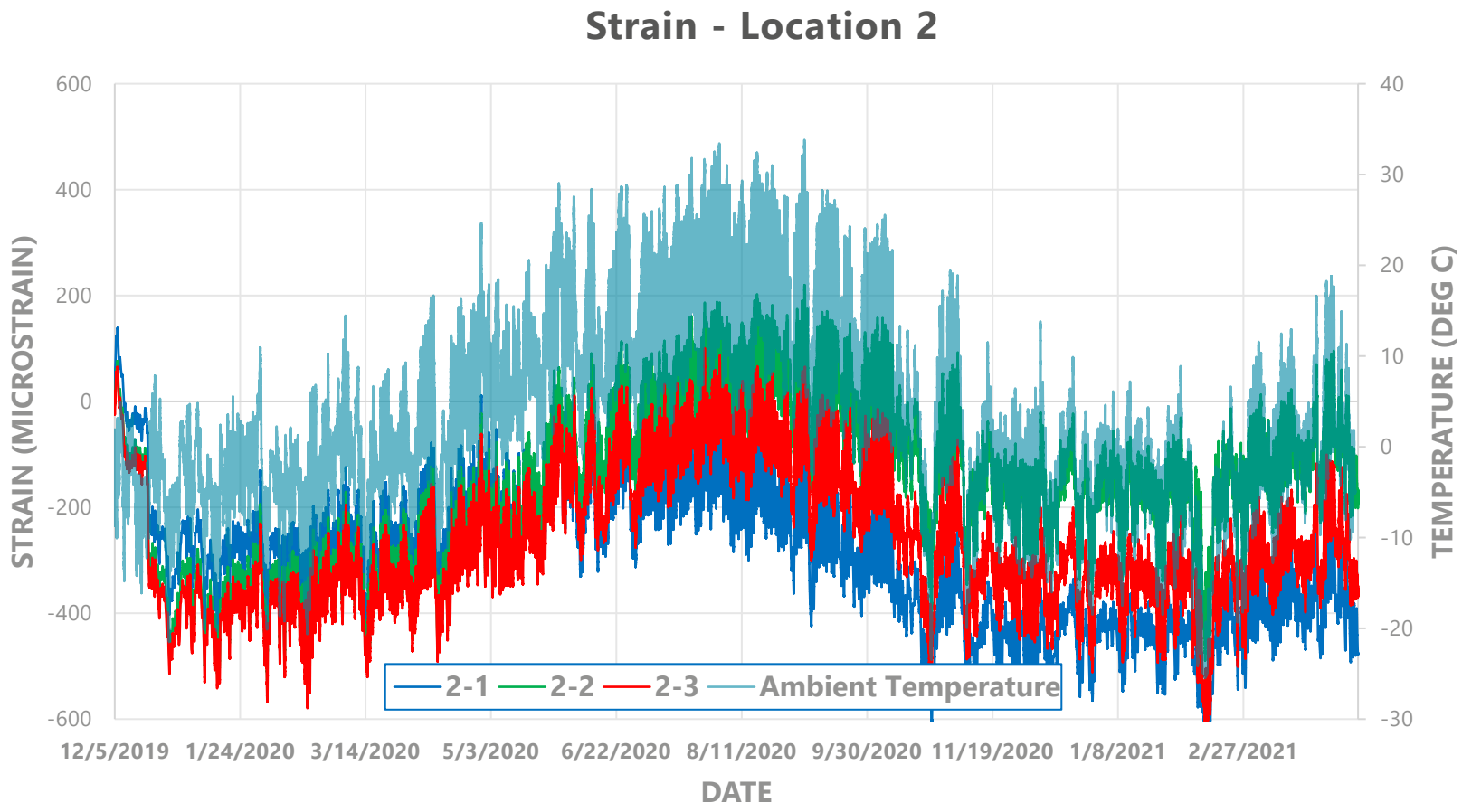
Strain - Location 2
600
400
200
0
-200
-400
-600
STRAIN (MICROSTRAIN)
40
30
20
10
0
-10
-20
-30
TEMPERATURE (DEG C)
2-1
2-2
2-3
Ambient Temperature
12/5/2019
1/24/2020
3/14/2020
5/3/2020
6/22/2020
8/11/2020
9/30/2020
11/19/2020
1/8/2021
2/27/2021
DATE

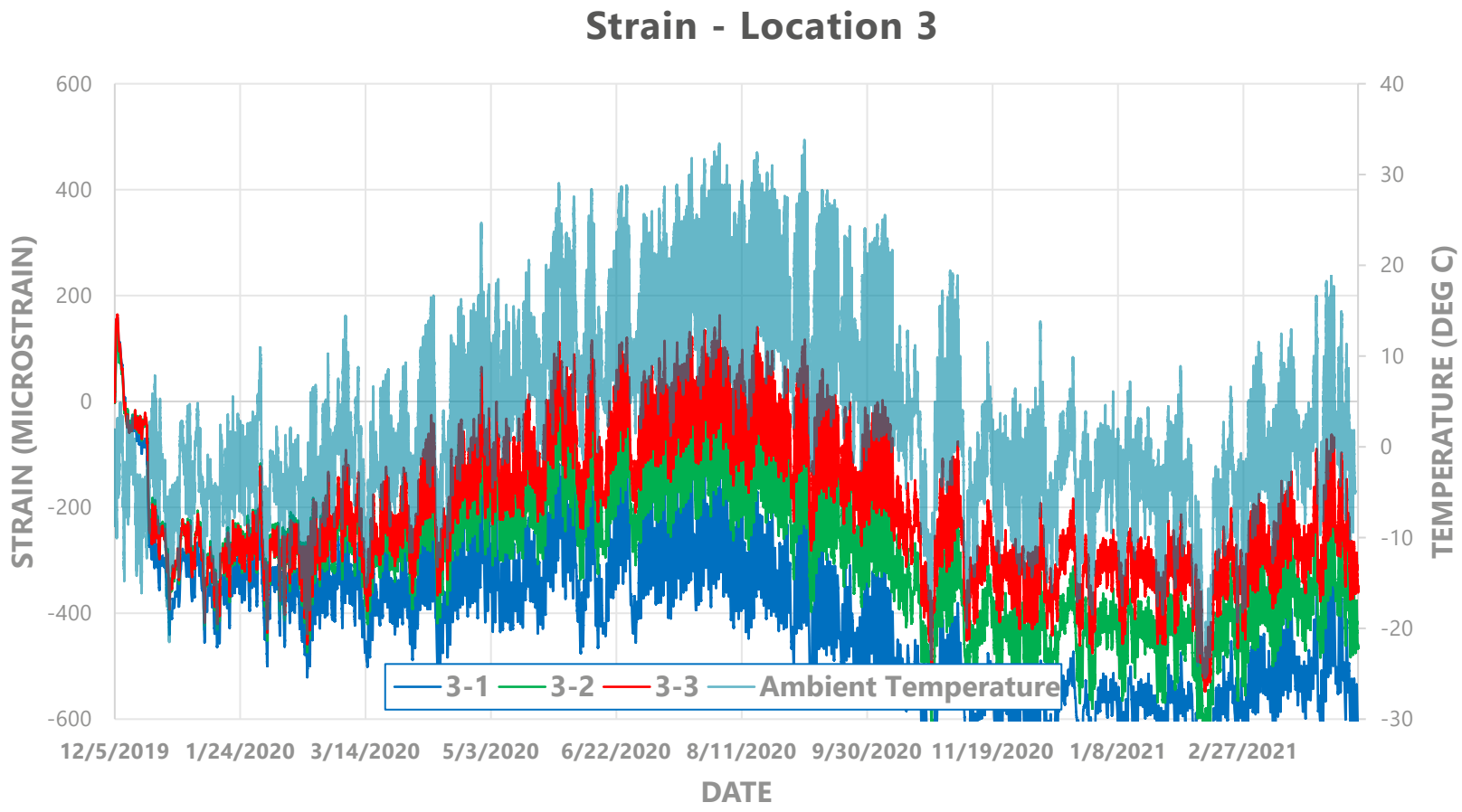
Strain - Location 3
600
400
200
0
-200
-400
-600
STRAIN (MICROSTRAIN)
40
30
20
10
0
-10
-20
-30
TEMPERATURE (DEG C)
3-1
3-2
3-3
Ambient Temperature
12/5/2019
1/24/2020
3/14/2020
5/3/2020
6/22/2020
8/11/2020
9/30/2020
11/19/2020
1/8/2021
2/27/2021
DATE

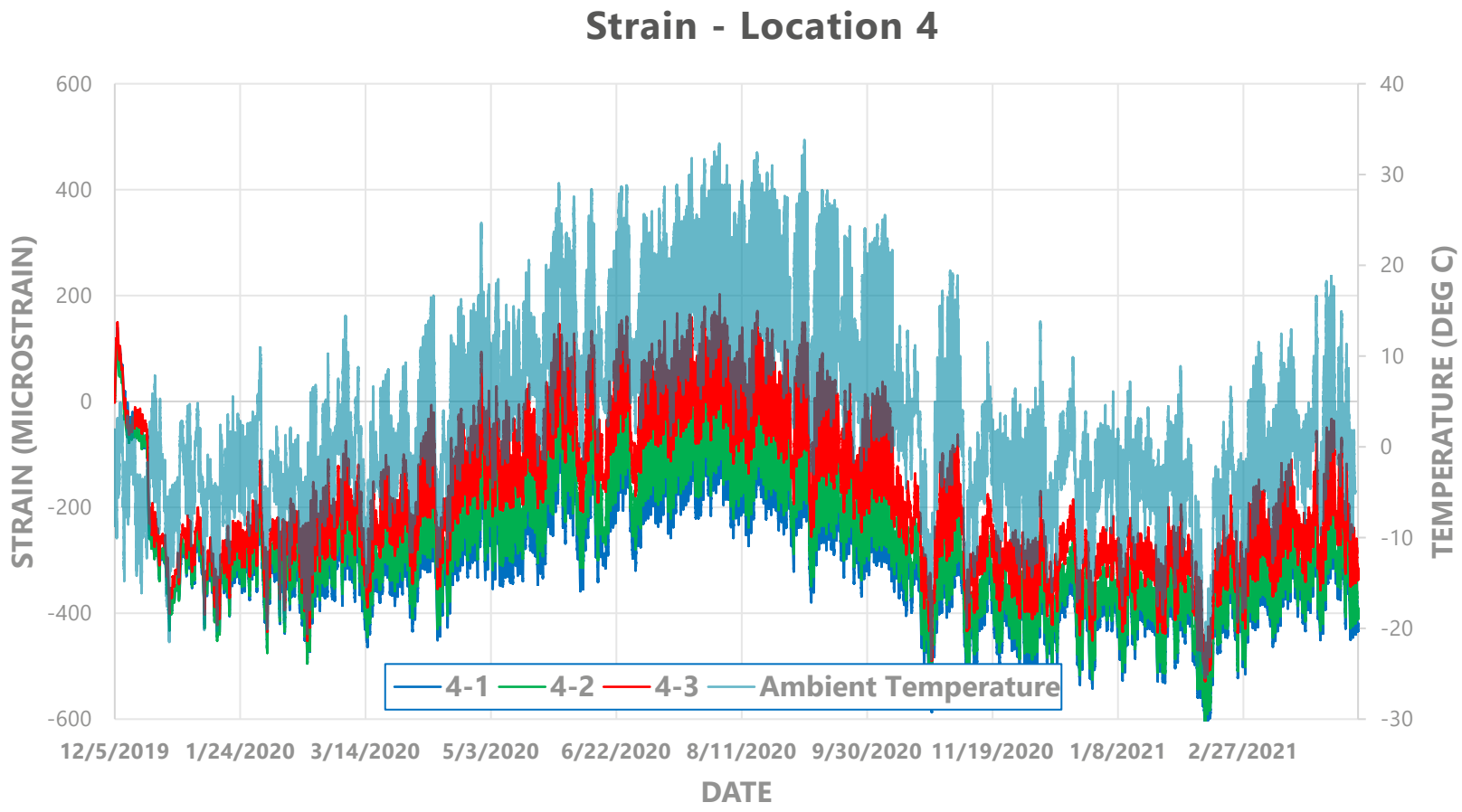
Strain - Location 4
STRAIN (MICROSTRAIN)
600
400
200
0
-200
-400
-600
TEMPERATURE (DEG C)
40
30
20
10
0
-10
-20
-30
4-1
4-2
4-3
Ambient Temperature
12/5/2019
1/24/2020
3/14/2020
5/3/2020
6/22/2020
8/11/2020
9/30/2020
11/19/2020
1/8/2021
2/27/2021
DATE

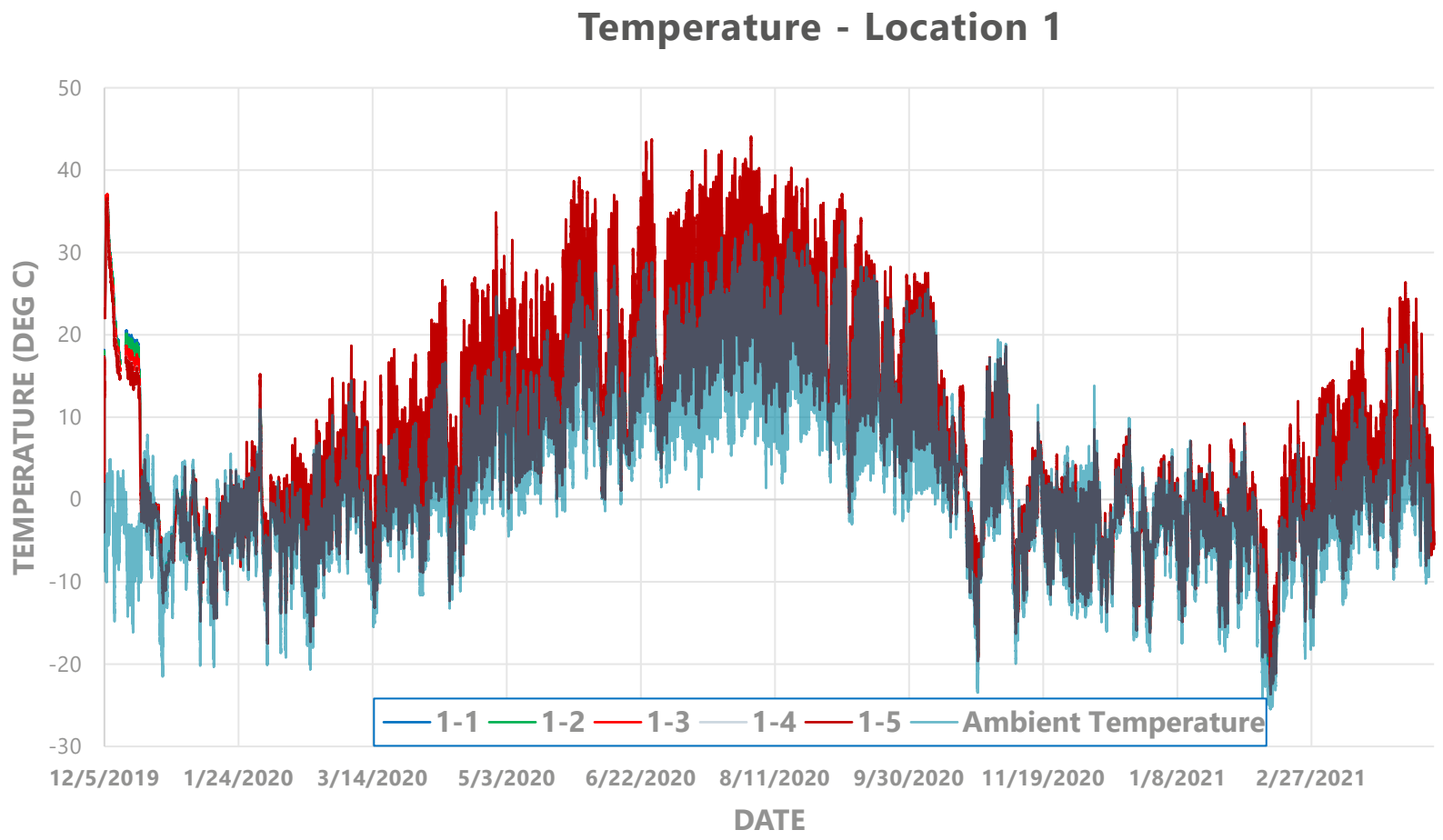
Temperature - Location 1
TEMPERATURE (DEG C)
50
40
30
20
10
0
-10
-20
-30
12/5/2019
1/24/2020
3/14/2020
5/3/2020
6/22/2020
8/11/2020
9/30/2020
11/19/2020
1/8/2021
2/27/2021
DATE
1-1
1-2
1-3
1-4
1-5
Ambient Temperature

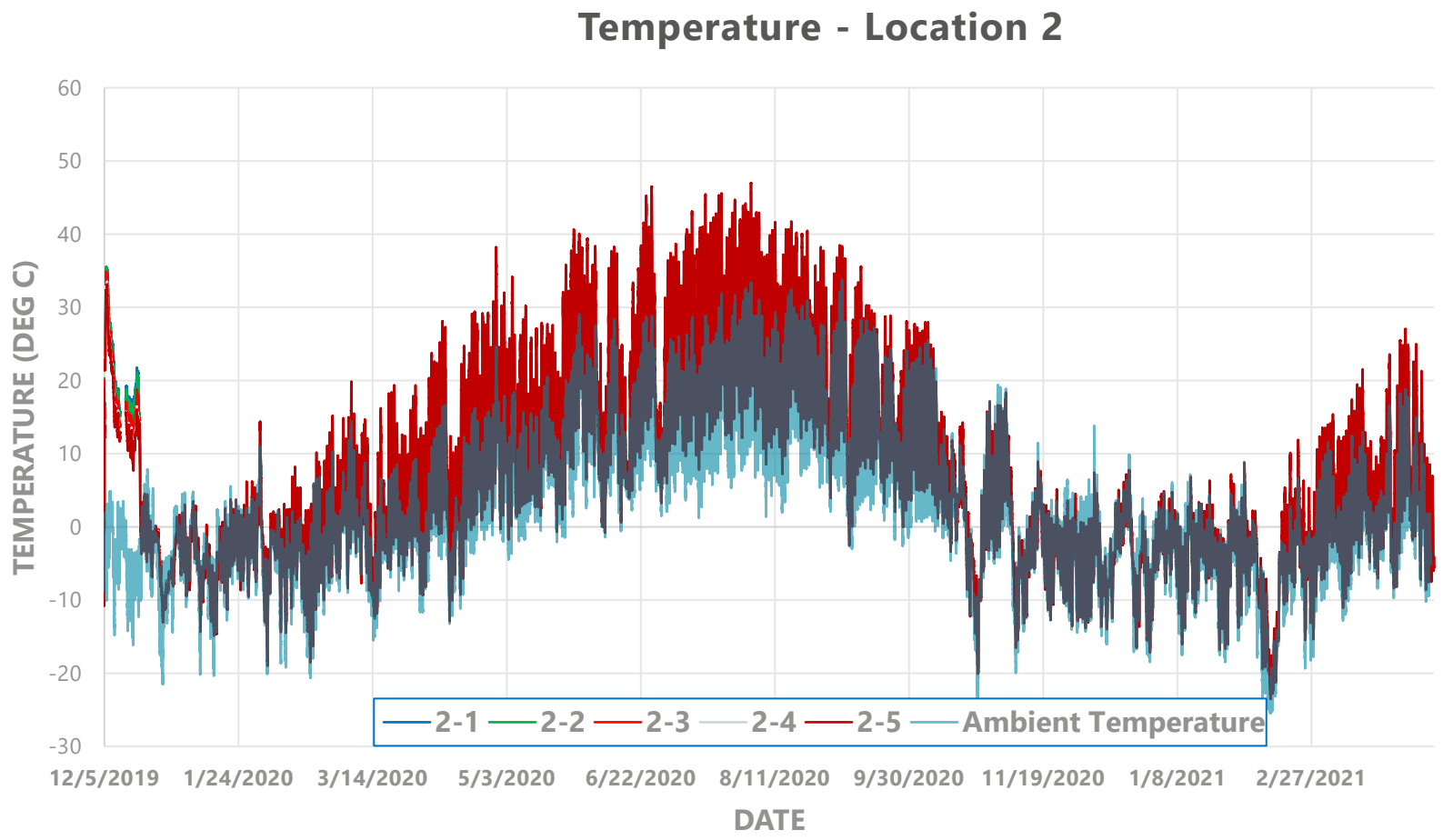
Temperature - Location 2
TEMPERATURE (DEG C)
60
50
40
30
20
10
0
-10
-20
-30
12/5/2019
1/24/2020
3/14/2020
5/3/2020
6/22/2020
8/11/2020
9/30/2020
11/19/2020
1/8/2021
2/27/2021
DATE
2-1
2-2
2-3
2-4
2-5
Ambient Temperature

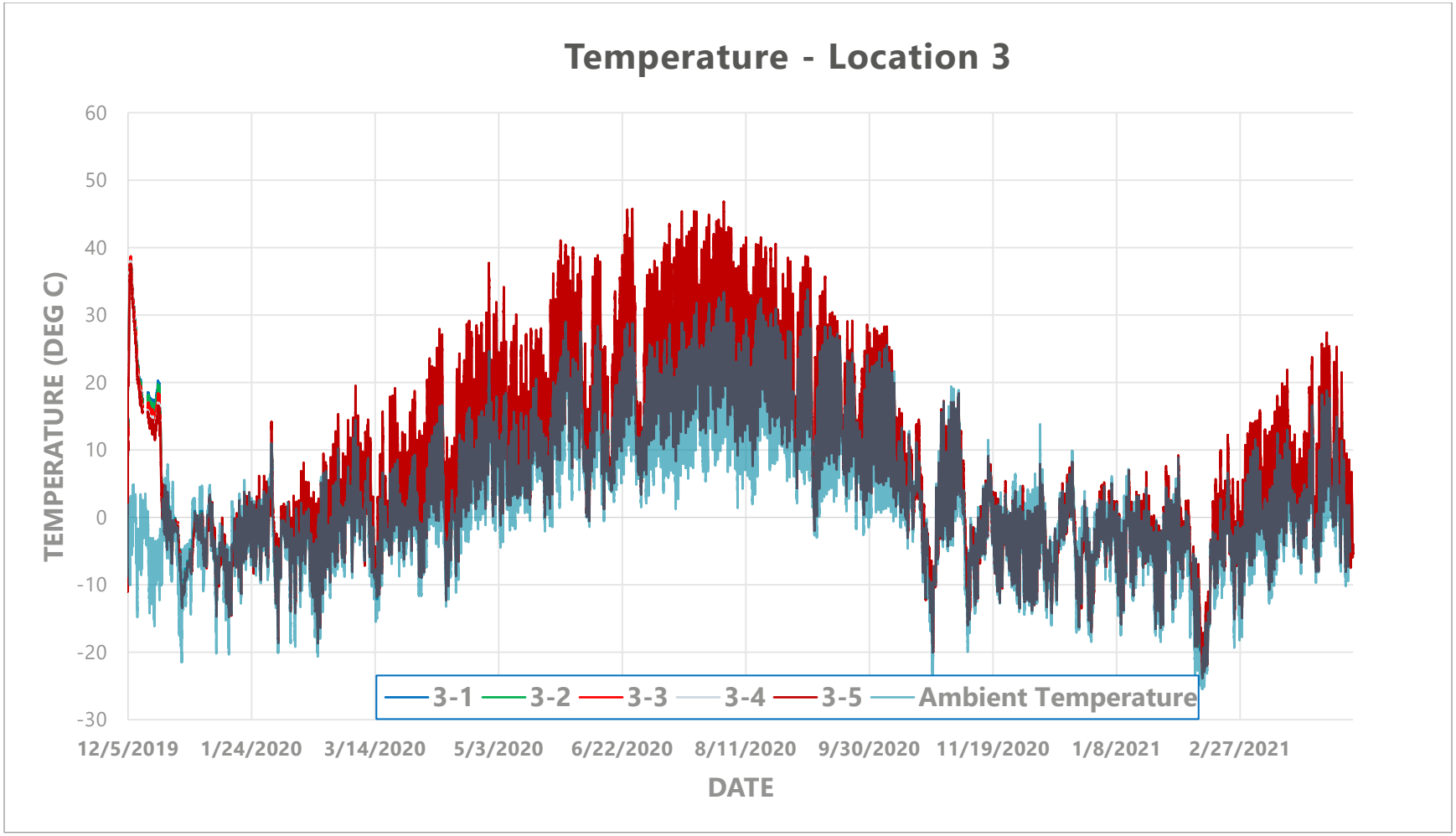
Temperature - Location 3
TEMPERATURE (DEG C)
60
50
40
30
20
10
0
-10
-20
-30
12/5/2019
1/24/2020
3/14/2020
5/3/2020
6/22/2020
8/11/2020
9/30/2020
11/19/2020
1/8/2021
2/27/2021
DATE
3-1
3-2
3-3
3-4
3-5
Ambient Temperature

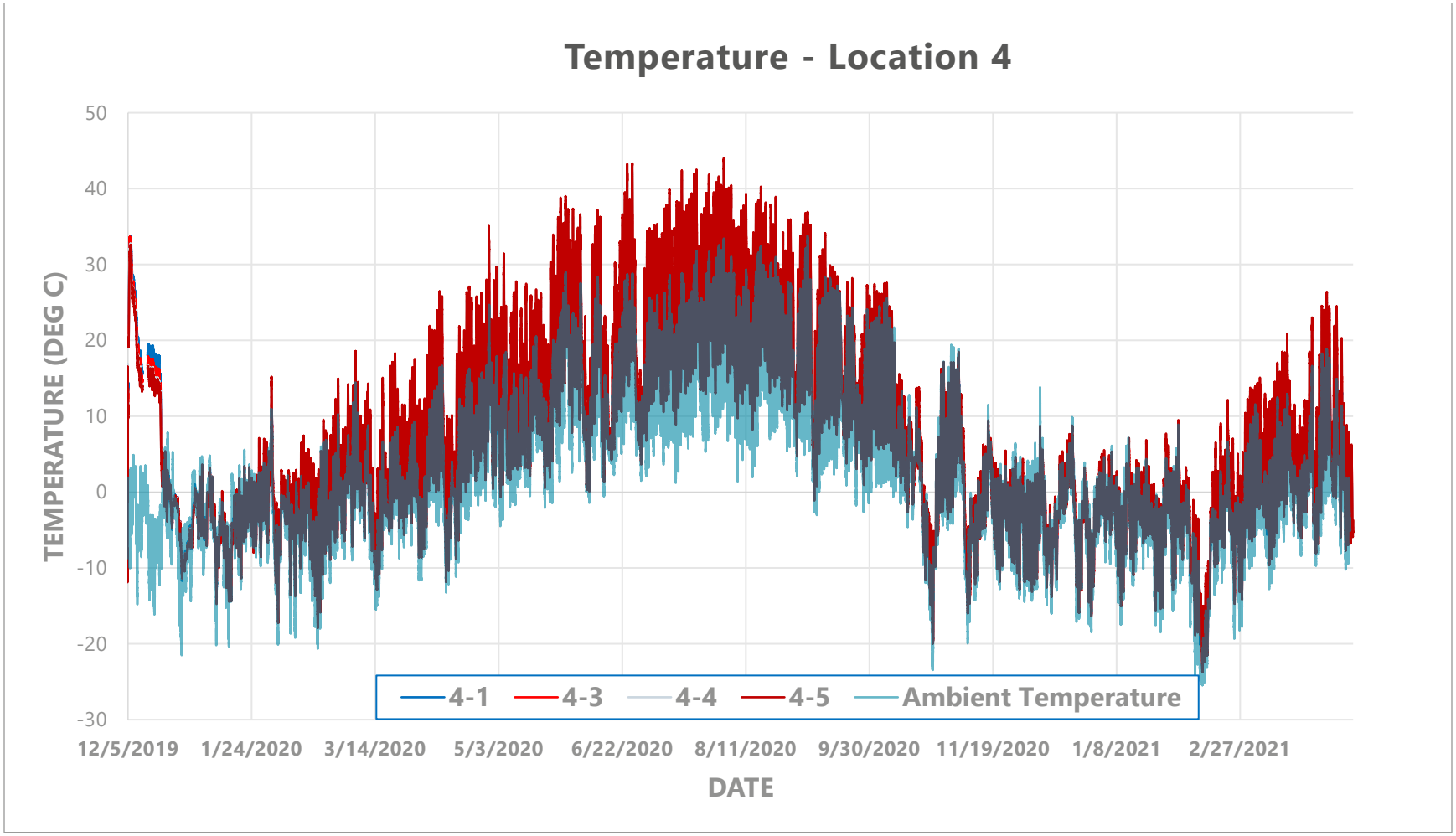
Temperature - Location 4
TEMPERATURE (DEG C)
50
40
30
20
10
0
-10
-20
-30
12/5/2019
1/24/2020
3/14/2020
5/3/2020
6/22/2020
8/11/2020
9/30/2020
11/19/2020
1/8/2021
2/27/2021
DATE
4-1
4-3
4-4
4-5
Ambient Temperature

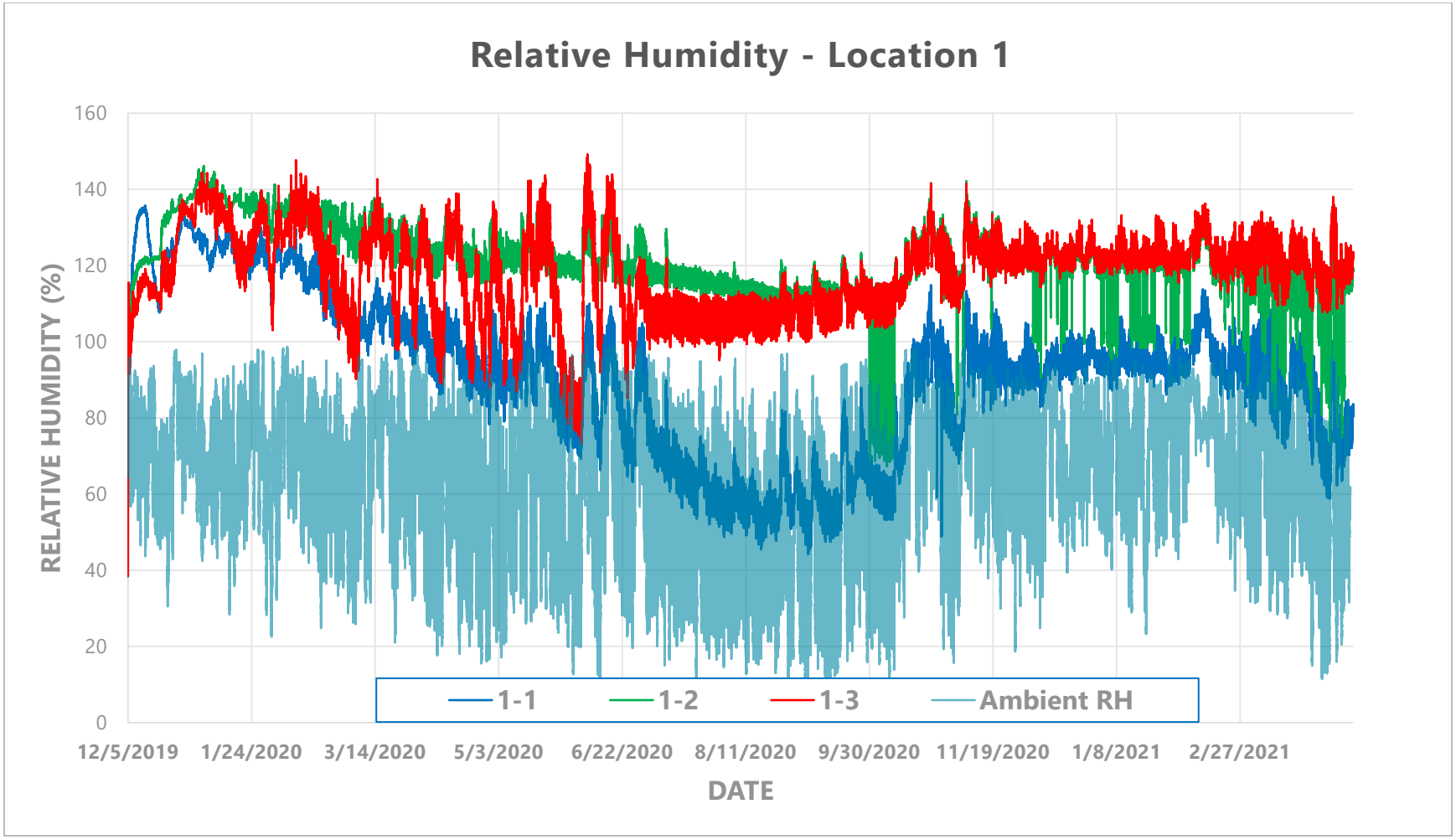

rH Location 2

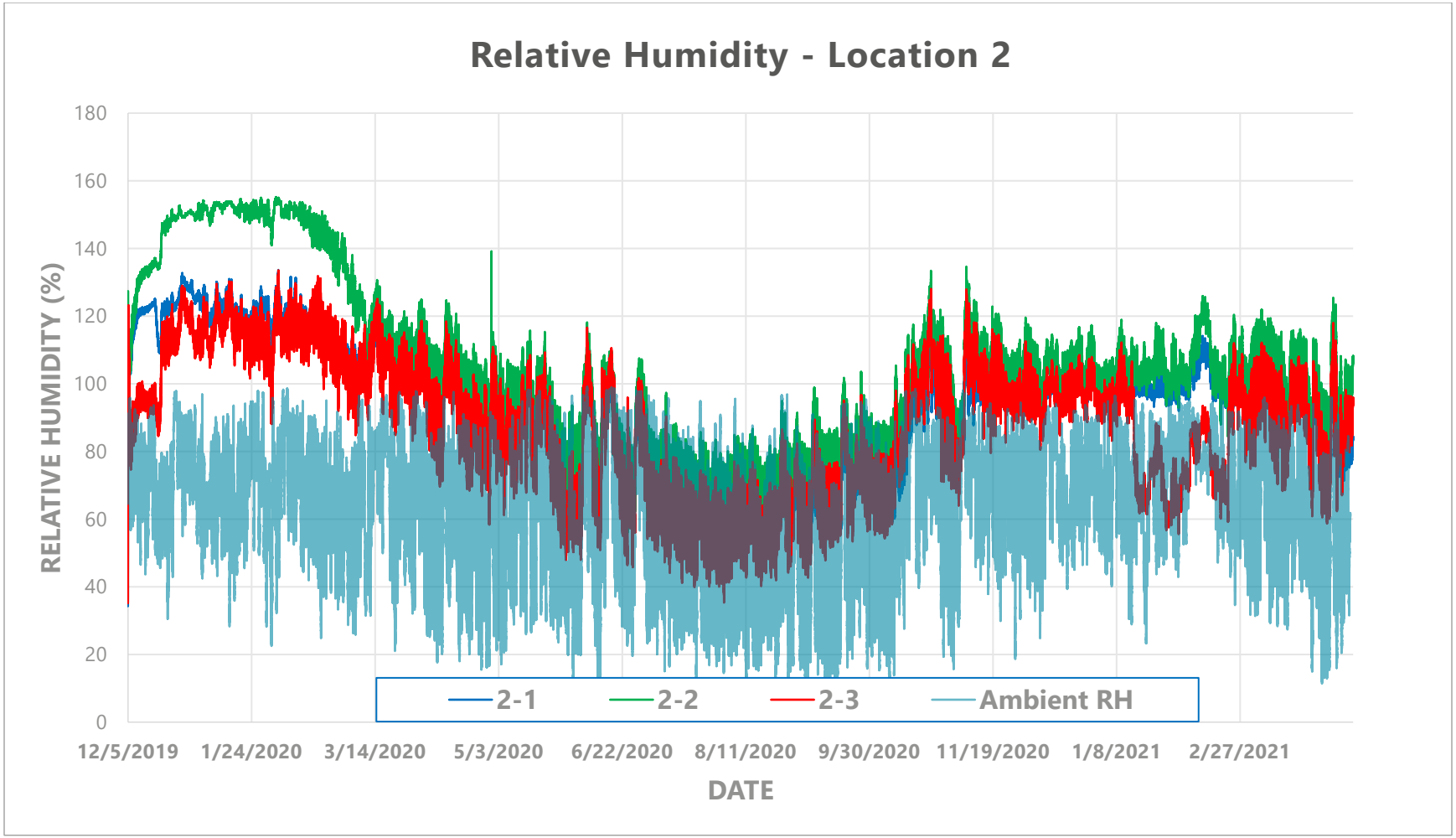
Relative Humidity - Location 2
RELATIVE HUMIDITY (%)
180
160
140
120
100
80
60
40
20
0
12/5/2019
1/24/2020
3/14/2020
5/3/2020
6/22/2020
8/11/2020
9/30/2020
11/19/2020
1/8/2021
2/27/2021
DATE
2-1
2-2
2-3
Ambient RH

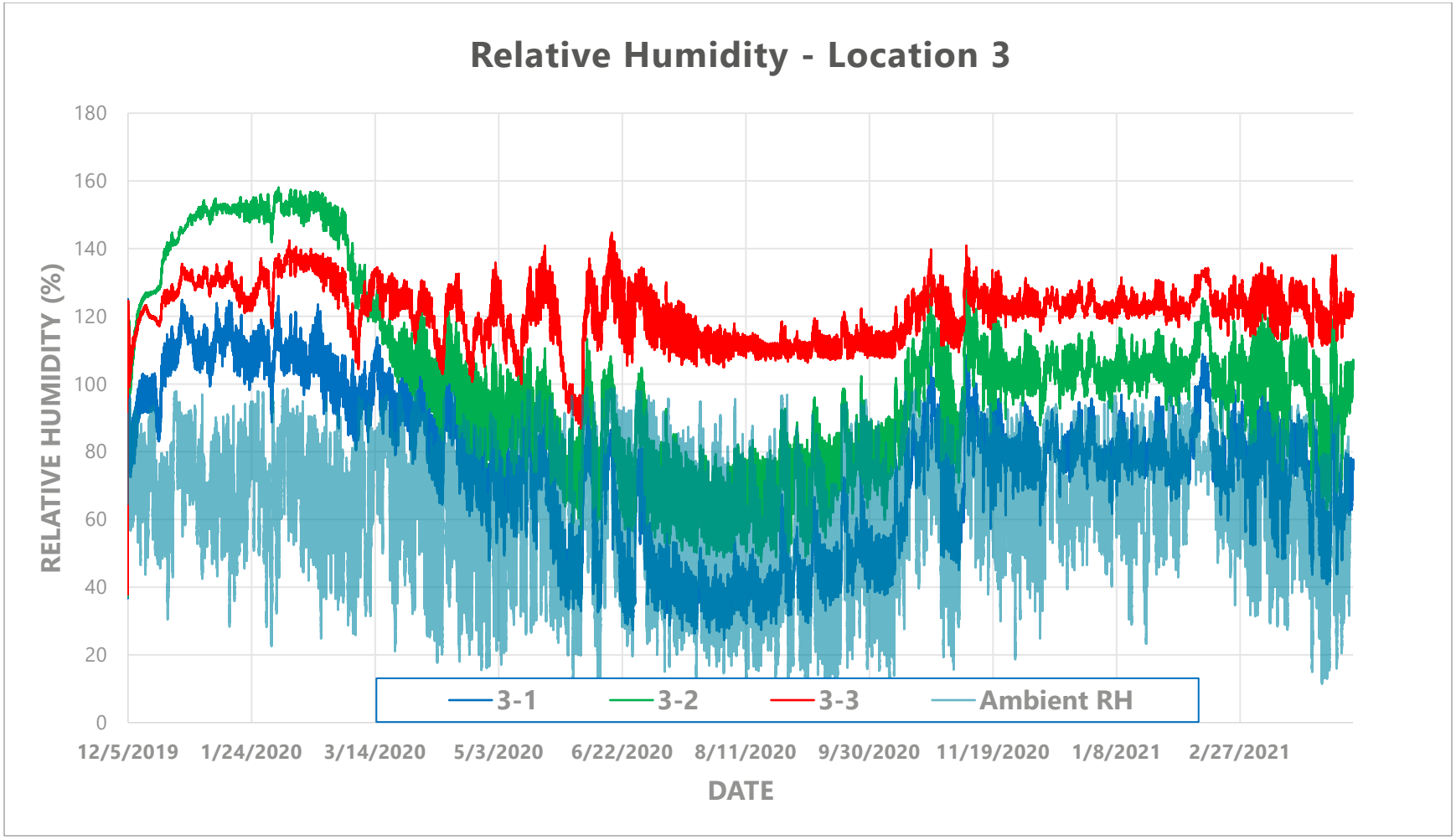
Relative Humidity - Location 3
RELATIVE HUMIDITY (%)
180
160
140
120
100
80
60
40
20
0
12/5/2019
1/24/2020
3/14/2020
5/3/2020
6/22/2020
8/11/2020
9/30/2020
11/19/2020
1/8/2021
2/27/2021
DATE
3-1
3-2
3-3
Ambient RH

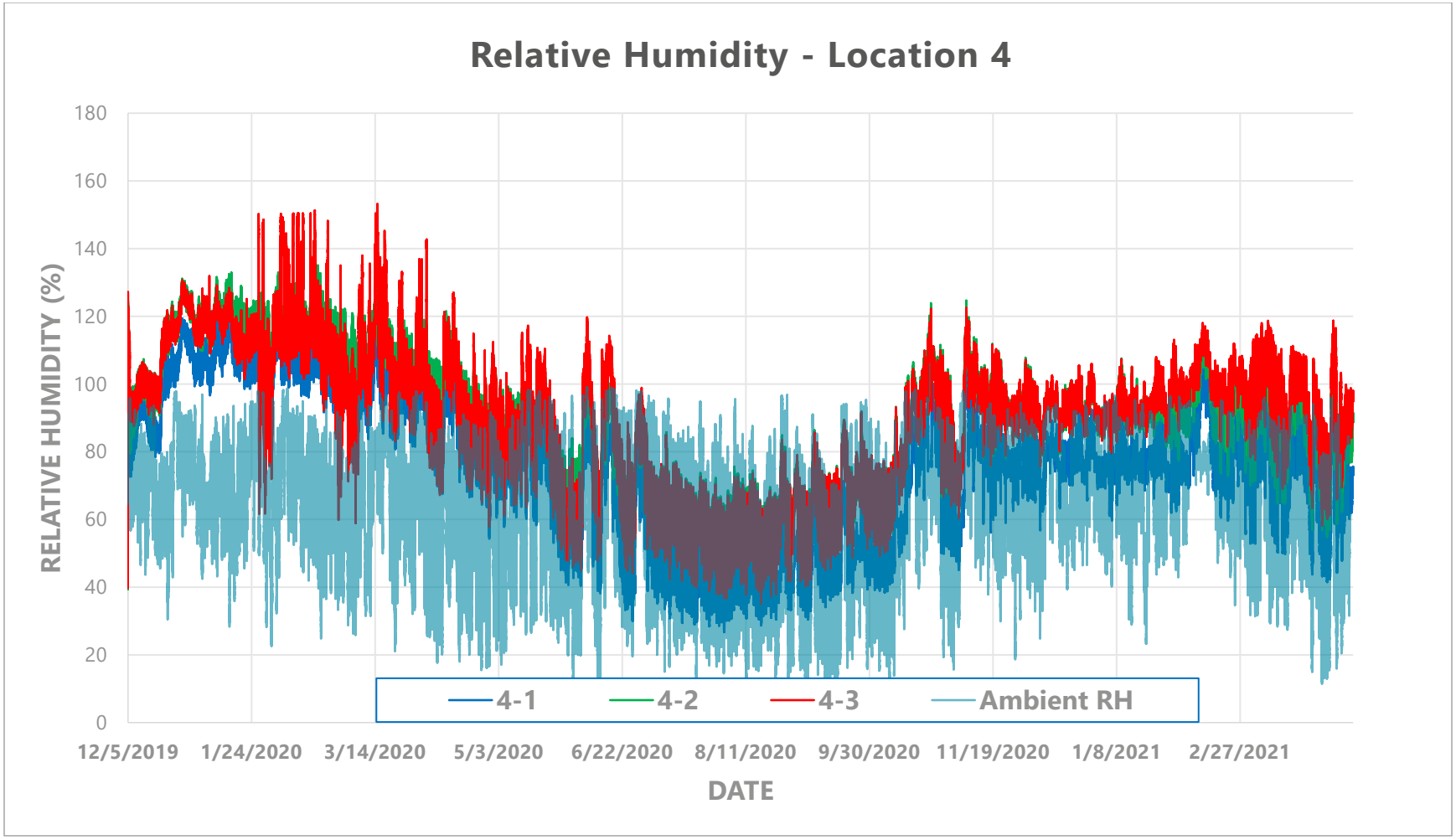
Relative Humidity - Location 4
RELATIVE HUMIDITY (%)
180
160
140
120
100
80
60
40
20
0
12/5/2019
1/24/2020
3/14/2020
5/3/2020
6/22/2020
8/11/2020
9/30/2020
11/19/2020
1/8/2021
2/27/2021
DATE
4-1
4-2
4-3
Ambient RH